

NASA CR-143806

TRADE-OFF ANALYSIS OF MODES OF DATA HANDLING FOR EARTH RESOURCES (ERS)

FINAL REPORT

VOLUME 2

(NASA-CR-143806)	TRADE-OFF ANALYSIS OF	N75-26471
MODES OF DATA HANDLING FOR EARTH RESOURCES		
(ERS), VOLUME 2 Final Report (TRW Systems		
Group) 286 p HC \$8.75	C5CL 05B	Unclas
	G3/43	25986

TRW Sales No. 22591.000

RFP No. 5-37612-212

28 MARCH 1975

Prepared for

GODDARD SPACE FLIGHT CENTER
 National Aeronautics and Space Administration
 Greenbelt, Maryland 20771



Prepared by



VOLUME 1

TABLE OF CONTENTS

	<u>Page</u>
1. INTRODUCTION	1-1
2. SENSOR CHARACTERISTICS	2-1
2.1 Sensor Selection	2-1
2.2 Cost Estimations	2-2
2.3 Sensor Descriptions	2-4
2.3.1 Individual Sensors	2-7
2.3.2 Sensor Characteristics Tables	2-21
3. MISSION MODEL DEVELOPMENT	3-1
3.1 Candidate Data Uses/Requirements	3-1
3.1.1 User Community Requirements	3-1
3.1.2 Data Products	3-19
3.2 Sensor Use Profiles	3-26
3.2.1 Mission 1 (Terrestrial Survey/Environmental Quality, Research)	3-27
3.2.2 Mission 2 (Ocean Survey/Meteorology, Research)	3-27
3.2.3 Missions 3 and 5 (Terrestrial Survey/ Environmental Quality)	3-28
3.2.4 Mission 4 (Ocean Survey/Meteorology, Research)	3-29
3.2.5 Mission 5 (Transient Environmental Phenomena Monitoring, Research)	3-29
3.2.6 Mission 7 (Ocean Survey/Meteorology, Operational)	3-31
3.2.7 Mission 8 (Meteorological, Research)	3-31
3.2.8 Mission 9 (Meteorological, Research)	3-32
3.3 Candidate Mission Descriptions	3-33
3.3.1 Mission Model No. 1	3-35
3.3.2 Mission Model No. 2	3-38
3.3.3 Mission Model No. 3	3-40
3.3.4 Mission Model No. 4	3-41
3.3.5 Mission Model No. 5	3-42
3.3.6 Mission Model No. 6	3-44
3.3.7 Mission Model No. 7	3-45
3.3.8 Mission Model No. 8	3-46
3.3.9 Mission Model No. 9	3-47
3.3.10 Payload Compatibility with Launch Vehicle and Spacecraft	3-48

TABLE OF CONTENTS (Continued)

	<u>Page</u>
4. DATA REQUIREMENTS SUMMARY	4-1
4.1 Data Handling System Requirements-Summary	4-1
4.1.1 Estimation of Data Volume/Time Profiles for Each Mission	4-1
4.1.2 Matrix Summaries	4-3
4.2 Data Handling System Driver Requirements	4-17
5. DATA ROUTING ANALYSIS	5-1
5.1 Method of Approach	5-1
5.2 Mission Requirements - Step 1	5-1
5.3 Data Storage - Steps 2 and 3	5-3
5.4 NASA Ground Stations - Step 4	5-4
5.4.1 TDRS	5-4
5.4.2 Space Tracking and Data Network	5-5
5.4.3 Real-Time Data Transmission	5-6
5.4.4 Remote Station Readout	5-6
5.5 Data Transmission Techniques - Step 5	5-7
5.5.1 Future Data Transmission	5-7
5.5.2 Cost Data	5-8
5.5.3 Data Link Characteristics	5-11
5.5.4 Parametric Cost Curves, Step 5	5-12
5.6 Mission Data Routing Trade Data - Step 6	5-18
5.6.1 Data Time Delay Factors	5-19
5.6.2 Mission Data Routing Analysis	5-20
5.6.3 Example of Mission Data Routing Analysis	5-20
References	5-27
6. ONBOARD PROCESSING CONSIDERATIONS	6-1
6.1 Image-To-Data Stream Conversion Techniques	6-4
6.1.1 The Multimegabit Operation Multiplexer System (MOMS) Concept	6-4
6.1.2 Low-Power A/D Conversion	6-6

TABLE OF CONTENTS (Continued)

	<u>Page</u>
6.1.3 Optical Processing Techniques	6-9
6.2 Formatting and Multiplexing Techniques	6-16
6.2.1 Line Stretching and Formatting	6-16
6.2.2 Digital Multiplexing	6-21
6.3 Data Compression	6-23
6.3.1 Effectiveness Measures	6-25
6.3.2 Classification of Techniques	6-26
6.3.3 Spectral-Spatial-Delta-Interleave (SSDIO) Algorithm	6-28
6.3.4 The Rice Coding Algorithm	6-30
6.3.5 Implementation of the SSDI/Rice Algorithm	6-31
6.4 Data Coding	6-33
6.4.1 Classification of Codes	6-33
6.4.2 Coding Candidates	6-33
6.4.3 Hardware Implementations	6-40
6.5 Synthetic Aperture Radar Data Processing	6-43
6.5.1 Processing Requirements	6-44
6.5.2 Feasibility of Implementation	6-
6.6 On-Board Correction and Calibration	6-50
6.6.1 Image Correction and Resampling	6-52
6.6.2 Ground Control Point Extraction	6-54
6.6.3 Reseau Extraction	6-55
6.6.4 Radiometric Correction	6-56
6.6.5 Additional Concepts	6-57
6.6.6 Conclusions	6-58
6.7 Storage Techniques	6-59
6.7.1 Magnetic Tape Recorders	6-61
6.7.2 Magnetic Bubble Memory	6-70
6.7.3 Charge-Coupled Device (CCD) Mass Memory	6-75
6.7.4 Optical Data Storage Technology	6-77
6.7.5 Plated Wire Technology	6-84
6.7.6 Conclusions	6-87

TABLE OF CONTENTS (Continued)

	<u>Page</u>
6.8 Digital Hardware Status and Trends	6-89
6.8.1 LSI Technologies	6-91
6.8.2 Tradeoffs and Projections	6-100
6.8.3 LSI, Bipolar and Other Techniques	6-103
References	6-105

VOLUME 2

TABLE OF CONTENTS

	<u>Page</u>
7. COMMUNICATIONS LINK CONSIDERATIONS	7-1
7.1 Summary of Projected Requirements	7-4
7.2 Current Capabilities and Constraints	7-8
7.2.1 Satellite Frequency Channel Allocations	7-8
7.2.2 Satellite Tracking and Data Network (STDN) and the Tracking and Data Relay Satellite System (TDRSS)	7-10
7.2.3 National Aeronautics and Space Administration Communications Network	7-15
7.2.4 Available Communications Time	7-16
7.2.5 Interference and CCIR Limits	7-19
7.2.6 Atmospheric Absorption and Weather Losses	7-20
7.3 System Considerations	7-20
7.3.1 System Overview	7-23
7.3.2 Modulation Considerations	7-24
7.3.3 On-Board Antennas	7-50
7.3.4 RF Power Sources	7-71
7.3.5 Path Losses	7-82
7.3.6 Ground Receiving Equipment Implications	7-84
7.4 ERTS Power Budget Analysis	7-101
7.4.1 Link Budget Technique	7-102
7.4.2 Link Sizing for STDN and TDRSS	7-111
7.5 Optical Communication Systems	7-114

TABLE OF CONTENTS (Continued)

	<u>Page</u>
7.6 Point-to-Point Ground Communications	7-116
7.6.1 Optical Ground	7-116
7.7 Summary and Conclusions	7-121
REFERENCES	7-124

APPENDIX 7A

7A.1 Atmospheric Absorption and Satellite-Ground Communications Links	7-128
7A.2 Weather Models	7-129
7A.3 Precipitation Rates	7-131
7A.4 Some Effects of Propagation Losses on System Performance	7-131
REFERENCES	7-134

APPENDIX 7B

7B.1 APK Signal Technique	7-135
7B.2 Candidate APK Signal Sets	7-136
7B.3 APK Thermal Noise Performance	7-139
REFERENCES	7-143

APPENDIX 7C

7C.1 PAPM Modulation Technique	7-144
7C.2 PAPM Implementation	7-146
REFERENCES	7-148

APPENDIX 7D

7D.1 Antenna Performance	7-149
7D.2 Antenna Tolerance	7-149
REFERENCES	7-159

TABLE OF CONTENTS (Continued)

APPENDIX 7E

	<u>Page</u>
7E.1 Neutral Gas Lasers	7-160
7E.2 Ionized Gas Lasers	7-161
7E.3 Molecular Gas Lasers	7-161
7E.4 Dye Lasers	7-161
7E.5 Rare Earth Liquid Lasers	7-162
7E.6 Commercial Laser Glasses	7-163

APPENDIX 7F

7F.1 Atmospheric Attenuation at Visible and Infrared Frequencies	7-165
8. GROUND DATA HANDLING SUBSYSTEM (GDHS) CONSIDERATIONS	8-1
8.1 System Analysis of GDHS Structure	8-1
8.1.1 Information Generation	8-2
8.1.2 Data Capturing Function	8-3
8.1.3 Central Data Processing Facility (CDPF)	8-5
8.1.4 Local User Data Processing Facility (LUDPF)	8-7
8.1.5 ERS Information Distribution Modes	8-8
8.2 Dominant Technology Areas of the ERS GDHS	8-9
8.2.1 ERS Data Formats	8-9
8.2.2 Ground Station Tape Recorder and Interface	8-10
8.2.3 Processing Algorithm Development	8-13
8.2.4 Filmwriter/Display	8-13
8.2.5 Computer Hardware Technology	8-15
8.2.6 Archiving Technology	8-16
8.2.7 Output Data Quality Specifications and Quality Assurance	8-18
8.2.8 ERS GDHS Management Considerations	8-18
8.3 Parametric Model for ERS GDHS Requirements and Estimated Costs	8-18

TABLE OF CONTENTS (Continued)

	<u>Page</u>
8.3.1 Data Processing Requirements	8-20
8.3.2 Hardware Technology Area Requirements and Estimated Costs	8-27
8.3.3 Applications of the Parametric Model	8-35
8.4 Conclusions of this Study of ERS GDHS Data Handling Considerations	8-39
9. POTENTIAL DATA MANAGEMENT SYSTEMS	9-1
9.1 Introduction	9-1
9.2 Mission 2	9-2
9.2.1 Mission Requirements	9-2
9.2.2 Orbit/Satellite-Constellation Design	9-3
9.2.3 Sensor Design	9-5
9.2.4 Communication System Design	9-8
9.2.5 Ground Data Handling System Design	9-10
9.2.6 Data Dissemination System	9-15
9.2.7 System Summary	9-15
9.3 Mission 6	9-16
9.3.1 Mission Requirements	9-16
9.3.2 Orbit/Satellite-Constellation Design	9-19
9.3.3 Sensor Design	9-21
9.3.4 Onboard Data Handling System Design	9-27
9.3.5 Communication System Design	9-27
9.3.6 Ground Data Handling System	9-31
9.3.7 Data Dissemination System Design	9-33
9.4 Mission 9	9-40
9.4.1 Mission Requirements	9-40
9.4.2 Orbit/Satellite-Constellation Design	9-41
9.4.3 Sensor Design	9-46
9.4.4 Communication System Design	9-48
9.4.5 Ground Data Handling System	9-49
9.4.6 Data Dissemination System Design	9-52
9.4.7 System Summary	9-53
9.5 SRT and ART Requirements	9-53

ILLUSTRATIONS

		<u>Page</u>
2-1	Data Rate versus Ground Resolution (Imaging Sensors- One Spectral Band)	2-6
2-2	Data Rate versus Resolution and Power in Synthetic Aperture Radar	2-7
3-1	Data Products Family	3-25
3-2	Mission 1 - Terrestrial Survey/Environmental Quality	3-27
3-3	Mission 2 - Ocean Survey/Meteorology	3-28
3-4	Mission 3 + 6 - Terrestrial Survey/Environmental Quality	3-29
3-5	Mission 4 - Ocean Survey/Meteorology	3-30
3-6	Mission 5 - Transient Environmental Phenomena Monitoring	3-30
3-7	Mission 7 - Ocean Survey/Meteorological, Operational	3-31
3-8	Mission 8 - Meteorological, Research	3-32
3-9	Mission 9 - Meteorological, Research	3-32
3-10	Candidate Mission Models	3-33
3-11	Earth Observations Working Group Mission Model	3-34
3-12	Mission Orbital Parameters Summary	3-34
3-13	Payload Compatibility with Launch Vehicle and Spacecraft	3-49
5-1	Mission Scatter Diagram	5-2
5-2	Sample Contact Plot	5-6
5-3	Projected Tariffs for Candidate Data Links	5-8
5-4	Performance and Cost for Various Data Link Configurations	5-14
5-5	Performance and Cost for Various Data Link Configurations	5-14
5-6	Performance and Cost for Various Data Link Configurations	5-15
5-7	Performance and Cost for Various Data Link Configurations	5-15
5-8	Performance and Cost for Various Data Link Configurations	5-16
5-9	Performance and Cost for Various Data Link Configurations	5-16
5-10	Performance and Cost for Various Data Link Configurations	5-17
5-11	Performance and Cost for Various Data Link Configurations	5-17
5-12	Performance and Cost for Various Data Link Configurations	5-18
5-13	Data Routing Analysis Flow Chart	5-21
5-14	Data Routing Analysis Log Sheet	5-22
5-15	Data Routing Analysis Log Sheet	5-23
5-15	Data Routing Analysis Log Sheet (Continued)	5-24
5-16	Data Routing Analysis Log Sheet	5-26

ILLUSTRATIONS (Continued)

	<u>Page</u>
5-17 Candidate Mission - Comparative Costs of Leased Transmission Lines Versus Delay Time	5-27
5-18 Performance and Cost for Various Data Link Configurations	5-29
5-19 Data Routing Analysis Flow Chart	5-32
5-20 Data Routing Analysis Log Sheet	5-33
5-21 Data Routing Analysis Log Sheet	5-34
5-22 Data Routing Analysis Log Sheet	5-37
5-23 Candidate Mission - Comparative Costs of Leased Transmission Lines Versus Delay Time	5-38
6-1 Projected Data Rate Capabilities of MOMS-Type Systems	6-6
6-2 Block Diagram for 8-Bit, 20 Million Samples/Sec A/D Connector Using SPFB Technique	6-8
6-3 Performance for Various Low-Power 8-Bit A/D Converters	6-8
6-4 Present Low-Power ADC Capabilities	6-9
6-5 Optical System Arrangement for Spatial Fitting	6-10
6-6 Wideband Data Handling System	6-18
6-7 Thematic Mapper and HRPI Wideband Formats	6-19
6-8 LCGS Format	6-19
6-9 Speed Buffer/Line Formatter	6-20
6-10 Projected Maximum Input Rate to a Typical On-Board Speed Buffer, Formatter, and Line Stretcher	6-21
6-11 Data Compression Techniques	6-27
6-12 Family Tree of Communication and Data Transmission Codes	6-34
6-13 Performance Data for Rate 1/2 Codes	6-36
6-14 SAR Data Rate versus Resolution and Power	6-43
6-15 SAR Processor Storage Requirements for Two Sample Designs	6-50
6-16 Genus of On-Board Data Storage Techniques	6-60
6-17 Projected Magnetic Tape Recorder Capacity	6-67
6-18 Project Magnetic Tape Recorder Cost	6-67
6-19 Project Magnetic Tape Recorder Packing Density	6-68
6-20 Projected Magnetic Tape Recorder Weight	6-68
6-21 Projected Magnetic Tape Recorder Power Requirements	6-69
6-22 Projected Bubble Memory Capacity	6-74
6-23 Projected Bubble Memory Packing Density	6-75
6-24 Current and Projected Capabilities of Plated Wire Memories	6-88
6-25 Projected Costs of Various Memory Technologies	6-89

ILLUSTRATIONS (Continued)

		<u>Page</u>
6-26	Types of LST Technologies (1973)	6-90
6-27	CMOS Power Dissipation Characteristic	6-95
6-28	Projection of LSI Density, Speed and Cost to 1980	6-102
7-1	Data Rate Projections for ERS Missions	7-6
7-2	Types of Communications Service	7-6
7-3	Data Perishability Considerations	7-7
7-4	Data Dump Time Versus Downlink Bit Rate	7-8
7-5	Allocated Bandwidth Versus Downlink Bit Rate	7-10
7-6	1976-79 STDN Network	7-11
7-7	Tentative 1979 Network with TDRSS	7-12
7-8	TDRSS User Coverage Capability	7-12
7-9	TDRSS Frequency Plan	7-14
7-10	Achievable STDN and TDRSS Data Rates Versus EIRP	7-14
7-11	Ground Station Coverage Considerations	7-16
7-12	Contact Time Versus Elevation	7-17
7-13	CCIR Power Flux Density Limits	7-19
7-14	EIRP Limitations Derived from CCIR Flux Density Recommendations	7-19
7-15	Atmospheric Absorption and Weather Losses	7-21
7-16	Cumulative Distribution Functions for Rainfall Rates at Washington, D. C.	7-22
7-17	Components of Typical Communication System	7-22
7-18	Spectral Density Functions Random Binary FSK Waveforms	7-27
7-19	FSK Waveform, Rectangular Pulses	7-28
7-20	Allowed Paths of the Phase for Continuous Phase FSK	7-28
7-21	PSK Signal, Rectangular Pulses	7-29
7-22	BPSK and QPSK Phase Decision Regions	7-30
7-23	Error Rates for Several Binary Systems	7-31
7-24	Typical MSK Waveform	7-32
7-25	MSK Visualized as Sine-Multiplied OQ-QPSK	7-32
7-26	Error Rates for Noncoherently Detected Orthogonal Multi-Tone Signaling	7-34
7-27	M-Phase Signaling	7-36

ILLUSTRATIONS (Continued)

		<u>Page</u>
7-28	Error Rates for Coherent Multi-Phase Signaling	7-37
7-29	Error Rates for Differentially Coherent PSK	7-37
7-30	Bandwidth Requirements of Ideal Optimized Systems	7-41
7-31	Spectral Density Functions of BPSK, MSK and QPSK	7-42
7-32	Power Loss Curves	7-42
7-33	Degradation Due to Transmission Filtering Versus Filter Cut-Off Frequency for QPSK	7-43
7-34	Correlation Loss Due to Filtering	7-45
7-35	Loss Due to Parabolic Phase Distortion and Finite Bandwidth	7-45
7-36	E_b/N_o Degradation Versus Normalized Bandwidth at 10^{-5} BER for MSK	7-46
7-37	Required Bandwidths Versus E_b/N_o	7-48
7-38	Antenna Configurations	7-54
7-39	Typical Pattern of 10-inch Linberg Lens with Open-End Waveguide at 6 GHz	7-62
7-40	Constant -K Lens Showing Focusing of Rays by Refraction	7-63
7-41	Relationship of Dielectric Constant and Radius of a Broad-Beam Luneberg Lens	7-65
7-42	Amplitude and Phases of Different Beam Signals in a 4-Element Matrix	7-67
7-43	Circular Array with Beam-Forming Matrix	7-70
7-44	Microwave Power Generators	7-72
7-45	State of the Art RF Power Amplifier Devices	7-77
7-46	Comparison of Magnetic Fields; Samarium-Cobalt and Alnico 8	7-79
7-47	RF Power Output for Several Mini-TWT's	7-80
7-48	Orbit Geometry	7-83
7-49	Gain Loss Versus Frequency, Due to Surface Tolerances	7-87
7-50	Gain of Large Antennas	7-90
7-51	State of the Art for Pre-Amplifiers	7-91
7-52	Parametric Amplifier Noise Temperature Versus Pump Frequency	7-92
7-53a	G/T for a 30 and 85 Foot Parabolic Antenna Operating at 2.2 GHz	7-94

ILLUSTRATIONS (Continued)

	<u>Page</u>
7-53b G/T for a 30 and 85 Foot Parabolic Antenna Operating at 8.2 GHz	7-94
7-53c G/T for a 30 and 12.5 Foot Parabolic Antenna Operating at 13.7 GHz	7-95
7-53d G/T for a 30 and 12.5 Foot Parabolic Antenna Operating at 21.6 GHz	7-95
7-54 Ground Antenna System Costs	7-97
7-55 Preamplifier Costs	7-98
7-56 Estimated Minimum Cost Antenna System at Specified G/T Levels	7-99
7-57 Cost Curves for "Maximum Cost Base" Antenna Systems Operating at 2.2, 8.2, 13.7 and 21.6 GHz at an Elevation Angle of 7.5 Degrees	7-100
7-58 Minimum Cost Loci	7-101
7-59 Link Power Budget Synthesis Sequence	7-104
7-60 Zenith Path Losses	7-107
7-61 Off-Zenith Incremental Path Losses	7-109
7-62 Spacecraft Parabolic Antenna Gain and Beamwidth	7-111
7-63 Tradeoff Factors Impacting Increase of EIRP	7-112
7-64 Impact of Increasing RF Power Output	7-112
7-65 Communications Link Sizing Nomogram	7-113
7-66 Maximum Repeater Spacings Anticipated for Fiber Optic Guide Ground Links Using 10 db/mile Media	7-120

APPENDIX 7A

7A.1 Contributions of Rain, Cloud, Oxygen and Water Vapor Absorption to Total Attenuation at 30-Degree Elevation During Moderate Summer Rain	7-128
7A.2 Total Attenuation and Antenna Noise Temperature at 30-Degree Elevation	7-130
7A.3 Total Attenuation and Antenna Noise Temperature at 30-Degree Elevation	7-130
7A.4 Example of Ground Station in the Vicinity of Washington, D. C.	7-132
7A.5 Loss Due to Water Film on Radome for Various Rain Rates	7-133

ILLUSTRATIONS (Continued)

	<u>Page</u>
APPENDIX 7B	
7B.1	Some Signal Set Candidate 7-136
7B.2	APK Performance Curves 7-140
7B.3	APK Performance Curves 7-140
APPENDIX 7C	
7C.1	PAPM Performance Characteristics 7-146
7C.2	Modulation Schemes 7-147
APPENDIX 7D	
7D.1	Tolerance Loss for Various Distributions of Surface Deviations 7-158
APPENDIX 7F	
7F.1	Approximate Variation of Attenuation Coefficients with Wavelength at Sea Level for Various Atmospheric Conditions 7-166
7F.2	Calculated Water Vapor Absorption at 10.59μ versus the Elevation Angle for Propagation Paths Traversing the Entire Atmosphere 7-167
7F.3	Calculated Carbon Dioxide Absorption at 10.59μ versus the Elevation Angle for Propagation Paths Traversing the Entire Atmosphere 7-167
8-1	GDHS Structure 8-2
8-2	Information Flow for ERS GDHS 8-3
8-3	Principle Components of the Data Capturing Function 8-4
8-4	Ground Data Handling Functional Block Diagram 8-5
8-5	Central Data Processing Facility Sizing Architecture 8-7
8-6	Distribution Modes from Data Processing Facility 8-8
8-7	Design Chart for Space Division Multiplex Recording 8-11
8-8	Software Development Costs 8-20
8-9	Large Data Rate Sensor Characterization 8-21

ILLUSTRATIONS (Continued)

		<u>Page</u>
8-10	Required Throughput for Continuous Sensors	8-22
8-11	Required Volume for Continuous Sensors	8-23
8-12	Input Data Frame Volume Requirements	8-25
8-13	Processing Data Volume Requirements	8-25
8-14	Calibration Data Volume Requirements	8-26
8-15	Daily Volume as Determined by Sensor Operation	8-26
8-16	Nadir Ground Speed as a Function of Spacecraft Altitude and Orbit	8-27
8-17	Estimated Range of Cost for Ground Station Tape Recorder and Interface	8-28
8-18	Input Data Tape Recorder Requirements - Two Shifts	8-29
8-19	CPU/Data Bus Processing Rate Requirements	8-30
8-20	Estimated Range of Cost for Input/Output Data Reformatting Memories	8-30
8-21	Estimated Range of Cost for Data Correction and Processing Data Memories	8-31
8-22	Special Purpose Hardware Processing Rate Requirements	8-32
8-23	Estimated Range of Cost for Special Purpose Hardware	8-32
8-24	Estimated Range of Cost for Filmwriter Technology	8-33
8-25	Estimated Archiving Capital Expense	8-34
8-26	Archiving Read Data Rate Replacement - Two Shifts	8-34
9-1	Mission 2 Coverage Geometry	9-6
9-2	A Comparison of the Coverage Frequency of Mission 2 Sensors in a 1562.2 km, 102.3° Orbit and the Observation Frequency Requirements	9-7
9-3	Mission 2 Ku-Band Link Requirements	9-8
9-4	Mission 2 S-Band Link Requirements	9-9
9-5	Data Routing for Mission 2	9-10
9-6	Mission 3 Data System Block Diagram	9-16
9-7	Coverage Pattern for Mission 6	9-22
9-8	A Comparison of the Coverage Frequency of the Mission 6 Sensors in a 1203.6 km, 102.3° Orbit and the Observation Frequency Requirements	9-22
9-9	Synthetic Aperture Radar Geometry	9-23

ILLUSTRATIONS (Continued)

		<u>Page</u>
9-10	Timing Relationship Between the Transmitted Pulses and Echo Returns for the Synthetic Aperture Radars in Mission 6	9-24
9-11	Geometry for Determining Pointable Imager Offset Angle Θ , and Ground Obliquity ϕ	9-26
9-12	On-Board Data Handling Subsystem	9-28
9-13	Sensor Interface Unit - Key Technology Item	9-28
9-14	Mission 6 Communication System Configuration	9-30
9-15	Data Routing for Mission 6	9-31
9-16	Coverage of CONUS Per Day	9-35
9-17	Data Dissemination Satellite Coverage	9-36
9-18	CONUS Data User Regions	9-37
9-19	Data Dissemination Satellite Configuration	9-37
9-20	Regional Coverage Antenna Gain	9-38
9-21	Mission 6 System Block Diagram	9-39
9-22	Coverage Pattern as a Function of Time for a Given Longitude of the Synthetic Aperture Radar for Mission 9	9-43
9-23	View of Orbital Geometry Looking East	9-44
9-24	A Comparison of the Coverage Frequency of the Mission 9 Sensors in a 1674 km, 6.3 Degree Orbit and the Observation Frequency Requirements	9-45
9-25	SAR Geometry for Mission 9	9-46
9-26	Passive Microwave Radiometer Geometry and Scan Pattern	9-48
9-27	Mission 9 Data System Block Diagram	9-54

TABLES

		<u>Page</u>
2-1	Revised Candidate Sensor List	2-1
2-2	Representative Parameters for DLCS	2-18
2-3	High Resolution Multispectral Point Scanners	2-22
2-4	Pointable Imagers	2-23
2-5	Synthetic Aperture Radar	2-24
2-6	Passive Multichannel Microwave Radiometer	2-25
2-7	Oceanic Scanning Spectrophotometer (Electronic Scan)	2-26
2-8	Oceanic Scanning Spectrophotometer (Mechanical Scan)	2-27
2-9	Sea Surface Temperature Imaging Radiometer	2-28
2-10	Advanced Atmospheric Sounder and Imaging Radiometer	2-29
2-11	Constant Resolution Meteorological Scanner	2-30
2-12	Dual-Mode Imaging Spectrometer	2-31
3-1	ERS Data Use Categories	3-2
3-2	Data Use Requirements Summary	3-4
3-3	Parametric Data Requirements - Air-Sea-Land Interactions	3-7
3-4	Parametric Data Requirements - Air Pollution	3-8
3-5	Parametric Data Requirements - Supper Atmosphere	3-9
3-6	Data Requirements - Hydrological Resources Inventory and Dynamics	3-10
3-7	Data Requirements - Agricultural, Forest, and Rangeland land Inventory and Dynamics	3-11
3-8	Data Requirements - Environmental Impact of Natural and Man-Induced Modifications to Earth Resources	3-12
3-9	Data Requirements - Geological Resources Inventory and Dynamics	3-13
3-10	Data Requirements - Ocean Pollution	3-14
3-11	Parametric Data Requirements - Mesoscale Meteorological Phenomena	3-15
3-12	U. S. Governmental Organizations Considered as Primary Destinations for Remotely-Sensed Earth Resources Data	3-16
3-13	Organizational Breakdown, U. S. Governmental Agencies	3-16
3-14	Analytical Modes	3-20
3-15	Mission/Sensor Grouping	3-26
3-16	Special Data Handling Considerations	3-37
4-1	Mission No. 1 - Terrestrial Survey/Environmental Quality, Research	4-4

TABLES (Continued)

	<u>Page</u>
4-2 Mission No. 2 - Ocean Survey/Meteorological, Research	4-5
4-3 Mission No. 3 - Terrestrial Survey/Environmental Quality Research	4-7
4-4 Mission No. 4 - Ocean Survey/Meteorological, Research	4-8
4-5 Mission No. 5 - Transient Environmental Phenomena Monitoring, Research	4-9
4-6 Mission No. 6 - Terrestrial Survey/Environmental Quality Operational	4-10
4-7 Mission No. 7 - Ocean Survey/Meteorological, Operational	4-11
4-8 Mission No. 8 - Meteorological, Research	4-12
4-9 Mission No. 9 - Meteorological, Research	4-13
4-10 Data Rate/Load Summary for Future Earth Resources Missions	4-14
4-11 Data Handling Requirement Summary for Candidate ERS Missions	4-15
4-12 Data Handling System Driver Requirement (Data Use Category: Terrain Mapping)	4-18
4-13 Data Handling System Driver Requirement (Data Use Category: Earth Surface Composition)	4-18
4-14 Data Handling System Driver Requirement (Data Use Category: Sea Surface Temperature)	4-19
4-15 Data Handling System Driver Requirement (Data Use Category: Severe Storm Warning)	4-19
4-16 Data Handling System Driver Requirement (Data Use Category: Surface Water Mapping)	4-21
4-17 Data Handling System Driver Requirement (Data Use Category: Sea Surface Composition)	4-21
5-1a Specifications of Conditioned Voice Lines in the U.S.A.	5-8
5-1b Technical Characteristics of Candidate Data Links	5-9
6-1 Figures of Merit in Common Use for Data Compression Systems	6-26
6-2 Candidate Information Preserving Compaction Algorithms and Their Relative Performance	6-28

TABLES (Continued)

	<u>Page</u>
6-3 DCU Unit Parameters	6-32
6-4 Binary Code for Error Correction and Detection	6-35
6-5 MSI and LSI Viterbi Decoder Parameters	6-40
6-6 Commercially Available Decoder Parameters	6-41
6-7 Recent Tape Transport Configurations	6-62
6-8 Projected Tape Recorder Specifications (Pre-1980)	6-63
6-9 Projected Characteristics of Data Storage Devices	6-69
6-10 Summary of Magnetic Bubble Technology	6-74
6-11 Summary of Projected Characteristics of Various Data Storage Devices (1975 - 1980)	6-84
6-12 Plated Wire Systems Comparisons (8,192 Words of 24 Bits Each)	6-86
6-13 Recent Plated-Wire Memory Configurations	6-87
6-14 LSI Terminology	6-90
6-15 LSI Tradeoff Comparison (1972)	6-100
6-16 LSI Parameter Summary 1973	6-101
6-17 LSI Technology Projections	6-101
7-1 Summary of Data Requirements	7-5
7-2 Space Telecommunications Frequency Allocations (1971)	7-9
7-3 STDN Data Handling Capabilities (without TDRSS)	7-13
7-4 TDRSS Data Handling Capabilities	7-13
7-5 Bandwidths for Practical Systems	7-47
7-6 Candidate Antennas for ERS Spacecraft	7-51
7-7 Beam Antenna Considerations	7-53
7-8 Typical Performance of High-Q IMPATT Oscillators	7-73
7-9 Typical Performance of Low-Q IMPATT Oscillators	7-74
7-10 Typical Performance: Mechanically Tuned Gunn-Effect Oscillators	7-75
7-11 Typical Performance: LSA Effect Sources	7-76
7-12 Technical Data for Miniature TWT's	7-80
7-13 Characteristics of Medium and High-Power TWT Amplifiers	7-81
7-14 Applicable Lasers	7-114
7-15 System Performance Limiting Values	7-119

TABLES (Continued)

	<u>Page</u>	
7-16	Equivalent Guide Loss	7-119
7-17	Maximum Repeater Spacing for Optical Repeater Using 10 db/mile Fiber Optic Guide	7-120

APPENDIX 7A

7A.1	Summary of Attenuation (30° Elevation) for Three Temperate Regions with Stratiform Weather Models	7-133
------	--	-------

APPENDIX 7B

7B.1	Candidate Signal Designs	7-138
7B.2	Comparison of Principal APK Sets	7-141

APPENDIX 7D

7D.1	Parabolic Antenna Performance	7-150
7D.2	Parabolic Antenna Performance and STDN System Capabilities	7-151
7D.3	Parabolic Antenna Performance for Satellite Space Research and Earth Exploration	7-152
7D.4	Parabolic Antenna Performance and STDN System Capabilities	7-153
7D.5	Parabolic Antenna Performance and STDN System Capabilities	7-154
7D.6	Parabolic Antenna Performance for Satellite Space Research and Earth Exploration	7-155
7D.7	Parabolic Antenna Performance for Satellite Space Research and Earth Exploration	7-156
7D.8	Parabolic Antenna Performance for Satellite Space Research and Earth Exploration	7-157

APPENDIX 7E

7E.1	Summary of Dye Laser Properties	7-162
------	---------------------------------	-------

APPENDIX F

7F.1	Laser Lines Absorbed by the Atmosphere	7-168
------	--	-------

TABLES (Continued)

		<u>Page</u>
8-1	Brief Characteristics of Terabit Archiving Technologies	8-17
8-2	Summary of Computer and Filmwriter/Display Estimated Costs	8-35
8-3	Example of Use of Parametric Model for Estimated Hardware Costs	8-38
9-1	Sensor Complement for Mission 2	9-4
9-2	Summary of the Data Requirements and Applicable Instruments for Each Data Use in Mission 2	9-5
9-3	Sensor Characteristics Considered in the Ground Data Handling System Parametric Model	9-11
9-4	Ground Data Handling Volume Requirements for the Mission 2 Design Driving Sensors	9-12
9-5	Cost Summary for the Error Processing System at the Data Station (\$ Thousands)	9-13
9-6	Satisfaction of User Format Requirements by the Output Product Generation Facility in Mission 2	9-14
9-7	GDHS Cost Summary	9-13
9-8	Sensor Complement for Mission 6	9-18
9-9	Summary of the Data Requirements and Applicable Instruments for Each Data Use in Mission 6	9-19
9-10	Summary of the Orbits Considered for Mission 6	9-21
9-11	Projected Characteristics of Data Storage Devices	9-29
9-12	Mission 6 Power Budget (Each of Three Channels)	9-30
9-13	Sensor Characteristics Considered in the Ground Data Handling System Parametric Model	9-32
9-14	Data Handling Volume Requirements for Mission 6 Design Driving Sensors	9-32
9-15	Cost Summary for the Ground Data Handling System (\$ Thousands)	9-34
9-16	Small Data User - Link Power Budget	9-38
9-17	Sensor Complement for Mission 9	9-42
9-18	Summary of the Data Requirements and Applicable Instruments for Each Data Use in Mission 9	9-43
9-19	Sensor Characteristics Considered in the Ground Data Handling System Parameter Model	9-50
9-20	Data Handling Volume Requirements for Mission 9 Design Driving Sensors	9-51
9-21	Cost Summary for the Ground Data Handling System (\$ Thousands)	9-52

7. COMMUNICATIONS LINK CONSIDERATIONS

This section addresses the considerations pertinent to proper link design and selection. The basic approach to the section is to review and/or develop the following:

- Projected requirements, including bit rates, types of service, data perishability and data quality
- Current capabilities and constraints, including frequency allocations and bandwidths, CCIR limits on interference, STDN, TDRSS and NASCOM
- Basic system considerations and major subsystem characteristics and options. This section represents the bulk of the task, and includes the basic data required for preliminary system synthesis
- Conclusions and recommendations.

The major subtasks of the study plan, listed below, are included in the above areas in the indicated section of this report.

- Choice of rf frequency for each link considering government allocations, application, bandwidth, propagation conditions, and ease of power generation, radiation and reception. (Section 7.1)
- Power budgets for each link with parametric relationships between power generated, on-board antenna gain, ground antenna gain, receiving system noise temperatures and data rates. (Section 7.3 and 7.4)
- On-board rf power sources considering efficiency, level of output, ease of modulation, reliability, etc. (Section 7.3.3)
- Modulation techniques relating the ratio between data rate and bandwidth with communication efficiency, ease of generation and ease of detection. (Section 7.3.1)
- On-board antennas relating gain and pointability to size, weight and influence on other system characteristics such as spacecraft pointing accuracy, ease of integration and checkout, shading of solar arrays, etc. (Section 7.3.3)
- Ground receiving equipment including antennas, receivers, and demodulators; specifically developing cost and installation data as a function of sensitivity and level of performance. (Section 7.3.6)

- Laser communication possibilities with emphasis on their application and feasibility for the various links of the paths covered in the routing analysis. (Section 7.3.5)
- Point to point ground communications for getting data from receiving stations to the processing center, including wide-band band lines and communication satellites. (Section 7.3.6)

Seven possible ERS communication frequencies have been identified at L-, S-, X-, K-, KU-, V-, and W-bands. The S-, K-, and Ku-band links are established consistent with STDN (spacecraft tracking and data network) service allocations. Link power budgets have been performed for four low altitude orbits (possible mission orbits) and a synchronous orbit and for four of the seven frequencies. These are at S-, X-, Ku-, and K-bands. All link evaluations have been performed on the basis of digital communication techniques, including link evaluation with ground receiver systems of the simplest variety and the best, and at each of the four frequencies.

For missions using low orbits, a means by which determination of the satellite contact time as a function of satellite elevation angle and tracking angle has also been provided.

The RF power source evaluation includes both microwave semiconductors as well as travelling wave tube (TWT) devices. Charts are presented giving current status in terms of efficiency and power output for Gunn, Trapatt, Impatt, and LSA semiconductor devices. CW TWT devices of the conventional line as well as the new miniature TWT's have been evaluated. The latter has some promising size and weight advantages due to the use of samarium-cobalt magnets. This recent technology addition has some exciting possibilities and is considered as part of the RF power source discussion.

As mentioned, link power budgets are worked on the basis of using high-data rate digital communication techniques. One of the newest modulation techniques that has been undergoing concentrated evaluation in the past few years is amplitude-phase keying (APK). This technique and its relative merits is described in Appendix B. A second technique also considered is called pulse amplitude phase modulation (PAPM) (Appendix C). This modulation technique when coupled with the high-energy short-pulse characteristics of Gunn, Impatt, or LSA semiconductor devices,

opens new and exciting possibilities by which communication links can be worked using analog pulse techniques.

On-board spacecraft antenna considerations include reflectors, optical lenses, spherical lenses, constrained lenses, beam forming array matrices, self-phasing and adaptive arrays and their relative advantages with respect to spacecraft stabilization, coverage, pointing control, and bandwidth.

The technical problem of establishing a ground station receiving system is considered as part of the link power budget problem already discussed. The problem is considered on the basis of using a 85- or 30-foot antenna already available at many of the STDN stations. A 12.5-foot antenna is included in this evaluation to serve for the higher link frequencies. A second aspect of the ground receiving problem is cost. This problem has been considered from three points of view. These include the cost of the antenna that may not be applicable in most cases except for the smallest 12.5-foot antenna. The preamplifier cost analysis, which has to be considered at most tracking centers, has been treated for the most sophisticated receivers, such as a maser, to the most conventional including TWT's and a tunnel diode amplifiers. A means by which cost optimization as a function of G/T and frequency has also been included.

Optical laser systems are considered for atomic gas, solid-state and molecular gas laser sources. Appendix F gives curves by which clear day attenuation can be determined as a function of source wavelength. Evaluation of optical links for point-to-point ground communication has also been considered, including charts giving the maximum laser power, required receiver sensitivity, and waveguide loss and loss margin (see Section 7.6).

The combination of PAPM modulation techniques and state-of-the-art RF power source technology in the Gunn, Trapatt, Impatt, and LSA device area requires exploring. The literature search performed as part of this report revealed little information indicating work done in this area.

The cost of ground station receiving equipment, presented as part of this report, is believed to have merit but is based upon information and reports which are approximately three years old. An area of specialized interest might include updating this information and extending

it into future years based upon cost-year extrapolation. Some information was found indicating the R&D work in the area of optical communications.

These reports dealt with current day link communication problems associated with laser communication technology. However, it is felt that most of these were superficial and/or only partially complete in their presentation and this area is one in which useful evaluation of current and projected technology could be performed.

7.1 Summary of Projected Requirements

Sections 2, 3 and 4 develop the communications requirements, in terms of mission parameters, orbit altitudes, sensors, real time data rates, and data perishability. Key elements of these requirements are listed in Table 7-1. The maximum data rates shown range from 0.6 Mbps to 728 Mbps, and represent the total real time data acquisition rate from all on-board sensors. Figure 7-1, shows the projected real time data acquisition rate for each mission, plotted against launch date. As one would expect, there is a gradual increase in data rates, with an upper bound represented by the solid curve, and a lower bound represented by the dashed curve.

A word of caution about data rates is in order. Table 7-1, and Figure 7-1 present maximum real time sensor acquisition rates, and not necessarily the probable communication rates. Depending on the on-board processing and storage capacity, orbit parameters, and perishability, one could expect the actual communications rates to vary up or down from sensor acquisition rates. This will also be proportional to the ratio of time the sensors are operating to the time the satellite is actually transmitting sensor data. Thus, a mission which continually gathers data that is only retransmitted when the satellite is in view of a ground station would have a higher data rate, whereas the reverse could be true of one that gathers data over a brief period of time.

Figure 7-2 illustrates four possible transmission modes:

- 1) Real time transmission to STDN (further described in Section 7.2.2).*
- 2) Store and forward to STDN.

* The maximum STDN bit rate is 30 mbit/sec. The maximum TDRSS bit rate is 300 mbit/sec.

Mission	Payload	Operating Data Rate (mbps)	Sensor Use Profiles (Appendix C)	Maximum Data Rate (mbps)	Data Load (mbits)		Data Perishability*	Orbit Altitude (km)	Orbit Period (min)	Time Above 5°	Time Above 15°	Avg Per 100 M
					Per Orbit	Per Year						
1. Terrestrial Survey/ Environmental Quality (R), 1978 Launch	• Scanning spectroradiometer (SSR)	72.1	Continuous (daytime) over CONUS and territories	154.3	741	4.5 x 10 ⁶	Moderate	852	101.47	13.5	9.5	0.1
	• Pointable imager (PI)	82.2	Continuous (daytime) 10 percent of time over CONUS and territories				Moderate (high for ISFW)					
	• Advanced atmospheric sounder (AAS)	-	Continuous over CONUS and territories				High					
	• Data collection and location system (DCLS)	-	Intermittent				High					
2. Ocean Survey/ Meteorology (R), 1980 Launch	• Oceanic scanning spectrophotometer (OSS)	1.1	Continuous (daytime) over U.S. coast (900 km swath)	126.5	426	2.6 x 10 ⁶	High (NWS, EDS, NESG)	895	102.87	14.0	10.4	0.0
	• (PI)	125	Continuous (daytime) over U.S. coast (1.6 km swath)				Moderate					
	• Sea surface temperature imaging radiometer (SSTIR)	0.36	Continuous over U.S. coast (900 km swath)				Low					
	• AAS	-	Continuous over U.S. coast (900 km swath)				High (NWSG)					
	• DCLS	-	Intermittent									
3. Terrestrial Survey/ Environmental Quality (R),	• Combined SSR/pointable imager	368.2	Continuous (daytime) over CONUS and territories	728	1.3 x 10 ⁵	7.7 x 10 ⁰	Same as for Mission 1	707	98.93	12	6.0	21
	• Imaging radar (IR)	360	Continuous over CONUS and territories									
	• AAS	-										
	• Film recovery system (FRS)	-	Intermittent									
4. Ocean Survey/ Meteorology (R), 1983 Launch	• OSS	1.1	Continuous (daytime) over global ocean and adjacent seas	3.6	2.5 x 10 ⁴	1.6 x 10 ⁸	Same as for Mission 1	995	105.0	15.0	11.1	-
	• Passive microwave radiometer (PMR)	1.19										
	• SSTIR	0.36										
	• AAS	-										
	• Constant resolution meteorological scanner (CRMS)	1.0	Continuous over global ocean and adjacent seas									
	• FRS	-	Intermittent									
5. Transient Environmental Phenomena Monitoring (R), 1983 Launch	• Dual mode imaging spectroradiometer (DMIS)	0.63	Continuous (daytime) approximately 25 percent of total time	0.6	---	5.0 x 10 ⁶	High for most users	35,870	Synch-			
	• AAS	-										
	• DCLS	-	Intermittent									
	• FRS	-										
6. Terrestrial Survey/ Environmental Quality (C), 1984 Launch	• Combined scanning spectroradiometer (SSR)/pointable imager (PI)	368.2	Continuous (daytime) over CONUS and territories	728	1.2 x 10 ⁵	7.7 x 10 ⁸	Same as for Missions 1 and 3	1,146	108.26	16.0	13.0	20
	• Imaging radar (IR)	360	Continuous over CONUS and territories									
	• Advanced atmospheric sounder (AAS)	-	Continuous over CONUS and territories									
	• Data collection and location system (DCLS)	-	Intermittent									
7. Ocean Survey/ Meteorology (C), 1986 Launch	• Oceanic scanning spectrophotometer (OSS)	13.2	Continuous (daytime) over global ocean and CONUS coast (1.6 km swath-high resolution mode)	32.3	1.8 x 10 ⁵	1.2 x 10 ⁹	Same as for Missions 2 and 4	1,133	107.77	-16.8	13.0	30
	• Passive microwave radiometer (PMR)	18.1	Continuous over global ocean									
	• Constant resolution meteorological scanner (CRMS)	1.0	Continuous over globe									
	• Film recovery system (FRS)	-										
	• DCLS	-	Intermittent									
8. Meteorology (R), 1986 Launch	• CRMS	1.0		2.2	---	1.4 x 10 ⁸	High	35,870	Synch-			
	• Imaging radiometer (IRAD)	1.22	Continuous over globe									
	• AAS	-										
	• FRS	-	Intermittent									
9. Meteorology (R), 1987 Launch	• Imaging radar	21.7	Intermittently, 10 percent of total time	41.3	1.5 x 10 ⁵	1.1 x 10 ⁸	High	1,852	123.85	24.2	20.1	2
	• Passive microwave radiometer	18.1	Intermittently, 10 percent of total time									
	• CRMS	1.0	Intermittently, 10 percent of total time									
	• Imaging radiometer	1.22	Continuous									
	• AAS	-	Continuous									
• FRS	-											
• DCLS	-	Intermittent										

* Perishability Legend: High = Near Real-Time to 1 Day
Moderate = 1 Day to 1 week
Low = >1 week

ORIGINAL PAGE IS
OF POOR QUALITY

FOLDOUT FRAME

Table 7-1. Summary of Data Requirements

Mission	Payload	Operating Data Rate (mbps)	Sensor Use Profiles (Appendix C)	Maximum Data Rate (mbps)	Data Load (mbits)		Data Portability ^a	Orbit Altitude (km)	Orbit Period (min)	Time Above 5°	Time Above 15°	Average Transmission Time (Min) Per Orbit at		
					Per Orbit	Per Year						100 Mbit/s	300 Mbit/s	720 Mbit/s
												Mbit/s	Mbit/s	Mbit/s
Satellite Survey/Imaging (R), Launch	Scanning spectroradiometer (SSR)	72.1	Continuous (daytime) over CONUS and territories	154.3	741	4.5 x 10 ⁵	Moderate Moderate (high for BSFV)	852	101.97	13.5	9.5	0.123	0.041	0.017
	Pointable imager (PI)	82.2	Continuous (daytime) 10 percent of time over CONUS and territories				High High High							
	Advanced atmospheric sounder (AAS) Data collection and location system (DCLS)	-	Intermittent											
Satellite Survey/Imaging (R), Launch	Oceanic scanning spectrophotometer (OSS)	1.1	Continuous (daytime) over U. S. coast (900 km swath)	126.5	426	2.6 x 10 ⁶	High (NWS, EDS, NESG) Moderate	895	102.87	14.0	10.4	0.071	0.0237	0.0098
	(PI)	125	Continuous (daytime) over U. S. coast (1.6 km swath)				Low High							
	Sea surface temperature imaging radiometer (SSTIR)	0.36	Continuous over U. S. coast (900 km swath)				High (NWSC)							
	AAS	-	Continuous over U. S. coast (900 km swath)											
	DCLS	-	Intermittent											
	Combined SSR/pointable imager	368.2	Continuous (daytime) over CONUS and territories	728	1.3 x 10 ⁵	7.7 x 10 ⁸	Same as for Mission 1	707	98.93	12	8.0	21.7	7.25	2.98
Satellite Survey/Imaging (R), Launch	Imaging radar (IR)	360	Continuous over CONUS and territories											
	AAS	-	-											
	Film recovery system (FRS)	-	-											
	DCLS	-	Intermittent											
	OSS	1.1	Continuous (daytime) over global ocean and adjacent seas	3.6	2.5 x 10 ⁴	1.6 x 10 ⁸	Same as for Mission 1	995	105.0	15.0	11.1	4.16	1.39	0.57
	Passive microwave radiometer (PMR)	1.19												
	SSTIR	0.36												
	AAS	-												
	Constant resolution meteorological scanner (CRMS)	1.0	Continuous over global ocean and adjacent seas											
	DCLS	-	Intermittent											
Satellite Survey/Imaging (R), Launch	Dual mode imaging spectroradiometer (DMIS)	0.63	Continuous (daytime) approximately 25 percent of total time	0.6	---	5.0 x 10 ⁵	High for most users	35,870	Synchronous					
	AAS	-	-											
	DCLS	-	Intermittent											
Satellite Survey/Imaging (R), Launch	Combined scanning spectroradiometer (SSR)/pointable imager (PI)	368.2	Continuous (daytime) over CONUS and territories	728	1.2 x 10 ⁵	7.7 x 10 ⁸	Same as for Missions 1 and 3	1,146	108.26	16.8	13.0	20.0	6.67	2.75
	Imaging radar (IR)	360	Continuous over CONUS and territories											
	Advanced atmospheric sounder (AAS)	-	Continuous over CONUS and territories											
	Data collection and location system (DCLS)	-	Intermittent											
	Oceanic scanning spectrophotometer (OSS)	13.2	Continuous (daytime) over global ocean and CONUS coast (1.6 km swath-high resolution mode)	32.3	1.8 x 10 ⁵	1.2 x 10 ⁹	Same as for Missions 2 and 4	1,133	107.99	~16.8	13.0	30.0	10.0	4.12
Satellite Survey/Imaging (R), Launch	Passive microwave radiometer (PMR)	18.1	Continuous over global ocean											
	Constant resolution meteorological scanner (CRMS)	1.0	Continuous over globe											
	Film recovery system (FRS)	-	-											
	DCLS	-	Intermittent											
	CRMS	1.0		2.2	---	1.4 x 10 ⁸	High	35,870	Synchronous					
	Imaging radiometer (IRAD)	1.24	Continuous over globe											
Satellite Survey/Imaging (R), Launch	AAS	-	-											
	FRS	-	-											
	DCLS	-	Intermittent											
	Imaging radar	21.0	Intermittently, 10 percent of total time	41.3	1.5 x 10 ⁵	1.1 x 10 ⁸	High	1,852	123.85	24.2	20.1	2.5	0.835	0.344
	Passive microwave radiometer	18.1												
	CRMS	1.0	Intermittently, 10 percent of total time											
	Imaging radiometer	1.22												
Satellite Survey/Imaging (R), Launch	AAS	-	Continuous											
	FRS	-	-											
	DCLS	-	Intermittent											

Legend: High = Near Real-Time to 1 Day
 Moderate = 1 day to 1 week
 Low = >1 week

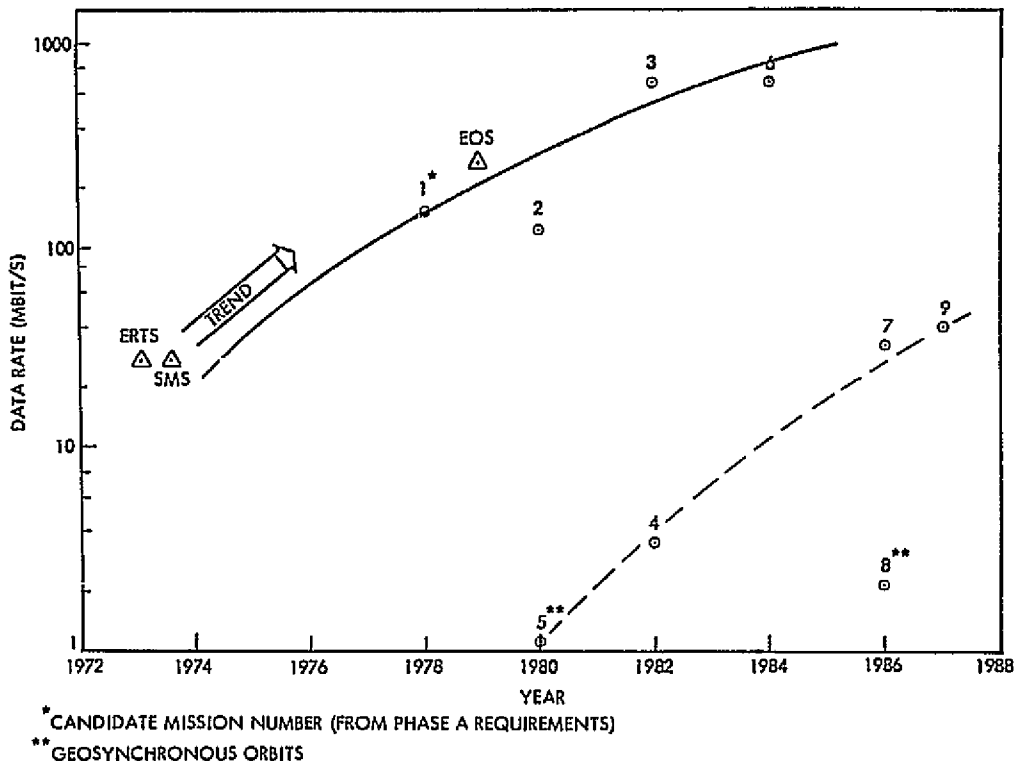


Figure 7-1. Data Rate Projections for ERS Missions

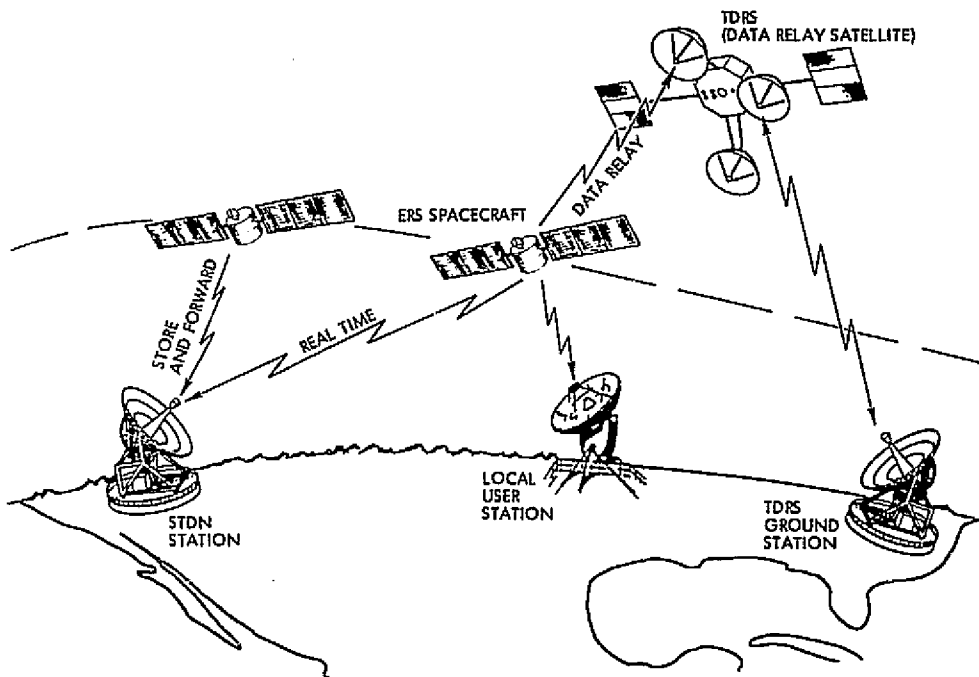


Figure 7-2. Types of Communications Service

- 3) Data relay via TDRSS (maximum STDN bit rate is 30 Mbps, maximum TDRSS bit rate is 300 Mbps)
- 4) Transmission to a local user station.

The data rate for missions employing real time transmission (Mode 1 and 3, possibly 4) will be the same as the sensor acquisition rate, modified by on-board processing, and limited by the channel capacity. The data rate for Mode 2 (and possibly 4) may be greater or less than the sensor acquisition rate, and is limited by the data acquired during the orbit, the record/playback rate of the on-board recorders, and the time the satellite is in view of the ground station and able to communicate (contact time).

The feasibility of evening-out the data load by using on-board recorders, of course also depends on the perishability of the data. Figure 7-3 illustrates data perishability and suggests that some data can be delayed on all but the geosynchronous Missions 5 and 8.

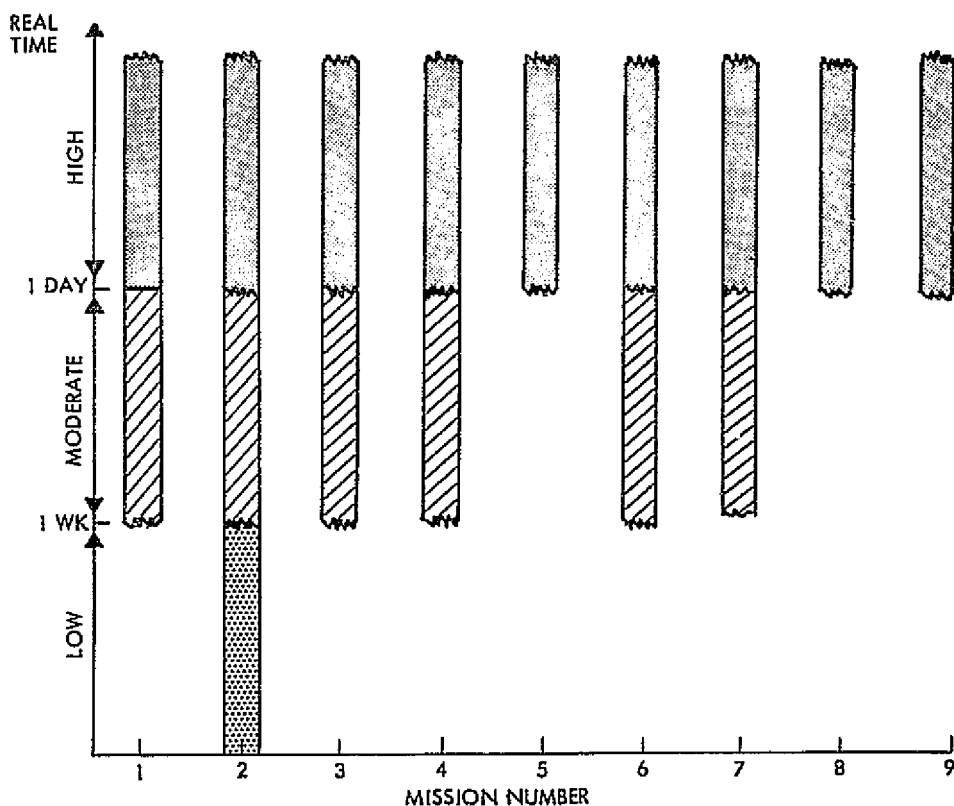


Figure 7-3. Data Perishability Considerations

Recorder storage/playback capabilities are reviewed in Section 5. Of concern here, however, is that near-term transports provide up to 100 channels at playback rates up to 2.5 Mbps, for a maximum capacity of 250 Mbps/. Projected pre-1980 capabilities will be limited to 300 Mbps. Thus, it would be desirable to design for a maximum record/playback rate of 300 Mbps, which incidentally is also the maximum data rate of the STDN/TDRSS system. With this in mind, required transmission times in minutes per orbit are indicated in Table 7-1. Other times can be computed from Figure 7-4. Available contact times are reviewed in Section 7.2.4

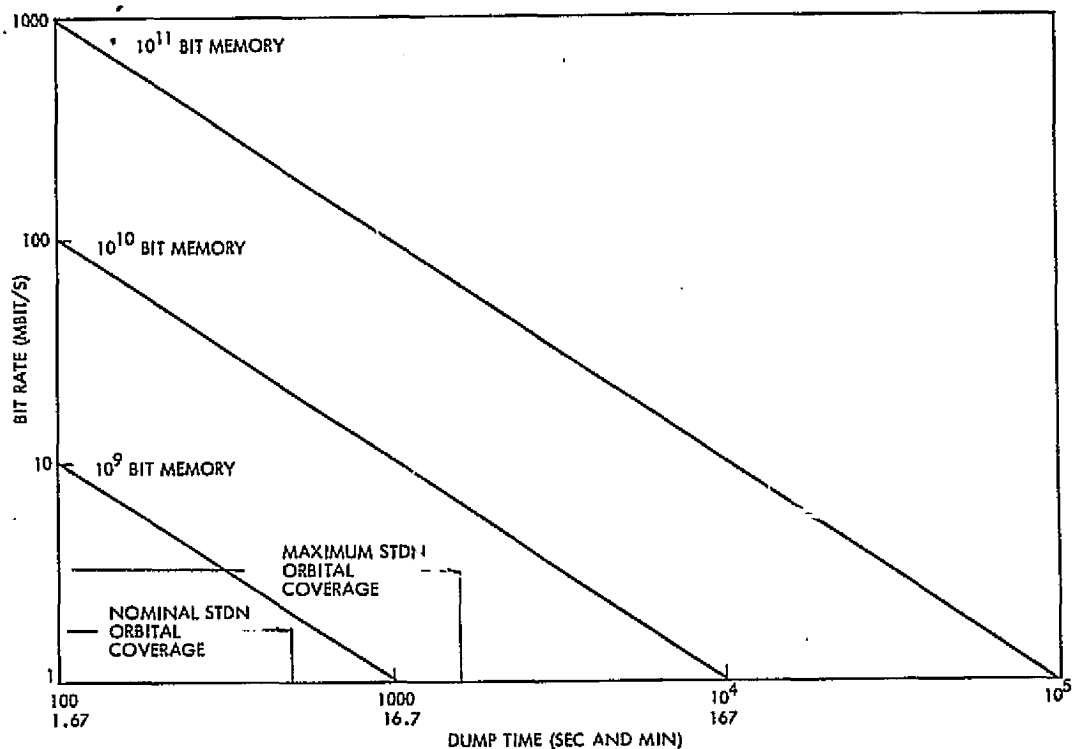


Figure 7-4. Data Dump Time Versus Downlink Bit Rate

7.2 Current Capabilities and Constraints

7.2.1 Satellite Frequency Channel Allocations

The sources considered in the establishment of communication bands for the earth exploration research satellite service, include the recent World Administrative Radio Conference on Space Telecommunications (WARC) held in Geneva, the FCC Rules and Regulations, Volume 2, September 1972, and the Spaceflight Tracking and Data Network (STDN)

plans as given for the 1979 to 1985 timeframe. The frequency allocations established by the June/July 1971 WARC are planned to be effective by 1 January 1973.

A number of bands were determined, running between 1.5 and 66 GHz and these are listed in Table 7.2. They include seven new earth exploration frequencies at L-, S-, X-, K-, V- and W-bands. Two are found at X-band. Forward and return link STDN service frequencies have been identified at S-band and Ku-band.

Table 7-2. Space Telecommunication Frequency Allocations (1971)

Frequency Band (GHz)	Bandwidth (MHz)	Service
1.525 to 1.535	10	Space operation (telemetry) Earth exploration satellite
1.750 to 1.850	100	S-band return (STDN service allocation)
2.025 to 2.120	95	S-band forward (STDN service allocation) Space research service Earth exploration satellite
2.200 to 2.300	100	S-band downlink (STDN service allocation)
8.025 to 8.175	150	Earth exploration satellite Fixed, fixed satellite Mobile
8.175 to 8.215	40	Fixed, fixed satellite Meteorological Mobile
8.215 to 8.400	185	Earth exploration satellite Fixed, fixed satellite Mobile
13.400 to 14.000	600	Ku-band return (STDN service allocation)
14.400 to 14.485	85	Government space research service Fixed satellite Mobile
14.515 to 15.350	835	Government space research service Fixed satellite Mobile
14.600 to 15.200	600	Ku-band forward (STDN service allocation)
21.200 to 22.000	800	Satellite space research Earth exploration
51.000 to 52.000	1000	Satellite space research Earth exploration
65.000 to 66.000	1000	Satellite space research Earth exploration

For the purposes of this study, frequencies selected for major consideration are 2.2 GHz, 8.5 GHz, 13.7 GHz; 21.6 GHz, 51 GHz and 66 GHz.

Figure 7-5 illustrates the present trend of allocating increasing bandwidths at the higher frequencies. Missions 1, 2, 3 and 6 will require data rates in excess of 100 Mbps, thus must look to the use of X-band (EOS), Ku-band (STDN/TDRSS) or higher frequencies.

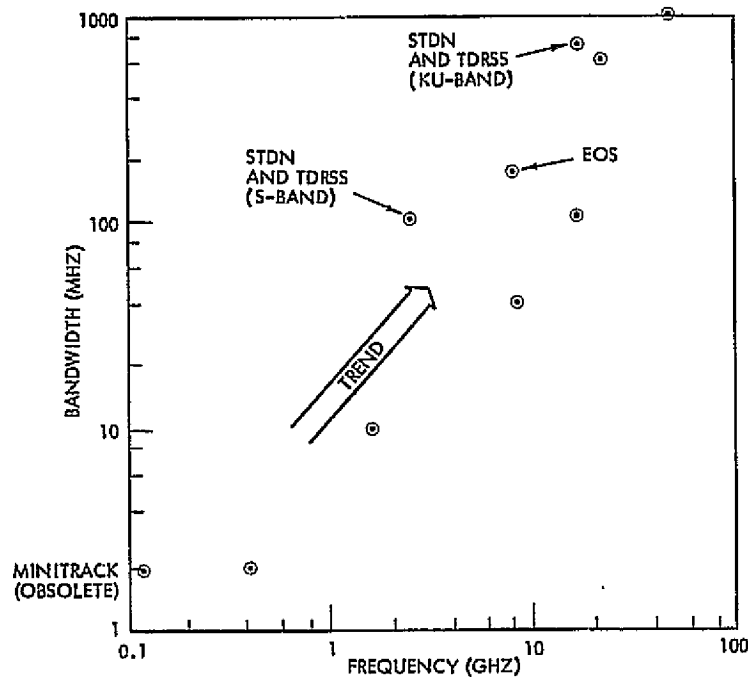


Figure 7-5. Allocated Bandwidth Versus Operating Frequency

7.2.2 Satellite Tracking and Data Network (STDN) and the Tracking and Data Relay Satellite System (TDRSS)

The STDN is composed of the facilities of two previously independent networks: The Space Tracking and Data Acquisition Network (STADAN) and the Manned Space Flight Network (MSFN). The STADAN was used primarily for unmanned spacecraft support while the MSFN was designed and equipped to support the U.S. manned flight programs.

Existing network equipment is being relocated in order to minimize the number of required stations without degrading coverage capability. The former STADAN station at Fort Myers, Florida, has been closed; a former MSFN station at Honeysuckle Creek, Australia, has been transferred to the JPL for use in support of deep space missions. The station at Corpus Christi, Texas, has recently closed. Carnarvon, Australia, and Johannesburg, South Africa, are scheduled to be closed in 1974 and 1975, respectively. The resulting network will consist of 15 stations shown in Figure 7-6.

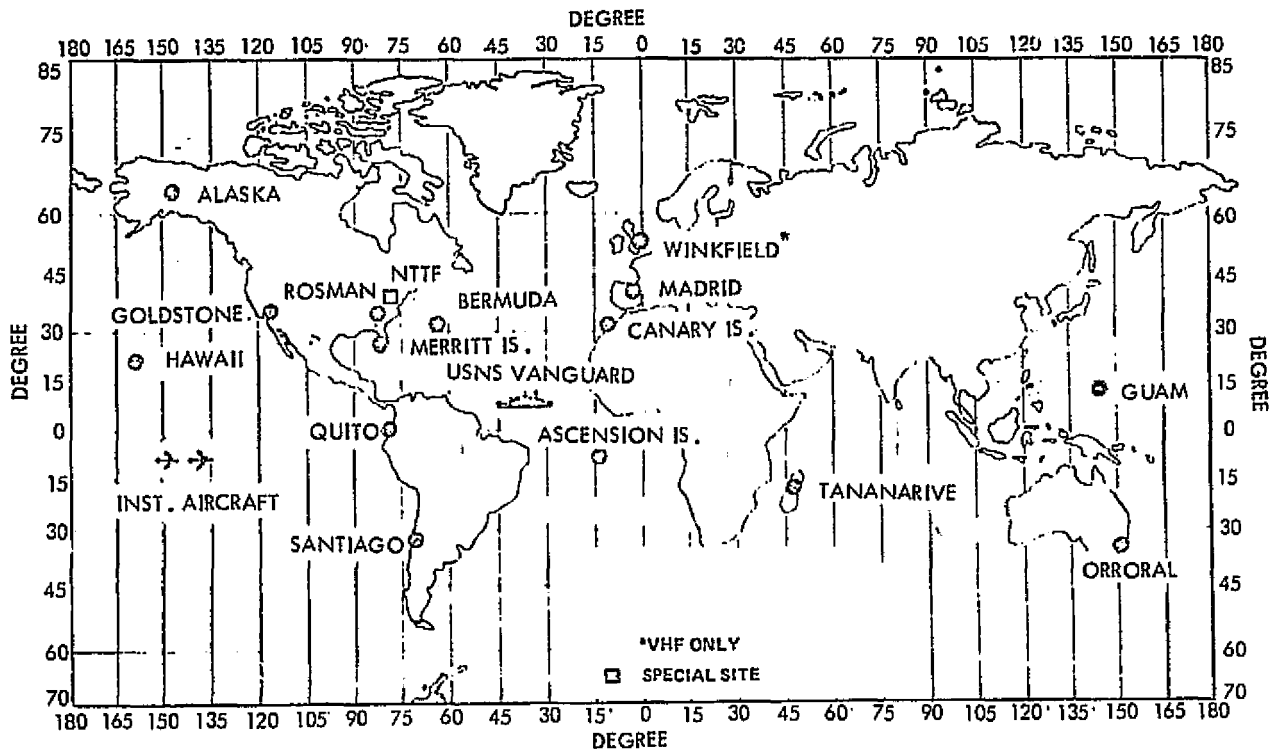


Figure 7-6. 1976-1979 STDN Network (15 Sites)

Future planning for the STDN includes the implementation of a Tracking and Data Relay Satellite System (TDRSS) in geosynchronous orbit into the STDN to provide service to payloads in low earth orbit. After the third TDRSS (including an in-orbit spare) is operational, plans include reducing the number of earth tracking stations in the STDN. Figure 7-7 shows a tentative configuration of the STDN with TDRSS. It is presently planned to reduce the STDN from 15 sites to the 7-8 station configuration.

Figure 7-7 and 7-8 also show a proposed configuration of the TDRSS, consisting of two geosynchronous relay satellites, 130 degrees apart in longitude, and a ground station facility planned to be located at White Sands, New Mexico. Coverage is such that real time data support will be provided to satellites orbiting between 120 km and 5000 km, with coverage below 1200 km reduced somewhat due to a small shadow zone, as illustrated in Figure 7-8b.

In combination, the TDRSS will provide primary support to low earth orbit payloads (below 5000 km) while the remote STDN sites will provide primary support to medium and high altitude payloads (above 5000 km).

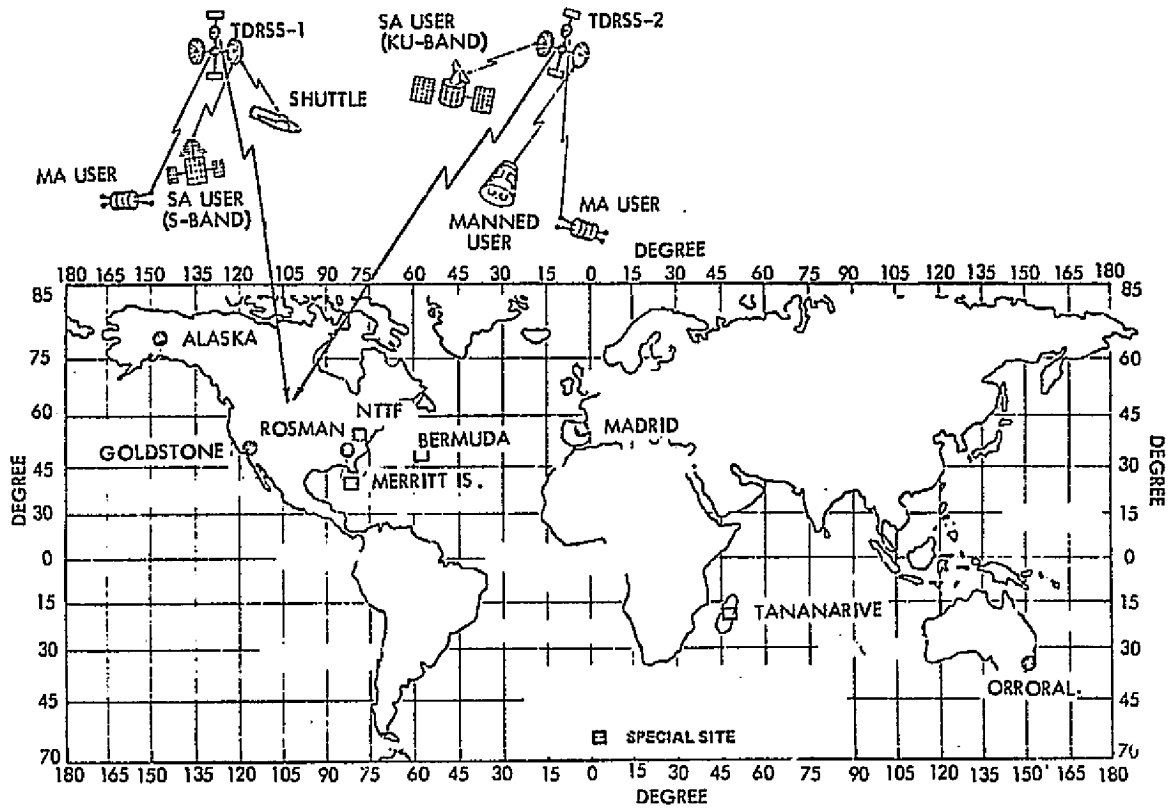


Figure 7-7. Tentative 1979 Network with TDRSS

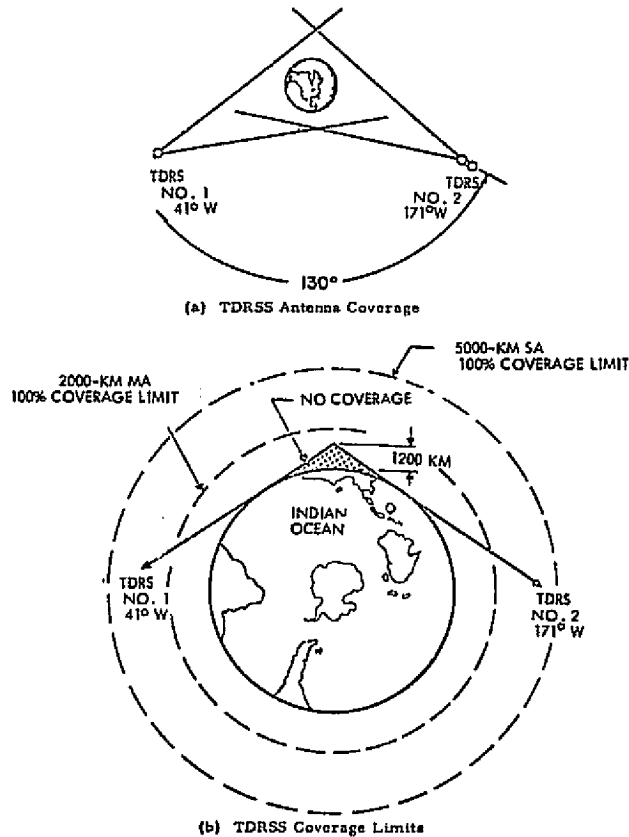


Figure 7-8. TDRSS User Coverage Capability

Characteristics of the STDN and TDRSS networks are presented in detail in references 29 through 33. Table 7-3 and 7-4 summarize the more important details. Frequency coverage is essentially S-band (2.2 to 2.3 GHz), and Ku-band from 13.4 to 15.25 GHz, according to Figure 7-9.

Table 7-3. STDN Data Handling Capabilities (Without TDRSS)

<p><u>S-Band (2.200 GHz - 2.300 GHz)</u></p> <p><u>Telemetry Data</u></p> <p>Receive, demodulate, bit synchronize, format and record - 1 mbps</p> <p>Receive, demodulate, and bit synchronize - 5 mbps</p> <p>Receive - up to 30 mbps (depending on modulation technique)</p> <p><u>NASCOM Point-to-Point Communications</u></p> <p>56 kbps minimum from earth site (50 kbps minimum real-time telemetry transmission capability)</p> <p><u>Coverage</u></p> <p>30 percent maximum (present network)</p> <p><u>Ku-Band (13.4 - 14.0 GHz)</u></p> <p>Selected sites by January 1978</p> <p><u>Future Network Utilization</u></p> <p>Post-1978 STDN will provide primary support to medium and high altitude (above 500 km) payloads</p> <p>S-band support with 85-foot antennas is available at Alaska, Rosman, Orroral, Madrid, and Goldstone. S-band support with 40-foot antennas is available at Tananarive and Alaska. S-band support with 30-foot S-band antennas is available at Merritt Island, Bermuda, Goldstone and the Vanguard (ship). Ku-band support will be implemented at selected STDN sites for wideband data use.</p>
--

Table 7-4. TDRSS Data Handling Capabilities

<p><u>S-Band (2.200 - 2.300 GHz)</u></p> <p>Multiple access antenna system up to 100 kbps (maximum 20 simultaneous users)</p> <p>Single access antenna system up to 5 mbps (maximum 2 simultaneous users)</p> <p><u>Ku-Band (13.4 - 14.0 GHz Uplink, 14.6 to 15.25 GHz return link)</u></p> <p>Single access antenna system up to 300 mbps (only one Ku-band user per TDRS if user's data rate exceeds 50 mbps (Biphase))</p> <p><u>NASCOM Point-to-Point Communications</u></p> <p>1.344 mbps from ground station (White Sands, New Mexico) to GSFC, redundant links, diverse routed</p> <p><u>Payload Support Function</u></p> <p>Will provide primary support to low earth orbit payloads (below 500 im)</p> <p><u>Coverage Capability</u></p> <p>85 percent (Minimum)</p>

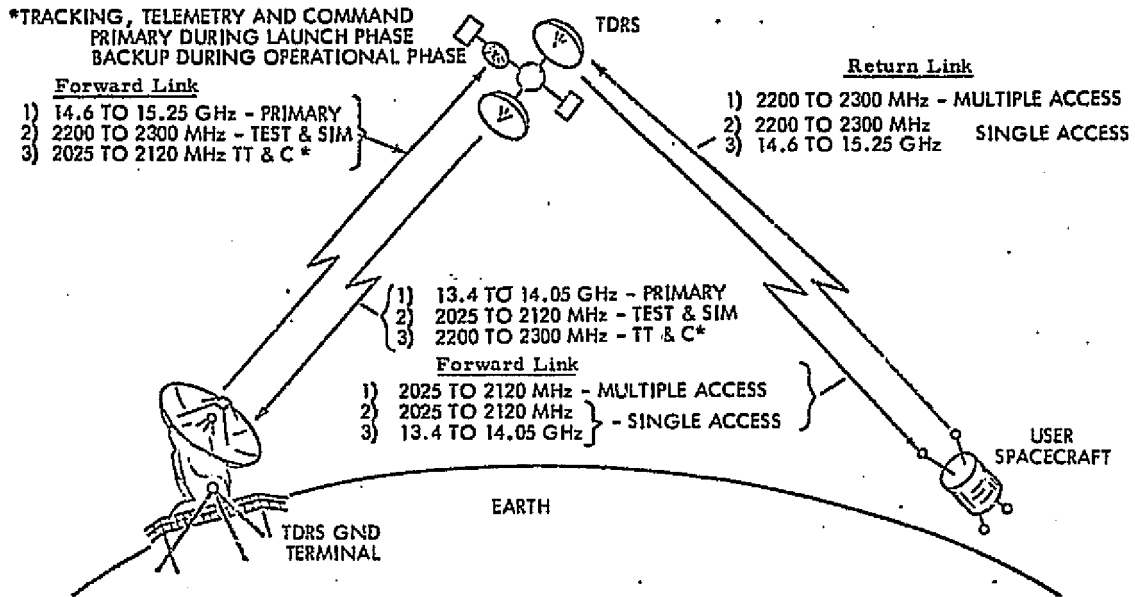


Figure 7-9. TDRSS Frequency Plan

Although the TDRSS will have both multiple-access and single-access channelization, anticipated data rates are such that the single-access mode will be of primary interest. Achievable data rates versus user EIRP are presented in Figure 7-10 for both the STDN and TDRS systems.

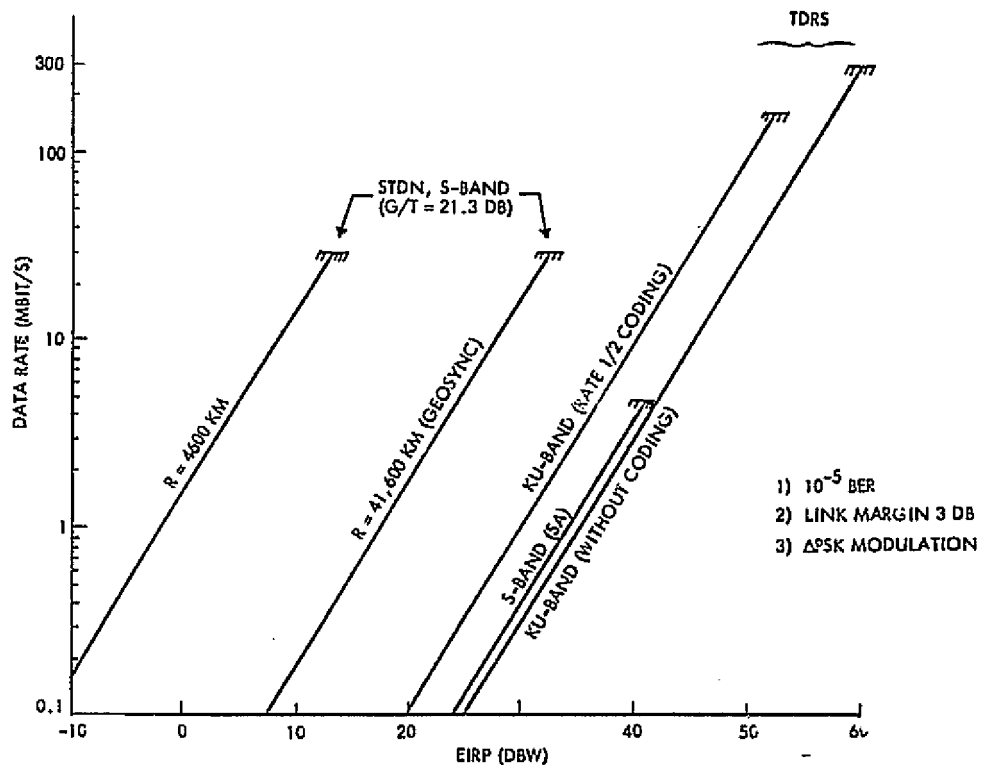


Figure 7-10. Achievable STDN and TDRSS Data Rate versus EIRP

7.2.3 National Aeronautics and Space Administration Communications Network

The National Aeronautics and Space Administration Communications Network (NASCOM) is a global system established and operated by NASA to provide long-line operational communications support of all NASA projects. NASCOM provides voice, data, and teletype communications between all ground tracking and data acquisition stations and the appropriate operations and control centers. It also provides for television and other wideband transmissions from selected stations. The network includes land lines, submarine cables, microwave and satellite links, and necessary terminal and switching facilities. In general, geographically diverse routes have been established from each station where possible so that no total communications loss will occur if the primary route fails.

Voice/Data Circuits. NASCOM provides a system of full period leased voice circuits (nominal 3-kHz bandwidth) to virtually all stations and terminal points in the NASCOM network. Essentially all voice/data circuits are routed either directly to the GSFC Switching, Conferencing, and Monitoring Arrangement (SCAMA) or through various overseas NASCOM switching centers where conferencing, monitoring, and test facilities are available. The voice links interface with Air-to-ground (A-G) voice equipment at manned flight support spacecraft voice communications in addition to the general mission support services.

High speed data modem (modulator-demodulator) sets are provided at all STDN and DSN stations. Modems at STDN stations operate at 7200 b/sec for transmission of telemetry data, and operate at 2400 b/sec (different modems) for transmission of high-speed tracking data. Channels to the DSN stations operate at 4800 b/sec. Analog data may also be transmitted over the 3-kHz voice/data lines either directly or using multiplex equipment.

Wideband Systems. Wideband communication links currently exist between GSFC and several STDN stations, and between GSFC and JSC. Group bandwidth (48 kHz) channels connect GSFC with Fairbanks, Madrid, Orroal, and with the MCC at JSC. Rosman is connected to GSFC by a wideband link with 1.5 MHz total available bandwidth (not continuous) in addition to a two-way 20-kHz wideband channel.

Generally, these circuits are capable of operating in a variety of modes to accommodate varying requirements. Typically a 48-kHz circuit can carry 28.5 kb/sec of data along with four voice bandwidth channels, or as with the three 48-kHz circuits to JSC, 50 kb/sec of data.

7.2.4 Available Communications Time

The time available for transmitting data directly to a ground site will be influenced by the time the satellite is in view of the ground stations and higher than a minimum elevation angle above the horizon. The former is influenced by the satellite orbit altitude, and the offset angle, or angle of closest approach to the zenith of the ground station, as illustrated in Figure 7-11 for elevation angles of 5 degrees and 15 degrees. Figures

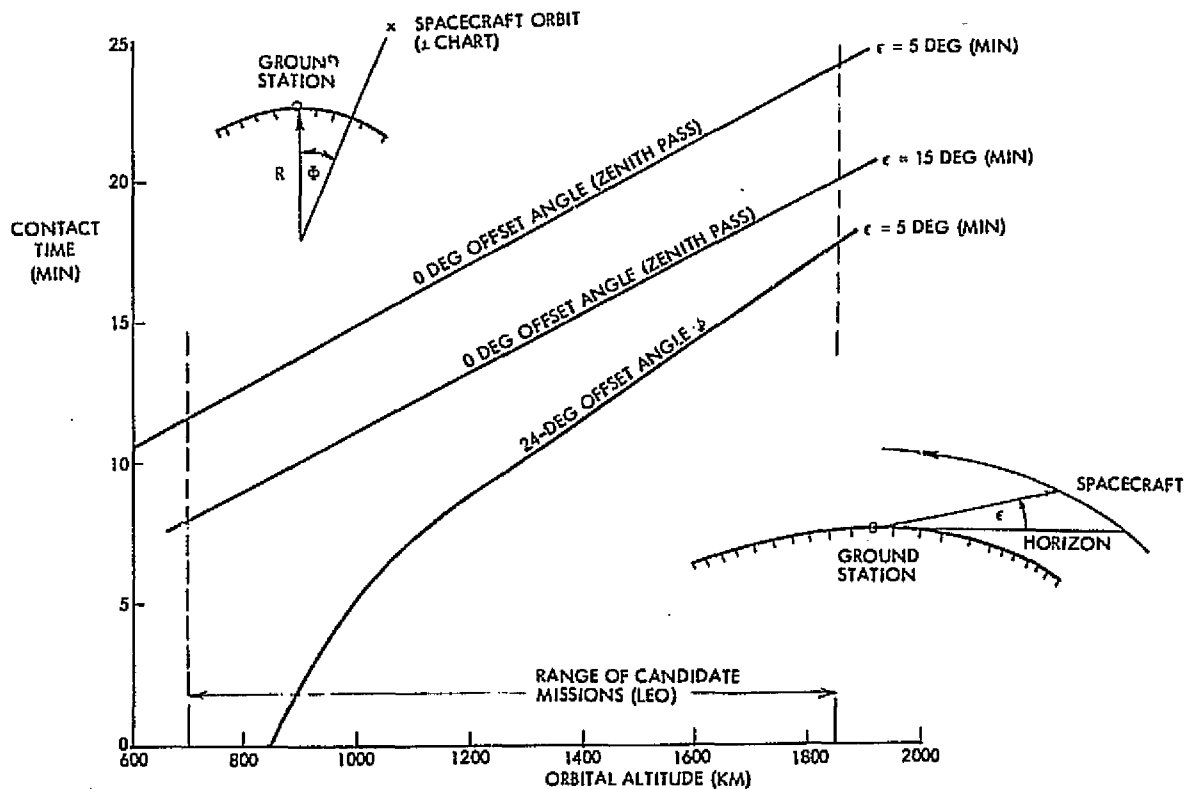


Figure 7-11. Ground Station Coverage Considerations

7-12a and 7-12d indicate the time the spacecraft are above a minimum elevation angle at altitudes of 707, 852, 1146 and 1852 km for offset angles up to 24 degrees. Note that the available transmission time is often as little as five minutes for offset angles of 21 or 24 degrees and minimum elevation angles on the order of 5 to 15 degrees.

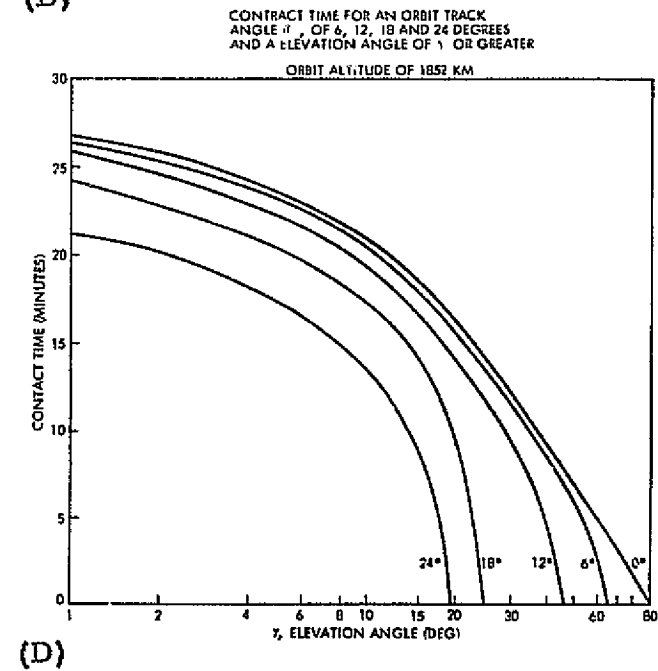
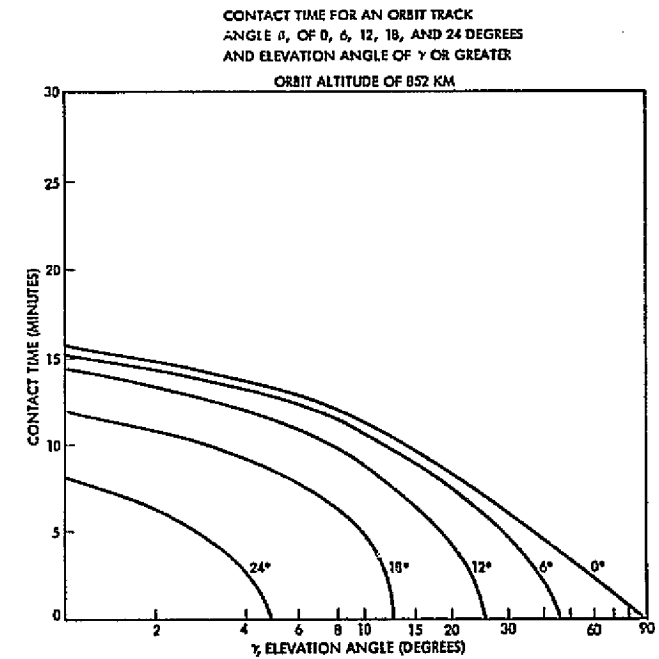
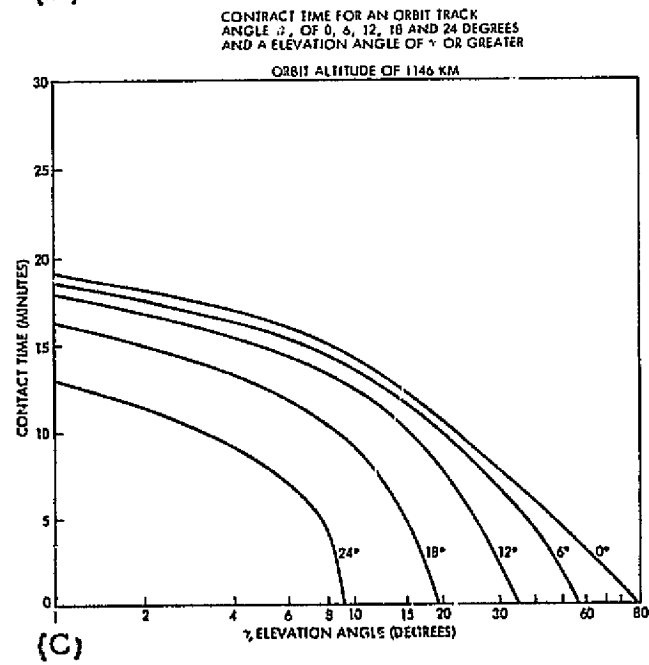
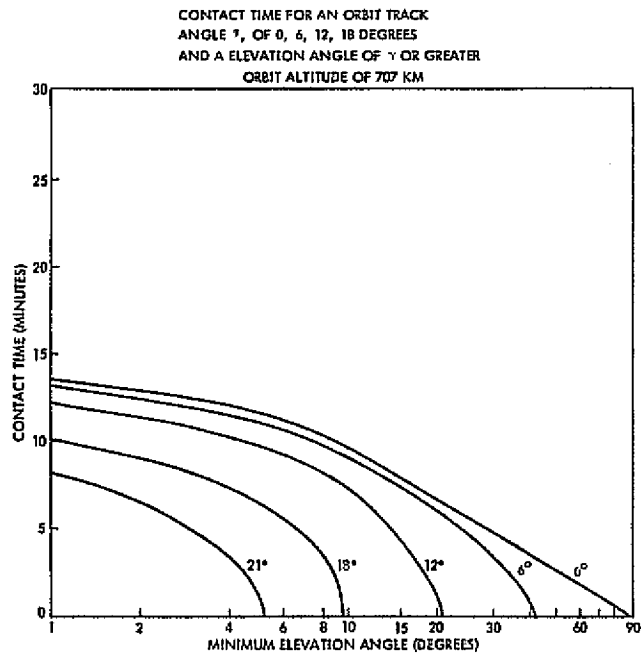


Figure 7-12. Contact Time versus Elevation

The minimum elevation angle is influenced by several factors, including CCIR limits on permissible flux density, atmospheric and other attenuation, multipath effects and antenna sensitivity. Flux density effects are reviewed in the next section. Weather effects are reviewed in Section 7.2.6 and in Appendix A. It is worth noting here, however, that atmospheric, cloud and rain losses become more severe with increasing frequency. At 8.2 GHz, the atmospheric and cloud losses without rain are not too severe above 5 degrees. However at 13.7 GHz, atmospheric losses alone rise to 3 db at 5 degrees, and at 21.6 GHz they are as high as 15 db. Rain and cloud losses at 13.7 or 21.6 GHz can be on the order of ten's of decibels at 5 degree elevation.

Multipath influences the minimum acceptable elevation angle by virtue of the deep nulls that occur when the reflected rays phase cancel the direct rays. The severity of the effect is influenced by the pattern of the ground receiving antenna, the nature of the terrain in the vicinity of the antenna, and the modulation. Multipath is the subject for a large study, in and of itself. However, as a rule of thumb, there will be few multipath problems if the bottom of the main beam of the antenna is above the tangent to the earth. The beam width of an 85-foot parabolic antenna is 0.4 degree at 2.2 GHz, that of a 30-foot parabolic is 0.3 degree at 8.2 GHz, and that of a 12.5-foot parabolic is 0.4 degree at 14 GHz. Since the first antenna null occurs approximately one beamwidth from bore-sight, multipath should present few limitations.

A final, very important limiting factor is the impact of terrain generated noise on the sensitivity of ground receiving systems. As the antennas are depressed, the lower atmosphere and terrain generated noise sources are included within the main beam and sidelobes, thus raising the effective antenna temperature. This is reviewed in Section 7.3.6.

In summary, it is evident that there are a number of factors inhibiting successful communications at low elevation angles and thus restricting available communications time. This in turn increases the required data rate during the portion of the orbit when communications can be established. It is for these reasons that a system design must occasionally be iterated, with parameters adjusted to allow for contact

time variations. Occasionally, it will be necessary to restrict the data rate, or to use an alternate path such as will be afforded by the TDRSS.

7.2.5 Interference and CCIR Limits

A major factor limiting satellite ERP is the power limitation established by international agreement and published in the form of CCIR rules. At present, the maximum flux density produced at the earth's surface by a satellite transmitter is as illustrated in Figure 7-13. Figure 7-14 illustrates the maximum allowable ERP permitted, as a function of slant range, bandwidth and satellite elevation angle, assuming no excess path attenuation caused by atmospheric absorption or weather.

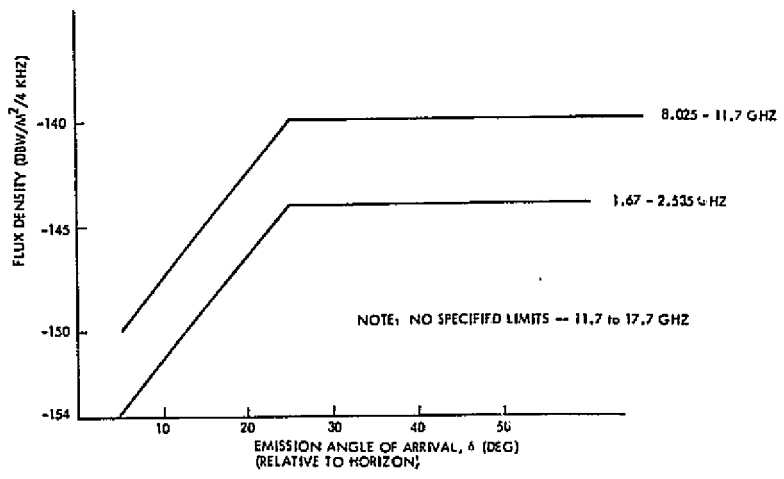


Figure 7-13. CCIR Power Flux Density Limits

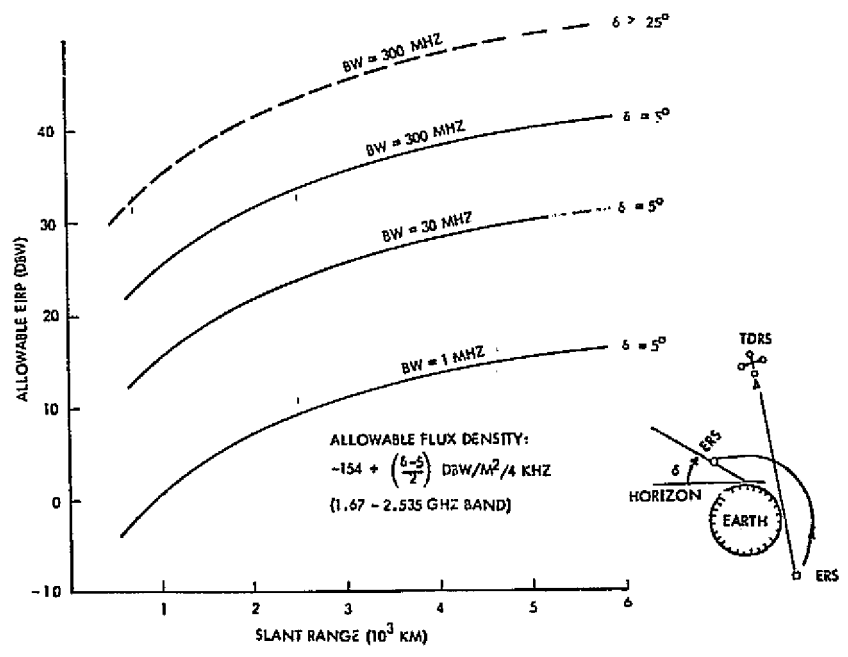


Figure 7-14. EIRP Limitations Derived from CCIR Flux Density Recommendations

It is interesting to compare allowable flux density with receiver noise temperature. For example, the maximum energy intercepted by a one meter square antenna at a low elevation angle of 5 degrees, is -154 dbw/4 kHz at S-band. This corresponds to -190 dbw/Hz which compares to $kTB = 204$ dbw for a one Hertz bandwidth when T is 290°K . Although the margin is 14 db, much of this would be required to overcome receiver noise figure and demodulation thresholds. It is apparent that one is driven to providing more sensitive receiving system with larger antennas, lower equivalent noise temperatures and to use increased modulation bandwidths when possible.

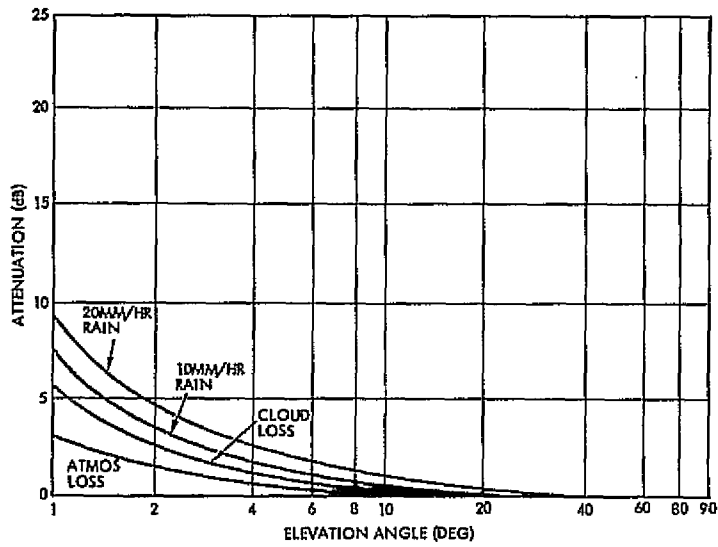
7.2.6 Atmospheric Absorption and Weather Losses

Atmospheric absorption and weather effects worsen with increased frequency, and with the length of the path passing through the atmosphere, clouds or rain storms. Inasmuch as the slant path length increases for low elevation angles, excess attenuation can vary considerably as the satellite rises from the horizon to directly overhead. This is illustrated by Figures 7-15 a - d for 2.2, 8.2, 13.7 and 21.6 GHz. Specific rainfall rates to be used will depend on outage requirements in terms of permissible link-downtime, and the geographical location of the ground terminal. An example of the cumulative distribution of rainfall rates is provided in Figure 7-16.

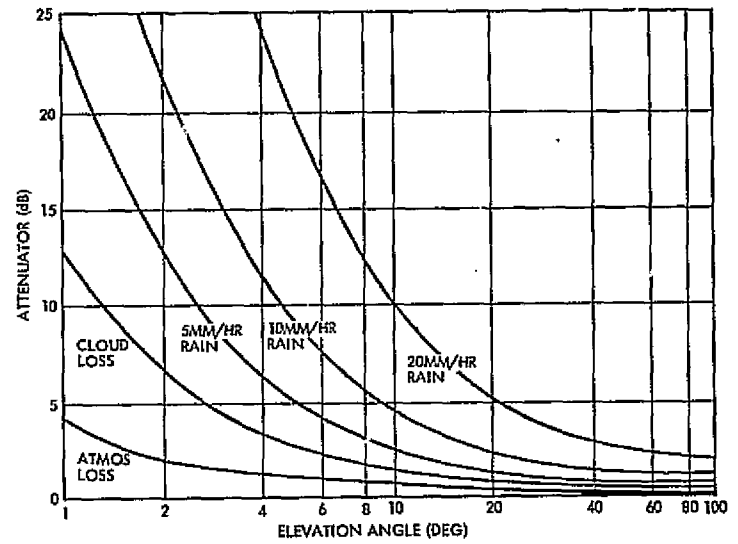
It is readily apparent that weather and atmospheric losses will have a significant impact on the minimum usable elevation for frequencies above 8.2 GHz. Factors influencing weather effects are reviewed further in Appendix A.

7.3 System Considerations

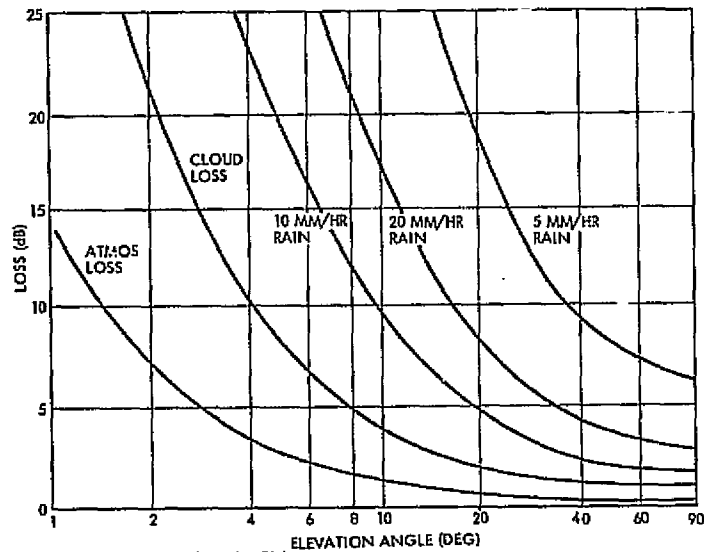
Communications link requirements are governed by a relatively simple equation that demonstrates the interplay of the system components of Figure 7-17. Before proceeding further, let us review this equation to place these components in perspective.



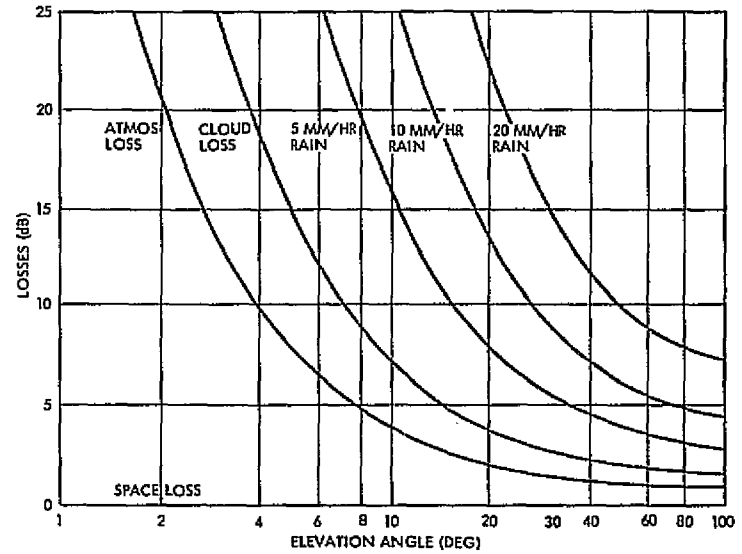
(A) $f = 2.2$ GHz



(B) $f = 8.2$ GHz

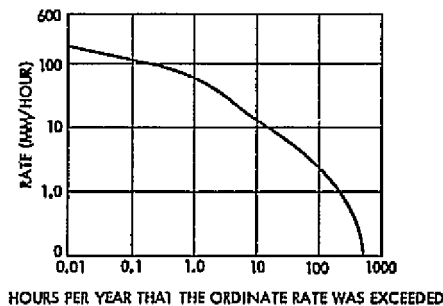


(C) $f = 13.7$ GHz



(D) $f = 21.6$ GHz

Figure 7-15 Atmospheric Absorption and Weather Losses



R MIN/HR	R (1) > R		R (1) < R % OF TIME
	TIME PER YEAR	% OF TIME	
150.00	1.5 MIN	2.8×10^{-4}	99.99972
100.00	9 MIN	1.7×10^{-3}	99.9983
50.00	1.3 HR	1.5×10^{-2}	99.985
25.00	4.3 HR	4.9×10^{-2}	99.951
12.50	11 HR	0.13	99.87
2.50	97 HR	1.1	98.9
1.25	185 HR	2.1	97.9
0 (0.125)	500 HR	5.7	94.3

TOTAL TIME PER YEAR A GIVEN RAINFALL INTENSITY IS EXCEEDED AND PERCENTAGE OF TIME A GIVEN RAINFALL INTENSITY IS EXCEEDED (FOR WASHINGTON, D.C.)

Figure 7-16. Cumulative Distribution Function for Rainfall Rates at Wash Washington, D.C.

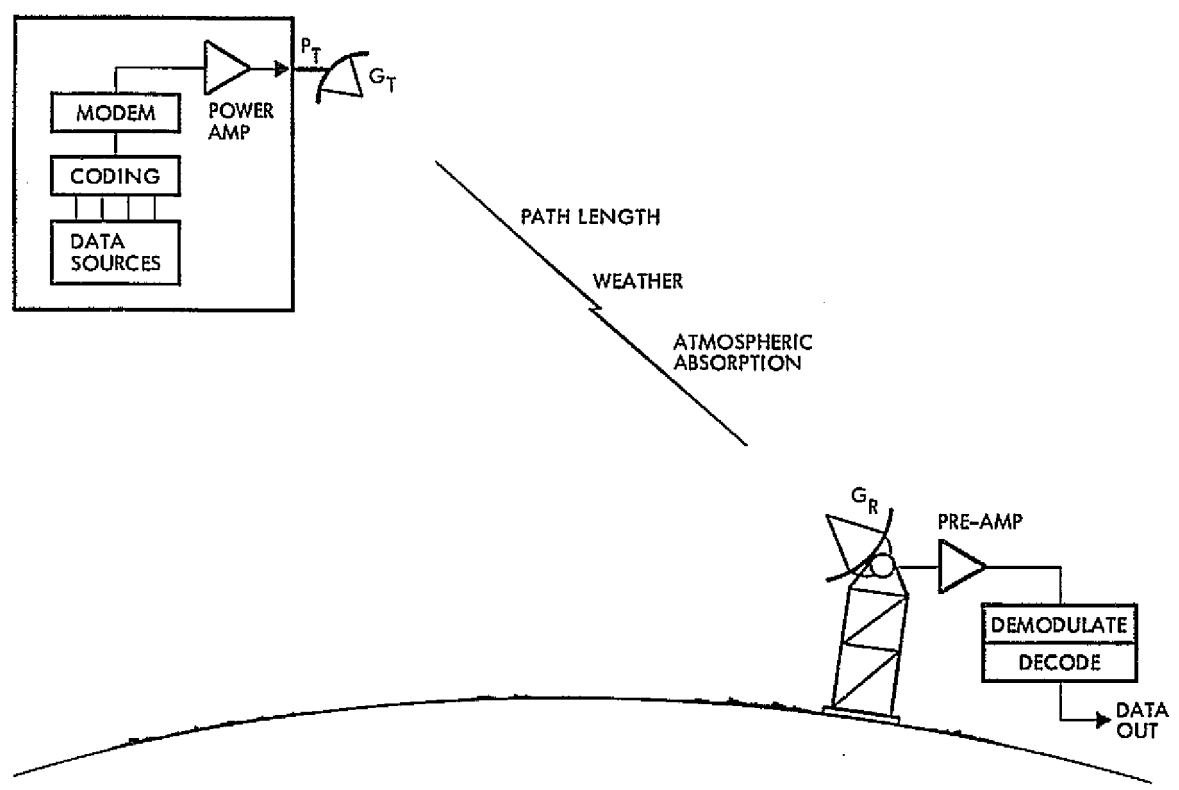


Figure 7-17. Components of Typical Communication System

7.3.1 System Overview

In general, one is concerned with communicating a given number of information bits over a link with no worse than a specified error rate. For each of the many modulation formats, when the received noise is gaussian, the bit error rates (BER) may be related to the ratio of the received energy per bit (E_b) to noise spectral energy density (N_o). Thus the starting point in the power budget derivation is to select a modulation format and maximum acceptable bit error rate. With these parameters, one is able to determine a minimum acceptable value of E_b/N_o .

Let E_b = Energy per information bit
 P_r = Received energy/second
 R_l = Information bits/second
 N_o = Received spectral noise density.

Then

$$\begin{aligned}\frac{E_b}{N_o} &= \frac{P_r}{R_l N_o} \\ &= \frac{P_t G_t G_r}{R_l k T_{eq} L_p}\end{aligned}$$

Where G_t = Transmitting antenna gain
 G_r = Receiving antenna gain
 L_p = Path losses
 k = Boltzman's constant
 T_{eq} = Equivalent antenna temperature.

But E_b/N_o must exceed E_b/N_o (threshold) by a safety factor, or margin, in order to provide reliable communications over the majority of operating conditions. If we denote the margin by m (where $m > 1$), we have

$$\frac{E_b}{N_o} = \frac{P_t G_t G_r}{R_l k T_{eq} L_p} \quad \text{must} \quad \geq \quad m \frac{E_b}{N_o} \Big|_{\text{Threshold}} \quad (1)$$

Rearranging

$$(P_t G_t) \cdot \frac{G_r}{T_{eq}} \geq \left(\frac{E_b}{N_0} \Big|_{\text{Threshold}} \right) (m L_p) (kR_1) \quad (2)$$

Thus the major factors influencing link design are revealed as:

$\frac{E_b}{N_0} \Big|_{\text{TH}}$ = the threshold condition for a given bit error rate (BER). This is influenced by acceptable BER, modulation format, coding and implementation losses. These are reviewed in Sections 7.3.2 and 7.4.1.

$P_t G_t$ = EIRP, or effective isotropic radiated power. This is a spacecraft design variable governed by the choice of transmitter power and spacecraft antenna. These factors are reviewed in Section 7.3.3 and 7.3.4.

$\frac{G_r}{T_{eq}}$ = Equivalent ground receiving antenna system figure of merit. This is governed by the ground antenna and preamplifier noise temperatures, and is reviewed in Sections 7.3.6 and 7.3.7.

L_p = Path losses, including spherical divergence, atmospheric attenuation weather and multipath. This latter is influenced by antenna pattern, elevation angle and modulation format. This is reviewed in Section 7.2.6 and Appendix A.

m = Link margin. This is essentially excess power provided as a safety factor to accommodate component degradation and link fading variables such as weather or multipath. Margin directly influences communication reliability in terms of the fraction of time the link will be available. Note that margin is provided to cover relatively long time-constant effects, as opposed to gaussian noise.

k = Boltzman's constant = 1.3×10^{-23} Joules/ $^{\circ}$ Kelvin. Note that $k = -228.6$ dBw/Hertz/ $^{\circ}$ Kelvin.

R_1 = Information bit rate to be supported by the link.

7.3.2 Modulation Considerations

7.3.2.1 General. The modulation technique to be selected will depend, to a great extent, on the ease of fitting the required bit rate into the available bandwidth, the maximum allowable error rate, the possibility of minimizing radiated power, and equipment complexity. Systems requiring

some immunity to jamming, or to multipath will also be influenced by these factors. However, we will assume that the latter considerations do not apply.

There are a variety of modulation possibilities, including amplitude, frequency and phase and combinations thereof. Each, in turn, may be developed in multistate formats ranging from binary and quaternary to as many as 32, 64, 128 or more.

Traditionally, binary modulation techniques have been used wherever bandwidth permits, since this leads to the simplest system. Furthermore, uniform amplitude systems permit the simplest transmitter design, and are compatible with the use of limiters in the receiver. Accordingly multilevel systems have found less favor than constant amplitude systems such as permitted by frequency or phase modulation.

Detection of a signal depends on the ability to make a decision in the presence of interfering noise. The usual practice is to assume gaussian noise as a basis for comparison, and will be followed here. More exotic noise sources often defy analytical tools, except in the case of specialized interferers such as cw signals, and will serve no useful purpose for comparison at this time.

Bit error probabilities have been derived by many workers, and are presented in numerous texts such as Bennett and Davey or Stern and Jones. The standard derivations lead to distributions of error probabilities as a function of signal-to-noise ratio at the detector input, after the signal and noise have passed through the transmitter and receiver filters and the intervening media.

The nature of the intervening transmission media and filters influence such signal characteristics as pulse shape and energy content in addition to the total noise energy at the detector input. Further, when there are adjacent channels to consider, the filter characteristics will influence channel aliasing or cross-talk.

In order to cope with filter effects, authors in the field introduce reasonable assumptions when deriving error probabilities, and then treat additional loss effects as implementation losses introduced by the particular system design. Bennett and Davey (Ref. 34, page 99) present an analysis to justify spectrum shaping according to a raised-cosine law.

Stein and Jones (Ref. 35, Chapter 13) also review filter effects, with analysis of matched filters, integrate and dump filters, maximum likelihood receivers etc. The approach taken here will be to present bit error rate curves based on signal-to-noise ratios, which for matched filter detection is equivalent to energy contrast ratios, E_b/N_0 . Implementation losses will be touched upon in a subsequent section.

The following sections will review modulation formats, spectral energy distributions and bit error probabilities. Bandwidth limiting factors will be reviewed, followed by implementation losses. Binary systems will be reviewed first, followed by a generalization to multi-state systems.

Because of the difficulties inherent in providing linear amplifiers required for non-constant amplitude wave forms, this review will concentrate on constant amplitude signals. However, two new non-constant amplitude waveforms that show considerable promise for the future are described in Appendix B and C.

7.3.2.2 Binary Wave Forms. Constant amplitude binary wave forms that merit review are the various forms of frequency shift keying (FSK), and phase modulation (PSK).

FSK. FSK with discontinuous phase is generated by switching between two oscillators at the "mark" and "space" frequencies f_1 and f_2 . Detection may be accomplished noncoherently with mark and space filters, or coherently with phase-locked loops (PLL's) tracking the discrete spectral components at f_1 and f_2 .

The spectral occupancy of discontinuous FSK is a function of the modulation index h , defined as

$$h = (f_2 - f_1) T$$

or

$$h = X_2 - X_1$$

where

$$f_0 = \text{reference frequency}$$

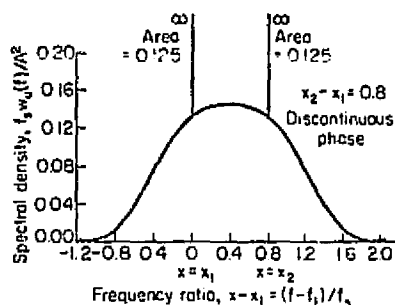
$$f_1 = \text{mark frequency}$$

$$f_2 = \text{space frequency}$$

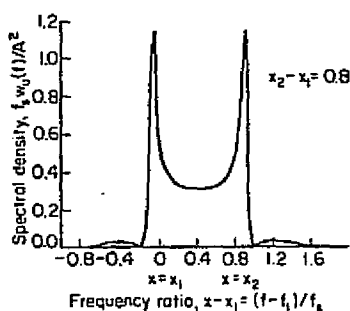
$$1/T = \text{bit rate}$$

$$X = (f - f_0) / \text{bit rate}$$

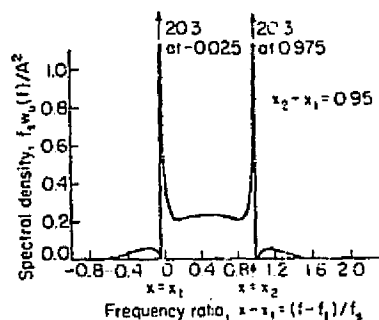
The modulation spectral density consists of $\sin^2 x/x^2$ functions centered at f_1 and f_2 containing 1/2 the total power, plus two discrete components containing the remaining power as shown in Figure 7-18. The spectral occupancy for reasonable values of h (say $h = 1$) is much greater than comparable PSK or QPSK systems.



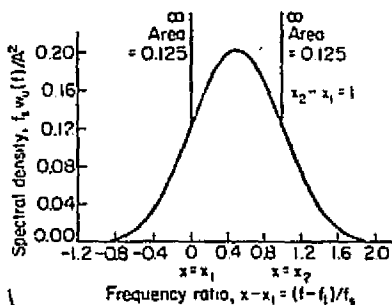
a) Discontinuous phase at transitions. Frequency shift = 0.8 times signaling frequency.



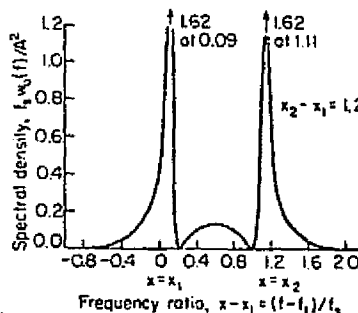
b) Continuous phase at transitions. Frequency shift = 0.8 times signaling frequency.



c) Continuous phase at transitions. Frequency shift = 0.95 times signaling frequency.



d) Continuous phase at transitions. Frequency shift = signaling frequency.



e) Continuous phase at transitions. Frequency shift = 1.2 times signaling frequency.

Figure 7-18. Spectral Density of Random Binary FSK Waveforms

Continuous-Phase FSK. Some bandwidth reduction is obtained if the phase transitions are continuous from bit to bit. The continuous-phase FSK signal is illustrated in Figure 7-19, and given by equation 7-1.

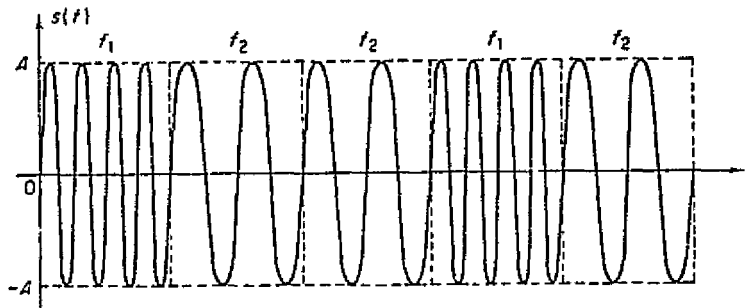


Figure 7-19. FSK Waveform, Rectangular Pulses

$$s(t) = \sin \left[2\pi \frac{(f_1 + f_2)}{2} t + \phi(0) + \phi(t) \right] \quad (7-1)$$

where

$\phi(0)$ = initial random phase

$$\phi(t) = \left(\sum_{i=1}^n a_i \pi h \right) + a_{n+1} \pi (f_2 - f_1)(t - nT),$$

$$nT \leq t < (n+1)T$$

$$a_i = \pm 1$$

The phase function $\phi(t)$ follows the continuously branching path sketched in Figure 7-20, increasing by $\pm \pi h$ during each bit interval.

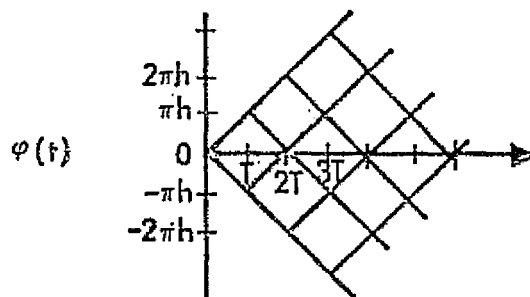


Figure 7-20. Allowed Paths of the Phase for Continuous Phase FSK

The value $h = 1$ for continuous phase FSK was proposed by Sunde. However, this modulation is inefficient because it contains discrete components at f_1 and f_2 , as shown in Figure 7-18d.

PSK. The binary PSK modulation signal is illustrated in Figure 7-21, and given by equation 7-2.

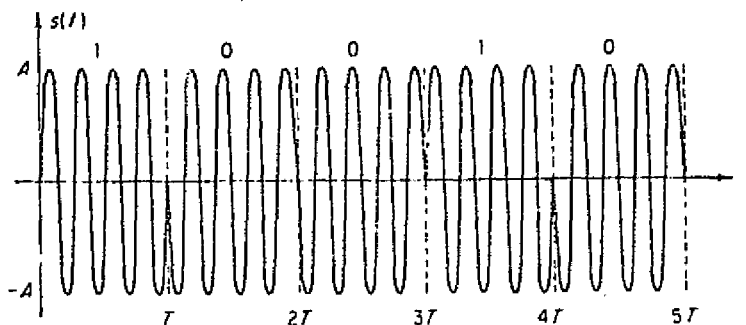


Figure 7-21. PSK Signal, Rectangular Pulses

$$s(t) = a_i \sin \left[\omega_c t + \phi(0) \right] \quad (7-2)$$

where

$$a_i = \pm 1$$

$$\omega_c = 2\pi f_c = \text{carrier frequency}$$

$$\phi(0) = \text{initial random phase}$$

Since this coding is antipodal, it uses both power and bandwidth very efficiently. The bit rate of PSK can be doubled in the same bandwidth by transmitting two 90 degree shifted biphasic carriers at a symbol rate equal to 1/2 the bit rate. The signal vectors for BPSK and QPSK are shown in Figure 7-22. The QPSK spectrum is a $\sin^2 x/x^2$ function with the frequency between the first nulls equal to the bit rate or twice the symbol or baud rate.

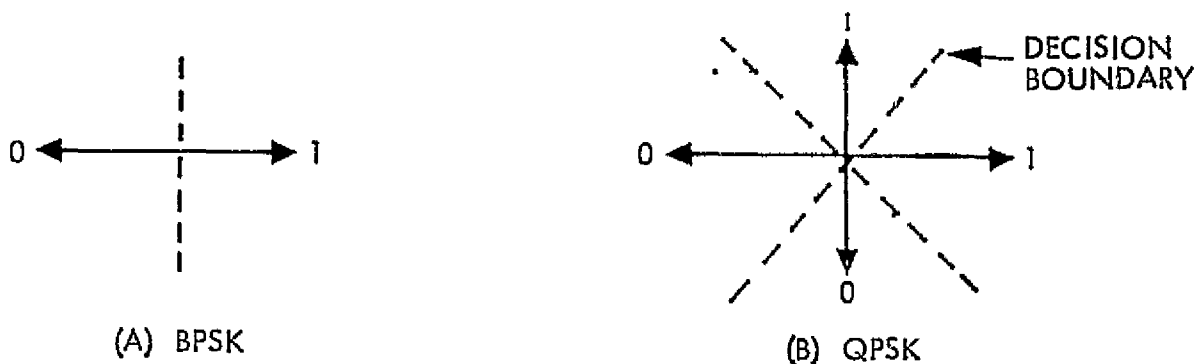


Figure 7-22. BPSK and QPSK Phase Decision Regions

Differentially Coherent PSK (DPSK). An alternative to ideal coherent PSK, with the required long-term stability and/or high-quality phase correction loops, is differentially coherent phase shift-keying and detection, often termed simply differential PSK or DPSK. In this technique, it is assumed that enough stability is present in the oscillators and the transmission medium that there is negligible change in phase from one information pulse to the next information pulse, aside from changes caused by actual encoding. Information is encoded, not by absolute identification of, say, 0 degree phase with Mark and 180 degrees with Space, but rather by differentially encoding the information in terms of the phase change between successive pulses. For example, no (0 degree) phase shift from the previous pulse could designate Mark, and 180 degrees phase shift would then designate a Space.

Bit error rates (BER) for FSK and PSK binary systems are given in Figure 7-23 as a function of γ , the signal to noise power entering the detector. The actual value of γ will be greatly influenced by the predetection filter which will limit both signal energy and noise. However for the special case of matched filter, γ assumes its maximum value, and is equivalent to E_b/N_o , the ratio of the energy per bit to the noise spectral energy density.

MSK. Minimum (frequency) shift keying (MSK) may be viewed either as a special case of continuous - phase FSK with $h = 1/2$, (peak frequency deviation equal to $\pm 1/4 R_L$) where R_L is the link bit rate), or as an offset-keyed QPSK modulation.

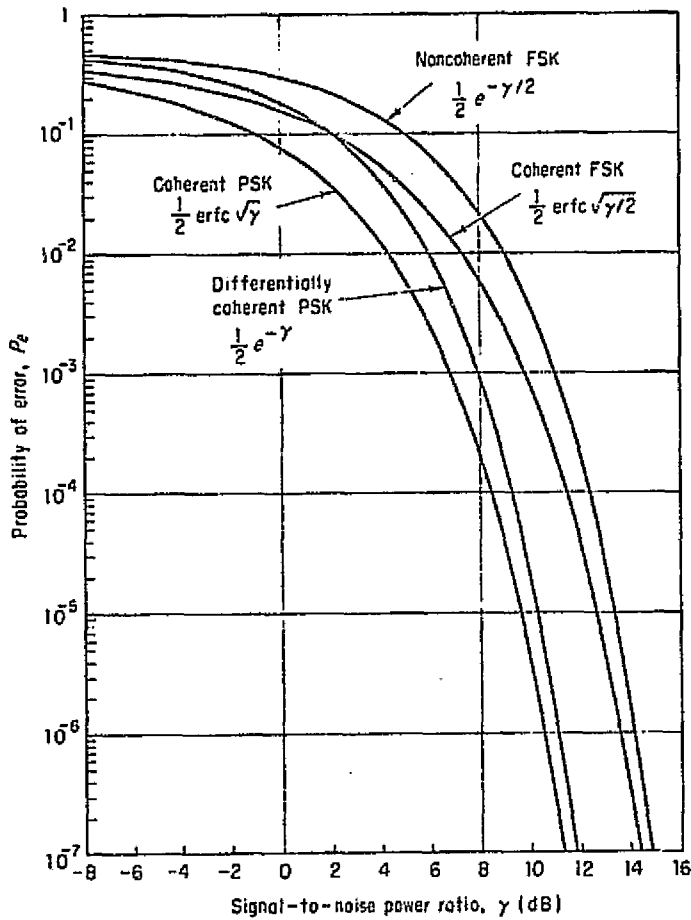


Figure 7-23. Error-rates for Several Binary Systems

In the first (FSK) view, MSK possesses the following properties.

The frequency deviation Δf is exactly $\pm (1/4) R_L$.

The RF phase varies linearly exactly $\pm 90^\circ$ with respect to the carrier during each $T = 1/R_L$ input bit interval.

There is phase continuity of the modulated RF carrier at the interbit switching instants.

With MSK, a phase difference of $\pi/2 - (-\pi/2) = \pi$ separates the mark and space frequencies. Hence a "space" (at frequency f_2) is exactly $1/2$ cycle longer than a "mark" (at frequency f_1). A typical MSK waveform is shown in Figure 7-24.

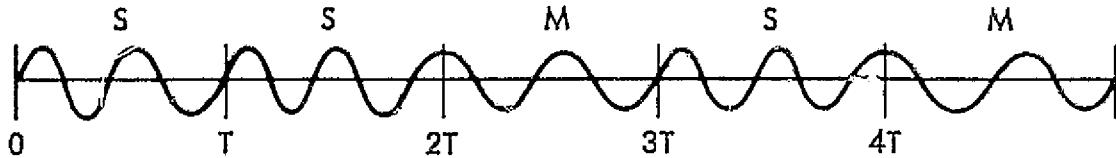


Figure 7-24. Typical MSK Waveform

A second approach views MSK as a quadriphase system with offset keying and sinusoidal symbol shaping.

A visualization of the waveforms is shown in Figure 7-25.

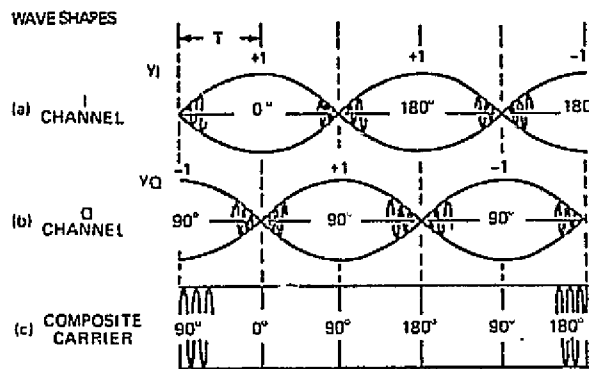


Figure 7-25. MSK Visualized as Sine-Multiplied OK-QPSK

In this second visualization, MSK possesses the following properties.

The composite signal can be viewed as two orthogonal (quadrature) phasors.

Each phasor is amplitude modulated by a half sinusoid.

The phase sense of the phasor is determined by the symbol sense.

Figure 7-25(c) illustrates that the sum of (a) and (b) yields a composite carrier identical to that of the FSK visualization.

Equations (7-2), (7-3), and (7-4) constitute the formal definition of MSK as used in Reference 36.

$$m(t) = y_Q \cos(\omega_c t) \cos\left(\frac{\pi}{2T} t\right) + y_I \sin(\omega_c t) \sin\left(\frac{\pi}{2T} t\right) \quad (7-3)$$

$$= y_Q \cos \left\{ \left[\omega_c + (y_Q \oplus y_I) \frac{\pi}{2T} \right] t \right\} \quad (7-4)$$

where y_Q and y_I are the quadrature and in-phase phasor symbols (± 1) and \oplus denotes modulo two addition

$$y_I(m) = y_L(n) \oplus y_I(m-1) \quad (7-5)$$

with a similar expression existing for y_Q . y_L is the last input bit to the modulator.

The optimal detector for MSK consists of in-phase and quadrature channels at baseband. These each perform an integrate-and-dump operation on interleaved pairs of bits rather than on a single bit, since bit phases are interrelated by the continuous phase restricted modulation.

A system using MSK to transmit unambiguous data has the same ideal E_b/N_0 as differentially encoded BPSK or OK-QPSK.

The probability of bit error p_e of coherently detected BPSK and conventional nonoffset QPSK is

$$p_e = 1/2 \left[1 - \operatorname{erf} \left(\frac{E_b}{N_0} \right)^{1/2} \right] \quad (7-6)$$

For MSK, this is modified by differential coding such that the combined probability bit error P_e is given by $P_e = 2p_e - p_e^2$. A typical value for E_b/N_0 is 8.8 db for $P_e = 10^{-4}$, and 9.9 for $P_e = 10^{-5}$.

7.3.2.2 Multi-State Systems

FSK and PSK may logically be extended from two frequency or phase values to several possible values. Usually, M is taken as some power of 2,

$$M = 2^k, \quad k = \text{integer}$$

Thus, we have 2, 4, 8 . . . possible tones in FSK, or phases in PSK, and detection of one of these values, M yields $k = \log_2 M$ bits of information.

Multiple FSK reception is usually via set of M bandpass filters, each centered on one of the possible tones, followed by non-coherent envelope detection. At low bit rates, more efficient integrate and dump filters may be used. Occasionally coherent detection is considered, but the problem of maintaining M coherent phase references mitigates

against its implementation, especially when doppler correction is required. Symbol error rates for M-ary single tone non-coherent FSK signals are presented in Figure 7-26. Note that the curves are presented as a probability of symbol error, with each symbol containing k bits of information. Bit error rates are related to symbol error rates by

$$P_{e,b} = 1/2 \frac{P_e}{[1 - (1/2)]} \quad (7-7)$$

For large k, bit error rates are approximately one half of the symbol error rates.

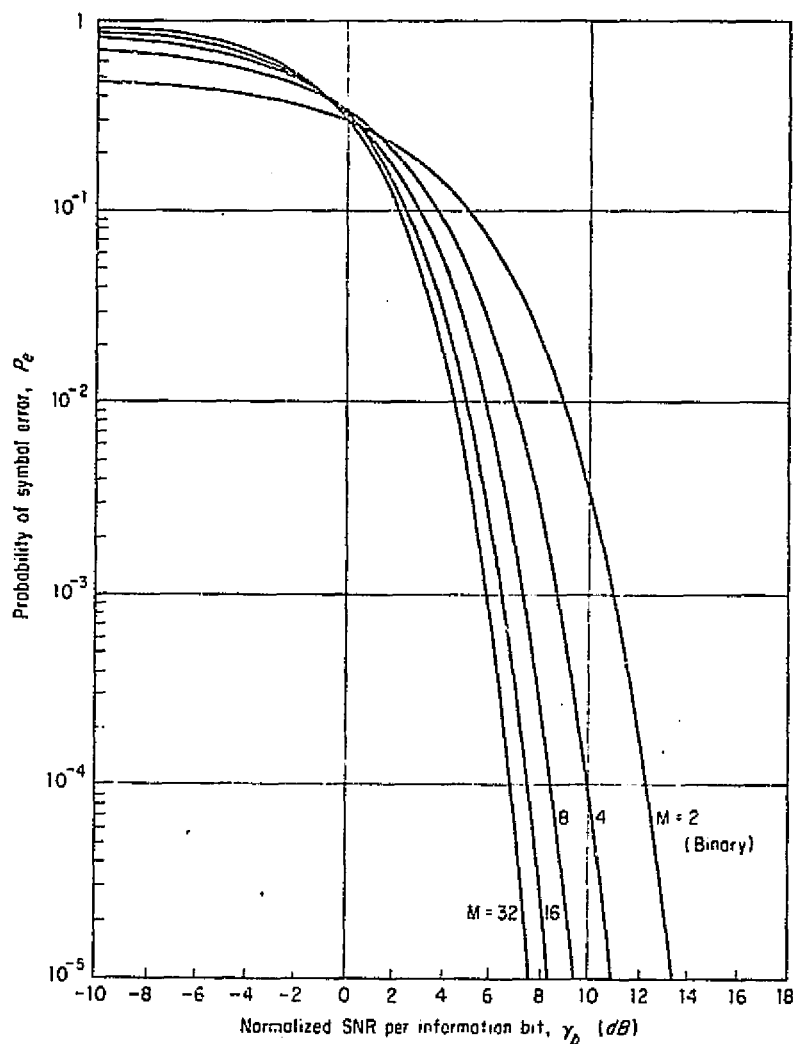


Figure 7-26. Error for Noncoherently Detected Orthogonal Multitone Signaling.

γ_b is the signal-to-noise ratio at the output of the tone filter containing the signal.

Figure 7-26 suggests that increasing M will permit reducing the transmitted power, while maintaining a constant symbol error rate and bit rate. This may be done, however, only at the expense of widening the total required spectrum. This is based on a relation between an increasing number of filters, each of which may be narrower by $\log_2 M$

$$\text{BW required} \propto \text{bit rate} \frac{M}{\log_2 M}$$

When multiple tones are simultaneously transmitted, the bandwidth need not be quite as wide, but signal power is again increased. As an example of simultaneous multiple tone keying, four bits could be transmitted by using four tones, each of which is allocated to one of four pairs of filters, for a total bandwidth equal to that of eight filters, as opposed to sixteen for the single tone case. Another possibility would be two tones allocated to each of two groups of four filters, thereby giving sixteen combinations within half the bandwidth of single tone keying. Each of these combinations is equivalent to combinations of lower-order single tone systems, insofar as signal to noise ratios are concerned, but with total required power proportional to the number of simultaneous tones used. Thus we again see a power bandwidth tradeoff.

Multiple PSK signalling is based on the possibility of signalling with several phases on a single tone, as illustrated in Figure 7-27.

For each signal pulse of length T ,

$$s(t) = \sqrt{2S} \cos(2\pi f_0 t + \theta), \quad 0 < t < T \quad (7-8)$$

where θ is one of a set of uniformly spaced values θ_m given, for example (see Figure 7-27), by

$$\theta_m = \frac{2\pi}{M} (m - 1), \quad m = 1, \dots, M \quad (7-9)$$

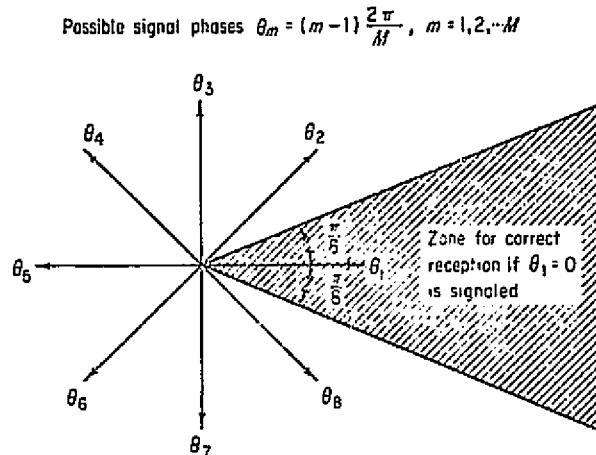


Figure 7-27. M-phase Signaling
(Illustrated for $M = 8$)

Again, each phase state represents a symbol with $k = \log_2 M$ information bits. The symbol probability error is presented in Figures 7-28 and 7-29 for coherent m-ary PSK and differentially coherent PSK as a function of signal to noise ratio at the detector input. Bit error probability, relative to symbol error probability is bounded by

$$\frac{1}{2} \frac{P_e}{1 - (1/2^k)} \approx P_{e_b} \approx \frac{1}{\log_2 M} P_e, \quad (7-10)$$

with the exact relationship determined by the randomness of the error in the phase bins and the conversion from symbol to bit sequence.

Signal to noise ratio for received signals will be maximum if matched filtering is used. In this case, γ_b will equal E_b/N_0 , as before.

For a constant PSK error rate, Figures 7-28 and 7-29 both show that γ_b , must be increased as the number of states is increased. This is a direct consequence of reduced allowable phase error between states. Since each symbol duration increases, as M increases, the required bandwidth decreases. Thus m-ary PSK will permit a reduced bandwidth for a given bit rate, but at the expense of additional power for the same bit error rate.

The bandwidth will be proportional to $(\log_2 M)^{-1}$, or to the increase of the number of bits per symbol.

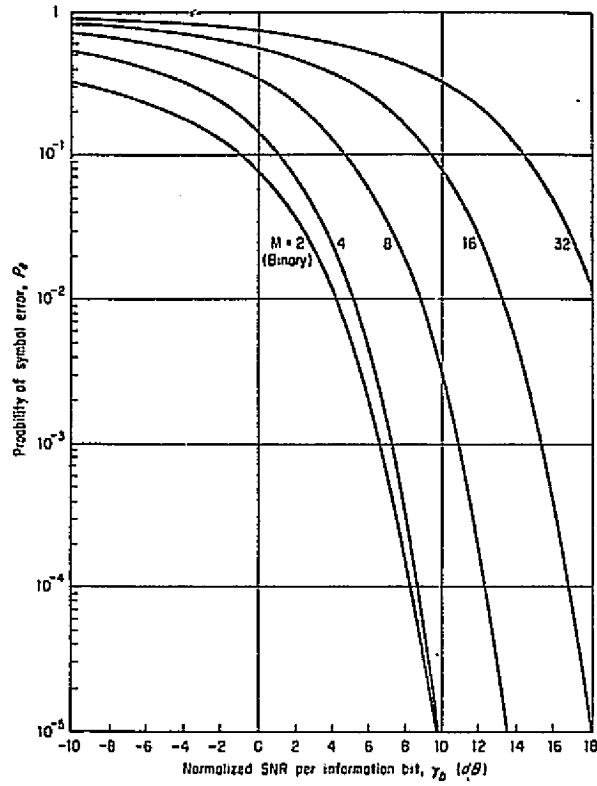


Figure 7-28. Error Rates for Coherent Multiphase Signaling

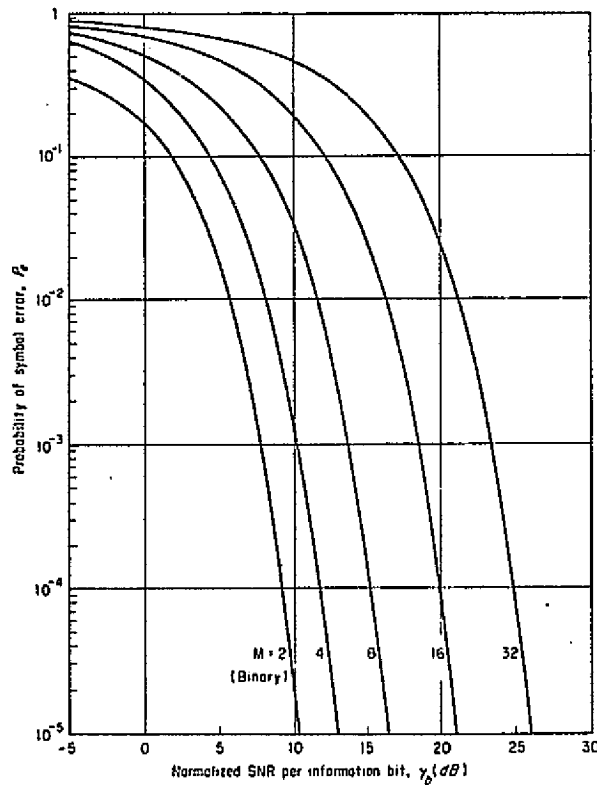


Figure 7-29. Error Rates for Differentially Coherent PSK

7.3.2.3 Analog Techniques. When the information is in analog form, PAPM is an attractive alternative to the more conventional SSB/AM or FM modulation methods as it provides some of the advantages of both.

TRW is currently investigating the performance of PAPM systems under a separate study which evaluates PAPM performance for several nonlinear mappings considering the effects of thermal noise, filtering, co-channel and adjacent channel interference, synchronization errors, and TWT nonlinearities. PAPM can provide a SNR improvement with a bandwidth that is determined by the baseband sampling rate, not the SNR improvement factor.

Although the use of more sophisticated modulation techniques such as APK or PAPM yield distinct performance advantages over more conventional methods, more complex and sophisticated modems are required at the high-data rates of interest. It is probable that the communications system would initially employ a conventional modulation technique such as biphase or quadriphase PSK perhaps with a rudimentary form of data compression. The system would have the capability for evolving into a more sophisticated and efficient network later as the state of the art permitted the use of high-speed APK or PAPM modulation. For additional information about APK or PAPM modulation techniques, see Appendix B, and Appendix C, respectively.

7.3.2.4 Bandwidth and Implementation Losses. The required bandwidth of a digital communication link must be considered in the light of spectrum utilization, and efficiency of information transfer. The former is concerned with the in-band bit rate and with minimizing modulation sidelobes and out-of-band energy. The latter two are very much a function of the modulation format, transmitter-induced non-linearities and transmitter filtering, all of which are transmitter-related. Information transfer efficiency is primarily related to in-channel factors such as modulation format, transmitter and receiver filtering and in-band effects of the transmission medium on both the signal and the total noise contribution at the detector input. We thus are concerned with the transmitted spectrum, as influenced by transmitter filtering, and with received signal and noise as influenced by receiver filtering.

The question that must be addressed is "what bandwidth is required for a given bit rate?", or "how many bits can be passed through a given channel?" There usually is no direct answer, since bandwidth can usually be restricted if one is willing to pay the price in terms of additional power to make up for additional implementation losses. Accordingly one looks for a way to answer the question for an ideal system, and a way to address implementation losses.

Recall that the error probability curves, previously presented, are plotted against signal to noise ratio, γ , normalized to signal energy per bit. For a given transmitter-receiver combination, γ will be largest when the receiver uses a matched filter having properties such that

- The filter's amplitude response versus frequency is proportional to that of the signal components.
- The filter's phase at each frequency negates the signal phase, with an additional phase variation which represents a time delay. (This phase characteristics results in phase-aligning all signal components so they add up to a maximum. This also distorts the pulse to a peak at the coupling instant).
- The noise power density spectrum, the weighting of the voltages at each frequency is inverse to the noise power density at that frequency.

Under these conditions, γ_b maximum will equal the energy contrast ratio, E_b/N_o , and the error rate will be minimized. Although the matched filter may or may not be realizable, it does not have an easily defineable bandwidth, but depends on the spectrum of the incoming signal. It does, however, offer the same advantage of maximizing signal to noise ratio and of causing $\frac{S}{N}$ to equal $\frac{E_b}{N_o}$. Thus, the error probability curves can be treated as referenced to E_b/N_o directly, with total received power equal to $E_b \times R$, where R is the bit rate. It follows that error probability curves with matched filtering make a convenient reference, with implementation losses charged to all factors which tend to aggravate the power budget to require increased transmitted energy.

We have not yet come to grips with bandwidth requirements, but we have defined a reference for implementation losses, i. e., the matched filter receiver.

Bennett and Davey distribute bandwidth limiting circuit elements between the receiver and the transmitter. They derive optimum filtering

conditions for flat gaussian white noise at the receiver input for common waveforms including baseband, FSK and PSK, and conclude in every case that an optimum configuration* is one in which

- The receiver uses a cosine filter.
- The transmitter output spectrum is adjusted to create a raised cosine spectrum at the input to the detector. Output power is charged to the after-filtering portion of the spectrum.

Since a raised cosine is equivalent to a cosine squared spectrum it follows that the receiving filter is a matched filter when the receivers' input noise spectrum is flat.

The base-band bandwidth of the optimum filter is chosen to be one half of the bit rate for binary signals. The equivalent RF bandwidth would be equal to the bit rate for Bennett and Davey's modulation formats. For the optimum filter, signaling efficiency, in bits/Hz of RF bandwidth is thus unity for binary systems. Higher order PSK systems will support $k = \log_2 M$ bits/Hertz. Multi-tone FM systems using one tone at a time, and matched filters, require a tone spacing equal to the symbol rate. For an optimum system with no inter-symbol interference, the required bandwidth between 3 db points of the outermost tone pulse is M times the symbol rate, or

$$B_t = \frac{2^k}{k} \cdot R \quad (7-11)$$

where R is the after coding bit rate. This is presented graphically in Figure 7-30 for optimized ideal systems.

In order to minimize implementation losses, practical systems tend to use bandwidths that are wider than the values shown in Figure 7-30. Even then, they also have implementation losses that vary from 1 to 4 db, depending on a variety of factors.

* Similar optimum results also apply for other less desirable filter forms.

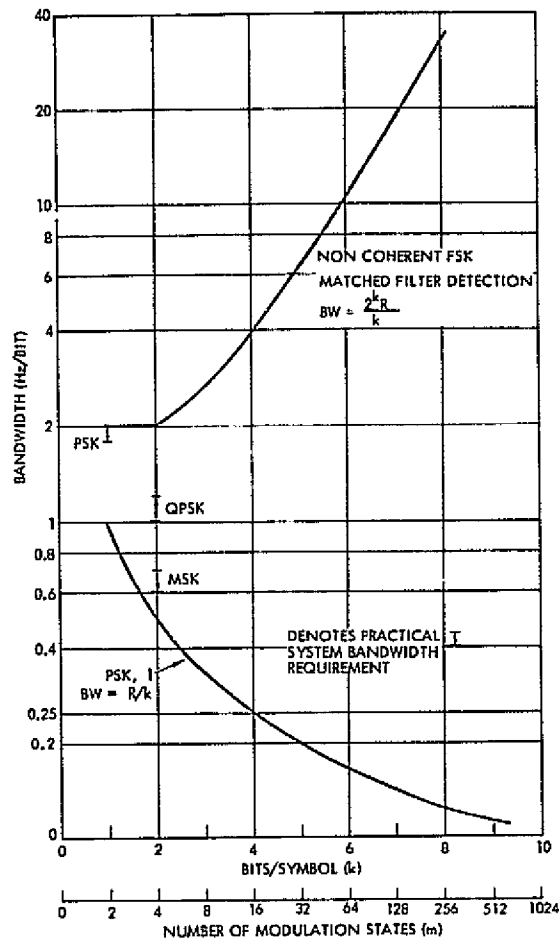


Figure 7-30. Bandwidth Requirement of Optimized Ideal System

To illustrate, consider Figure 7-31, which presents the spectrum of PSK, QPSK and MSK binary signals, as a function of the bit rate.

For the MSK spectral density the bandwidth between first nulls is 1.5 times the bit rate. This bandwidth is exactly intermediate between the nulls of the BPSK and QPSK modulations

The power excluded by an ideal rectangular filter should be as small as possible. The signal normally passes through a link whose overall bandwidth is about equal to the bit rate. The amount of power lost by bandpass filtering gives a lower bound to the link degradation (inter-symbol interference and adjacent channel interference may also contribute degradation). The power loss for MSK, BPSK and QPSK is shown in Figure 7-32.

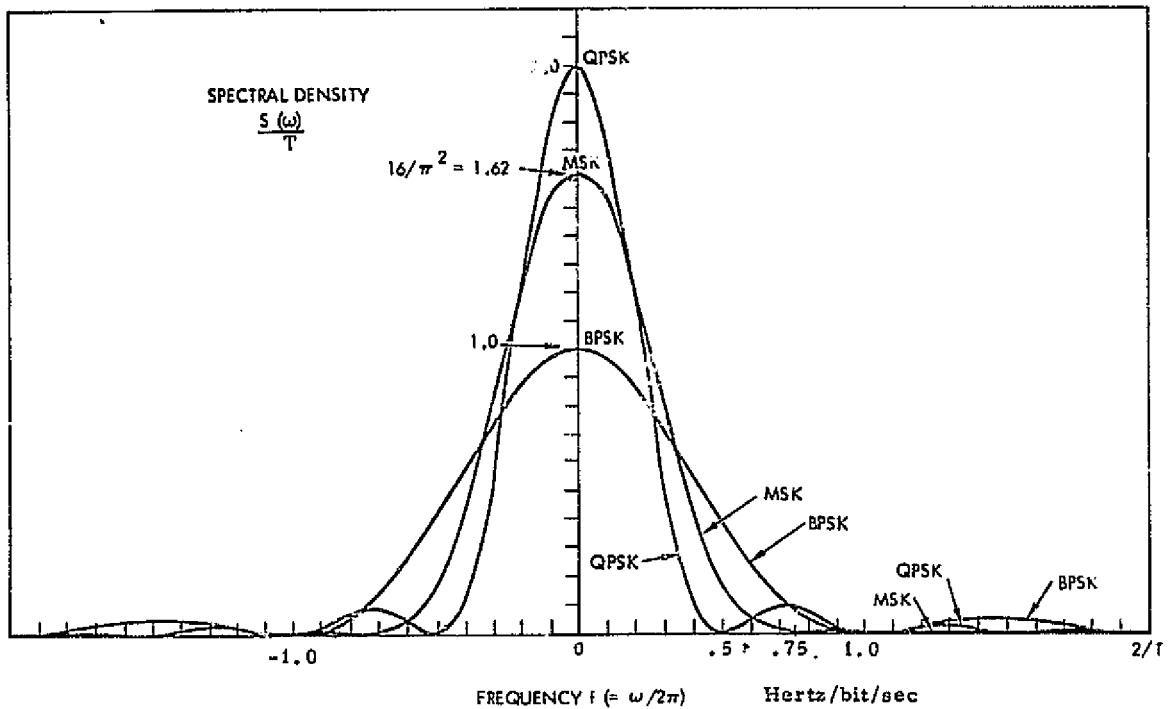


Figure 7-31. Spectral Density Functions of BPSK, MSK and QPSK

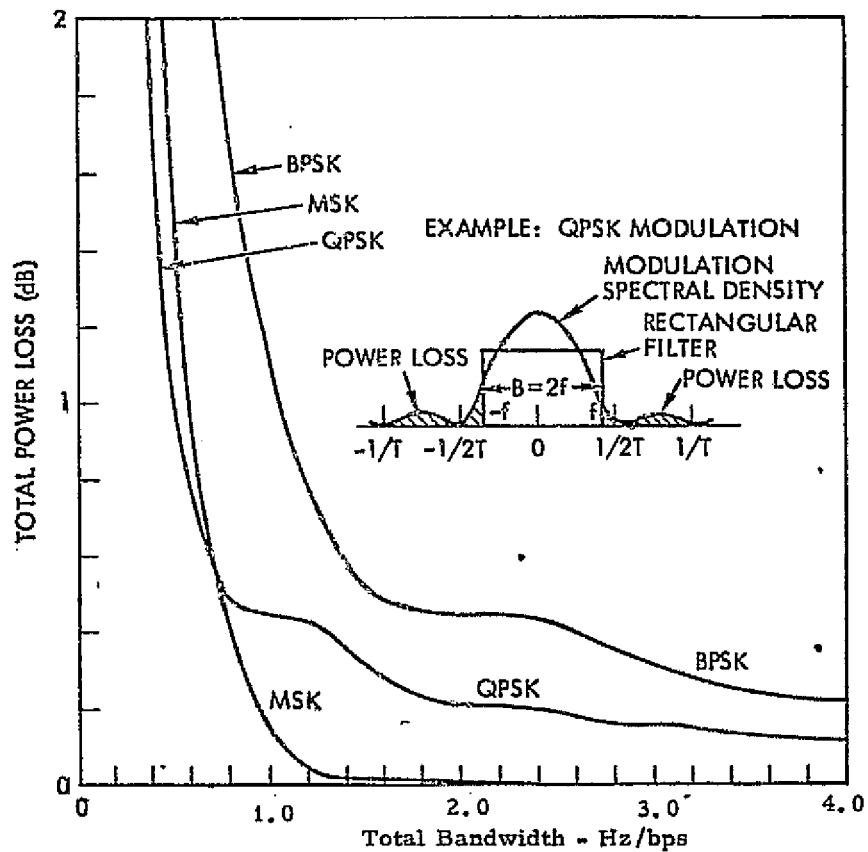
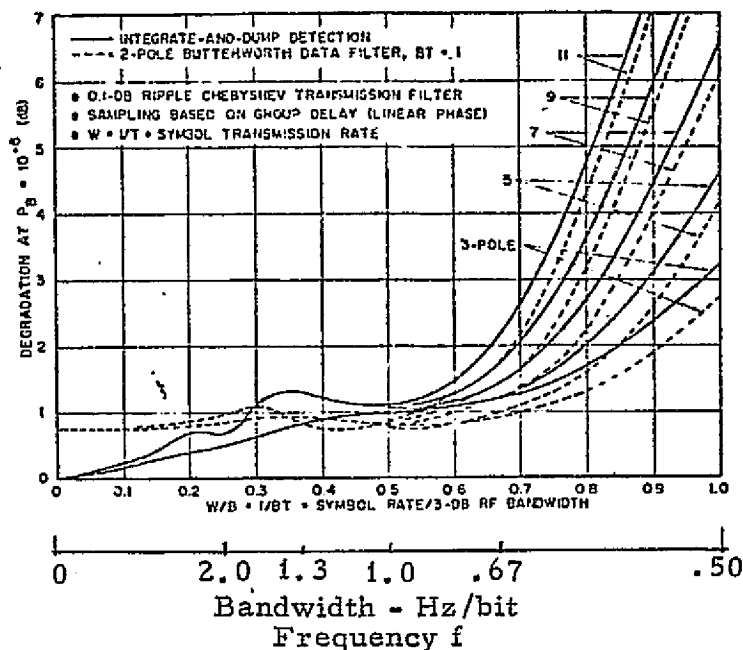


Figure 7-32. Power Loss Curves

For example, consider a filter with bandwidth equal to the bit rate. The power loss for MSK is negligible, but about 0.44 dB for QPSK and about 1.1 dB for BPSK. Notice that the QPSK loss curve is almost flat at this point and down to a bandwidth of about 0.8 times the bit rate. The QPSK power loss even at this narrow bandwidth is less than 0.5 dB.

The total degradation $\Delta E_b/N_0$ ratio for QPSK at bit error rate 10^{-6} is shown in Figure 7-33. A chebyshev transmission filter with between 3 and 11 poles is assumed. This curve includes degradation due to power loss, degradation due to intersymbol interference, mismatched detection filter and group delay of the signal. Data filters, for detection, after the input filters are either integrate-and-dump filters, or 2 pole butterworth filters.



(Transmission filter 3 dB RF bandwidth = $2f$)

Figure 7-33. Degradation due to Transmission Filtering Versus Filter Cut-off Frequency f for QPSK

For a bandwidth equal to the bit rate the degradation is about 1 dB for all the filters. This 1 dB includes the previously specified 0.44 dB due to power loss only, plus the additional degradation sources. Furthermore, the degradation is approximately 1 dB for all bandwidths between 0.9 and 1.4 times the bit rate.

Jones has shown that for QPSK the total degradation due to symmetrical band-pass filtering (including power loss) is 1.0 dB for a bandwidth of two times the symbol rate (symbol rate = 2 x bit rate) and a bit error rate of 10^{-6} . Increasing the bandwidth does not improve performance at all for symmetrical filtering. However, Jones' analysis shows that degradation increases rapidly for bandwidth less than 2.0 times the symbol rate. For example, a bandwidth of 1.4 times symbol rate causes a degradation of from 1.5 dB to almost 3 dB depending on the number of poles in the transmission filter.

Cuccia indicates that the bandwidth used for a QPSK system should be 1.3 times the bit rate in order "to avoid undue degradation due to group delay distortion." However, Jones' analysis indicates that a QPSK signal which has been bandlimited to 1.0 times the bit rate is not sensitive to parabolic or cubic phase distortion. Cuccia does not elaborate on what is meant by "undue degradation"; however, the extra degradation caused by decreasing the bandwidth from 1.3 to 1.0 times the bit rate is probably less than about 0.7 dB in a real system.

Jones curve of Figure 7-33 applies to PSK signals when "bits" are replaced by "symbols", and it is recalled that there is one bit per PSK symbol instead of two as for QPSK. Thus, the bandwidth for PSK would be double that for QPSK, or in the range of 2.0 Hz per bit.

For further comparison, the losses incurred by a pseudo-noise DPSK sequence when filtered by a sharp out-off linear phase band-pass filter causes correlation losses illustrated in Figure 7-34. The two curves shown correspond to the losses referenced to the signal power before and after filtering. Losses introduced by parabolic phase distortion and finite bandwidth are as shown in Figure 7-35. From these two curves, one is inclined to agree with commonly accepted values of bandwidths equal to 1.8 Hz/bps for binary PSK with filtering implementation losses on the order of 1.0 db.

Mathwisch, et al develop bandwidth requirements for MSK systems with and without limits, using a 4 pole butterworth transmitter filter and a linear phase gaussian channel filter ahead of an ideal receiver. For this

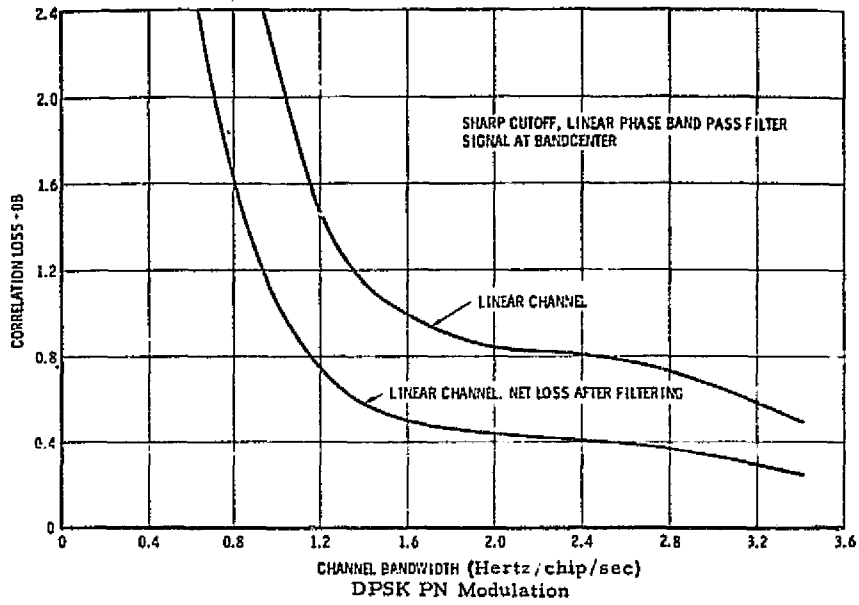


Figure 7-34. Correlation Loss Due to Filtering

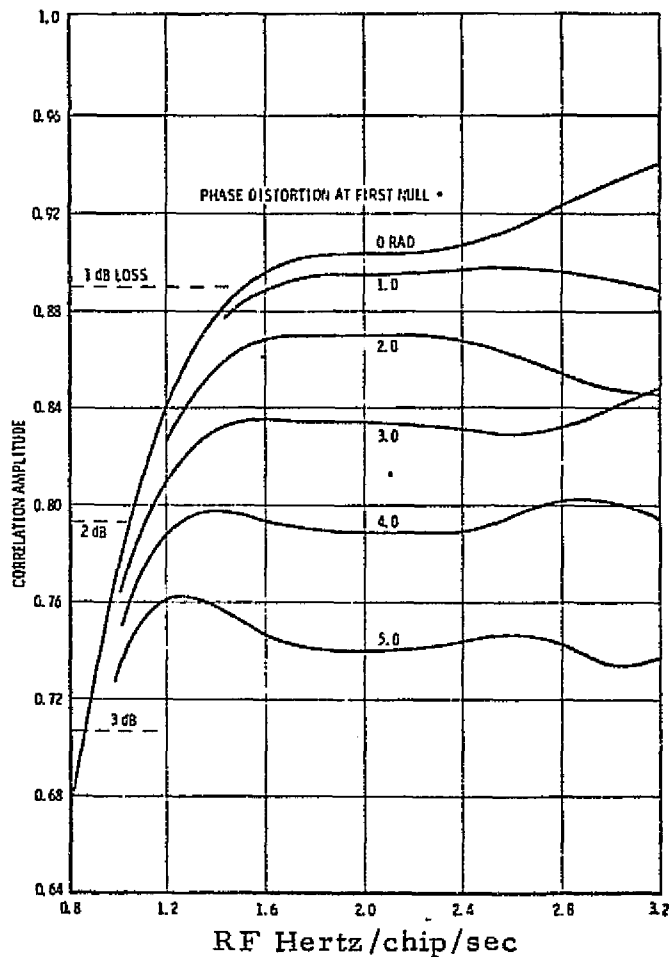
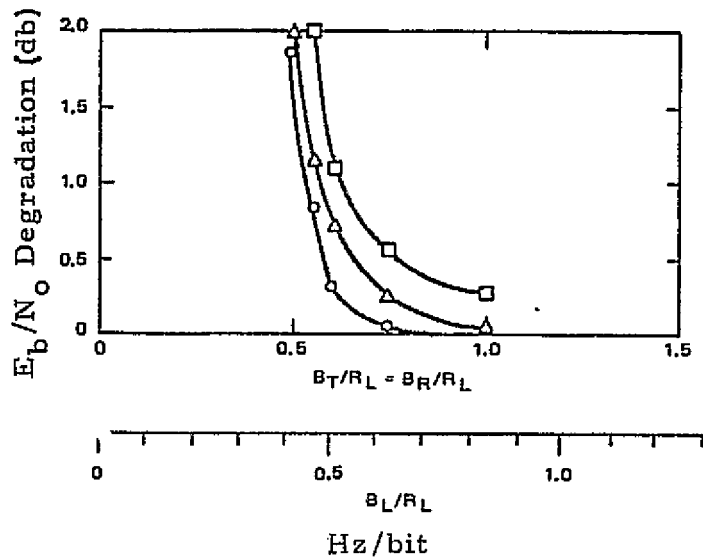


Figure 7-35. Loss Due to Parabolic Phase Distortion and Finite Bandwidth

combination, 3 db system bandwidth ratios of 0.6 Hz/bit cause a theoretical degradation of less than 1 db. Figure 7-36 illustrates their theoretical results for a BER of 10^{-5} .



Legend

- Δ Band and amplitude limiting
- Band limiting only; normalized to transmit filter input power
- Band limiting only; normalized to average transmit filter output power
- BR Receiver bandwidth
- BT Transmitter bandwidth
- BL Bandwidth of composit system
- RL Link bit rate

Figure 7-36. E_b/N_0 Degradation Versus Normalized Bandwidth at 10^{-5} BER for MSK

Note, however, that they reference degradation to over-all system bandwidth. Transmitter and receiver 3 db bandwidths are approximately 20 percent greater. Their experimental verification produced additional implementation losses of approximately 1.4 db, not including losses related to synchronizing the integrate and dump circuits. It seems prudent, at this time to assume a practical link bandwidth of 0.6 - 0.7 Hz/bit with approximately 2 db implementation losses.

FSK systems with non-coherent detection often use integrate-and-dump detection filters for data rates in the kilo-bits to low mega-bit range. For tone spacings equal to the multiples of the bit rate, I&D matched filters centered on each tone, and perfectly synchronized, will give zero inter-symbol distortion and cross-talk. At the higher bit rates, losses associated with synchronizing the I&D switching circuitry, discharge times, etc., become significant. For these higher frequencies, 2-pole Butterworth filters followed by envelope detectors become more practical to discriminate between the tone-channels. The tone-spacings will depend on acceptable inter-symbol interference and implementation losses. For a simple one-pole filter, channel spacings need be 1.5 for 20 db inter-symbol interference, or $2.1 R_1$ for 30 db intersymbol interference. Pre-detection filters will increase cross-talk, depending upon their phase and envelope distortion. For planning purposes, however, bandwidth ratios of 2.0 are reasonable, with insertion losses of 1.5 to 2 db.

In summary, it is proposed that reasonable bandwidth design goals, and initial implementation loss estimates for MSK, PSK and QPSK be as shown in Table 7-5. Higher level systems would be adjusted in the same

Table 7-5. Bandwidth Ratios for Practical Systems

Modulation	Bandwidth Hz/Bit/Sec	Representative Implementation Losses - db
<u>MSK</u>	0.6 - 0.7	2
QPSK	1 - 1.2	2.0 - 1.5
PSK	1.8 - 2.0	2.0 - 1.5
FSK	2.0	1.5 - 2.0

ratios, relative to symbol rates. The values listed in Table 7-5 are plotted in Figure 7-37 for comparison to ideal values.

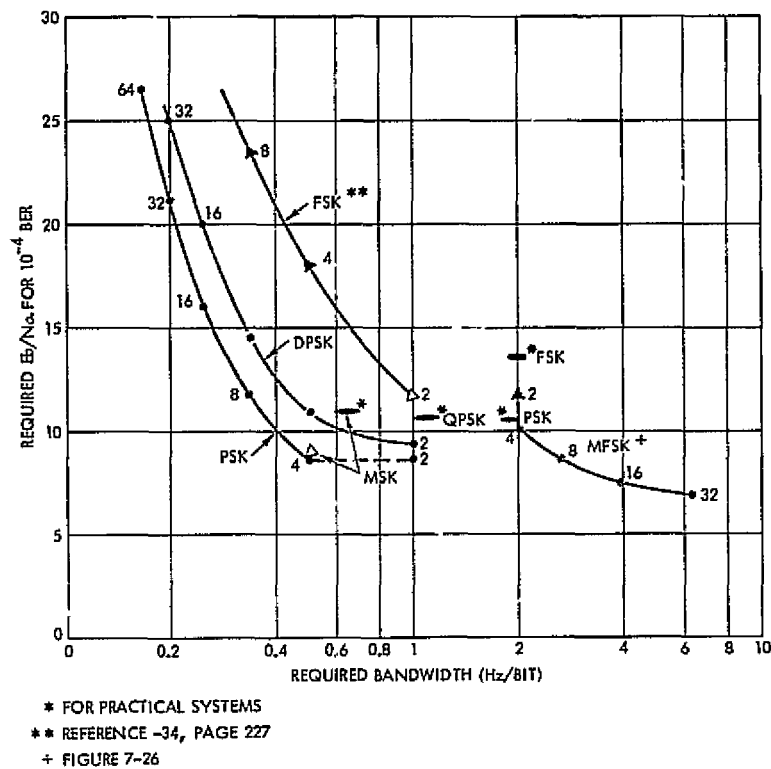


Figure 7-37. Required Bandwidths Versus E_b/N_o

7.3.2.5 Comparison of Higher Order Modulation Systems. Bennett and Davey compare modulation systems, with varying number of states, by comparing required S/N to bits/hertz of bandwidth at 10^{-4} BER level. They choose a form of multi-tone FM modulation which packs more and more filters into the given bandwidth, and as one would expect the higher SNR's since required bandwidth per bit is diminishing. This is also true of PSK systems, but one expects narrower bandwidth with PSK, whereas FSK usually is implemented to use wider bandwidths at lower E_b/N_o . In use wider bandwidths at lower E_b/N_o . In order to put things in perspective, PSK, DPSK and FSK are compared in Figure 7-37 which presents required E_b/N_o against bandwidth requirements in Hertz/bit of information. Ideal bandwidth efficiencies are used as a point of reference. The FSK curve is extended from the high channel packing region, a la Bennett and Davey, to the wider bandwidth case reviewed in Section 7.3.2.3.

As one would expect, increasing bandwidth permits reducing the required signal to noise ratio. Regions with good bandwidth efficiency

towards the left of the abscissa require increased signal to noise ratio, with PSK, DPSK and FSK requiring increasingly more energy.

Further, the usual perversity of nature sets in, and we find that the simplest system to implement (FSK), requires more power, whereas PSK which require less power also requires more complex hardware to implement. The latter includes such circuits such as phase-lock loops, or Costas loops to track or generate a reference carrier.

In general, when one is confronted with a starved bandwidth situation, it will be necessary to determine the bandwidth efficiency required in Hertz/bit, then to select the simplest modulation structure compatible with available system power budget, i. e., FSK is simpler, but requires increased transmitter ERP and increased receiver sensitivity.

In summary, the key aspects of candidate modulation techniques are as follows:

Type	Characteristics
PSK	<ul style="list-style-type: none"> ● Most efficient binary scheme ● May be suppressed carrier or not ● Requires receiver phase reference
QPSK	<ul style="list-style-type: none"> ● Same efficiency as PSK, 1/2 bandwidth
M-ARY PSK	<ul style="list-style-type: none"> ● Bandwidth conserving ● Decreased efficiency
MFSK	<ul style="list-style-type: none"> ● No phase coherence ● Efficient for large alphabet (>8) but increased bandwidth
APK	<ul style="list-style-type: none"> ● Bandwidth conserving ● Nonconstant envelope ● More efficient (>bits/Hz) than M-ARY PSK ● More complicated demodulator
MSK	<ul style="list-style-type: none"> ● Bandwidth conserving ● Efficiency approaches QPSK

7.3.3 On-Board Antennas


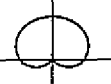

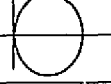

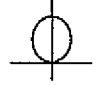


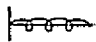
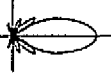
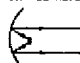
7.3.3.1 General. An interesting variety of special communication problems are generated for the spacecraft antenna system that involve unique considerations and difficulties differing in both degree and kind from those associated with earth-based facilities and terminals. Highly efficient point-to-point communications are going to be required in which the space vehicle itself may constitute either a point of origin of transmissions or a relay station, depending on the particular mission. A higher SNR will be required of the energy from the satellite, especially in the final, possibly power-limited, link down to earth. Also, motion is to be expected of either or both terminals of a communication link with respect to any particular choice of reference frame. New environmental demands must be met including those imposed by the ambient vacuum, temperature extremes, and micrometeorite bombardment. Reliability assumes extreme importance with spacecraft antenna systems since neither repair nor servicing is possible with present-day technology.

The stringent weight restriction on equipment that is inherent in all space missions translates for the antenna system rather directly into limitations of the available power and size of communication equipment. Transmission of signals to and from space vehicles will involve communication data rates over distances which, even for an earth-orbiting satellite, are great. The implications of the weight limitations and the high communication data rates joint to the desirability and necessity of achieving as much directivity and efficiency in the antenna structure as the mission situation will permit.

Not all missions, however, will permit an arbitrary selection of the antenna to be used, since beamwidth and gain are inversely proportional. There will be classes of missions requiring simultaneous access to terminals anywhere on the earth's surface within view of the spacecraft. For these missions broad-beam or earth-coverage patterns are required. Other missions may not be so constrained, and high gain narrow beam antennas, will be permitted. Accordingly, selection of the spacecraft antenna system depends upon the antenna pattern constraints.

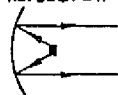

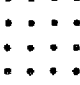
Tables 7-6a and 7-6b summarize key characteristics of representative low, medium and high gain antennas suitable for spacecraft

Table 7-6a. Candidate Antennas for ERS Spacecraft Low/Medium Gain

TYPE	PATTERN	POLARIZATION	GAIN (DBI)	BEAM-WIDTH (DEG)	MAXIMUM FREQUENCY (GHz)	BAND-WIDTH (PERCENT)
LOW-GAIN (OMNI) 1. LOG CONICAL SPIRAL 		CP	2 - 5	120 - 220	X-BAND	65
2. ARCHIMEDEAN SPIRAL 		CP	5 - 7	70 - 90	X-BAND	65
3. CROSSED-DIPOLE 		LP, CP	4 - 7	70 - 110	X-BAND	20-30
MEDIUM-GAIN 1. HORN 		LP, CP	8 - 20	15 - 65	Ku-BAND	30
2. HELIX 		CP	8 - 15	30 - 65	X-BAND	50
3. ARRAYS HELICAL CROSSED DIPOLE PC CROSS SLOT WG SLOT	SIMILAR TO HORN	CP CP CP CP	18 - 25	8 - 18	X-BAND X-BAND S-BAND Ku-BAND	30 8-10 8-10 5-6
4. SMALL REFLECTOR 	SIMILAR TO HORN	CP, LP	18 - 25	9 - 20	DETECTED BY FEED	30

ORIGINAL PAGE IS OF POOR QUALITY

Table 7-6b. Candidate Antennas for ERS Spacecraft High-Gain

TYPE	PATTERN	POLARIZATION	GAIN (DBI)	BEAM-WIDTH (DEG)	MAXIMUM FREQUENCY (GHz)	BAND-WIDTH (PERCENT)
1. PARABOLIC REFLECTOR 	 "PENCIL" BEAM	LP, CP	20 - 50	0.5 - 16	DETERMINED BY FEED	30
2. PHASED ARRAY * 	SIMILAR TO REFLECTOR	LP, CP	20 - 50	0.5 - 16	DETERMINED BY ELEMENTS	DETERMINED BY ELEMENTS
3. WAVEGUIDE ARRAY	SIMILAR TO REFLECTOR	LP	20 - 50	0.5 - 16	X-BAND	5 - 6
4. ARTIFICIAL DIELECTRIC LENS	SIMILAR TO REFLECTOR	LP, CP	20 - 50	0.5 - 16	Ku-BAND	30

* KEY TECHNOLOGY AREA.

use. The higher gain antennas have increased directivity and the necessary degree of pointing accuracy required of the spacecraft antenna also increases. Two limitations are encountered here: 1) in the capability of a vehicle to control its mechanical orientation, and 2) in the accuracy to which this orientation may be determined at any given time. To achieve good performance, high gain is the basic requirements and controls the characteristics of a satellite communications antenna. High gain implies:

- A beam from the satellite that is narrower than a beam that would subtend the earth
- An aperture that is large compared to wavelength
- A steering mechanism that points the beam continuously at one or more selected locations on earth.

The beam motion is an integral part of the antenna problem. Three types of beam motion are possible, of which the most promising is also the least developed: 1) mechanical, including large appendage antennas, 2) electromechanical, and 3) electronic or inertialess. Short of these limitations, the question exists of the extent to which control of the vehicle attitude is advisable in a given set of circumstances. The answers from an engineering standpoint entail practical compromises and depend on the techniques available for antenna searching and tracking as compared with vehicle control methods. A consideration of antenna techniques must thus be incorporated into any overall system design for a mission, in order that essential tradeoffs in weight, accuracy, and reliability can be determined. Some of these factors are tabulated in Table 7-7.

Various kinds of space communication links have been considered in this study in an effort to provide descriptions of antenna and antenna system techniques that would improve overall gain characteristics. Available techniques for all-electronic beam formation, shaping, and steering, were surveyed and their applicability to specific space missions assessed, even though the devices presently available for the reliable control of individual radiating elements involve considerable bulk and weight.

The functions of the communication systems studied demand high-gain beams that can be despun and pointed at electronic speeds. This

Table 7-7. Beam Antenna Considerations

Type of Antenna	Applicable Type of Stabilization	Coverage	External Pointing Control	Bandwidth	Reliability Factors	Problem Areas
Reflectors and Feeds	Gravity	A few beam-widths off axis	Pilot signals or pre-programmed controls	Inherently broadband; limited by feed and crossover level changes	Failure of switch causes loss of beam(s)	Gain degradation beyond a few beam-widths Aperture blockage
Thin optical lenses and feeds	Gravity	A few beam-widths off axis	Pilot signals or pre-programmed controls	Unzoned solid dielectric broadband Zoned: less broadband $BW = \frac{25}{M} \%$ (dielectric)	Failure of switch causes loss of beam(s)	Weight and feed array
Spherical optical lenses and feeds	Gravity	Beams may be positioned within cone of half-angle $60^\circ - 70^\circ$	Pilot signals or pre-programmed controls	Solid dielectric: broadband (octave) Artificial: less broadband	Failure of switch causes loss of beam(s)	Weight
Constrained lenses and feeds	Gravity	Beams may be positioned within cone of half-angle 50°	Pilot signals or pre-programmed controls	Narrow band (on the order of 10 percent)	Failure of switch causes loss of beam(s)	Feed array
Arrays with beam-forming matrices	Gravity	Beams may be positioned within cone of half-angle 45°	Pilot signals or pre-programmed controls	Matrices can be made broadband (octave)	Failure of switch causes loss of beam(s)	
Self-phased arrays	Gravity Unstabilized spin	All require r-f pilot	Pilot signals or pre-programmed controls	Limited by size of array and by scan coverage	Fails gracefully	Lightweight components are needed; phase coherence required between channels is limited by component characteristics
Adaptive arrays	Gravity Unstabilized				Fails gracefully	

demand implies lightweight antennas that can be integrated into the surface of the vehicle. Those functions that require high power gains in certain areas of space need antennas of sufficient size in wavelengths to effectively collimate the radiated or received energy. Each antenna system must be capable of finding a small target and tracking it under diverse operating conditions. Various stabilization configurations were also considered and suitable antenna techniques were juxtaposed with the missions (see Figure 7-38).

As a result of the antenna techniques survey embodied in this report, several conclusions for applicability of the various methods have been reached. The following sections briefly review key considerations related to earth coverage antenna and to the more directive antenna subsystems.

7.3.3.2 Earth Coverage Considerations. A well known rule-of-thumb for antenna gain, is

$$G = \frac{27,000}{\Theta_E \Theta_H} \quad (7-13)$$

where Θ_E and Θ_H are the E and H plane half power beamwidths. This

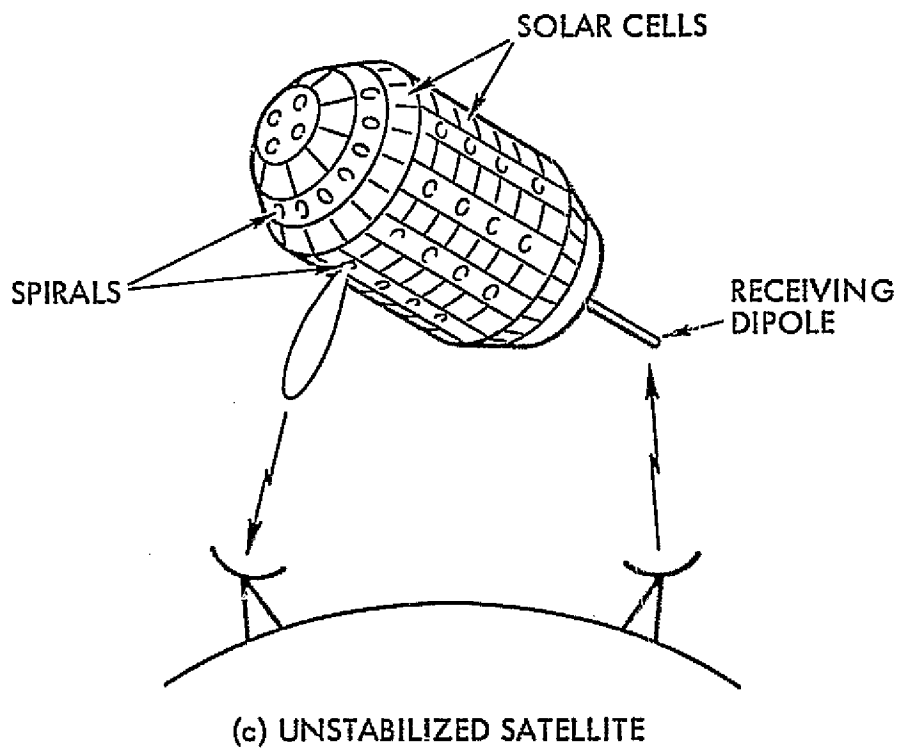
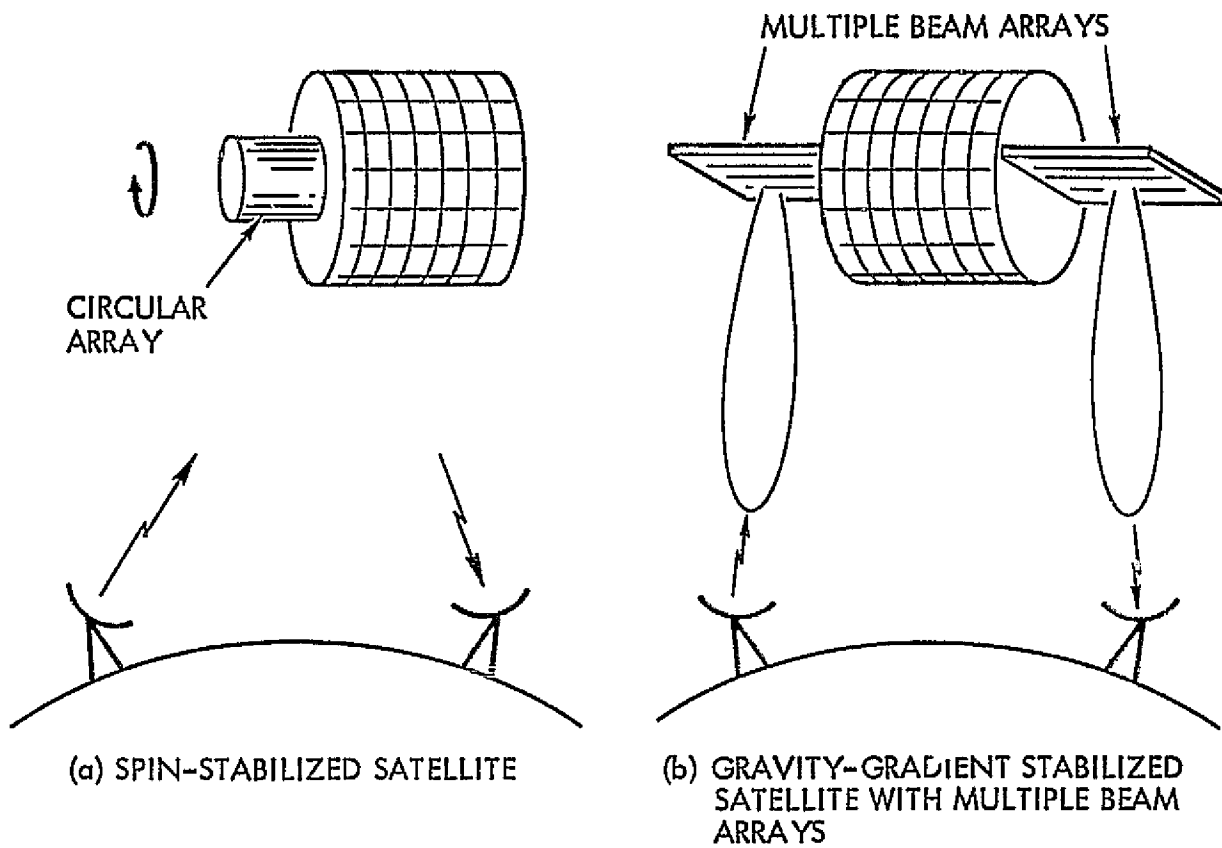


Figure 7-38. Possible Antenna Configurations

equation is often used to estimate directivity gain from pattern measurements. The equation is felt to be accurate to within 25 percent, or approximately 1.25 db, with accuracy improving for narrow beam high gain antennas.

A spacecraft mounted antenna whose pattern subtends the earth's disc at the 3 db point would have a gain of approximately

$$G = 44.3 - 20 \log_{10} \left[2 \sin^{-1} \frac{r}{r+h} \right] \text{ decibels} \quad (7-14)$$

where

$$2 \sin^{-1} \frac{r}{r+h} \text{ corresponds to the subtended angle, } \beta.$$

For a geosynchronous altitude spacecraft, the included angle would be 17.5 degrees, and the gain approximately 19 db. For lower altitude orbits, the gain is correspondingly lower, ranging down to 2 db for a spacecraft orbit altitude of 707 km.

We see that earth-coverage antennas to be used for low orbit spacecraft have low to medium gains, represented by the antenna of Table 7-7. Each of these is relatively straightforward to design and build, with the important details contained in the standard handbooks such as Jasik's "Antenna Engineering Handbook."

7.3.3.3 High Gain Antennas

Paraboloidal Reflectors. The possibility of using a paraboloidal reflector on a gravity-gradient stabilized satellite has been considered. In this application; the reflector would be located on the base of a cylindrical or cubical satellite structure with the antenna axis directed along the satellite axis. In the absence of librations this axis would be directed through the center of the earth. These antennas are not desirable for electronically scanning a beam over large angular regions. Problems of aperture blockage are severe and array type feeds are required to obtain proper beam positions and small spillover. They might be used for restricted angular coverage since, in general, scans of a few beamwidths can be achieved without pattern deterioration.

Reference 41 reports the off-axis scanning capabilities of paraboloidal reflectors. It shows that only limited scan angles may be

achieved without serious sidelobe and gain degradation. For example, a scan of about 5 half-power beamwidths with a 30-inch reflector, which has a 3-degree half-power beamwidth and a 20-db aperture taper, has a gain loss of about 1.5 db. The sidelobe level increases from about -26 db to -14 db, an increase of approximately 8 db. These measurements were taken using a single-feed horn mechanically moved off the axis.

Spherical Reflectors. These antennas are also not desirable for satellite communication application. They are capable of wide-angle scan with a single mechanically moved feed, but electronic scanning requires the presence of array feeds that result in aperture blockage. With either type of scanning, inefficient use is made of the aperture. As shown in Reference 17 symmetry of the spherical surface eliminates beam deterioration over wide-scan angles, at least when a single movable feed is used to scan the beam. When a cluster of switched feeds is used for electronic beam steering, however, perfect symmetry is not maintained as various feeds are connected, so that some beam shape changes might be expected to occur as the beam is stepped throughout the required coverage region. Other factors also affect the applicability of the spherical reflector to electronically scanned antennas.

The spherical reflector does not have a well defined focus so that a point-source feed gives a rise to phase errors over the aperture. If it is assumed that the aperture is uniformly illuminated (the primary pattern must in reality be tapered in order that the aperture be limited to a (specific value), that a 3 degree beamwidth is preserved, and a maximum scan angle of 18 degrees (corresponding to a synchronous altitude orbit) is used, about 41 percent of the physical aperture available may be used to produce the beam. If the aperture taper is taken into account, this area is further reduced. It is apparent that such a system makes very inefficient use of the physical aperture. In addition, aperture blockage will also be a problem area when clusters of feeds are used. The feed problem might be solved by using arrays to form the primary aperture as discussed in the previous section on paraboloidal reflectors. For these reasons, the spherical reflector is not too attractive for a scanning antenna.

Other types of reflectors may appear to be adaptable to electronic scanning requirements in certain respects. However, it is felt that the

aperture blockage and feeding techniques will remain problem areas and this type of antenna system has not been pursued further.

Thin Optical Lens and Wide-Angle Scanned Dielectric Lens Antennas.

The use of lenses with multiple switched feeds for electronic scanning would apply most readily to a satellite using the gravity-gradient type of stabilization. Various types of dielectric and metal plate lenses have been studied by a number of investigators and are reported in several places. These antennas have a problem as they require array feeds to obtain proper beam spacing. Unless primary phased arrays are used to feed them they are limited in their achievable scan angle before pattern deterioration occurs. However, aperture blockage is not a problem with lenses. Solid dielectric lenses are broadband but may be heavy. Zoned lenses are less broadband but lighter. The use of artificial dielectrics can decrease weight but will increase dissipative losses and frequency sensitivity.

Both dielectric lenses and metal plate lenses whose radiation characteristics are optimum along, or symmetrical about, a certain axis fall into the class of lenses with an optical axis.

Dielectric lenses are designed on the basis of geometrical optics (Snell's law). The surfaces are chosen in such a way that rays emanating from a point (focus) on one side of the lens emerge as parallel rays on the opposite side of the lens. The radiation pattern of the lens is computed from the resulting field distribution over an aperture near the lens surface.

Metal plate lenses may be designed on a similar optics basis, but one type, the so-called constrained lens, does not depend on Snell's law for its operation and merits separate discussion.

Most optical systems can be designed so there are no phase errors over a given plane aperture for one particular position of the feed, usually the lens axis. When the feed is removed from this position, however, the resulting aperture distribution has phase errors, which contribute to beam pointing error, pattern asymmetry, gain reduction, and increased sidelobe levels. With dielectric lenses it is possible, through use of the Abbe sine condition (Reference 18) to improve the off-axis pattern characteristics. When this condition is satisfied, "coma" effects are

reduced for source positions near the lens focus and lens scanning performance is improved. Even with this improvement, scanning is still restricted to relatively small angles. An example of a wide-angle scanned dielectric lens that employs the Abbe sine condition to improve scanning performance is discussed by Friedlander in Reference 19. The lens has a constant dielectric with a plane surface on the feed side. The ideal value of the index of refraction, \underline{n} , was found to be $n = 1.618$ but Friedlander used a slightly different value. For a lens in which $D = 50\lambda$, he was able to obtain a scan of ± 10 degrees from the axis with satisfactory beam performance. If it is assumed that the aperture illumination was tapered as $\left[1 - \left(\frac{\rho}{2D}\right)^2\right]$, then the half-power beamwidth of the antenna is given by

$$\text{Beamwidth}_{1/2} = 1.27 \frac{\lambda}{D} \text{ radians}$$

$$\text{Beamwidth}_{1/2} = 1.45 \text{ degrees}$$

Thus, the scan angle is equivalent to 6.9 half-power beamwidths. If the D/λ ratio is halved by reducing the frequency, the beamwidth would increase to about 3 degrees and a scan angle of ± 15 to 20 degrees might be achievable within the same limits of phase error over the aperture. These results would depend on how the phase error distribution over the aperture varied with feed position, so the number of beamwidths that would be scanned is not independent of frequency. Even lenses designed for wide-angle scanning of fairly narrow beams are still restricted rather severely in their scan capabilities. Thus, an array technique would be required for feeding such a lens. However, in order to obtain wide angle scan, this primary feed array would have to be phased to correct for lens aberrations; otherwise, only limited scan is achievable. In view of the rather limited scan angle achievable without phasing, this lens system is apparently not generally applicable to the space missions of interest.

Wide-Angle Scanned Constrained Lens. These antennas, which force rays to follow prescribed paths, can be designed for wide-angle coverage. They still have the requirement that array feeds are necessary

to obtain overlapping beams. They may also be frequency sensitive because of dispersion in the constraining paths. Constrained lenses, which do not obey Snell's law, may be designed to scan over fairly broad angular regions. These lenses use parallel metal plates which constrain the waves to follow prescribed paths. If the metal plates are arranged in an egg-crate fashion so that they form square dominant mode waveguides, then waves of any polarization will be accepted and constrained to follow these waveguides. By adjustment of the input and output surfaces of these lenses, desirable radiation characteristics may be obtained over relatively wide-scan angles. Such lenses are discussed by Ruze (Reference 20) and are considered in two-dimensions. However, the general technique applies to three-dimensional lenses. For example, if a lens aperture \underline{D} , is 72 wavelengths and $f_o/D = 1.5$, it is possible that with the feed located on a feed locus of radius f_o , there are no phase errors in the aperture for feeds positioned at angles of ± 45 degrees with the axis. With the feed on axis at f_o , there is no quadratic phase error over the aperture. Under these conditions the antenna was capable of scanning a 1 degree (half-power beamwidth) beam over a ± 50 degree range. Reference 20 also gives a relation between the f/D ratios, half-power beamwidth, θ_s , and the total scan angle for this type of lens as

$$\theta_s = 93^\circ \left[BW_{1/2}^o \left(\frac{f_o}{D} \right)^2 \right]^{1/3}$$

For the particular antenna considered, it can be found that $BW_{1/2}^o = 65^\circ \lambda/D$ so that

$$\theta_s = 374^\circ \left[\lambda/D \left(\frac{f_o}{D} \right)^2 \right]^{1/3}$$

For $D = 75\lambda$ and $f_o/D = 1.50$, this relation gives $\theta_s = 113^\circ$, in substantial agreement with the experimental results. If D/λ were decreased by a factor of three, i.e., if the beam had a half-power width of 3 degrees, then the scan angle θ_s , is increased to $\theta_s = 163$ degrees so that a sector of ± 81 degrees could be scanned.

Feeding Techniques. In all the reflector and lens antennas considered, it was shown that the primary aperture dimensions required are greater than the displacement of the primary aperture necessary to obtain a scan of 0.5 power beamwidth. Thus, to obtain electronic scanning, it appears that the primary aperture must be composed of an array of small (i.e., approximately half wavelength) radiations, which can be excited in combinations, to produce the desired effective primary aperture. If this array were conformal with the locus of the focal point as the array is scanned, then the array elements could be fed in phase and only on-off switching or a smooth transfer of power between elements would be required to obtain beam scanning. This technique would not be able to correct for aberrations resulting from the effective motion of the primary aperture.

The technique of White and DeSize (Reference 21), on the other hand, uses a surface that usually does not coincide with the locus of focal points and thereby requires phase as well as amplitude control to achieve proper illumination. It is capable of correcting the various aberrations that might otherwise occur in electronic scanning but is more complicated than the system without phase control. Since in lens antenna systems, aperture blocking would not be a problem, either technique might be applied. The relative merits of each would depend on the particular system requirements. In any event, additional investigation of the techniques would be required before any specific recommendations could be made.

Losses. Several effects contribute to losses in lens antennas. In both dielectric and metal-plate lenses, reflection losses occur at the air-dielectric or air-metal plate interfaces. These losses depend on polarization and incidence angle of the radiation as well as on the effective lens dielectric constant and may result in a gain reduction of 0.5 dB. They may be reduced by the use of matching techniques into and out of the lens. Dissipation losses in dielectric lenses may also be a problem; however, they depend on the type of lens and the loss tangent of the material used. For low-loss dielectric lenses (loss tangent = 0.001), which are zoned to keep them thin, dissipative losses are on the order of less than 0.1 dB.

Spherical Lenses With Multiple Feeds. This variety of lenses provides wide angular coverage, and with a cluster of feeds arranged on a spherical cap, the antenna is applicable to a gravity-gradient stabilized satellite. With a belt of feeds surrounding the lens on a great circle, the antenna is applicable to a spin-stabilized vehicle. In the first configuration, for example, the antenna could be placed on the earth-directed face of the satellite. The feeds, and somewhat less than half the lens, would be set in a recessed portion of the satellite. In the second configuration, the lens and feeds would have to be supported on the satellite spin axis but far enough away from the satellite to avoid interference between lens and satellite. In this form, it would be an appendage antenna. Weight is a problem if solid dielectrics are used for the lenses. Artificial dielectrics are lighter but have higher losses that can be up to 3 db more than for the solid lenses. In addition, the volume of these lenses, as with thin optical and constrained lenses, is relatively large since their depth is equal to their aperture.

Since spherically symmetric lenses do not have any preferred optical axes and, therefore, maintain their radiation characteristics for all positions of a feed, they are inherently wide-angle scan lenses. Several types are of interest: 1) Luneberg lens, 2) Constant dielectric lens, and 3) Broadbeam Luneberg lens.

Luneberg Lens. The Luneberg lens is a sphere of dielectrically loaded, radar-transparent material. The dielectric constant increases from that of air at the periphery to twice this value at the center. The rate of increase is such that a plane striking the lens from any one direction is focused at a point on the opposite side of the sphere. If an open waveguide feed is placed at this focus, the energy will propagate down the waveguide. A second waveguide placed adjacent to the first will produce a second beam adjacent to the first, and if the two waveguides are sufficiently close, the two beams will overlap. Because of diffraction effects, the beams that are formed have finite angular beamwidths and sidelobes; in fact, the complete radiation pattern of one of these beams is very much like the radiation pattern of a planar aperture of the same diameter.

Eaton (1954), and others have shown that the paths followed by the rays in an ideal Luneberg lens lie in planes and have elliptical shapes.

A mosaic arrangement of feeds on the surface of the Luneberg lens will generate a similar mosaic of overlapping beams in space on the diametrically opposite side of the lens. The amount of beam overlap can be controlled by the spacing between adjacent feeds. Use of loaded waveguide feeds allows their size and spacing to be tailored to the particular requirements for any application. Beam overlap at the 3-dB points is easily obtained. The gain, beamwidth, and radiation pattern of each beam would be essentially identical. Overall gains of about 3 and 2.5 dB below area gain have been obtained, respectively, with an 18-inch diameter Luneberg lens operating at 12.4 GHz and with a 10-inch diameter Luneberg lens operating at 6 GHz (Shapiro, Reference 22). The pattern of the 10-inch diameter lens fed by open-ended waveguides at 6 GHz is shown in Figure 7-39. Such a pattern would be acceptable for communication systems.

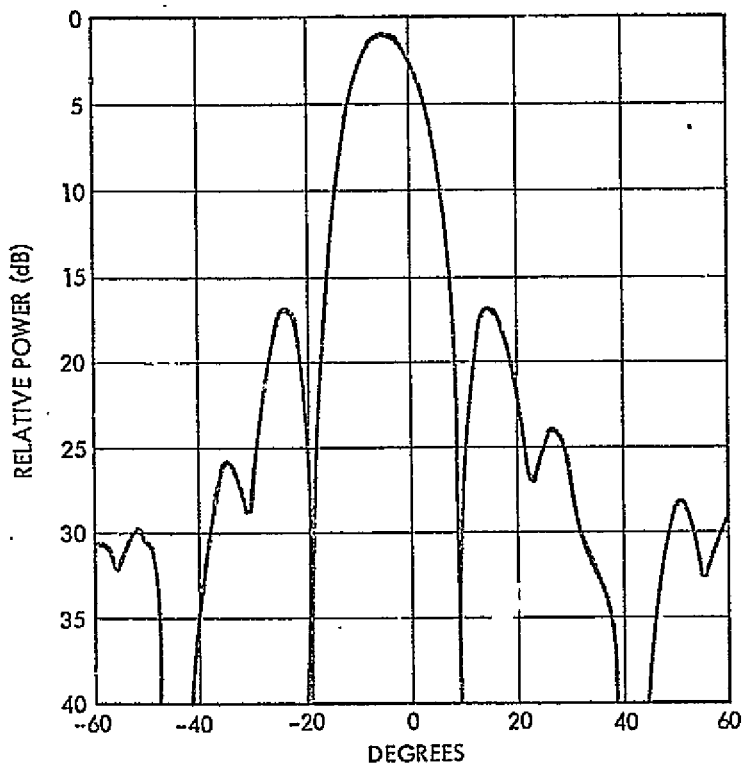


Figure 7-39. Typical Pattern of 10-Inch Luneberg Lens with Open-End Waveguide at 6 GHz

In addition to the effects of adjacent feeds on the radiation pattern, the effects of aperture blockage at wide scan angles due to the presence

of multiple feeds distributed over the rear of the lens have been measured experimentally. It was found that the effect was negligible for scan over cones of half-angle less than 67 degrees.

Several problems exist in the use of Luneberg lenses. One of these is weight; for example, the 18-inch lens discussed above weighs about 36 pounds. A Luneberg lens cannot be zoned to reduce weight as can the other lenses, but artificial dielectrics can be used. A light-weight version of the 18-inch lens would weigh 9 pounds. The artificial dielectric material restricts the use of these lenses to frequencies for which the loading objects and their spacings are small in terms of wavelength. The problem of controlling the dielectric constant in sufficiently small steps also limits the high frequency application of such lenses. In addition, less gain (about 2 db) is to be expected because of the artificial dielectric material. The beamwidth, however, would be unchanged.

Constant Dielectric Lenses. A spherical lens of uniform dielectric material, commonly referred to as the "constant-K" lens, can be used to obtain wide angle scan. This type of lens has focusing properties similar to those of Luneberg lenses, except that small aberrations sufficiently small to be negligible for most practical applications, are present. Figure 7-40 shows a constant-K lens and indicates the manner by which the rays are brought to a focus with ray refraction. Such lenses are inherently of simpler mechanical design than Luneberg lenses and should therefore have electrical symmetries far more accurate than those attainable for Luneberg lenses.

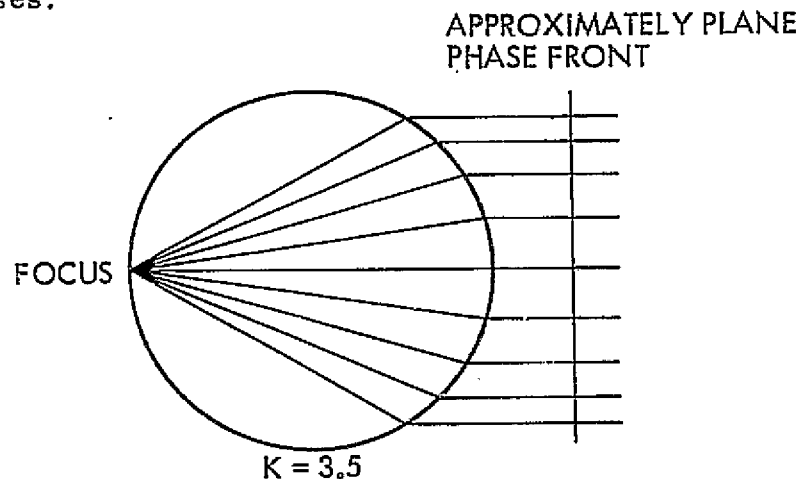


Figure 7-40. Constant-K Lens Showing Focusing of Rays by Refraction

The focus is within the lens if the dielectric constant of the constant-K lens is greater than 3.5. As the dielectric constant is reduced from 3.5, the focus progressively moves away from the surface.

Constant-K lenses with diameters in excess of 100 wavelengths should perform well according to theoretical investigations. However, as the aperture gets larger in terms of wavelength, the aberrations become more significant and degrade the pencil-beam pattern and reduce the gain. Overall gains of about 3 dB below area gain have been obtained with a constant-K-type lens of diameter equal to 12 wavelengths (15.5 inches) operating at 9.375 Gc.

A multiple-beam antenna formed by a constant-K lens or a Luneberg lens backed with a mosaic or array of feed elements has a unique advantage over multiple-beam antennas that use beam-forming matrices. In the lens array, the pointing direction of each beam is independent of frequency; it depends only on the location of the feed with respect to the center of the lens. This advantage will reduce the complexity of a wide-band system that must operate at widely different frequencies with the multiple beams.

The weight of a constant-K-type lens would probably be greater than that of a luneberg lens of similar size, and would be a serious problem in many space applications.

Broadbeam Luneberg Lens. To minimize the problem of aperture blockage by increasing the size of the lens and retaining the same beamwidth, a shaped beam modification of the Luneberg lens is considered. This lens has a broader pencil beam than a Luneberg lens of the same diameter, since the emergent phase front is not plane but rather a slightly curved sphere. The rays are not collimated, and the lens design may be thought of as being of the "shaped beam" type. Geometrical optics should give a reasonable first approximation to the actual patterns achieved by these lenses, just as it does for the shaped-beam metal reflectors described by Silver (Reference 23). Since this type of analysis leads to patterns that are frequency independent, one application of the shaped beam lens is for "pencil-beams" with constant beamwidth over a broad-band. This application permits broadband, wide-angle coverage with a

multiplicity of fixed feeds without failure of coverage at the high-frequency end of the band or wasteful overlap at the low-frequency end.

References 24 and 25 show design procedures for finding the index variation of a spherically symmetric lens that will produce a uniform exit beam of any desired width. For the broadbeam Luneberg lens with a cosine-tapered feed at the surface, Morgan has verified Kay's work and derived the index of refraction of a lens with a specified sector beam to allow fourteen beams to cover the earth from a synchronous orbit of approximately 22,000 miles.

The broadbeam Luneberg lens would produce a constant beamwidth regardless of size and frequency, when fed with a cosine primary pattern. It has a dielectric constant that varies with the normalized lens radius as plotted in Figure 7-41.

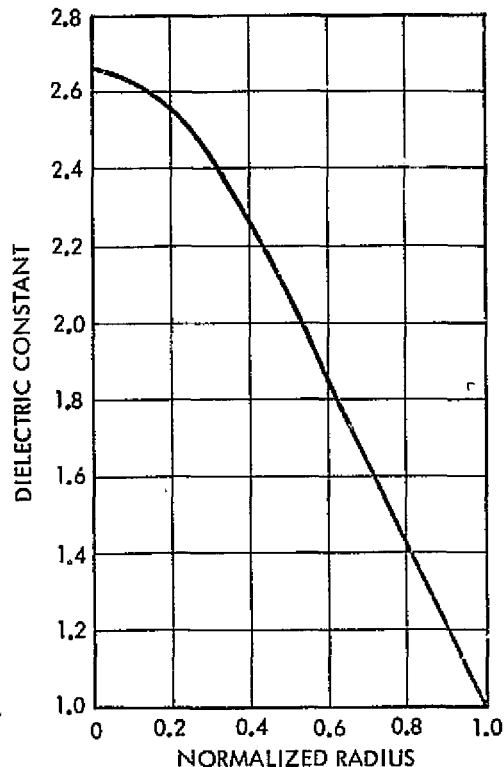


Figure 7-41. Relationship of Dielectric Constant and Radius of a Broad-Beam Luneberg Lens

As far as is known, there are no lenses of this design available commercially. Thus, the potential of the theoretical work remains to be reduced to practice.

Multiple-Beam Arrays Using Beam-Forming Matrices. These antennas use a single array of radiators that are fed by a matrix with multiple inputs, which forms a number of independent beams. The beam-forming matrices require combinations of hybrids or directional couplers. The fact that the matrix consists of passive elements makes it inherently reliable; however, their number depends on the number of beams required and rapidly becomes very large. At frequencies up to X-band, strip transmission line techniques can be used in the matrix to keep down size and weight. The extensive networks required can introduce dissipation losses of several db into the antenna.

Of the multiple-beam arrays studied, the most attractive appears to be a hybrid of the spherical lens and an array with a beam-forming matrix, the former for its wide angle scan capability and the latter for its capability to be arranged in a compact planar configuration. A promising example of an array is the so-called Butler array that consists of an RF beam-forming matrix circuit in which extensive use is made of 3-dB directional couplers and fixed-phase shifter. The beam-forming matrix technique has been modified and adapted to use in circular arrays (Chadwick and Glass, Reference 26).

The Butler Array. One of the basic components of the Butler type of beam-forming array is the 3-dB directional coupler that connects the antenna elements to the output terminals.

A four-beam array can be built by the interlacing of two two-beam arrays with a second level of directional couplers provided to combine the outputs into beams. Fixed-phase shifters must be inserted between the upper and lower levels of couplers to form the output beam. Figure 7-42(a) shows such a four-element, four-beam array using directional couplers. The amplitudes and phases of an incident "Beam 1-Left" signal are shown at various points in the matrix. Figure 7-42(b) shows the amplitudes and phases of an incident "Beam 2-Left" signal. Beam 1-Right and Beam 2-Right are obvious because of the symmetry of the matrix. The shaded directional couplers are the ones used to form the particular beam. It can be noted that the beam-forming matrix behaves like a multiple corporate feed structure that routes a signal originating at a particular point in space to a particular output part of the matrix.

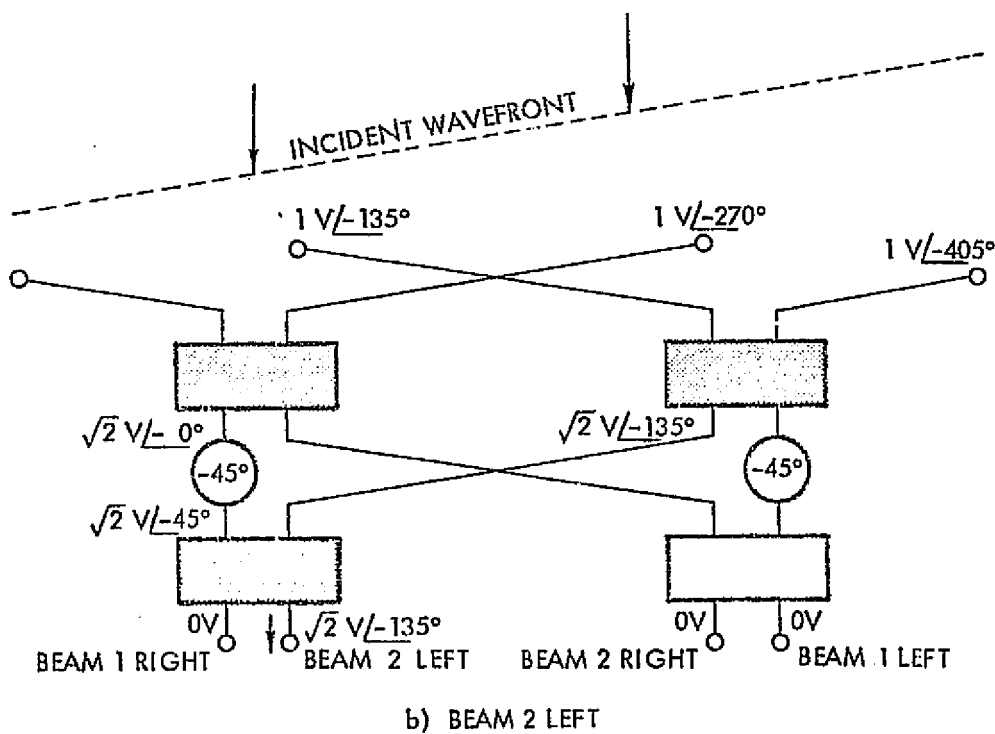
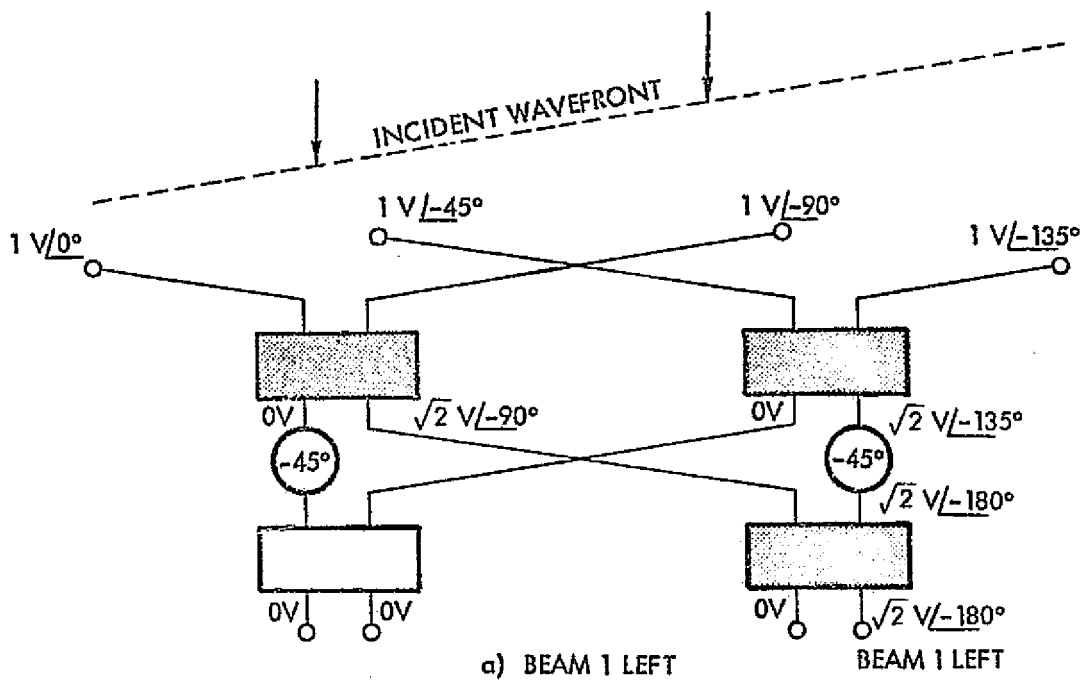


Figure 7-42. Amplitude and Phases of Different Beam Signals in a 4-Element Matrix

The number of directional couplers required to build the matrix of the Butler array can be shown to be equal to $n/2 \log_2 n$, where n is the number of elements in the array. The number of fixed phase shifters required is $n/2 (\log_2 n - 1)$. A major drawback of this beam-forming technique, when large arrays are considered, is the complexity of the matrix arrangement.

These arrays can be built to have any power of two beams, 2, 4, 8, 16, 32, and so on. The number of beams is equal to the number of array elements. This beam-forming technique can be used in two-dimensional (planar) arrays by first combining the outputs of the columns of antenna elements into matrices and then combining the outputs of the column matrices in a group of row matrices.

Theory of Butler Array. The normalized magnitude of the field intensity in the far field of a linear array of n isotropic sources is given by Reference 16 as:

$$|E| = \frac{1}{n} \frac{\sin(n\psi/2)}{\sin(\psi/2)}$$

The number of 3-dB couplers required for an 8 x 8 array is 768, while 512 fixed-phase shifters are required. The phase shifters may consist of only sections of transmission line and would be no problem but the number of 3-dB couplers is quite large. However, it appears that all relatively high-gain scanning systems require a large number of elements.

Shelton and Kelleher describe alternative methods for building up the feed matrix of uniformly illuminated multiple-beam arrays. In addition to the hybrid junctions of the Butler matrix, they consider the use of 6- and 8-port junctions. With these, it is not necessary that the number of radiating elements equal a power of two. The number of elements may take on the values $2^k 3^m 4^n$, where k , m , and n are integers (including 0). By using a combination of 4- and 8-port junctions, it is possible to obtain a 128-element linear array that requires 64 hybrids and 96 8-port junctions for a total of 160 junctions. A Butler matrix for the same number of radiating elements requires 448 hybrids. Thus, the use of different building blocks can drastically reduce

the number of junctions required and might more than offset the increased complexity of the multiport junctions. As a further comparison, a 16 x 16 element planar array using 8-port junctions would require only 256 such junctions as compared to the 8192 2 x 2 hybrids required for the same aperture using a Butler matrix. It appears that development of low-loss, 6- and 8-port junctions for use in such matrices, might make such a system feasible.

Multibeam Circular Arrays. Adaptation to circular arrays of the Butler beam-forming matrix technique (Chadwick and Glass, Reference 24) makes use of an approximate analogy between the exponential Fourier series expansion in ϕ of the azimuth pattern of a circular array and the pattern of a linear array in the variable $u = kd \sin \phi'$. If the excitations of the elements of a circular array are expressed in terms of their phase sequence modes, then each phase sequence mode is responsible for exciting primarily one specific term in the exponential Fourier expansion of the pattern in ϕ . For example, the zero phase sequence mode excited an essentially omnidirectional pattern with uniform phase; the first positive phase sequence excites a pattern that is essentially omnidirectional in ϕ , but whose phase varies linearly in ϕ ; the second phase sequence mode excites an essentially omnidirectional pattern whose phase varies as 2ϕ ; etc. Actually, the phase sequence mode patterns are not ideal and have additional harmonics that are error terms. If the error terms are sufficiently small, then excitation of the phase sequence modes with the same relative amplitudes and phases as those of the element excitations of the equivalent linear array will result in a pattern as a function of ϕ , which is identical with the linear array patterns as a function of $kd \sin \phi'$. Therefore, techniques for synthesizing linear array patterns, as a function of $kd \sin \phi'$, may be applied to synthesizing patterns of circular arrays as a function of ϕ .

The heart of the technique is the so-called mode-forming matrix that transforms the excitation coefficients of the reference linear array into the proper phase sequence component of the circular array excitation and combines these excitations at the elements of the circular array to produce the desired pattern in ϕ . This matrix is illustrated in Figure 7-43.

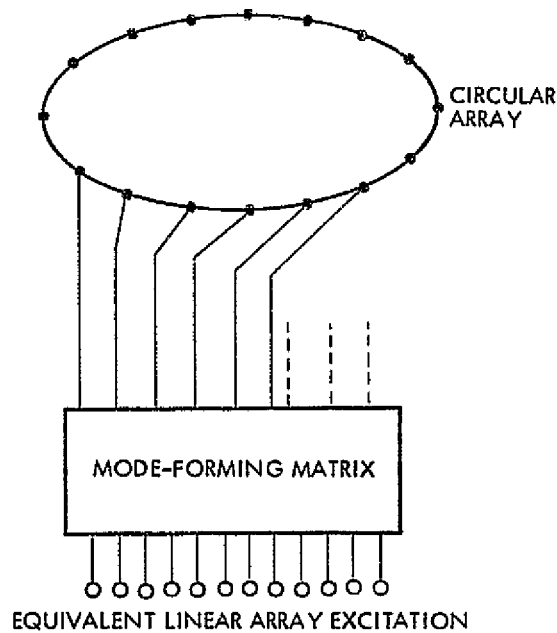


Figure 7-43. Circular Array with Beam-Forming Matrix

The errors in the fields of the various phase sequence modes are greatest for the modes whose numbers are approximately equal to half the number of array elements. These errors increase with element spacing. They appear to be relatively small for spacings less than 0.25 wavelength but increase beyond this spacing. As an example, for a 16-element array with half-wavelength spacing, whose elements have patterns of the form $\cos^{16}(\phi - \phi_n/2)$, where ϕ_n is the angular position of the n^{th} element, only 10 out of 16 phase sequence modes are very pure. This means that a pattern corresponding to a linear array of only ten elements can be faithfully reproduced. As the patterns of the individual elements become more nearly omnidirectional, even fewer phase sequence modes have sufficient purity; i.e., the number of elements in the equivalent linear array whose pattern can be faithfully reproduced becomes less.

7.3.3.4 Self-Steerable Antennas. The class of antennas termed "self-steerable" are those which, through the use of electronic processing equipment, can automatically form a beam in the direction of an incident pilot signal. These antennas may be subdivided into several groups, depending on how the steering is accomplished. These groups are listed here as: 1) switched multiple-beam antennas, 2) self-phased arrays, and 3) adaptive arrays.

Group 1) may use the multiple-beam antennas mentioned with appropriate switching and control circuitry to select the proper beam automatically as indicated by the pilot signal. Group 2) is composed of conformal arrays of elements, each of which has its own electronic circuitry that automatically phases the elements or produce a beam in the direction dictated by the pilot. Group 3) is closely related to Group 2) but uses phase-locked loops at each element to accomplish the element phasing. The term adaptive comes from certain properties of the phase-locked loops.

Conventional Phase Arrays. These arrays obtain beam-pointing direction through the use of phase shifters to control the phase distribution across the aperture. They differ from the self-phased and adaptive antennas in that the beam-pointing information is not obtained directly at each element but must be obtained from some other information, such as the inter-element phase shift of a pair of elements, an IR sensor, or some pre-programmed pointing instructions. This information must then be used to generate control signals that will adjust the individual phase shifters to point the beam in the proper direction. The control functions must be tailored to the phase shifter characteristics.

7.3.4 RF Power Sources

7.3.4.1 Microwave Semiconductors. The use of semiconductors as sources of microwave energy has relentlessly expanded in the area of upper frequency operation and efficiency for a number of years with breakthroughs most noteworthy in the areas of IMPATT, TRAPATT, and Transferred Electron Devices (TED's) devices. Along with the use of diodes as RF sources for both pulsed and CW purposes, the transistor market has steadily been pushing its own upper frequency limit.

Figure 7-44 shows the current state of both the transistor and diode markets with transistors making a good showing up to 3 GHz with 10 watts power output at 30 percent efficiency. Pulse application diodes deliver a wide range of power outputs for frequencies from 1 to 90 GHz. CW diode applications are limited between 0.02 and 5 watts over the same frequency range. This is described in some detail in the following sections.

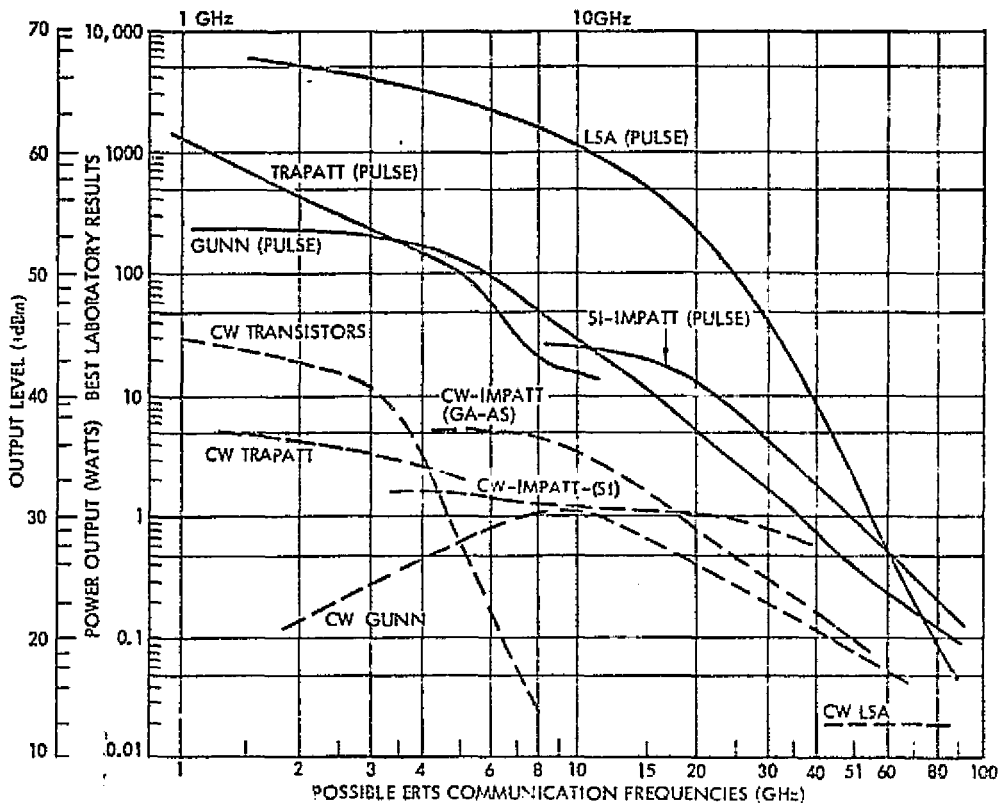


Figure 7-44. Microwave Power Generators

IMPATT (Avalanche) Diode Devices. IMPATT is an acronym for "impact ionization avalanche transit-time." This junction device operates under a reverse-bias field with the junction in deep avalanche breakdown. If the avalanche (carrier discharge) region is at one end of a high-resistance region the rest of which serves the generated carriers as a transit-time drift space, then the device can exhibit a negative resistance. (Such a diode was first proposed by W. T. Read). The IMPATT phenomenon involves an exchange of energy between a DC field and the desired RF field. When the DC field forces carriers to move against the RF field, then those carriers give up energy to the RF field which, in turn, transfers it to an external load. At the start of a cycle, the DC field is at a critical level, just below threshold. The RF field at its positive maximum, adds to the DC level to establish avalanche. Carrier charge-density rapidly builds in the avalanche region, and moves into the drift region just as the total field drops below threshold. The charge (a current) moves through the transit-time region at saturation drift velocity as the RF field passes through its negative maximum and is collected just as the RF field (a voltage) reaches a minimum. The combination of

1) delay between carrier generation rate and carrier accumulation and
 2) the time delay associated with the transit time through the drift region accounts for a 180 degree phase shift between RF electric field and RF current density. thus producing a current-controlled, dynamic, negative resistance.

IMPATT diodes are generally epitaxial silicon devices. They are noisy, because avalanche breakdown is a noisy phenomenon; but there are circuit techniques to reduce this problem. Gallium-arsenide IMPATTs are available; these are less noisy than silicon devices, but do not have silicon's thermal conductivity. However, they offer better efficiency operation; impressive results have been achieved with special profile Ga As diodes at X and Ku-bands; 5-10 watts CW and efficiencies in the 20-30 percent range have recently been obtained.

IMPATT oscillators are ultra-reliable, fixed-frequency or tunable solid-state sources for use as local oscillators or parametric-amplifier pumps in applications or as RF low power sources.

High-Q oscillator configurations provide up to 200 mW of low-noise RF power output in both X- and Ku-bands up to 16.0 GHz. From 16.0 to 18.0 GHz up to 100 mW is available, with either fixed-frequency or mechanical tuning. Operating lifetime in excess of 16,000 hours at these power levels has been achieved without failure. Table 7-8 shows the typical performance for High-Q IMPATT oscillators.

Table 7-8. Typical Performance: High-Q IMPATT Oscillators

	Mechanically Tunable		Fixed Frequency	
	From	To	From	To
Frequency ranges	7.0 to 8.2	12.4 to 16.0	7.0 to 8.2	12.4 to 16.0 GHz
Tuning range	± 100 to 300	± 50 to ± 500	-	- MHz
Power output	10 to 150	10 to 150	25 to 200	25 to 200 mW

Low-Q IMPATT Oscillators deliver up to 1 watt of RF power output for applications where noise performance is less critical but power output and DC to RF efficiency are of prime importance (Table 7-9). They are ideal for injection-locking use, with locking bandwidths up to 200 MHz and 10 decibels of locking gain.

Table 7-9. Typical Performance: Low-Q IMPATT Oscillators

	Mechanically Tunable		Fixed Frequency	
	From	To	From	To
Frequency ranges	5.85 to 8.20	8.20 to 12.4	3.95 to 5.85	8.20 to 10.00 GHz
Tuning range	+150	+250	-	- MHz
Power output	750	750	100 to 500	100 to 1000 mW

Expected performance for both silicon and Ga-As IMPATT diode devices are shown in Figure 7-44 for both CW and pulse applications. Typical device bias conditions at 100-200 mA vary from around 100V at X-band to 30 volts at Ka-band to 15 volts at 60 GHz.

TRAPATT Diode Devices. TRAPATT diodes, first reported by K.K. N. Chang, give higher power, and at higher efficiencies, than do ordinary IMPATT. They are called TRAPATTS, an acronym for "trapped plasma avalanche-triggered transit." A TRAPATT cycle starts in a normal IMPATT mode. But then a second, IMPATT triggered avalanche occurs, forming an avalanche zone which moves through the diode in much less than the normal transit time. (for this reason, one should not expect useful TRAPATT operation much above 20 GHz). Carrier velocity decreases because the electric field rises in front of this zone and drops behind it, developing a space-charge-neutral, trapped plasma. This plasma (output signal) is bled off by external circuitry and the cycle starts anew, with output frequencies about half those of corresponding IMPATTS. High efficiency comes from the diode's alternate cycling between a low-voltage, high-current plasma state, and a high-voltage, low-current IMPATT state.

TRAPATT diode efficiency as a pulsed device will be between 45 percent at 1 GHz and 20 percent at 10 GHz.

TRAPATT operation requires circuit techniques for more complex than pure IMPATT operation; and although CW operation was recently achieved more work needs to be done before the TRAPATT device reaches the stage of genuine usefulness for a real systems application.

Gunn-Effect Devices. J. B. Gunn was the first to observe that a junctionless, bulk sample of GaAs (InP, CdTe, ZnSe are also suitable)

produces a current which rises with voltage, then becomes oscillatory as the field reaches several thousand volts per cm. In the most simple mode, the oscillation is in the form of domains of high field strength which travel across the material between its ohmic contacts. The period of the RF energy corresponds to the transit-time of the high-field domains across the device. As one domain disappears at the anode, the field builds up behind it, forming a new domain at the cathode, and so the cycle goes. Gunn or "transferred electron" devices (TED's) exhibit a voltage-controlled negative resistance. Above a critical field value (threshold) the average electron velocity and current begin to decrease. This quantum-mechanical effect excites high-energy electrons into a low-mobility conduction band from one with higher mobility (the two-valley theory), and the loss of high-mobility electrons produces a differential negative resistance. Avalanche and bulk-effect devices show negative resistance along with a capacitance, and they oscillate when embedded in an inductive structure such as a cavity.

Gunn-Effect devices can be designed to constitute a line of CW and pulse oscillators for low-power transmitters, local oscillators, and parametric amplifier pump experimentation from C through Ka bands. FM noise characteristics are comparable to those of good reflex klystrons; AM noise characteristics are superior. Mechanical tuning ranges greater than 1 GHz are standard, with little power variation. Typical DC potentials at Ka-band are 5 volts, and at X-band, 9 volts, while typical currents are 500 ma. Life tests indicate an MTBF in excess of 100,000 hours. Typical performance for mechanically tuned Gunn-effect oscillators is shown in Table 7-10.

Table 7-10. Typical Performance: Mechanically Tuned Gunn-Effect Oscillators

	From	To	
Frequency ranges	4.8 to 8.0	50 to 60	GHz
Power output*	25 to 100	5	mW
Tuning range	± 250	± 100	MHz
* 250 mW power output available from 8.0 to 12.4 GHz 100 mW up to 50 GHz			
** Up to ± 500 MHz tuning available from 8.0 to 50.0 GHz			

Phase locked transferred electrons oscillators have become available recently which permit crystal derived frequency stability at 8 to 18 GHz with output powers of 500 to 50 mW without the use of multipliers. The technique utilizes sampling the fundamental oscillator output up to 18 GHz. The input frequencies are typically 80 - 130 MHz.

LSA Devices. IMPATT diodes and transferred electron (Gunn) devices are transit-time limited; the power-impedance product is proportional to $1/f^2$. But the Limited Spacecharge Accumulation (LSA) mode of a bulk device - an effect discovered by J. A. Copeland - has lower capacitance and greater power output capability than either IMPATT or Gunn devices, and a power-impedance product nearly independent of frequency. High-field, traveling domains characteristic of bulk-effect devices are not permitted to form. The oscillating field across the device rises above and falls back to the threshold level too quickly for domains to take shape. Any small charge which does manage to accumulate dissipates rapidly when the field drops below thresholds. Thus, the charge density is essentially uniform within the bulk sample; almost the entire device acts as a negative resistance independent of the sample's length, and without any transit-time effects. In this way, pulsed LSA devices can operate at much higher peak power levels than can Gunn or IMPATT diodes. The LSA mode needs a DC bias several times threshold, but the RF field still must be able to drop below the threshold. This situation implies a very lightly loaded device: an LSA diode must work into a circuit impedance about ten times as large as that of the diode itself.

To date, the LSA devices have not fulfilled the promise of high power, high efficiency devices in those frequency bands complimentary to IMPATTs, say at 100 GHz and above. Typical performance is summarized in Table 7-11.

Table 7-11. Typical Performance: LSA Effect Sources

	From	To
<u>Oscillators</u>		
Frequency range	40-45	90-90 GHz
Power output	+ 20 MW	
Nominal efficiency	1 to 2 percent	
<u>Pulses Sources</u>		
Frequency range	1.5	75 GHz
Power output	5K	0.05W
Nominal efficiency	6 to 12 percent	

C-2

7.3.4.2 Broadband CW Devices. The perennial race for supremacy among the various microwave broadband, CW devices now narrows down to solid-state devices attempting to overtake traveling-wave tubes (TWT's). Latest estimated contour plots of RF CW power as a function of frequency for promising microwave devices, including high power TWT devices, are shown in Figure 7-45

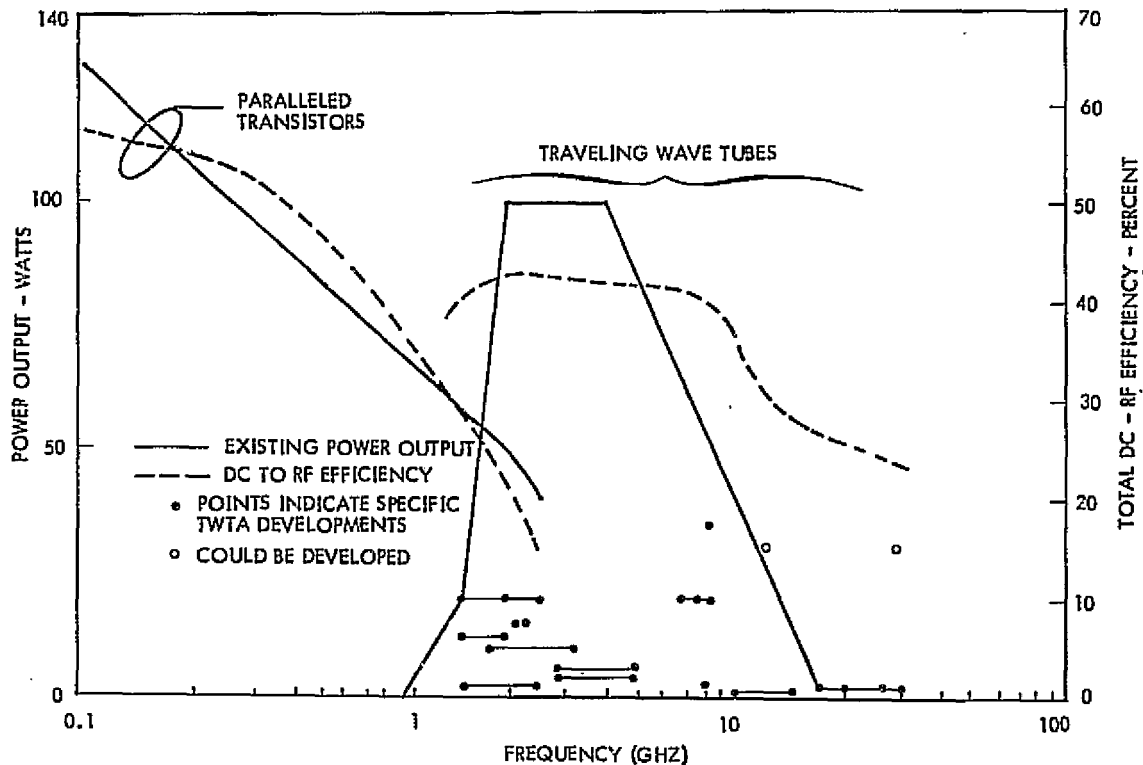


Figure 7-45. State-of-the-Art RF Power Amplifier Devices

For solid-state amplifiers, as indicated, the transistor prevails below 4 GHz. Above this frequency, the transistor and single-port reflective devices (IMPATT, TRAPATT, and TEA) are collectively in competition. Nevertheless, distinctive performance differences among these amplifiers tend to separate one from the other readily. The CW capabilities of microwave solid-state devices, although still embryonic and undergoing exciting improvements, are:

- All of the reflection-type amplifiers, when optimized for bandwidth, have low gain per stage (6 to 3 dB). Consequently, five to seven stages are needed for 40-dB overall gain. The device simplicity virtually disappears as one adds the required circulators to isolate input and output ports, biasing networks, and temperature compensation for each of the stages.

- The TRAPATT amplifier, requiring harmonic and sub-harmonic tuning as well as initiation through the IMPATT mode, has excellent efficiency (25 percent but relatively narrow instantaneous bandwidth (5 to 10 percent).
- The IMPATT amplifier has a bandwidth capability greater than the TRAPATT (10 percent but less than one-third to one-half that of the TEA.
- The TEA has the widest bandwidth (50 to 100 percent) and lowest noise figures of all the single-port devices, but its efficiency (~3 percent) and power output are low.
- The transistorized amplifier has narrow bandwidth and relatively low power and efficiency above 3.5 GHz.

A review of the limitations of the aforementioned solid-state amplifier devices for CW performance serves to highlight the superiority of the helix-type TWT. For the TWT, gains of the order of 40 to 50 dB over octave bandwidths and conversion efficiencies over 20 percent are routinely achieved. Moreover, as indicated in Figure 7-45. The CW power-output capability of the conventional TWT is two to three orders of magnitude in excess of that achieved for those solid-state devices previously described.

More recent advancements — miniaturization of the TWT — have added significantly to the advantages inherent in these broadband, high-gain devices.

7.3.4.3 TWT's. A generic line of miniature TWT's intended for aerospace or ground-based applications at the 10- to 30-watt RF output power levels has been developed. These miniature tubes, which cover the frequency range from 2.6 to 18 GHz, are unique in their performance, size, and weight. The tubes use samarium-cobalt magnets, have a volume as low as 4 cubic inches and weigh as little as 9 ounces. These tubes which provide greater than octave bandwidth coverage, can be used whenever high-performance RF amplifiers are required.

The miniature TWT uses a conduction-cooled heat sink and depressed collector operation for improved overall DC to RF efficiency. They are specifically designed for side-by-side operation — a prerequisite in an antenna array — with minimal interaction between adjacent tubes.

TWT Design Considerations. Miniature TWT's have been designed with rare-earth samarium-cobalt magnets. These magnets produce extremely large axial flux fields to maintain stable beam focusing and, at the same time, make small packaging dimensions possible.

A comparison of the flux fields obtained for a specific configuration with samarium-cobalt and with Alnico 8 magnets for PPM focusing is shown in Figure 7-46. The curves illustrate the increased axial flux that can be obtained for a fixed magnetic pole piece inside diameter (ID) (0.2 inch) as the outside diameter of the magnetic material is increased. For this configuration, the Alnico material is limited to a flux density of 1200 gauss with a magnet outside diameter (OD) of 0.75 inch; the samarium-cobalt provides a flux of 2000 gauss for an OD of 0.4 inch. This dimension is well within the form factor to enable the fabrication of a packaged 0.5-inch width TWT. The magnetic-focusing stack is processed before use at an elevated temperature (200°C) which exceeds the maximum operating temperature, to eliminate an inherent irreversible flux (-10 percent) loss and to obtain high-temperature operation independent of time.

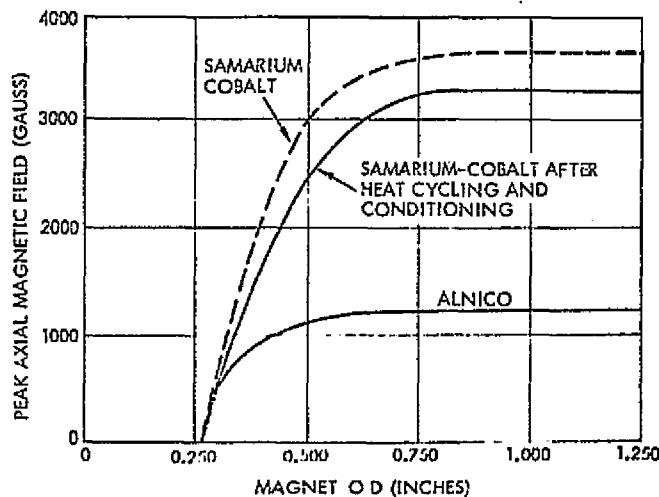


Figure 7-46. Comparison of Magnetic Fields: Samarium-Cobalt and Alnico 8

Performance Capabilities. The characteristics of the miniature TWT's, now under development or being sampled for system usage, are given in Table 7-12. RF power output contours as a function of frequency, typical of some of the tubes, are shown in Figure 7-47. These tubes have

demonstrated the capability of meeting RF power-output requirements greater than 30 watts over octave frequency bands from 2.6 to 18 GHz.

Table 7-12. Technical Data for Mini-TWT's

RCA Type Dev #	Freq Range GHz	RF ¹ Output W	S/S Gain dB	Noise Figure db	Heater Power		Collector Power		Holtz Power		Anode Voltage V	Dimensions ² (inches)			Weight Approx LB
					V	A	V	mA	V	mA		L	W	H	
A1485	2.6-6.2	25	40	3.5	6.3	1.0	1200	120	2400	8.0	3800	10.0	0.75	1.0	1.0
A1481	5.2-10.4	25	40	3.5	↓	.5	1300	100	2500	8.0	3900	8.0	0.6	0.85	0.6
A1487	7.0-17.0	10	50	3.5		.4	1700	70	3000	5.0	2900	10.0	0.6	1.0	1.0
A1484	8.0-18.0	10	45	3.5		.35	1700	60	3300	6.0	2300	9.0	0.63	1.35	0.75
A1478	9.0-18.0	15	40	3.0		.4	2000	75	3000	8.0	2900	7.0	0.5	1.0	0.5
A1486	10.4-18.0	25	40	3.5		.5	1800	95	3000	8.0	3400	7.0	0.6	0.85	0.6
A1480	11.0-18.0	20	40	3.0		.3	1600	70	3200	8.0	2800	7.0	0.5	1.35	0.6

1 Saturated
2 Excludes connectors

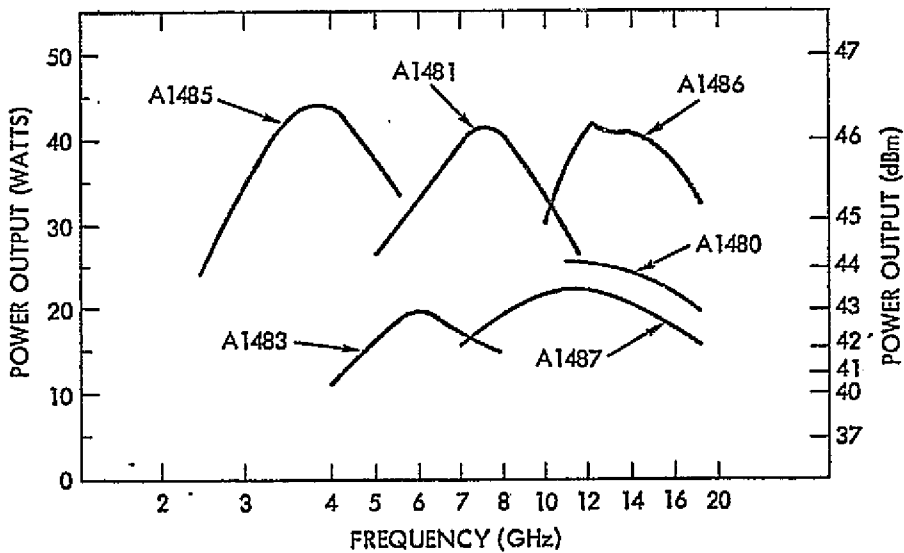


Figure 7-47. RF Power Output for Several Mini-TWT's

High Power TWT's. The availability of high power TWT tubes of proven reliability makes it possible to consider future communication links with considerably higher values of ERP. Table 7-13 indicates representative parameter values for a range of TWT devices, with outputs of 1 to 500 watts. Tubes are available for power of up to 8 kw.

Table 7-13. Characteristics of Medium and High Power TWT Amplifiers

Manufacturer	Part Number	Frequency Range (GHz)	Power Output (Watts)	Power Gain (dB)	Noise Factor (dB)	Form of Cooling
RCA	A-1429	4 to 8	2	40	-	
Keltec	CXR-600-1	4 to 12.4	1	30	30	
Keltec	CSR-602-2	4 to 12.4	2	30	30	
Watkins Johnson	WJ-231-5	(opt 4-9) 5 to 8.5	35	30	-	Cond.
RCA	A-1397	5 to 10	4	43	-	
Watkins Johnson	WJ-440	5.2 to 10.4	500	30	-	FA (also Liq 440-2)
Keltec	CXR-602-1	5.4 to 10.7	1	55	30	
Keltec	CXR-601-2	5.4 to 10.7	2	60	30	
Keltec	CSR-600-20	6 to 11	20	35	35	
Keltec	CXR-601-20	7 to 11	20	50	35	
Watkins Johnson	WM-231-4	(opt 5 to 10) 7 to 8	35	40	-	Cond.
Keltec	XR-601-1	7 to 12.4	1	50	30	
Keltec	XR-600-2	7 to 12.4	2	36	30	
Keltec	CXR-601-1	7 to 11	1	33	30	
Keltec	CXR-600-2	7 to 11	2	36	30	
Watkins Johnson	WJ-1128	7 to 11	2	37	-	Cond.
Watkins Johnson	WJ-1116-2	7 to 11	2	37	-	Cond.
RCA	A-1428	7 to 11	2	40	-	
Watkins Johnson	WJ-492-1	7 to 11	3	37	22	Cond.
Watkins Johnson	WJ-1115	7 to 11	4	45 to 60	-	Cond.
Watkins Johnson	WJ-391	7 to 11	5	36	-	Cond.
Keltec	CXR-600-10	7 to 11	10	40	35	
RCA	A-1378	7 to 11	10	40	-	
Keltec	CXR-601-10	7 to 11	10	60	35	
Keltec	CXR-600-100	7 to 11	100	30	35	
Keltec	CXR-600-200	7 to 11	200	37	35	
Watkins Johnson	WJ-1116-1	7 to 13	2	45	-	Cond.
RCA	A-1427	7.9 to 8.4	5	50	-	
Hughes	722H	8.4 to 9.2	1 kw	40	-	
Hughes	710H	8.7 to 9.3	8 kw	50	-	
Hughes	732H	8 to 10	5	40	-	
Keltec	XR-600-1	8 to 12.4	1	30	30	
Watkins Johnson	WJ-2503-3	8 to 12.4	1	30	-	F. A.
Watkins Johnson	WJ-492-2	8 to 12.5	3	54	22	Cond.
Keltec	XR-600-10	8 to 12.4	10	30	35	
Hughes	771H	8 to 12.4	10	30	0	
Keltec	XR-500-10	8 to 12.4	10	35	25	
Keltec	XR-600-20	8.2 to 12.4	20	35	35	
Keltec	XR-601-20	8.2 to 12.4	20	50	35	
Watkins Johnson	WJ-350-1	8 to 12.4	30	38	-	Cond.
Keltec	XR-600-100	8 to 12.4	100	30	35	
Keltec	XR-601-100	8 to 12.4	100	50	40	
Keltec	XR-600-200	8 to 12.4	200	40	35	
Hughes	773H	8 to 14	100	40	-	
Keltec	XR-602-125	8 to 14	125	30	40	
RCA	A-1427	10.7 to 11.7	5	50	-	

ORIGINAL PAGE IS
OF POOR QUALITY.

7.3.5 Path Losses

A major factor in a power budget analysis is the signal loss between antennas. Nominally the loss contributors are the spreading or $1/R^2$ loss due to spherical divergence, and the attenuation caused by absorption in the atmosphere, clouds or rain through which the signal passes. A third contributor sometimes encountered is fading caused by multi-path induced phase cancellation that can occur whenever energy reaches the receiving antenna via two or more paths. This latter should not be a serious problem for systems using narrow-beam ground antennas when the satellite elevation angle exceeds the beamwidth.

The usual derivation of energy transfer is based on isotropic transmitting antennas having a spherical radiation patterns, and on isotropic receiving antennas having an effective intercept area equal to $\lambda^2/4\pi$. The received energy is proportional to the transmitted energy and the ratio of the receiving antenna's effective area to the area of a sphere centered on the transmitting antenna. Accordingly, path loss becomes

$$L_p = \frac{\text{Area Receiving}}{\text{Sphere Area}}$$
$$L_p = \left(\frac{\lambda}{4\pi R} \right)^2 \quad (7-15)$$

The term that varies with R^2 is caused by spherical divergence, whereas the frequency sensitivity is related to the effective area of the isotropic receiving antenna. Taken together they form a term referred to as path loss.

When one terminal of the communications link is on the ground, and the other in a spacecraft, path losses are sometimes computed on the basis of orbit altitude h , and frequency. However, when the spacecraft is not at the zenith, the path loss increases slightly according to the square of the ratio of path lengths, illustrated by Figure 7-48. For convenience, Figures 7-60 and 7-61 for zenith and off-zenith losses are provided in Section 7.4, (link power budgets). The first relates zenith path loss at each of the candidate orbit altitudes versus frequency. The second, presents the incremental path loss as a function of elevation angle.

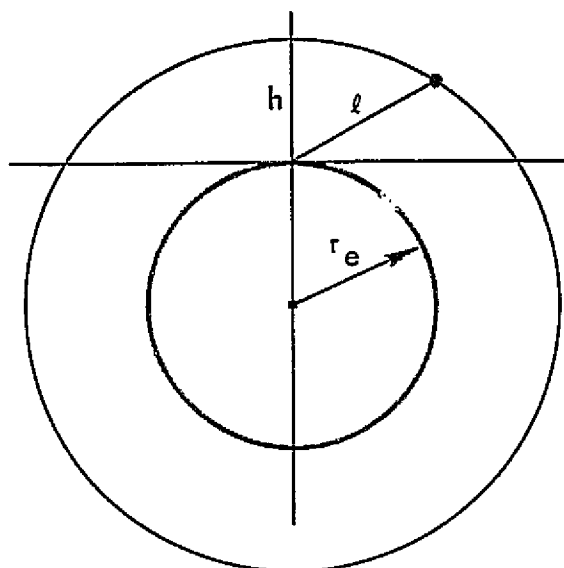


Figure 7-48. Orbit Geometry

Atmosphere, Clouds and Rain. Losses caused by the atmosphere and adverse weather vary with frequency, precipitation and its form (humidity, ice crystals or rain). The losses to be expected from these phenomena are well understood for uniform weather masses. Unfortunately, actual weather conditions are highly variable in both uniformity and frequency of occurrence. Accordingly, there is usually a great deal of uncertainty about how to plan for weather losses before a link is developed.

When interest in communications lie in frequencies below a few GHz, or even up to 8 GHz, weather losses are not significant more than a few hours a year, and then only for the heavier rains. With interest now extending upward in frequency, including Ku-band and up, weather losses can be significant, and should be accounted for. The ability to account for these losses will be heavily dependent upon the weather data available for the terminal area, and all portions of the path likely to pass through adverse weather.

The TDRSS ground site will be in Roswell, New Mexico, which is known to have predominantly clear weather, and will thus require less of a margin than will other sites, for other systems, that might be located in Europe, South East Asia, Washington, D. C. and other locations with a significant amount of adverse weather.

There is usually little statistical weather data in the form desired. The available weather data is usually recorded at fixed observation posts at hourly or six-hourly intervals. Rain gauges provide the integrated effect since the previous measurement; observers estimated cloud cover, in 10ths, at the instant of the observation. Accordingly there is little data to indicate how long a particularly heavy rain lasted, how wide an area was included or what the distribution of heavy rain cells was. This in turn, makes it difficult to develop fine-grain outage time statistics, or to estimate path attenuation for narrow beam antenna systems, when the fraction of the path in the loss region is uncertain.

With interest in the use of frequencies above X-band increasing, and a recognition that weather conditions present serious problems in Europe and South-East Asia, the USAF Environmental Technical Applications Center (USAFETAC) has recently started to develop analytical and statistical data. References 43 - 46 list a few of their more applicable reports.

In recent years, major meteorological stations have begun to record data in a form to assist in predicting weather losses, and should be solicited as a part of a link design and site selection program.

Typical weather losses are reviewed in Appendix A. Parametric curves generated for 2.2, 8.2, 13.7 and 21.6 GHz are provided in Section 7.2.6 as a part of the discussion on constraints imposed upon the system engineer.

7.3.6 Ground Receiving Equipment Implications. A ground receiving system used for communications at microwave frequency today is specified in terms of the antenna system figure of merit. This is the ratio G/T of the antenna gain G to the system noise temperature, T referenced to the same point.

There are three contributors to the system noise temperature: 1) the noise temperature (T_a) of the antenna, 2) the insertion loss and resultant noise temperature (T_f) of the diplexer and feeder system, and 3) the noise temperature (T_R) of a high-gain, ultra-low-noise amplifier, (LNR).

$$\text{Figure of merit} \approx G / (T_a + T_f + T_R) \approx G/T$$

There are two contributors to antenna gain, namely antenna diameter, D and antenna efficiency, η .

From the cost standpoint, an antenna of diameter D , and efficiency will cost so many dollars for the gain involved. If the antenna is increased, the gain and the cost will both increase. If the gain can be increased by an increase in efficiency, then the cost may not increase as much since the increase in structure cost may not be significant. In like manner, there is a relationship between receiver noise temperature and preamplifier or receiver cost. As the receiver noise temperature is reduced, costs increase.

The following sections review the important factors relating to antenna and preamplifier design, then relate the tradeoffs involved in minimizing costs.

7.3.6.1 Antenna Considerations

As microwave frequencies increase, the most predominant factor in establishing the effective gain or efficiency of a large aperture antenna is the phase error associated with the received signal. Assuming that the antenna is located in a radome for security or environmental protection, the following sources of phase error would be present in the signal ultimately delivered to the receiver:

- Random phase errors due to non-uniformity of the radome material dielectric constant and thickness tolerances
- Random phase errors due to the manufacturing tolerances of the main reflector and subreflector
- Systematic phase errors due to axial defocussing of the subreflector-feed combination
- Systematic phase errors due to structural sag in the total reflector, causing the reflector to assume a quasi-elliptical shape
- Systematic phase errors due to a difference in the E- and H-plane feed phase centers.

The phase shift through a dielectric material is given by

$$\phi = \frac{2\pi d}{\lambda_0} \sqrt{\epsilon' - \sin^2 \theta}$$

where

- d is the radome wall thickness
- λ_0 is the free space wavelength
- ϵ' is the dielectric constant of the radome
- θ is the angle of incidence ($\theta=0$ =normal incidence).

The minimum thickness for a space frame radome is in the order of 0.020 inch, with a tolerance of approximately 20 percent. Average dielectric constants of materials employed (epoxy-dacron) is 3.0 with a tolerance of 20 percent. Assuming a random distribution of both thickness and dielectric constant, the radome phase error will be in the order of ± 0.003 inch at angles of incidence between 0 degree and 30 degrees.

Ruze's work is widely utilized to account for gain loss due to random errors in the surface tolerances of parabolic reflectors. For a dual reflector antenna, employing a radome with phase errors, the random phase error efficiency is given by:

$$N_T = e^{-16 \frac{\pi^2}{\lambda_0^2} (\sigma_M^2 + \sigma_S^2 + \sigma_R^2)} \quad (7-16)$$

where

- λ_0 is the free space wavelength
- σ_M is the RMS surface tolerance of the main reflector
- σ_S is the RMS surface tolerance of the subreflector
- σ_R is the combined RMS thickness-dielectric constant tolerance of the radome.

For most large aperture antennas it can be reasonably stated that main reflector surface tolerances can probably be maintained to 0.010 inch RMS under controlled environmental conditions, while subreflector

tolerances will be 0.005 inch RMS. This includes antenna sizes up to 66 feet in diameter. For smaller aperture antennas, below 36 feet in diameter, main reflector surface tolerances of 0.005 inch have been achieved, while a subreflector surface tolerance of 0.003 inch can be achieved. The loss in gain versus frequency for these two cases is plotted in Figure 7-49

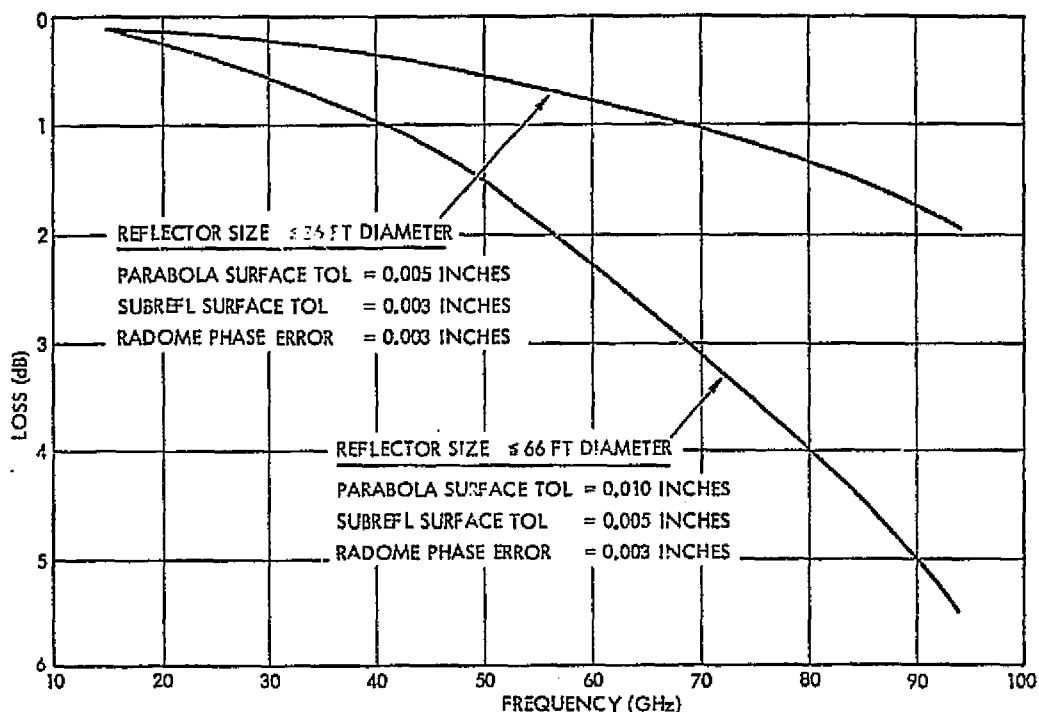


Figure 7-49. Gain Loss versus Frequency due to Surface Tolerance

Systematic phase errors can be treated in a somewhat different manner, especially where the antenna is to operate over a small angular region and is located in a controlled environment. Axial defocussing, due to subreflector displacement would be caused by temperature changes and structural deformation for large movements of the antenna. Structural sag in the total antenna aperture is highly dependent upon the design of the structure. If the antenna is to operate over a limited region, then the parabola would normally be designed to have minimum deflection over that region. In the area of feed design, very efficient designs are available, having well-defined phase centers and very low spillover in a cassegrainian geometry. These include the corrugated conical horn, the dual or multimode horn, and finned conical or rectangular horns. Thus, it

can be concluded that systematic phase errors of the types mentioned can be minimized when

- The antenna is in a controlled environment (radome with air conditioning and/or heating)
- The antenna look angle is confined to a small angular region as would be the case with a synchronous satellite
- Exploitation of the above conditions and the feed design techniques are fully utilized.

Other factors affecting the efficiency of a high frequency cassegrain antenna include the following:

- N_I , the aperture illumination, or amplitude taper
- N_{SS} , the spillover or lost energy not collected by the subreflector
- N_{SR} , the spillover or lost energy not collected by the parabolic aperture
- N_{BSUB} , the blockage of the subreflector
- N_{BSOP} , the blockage by the subreflector supports
- N_{XP} , the cross polarization of energy inherent in the feed design and incurred by the reflecting surfaces
- N_{LS} , the losses, ohmic in nature, caused by the reflecting surfaces
- N_{LF} , ohmic losses of the feed subsystem including polarizer
- N_{LD} , ohmic losses of the diplexer
- N_R , reflective loss due to finite VSWR of feed subsystem (negligible for good designs).

In order to achieve the highest possible efficiency from a given aperture, various techniques have been devised to obtain very nearly uniform illumination across the aperture. These include shaping of the subreflector and main reflector, multi-feed horn arrangements, and feed-compensated lenses. In general, these techniques have worked quite well and illumination efficiencies in excess of 90 percent have been obtainable. However, in a radome-enclosed situation where the metallic members of the space frame radome produce increased blockage toward the edge of the aperture, there may be little, if any efficiency improvement unless the radome is large compared to the diameter of the antenna.

This can be intuitively visualized when one considers that the metallic members of the radome are essentially thin radials of a sphere, such that an optical projection across an aperture causes greater and greater blockage towards the edge of the aperture. This blockage, for normal radome diameter to antenna diameter ratios (about 4/3) can almost obviate any sophisticated attempts at increasing efficiency by obtaining uniform illumination. Furthermore, the computation of surface error efficiency by Ruze's method is based upon a tapered or weighted illumination function which is nominally a 10 db illumination taper. Toward the outer edge of the aperture of a physically realizable parabola, or quasi-parabola the actual surface tolerance will be lessened due to the reduced rigidity of the structure. Thus, while the RMS surface tolerance of the reflector surface may be measured to be, say 0.010 inch, the outer portion of the aperture, which has the least stiffness, but the greatest area, could logically cause the greatest phase error. For very high frequency systems, then, the Ruze phase error equation for uniformly illuminated apertures would predict an optimistic efficiency.

While no numerical results were obtained from the above discussion, it can be seen that certain flaws exist in the "uniform illumination - 100 percent aperture efficiency" design approach, and that this is especially true where a metal space-frame radome is employed.

As with everything in nature, there is an ultimate limit which cannot be exceeded. This holds true where the gain of an antenna is concerned. The gain of an antenna is given by

$$G = N \frac{4\pi A}{\lambda^2} \quad (7-17)$$

where

N is the efficiency

A is the area of the aperture

λ is the free space wavelength

Assuming a fixed efficiency, higher and higher gain is achieved with increasing aperture size. Unfortunately, the assumption of fixed efficiency with increased aperture size is not experienced in practice. For fixed efficiency, a fixed tolerance value must be held as the aperture is increased, i. e., mechanically a smaller and smaller percentage

variation is required. At the present state of the art, antenna gain limits have fallen between 73 to 75 dbi. This is illustrated in Figure 7-50 which plots the gains of several of the state of the art ground antennas.

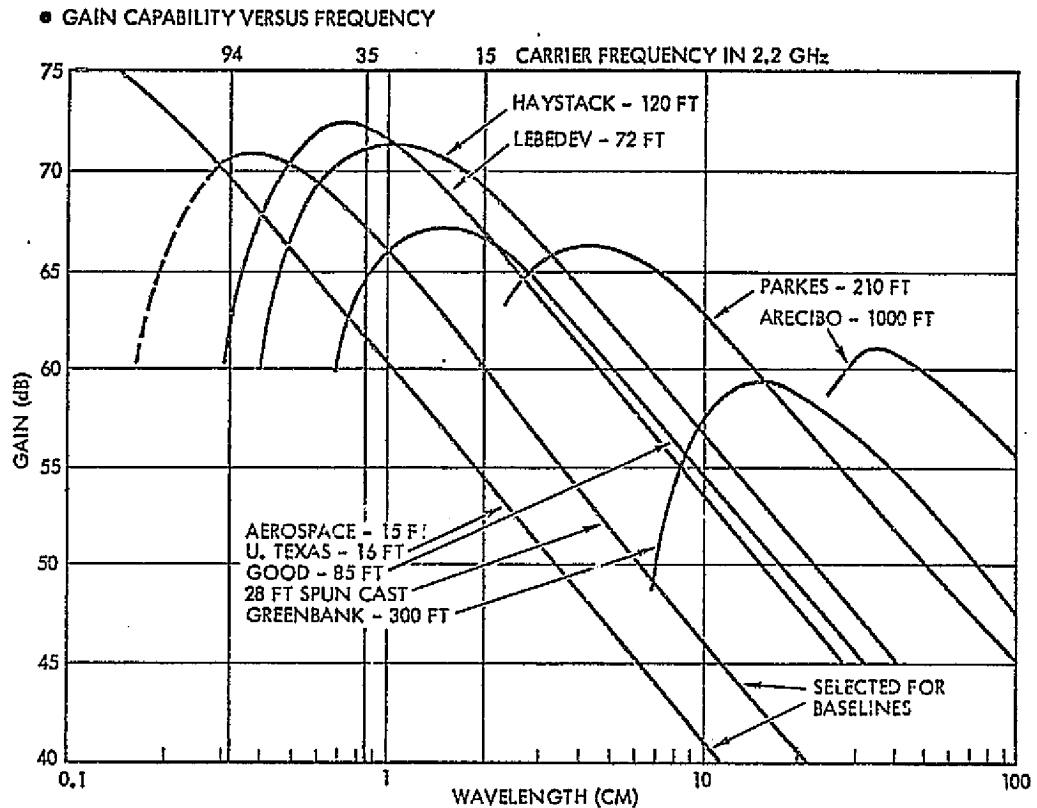


Figure 7-50. Gain of Large Antennas

7.3.6.2 Low Noise Amplifier Considerations. Many types of LNA's are available for frequencies well into the microwave range. Figure 7-51 presents noise temperatures that are representative, in mid-1974, of the cooled and uncooled parametric amplifier, the mixer, tunnel diode amplifier and field-effect transistors (FET's).

The maser exhibits bandwidth limitations of about 150 MHz. It also requires a very expensive liquid helium cryogenic refrigerator. The traveling-wave tube has been subject to obsolescence wherever it could be replaced by solid-state device. As a result of the liabilities in the maser, and the general trend away from TWT's, development efforts are concentrated on the cooled paramp, which despite its slightly higher noise temperature, than the maser is much lower in

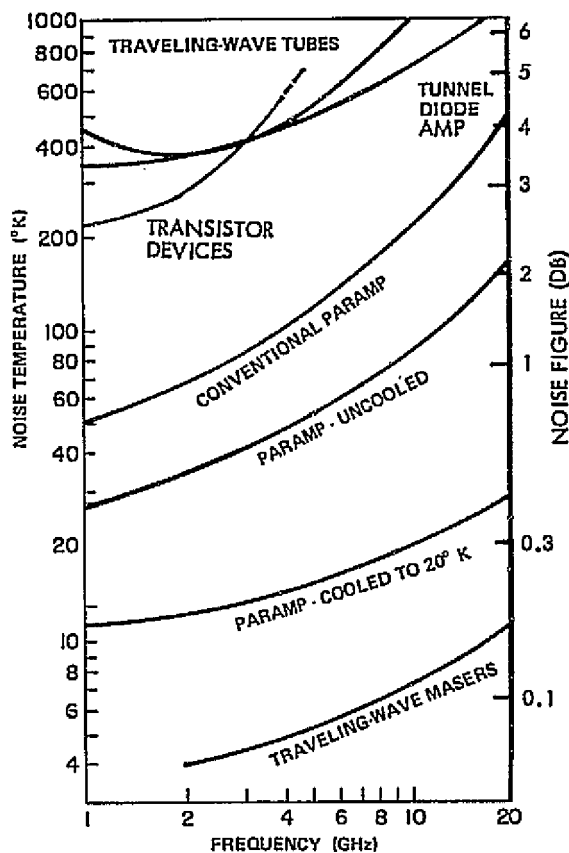


Figure 7-51. State of the Art for Preamplifiers

cost, has a much wider bandwidth, and can operate reliably unattended for thousands of hours.

Many of the technologies required for stable wideband cooled and uncooled paramps matured between 1966 and 1970. A highly reliable 17°K cryogenic refrigerator was developed. Gallium arsenide varactors with cutoff frequencies in excess of 200 GHz were procured. Capricious and unstable reflex klystrons gave way to the stable long-life two-cavity klystron, which then were superseded by the solid-state pump utilizing the Gunn diode oscillator.

Uncooled paramps of extremely low noise temperatures, approaching what would have been considered to be the noise temperature of a cryogenic paramp ten years ago, are now being built in many frequency ranges. Wideband paramps are available at frequencies from 2 GHz all the way up to 94 GHz. The klystron has now been virtually entirely supplanted by solid-state pumps for most new communication paramps.

The development of new varactors for use in either cartridges or waveguide mounts, with cutoff frequencies well above 500 MHz and capable of being pumped in the 60-80 GHz range, are now being made.

Modern paramps utilize significant thermal stabilization techniques to assure that the varactor temperature is very stably maintained. The two most common stabilized temperature environments in use today are: 1) around 17°K , which is found in the dewar of a cryogenic refrigerator or 2) on a temperature-stabilized plate using Peltier cooling, usually at 20 degrees below zero. In today's terminology, the former would be a cooled paramp, whereas the latter would be on "uncooled" paramp.

Effective temperature is related to varactor thermal temperature by cut-off frequency and pump frequency.

One favorable technical aspect of the cryogenic paramp is the fact that, to achieve noise temperatures usually below 50°K even into the 10-20 GHz range, a pump frequency as low as around three times that of the signal frequency can be used.

On the other hand, the uncooled paramp- and this refers to paramps whose varactor temperature can be maintained thermoelectrically as low as at -40°C has a significant problem since it requires that the pump frequency be as far removed from the signal frequency as is practical. Figure 7-52 illustrates the performance improvement achievable by increasing the pump frequency of 4 GHz paramp whose varactor is maintained at -18°C .

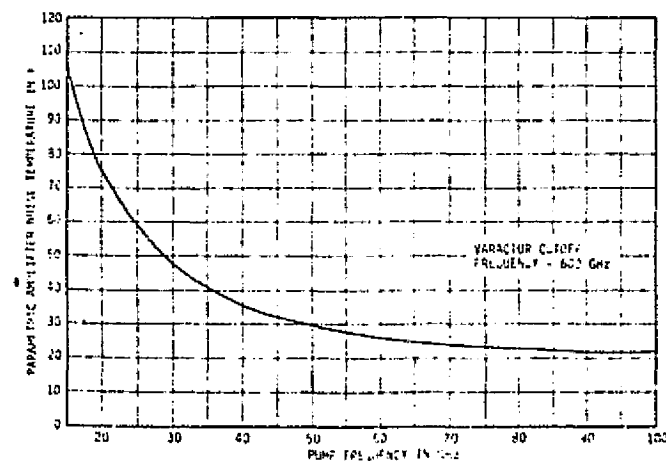


Figure 7-52. Parametric Amplifier Noise Temperature Versus Pump Frequency

Uncooled paramps above 15 GHz use pump frequencies from 70-120 GHz and have noise temperatures in the 4-6 db range. This high noise figure makes these amplifiers still very attractive, but now significant competition comes from mixer down-converters with 5.0 db conversion loss, which can operate into a 1-db noise figure transistor amplifier at UHF or VHF.

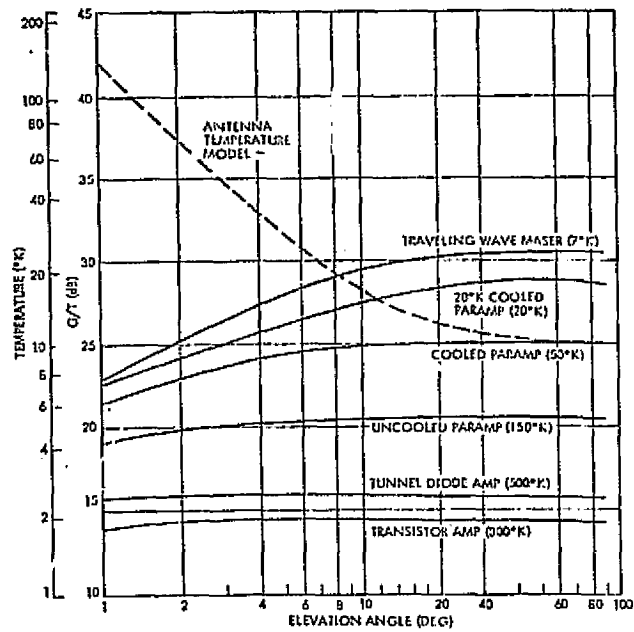
Pump power level variation. The pump power level is one of the key elements of paramp stability with respect to gain. In general, a change of approximately 0.1 db of pump power will result in about 1 db of gain change. Modern practices now provide leveling loops and thermal controls adequate to maintaining gain stability to approximately 0.5 db.

7.3.6.3 System G/T. The system noise temperature substantially represents the thermal sum of the antenna, the feed and feeder, and the low noise receiver.

Principal contributors to noise temperature of a parabolic antenna at received frequencies include cross-polarization loss, forward spillover loss, and blockage and scattering loss. Also, the antenna looks into a sky having various temperature values; when the antenna is at the zenith, the sky temperature is approximately 3.5°K ; at 7.5 degrees above the horizon, the sky temperature is 22.7°K ; and on the ground, the antenna temperature is 240°K . The antenna will sum various noise contributions depending on elevation angle beamwidth, side lobes, and back lobes and provide antenna noise temperature, T_a .

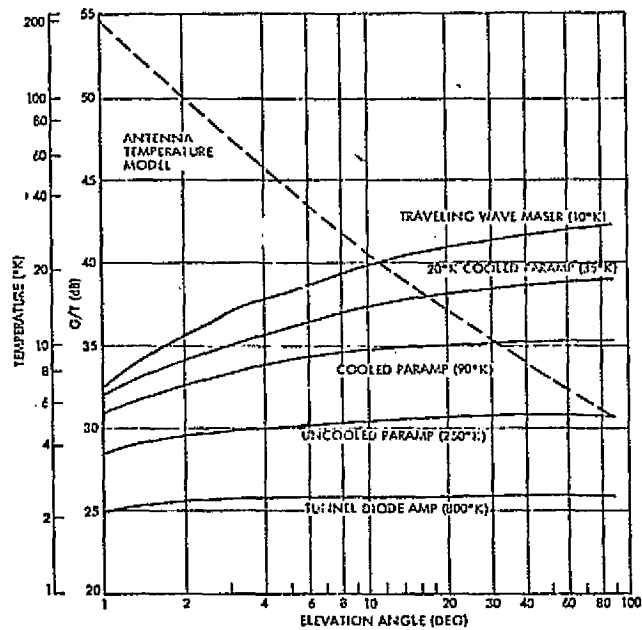
Antenna temperature will never be significantly below 10°K , even when pointed at the zenith. At low elevation angles, this noise temperature will be in the 30° - 60°K range. Feed and feeder loss noise contributions will never be less than about 15°K and most earth terminals will be in this range.

Based on a reasonable antenna temperature assumptions, G/T curves have been developed for the four key frequencies of interest, 2.2, 8.7, 13.7 and 21.6 GHz for probable antenna sizes and candidate pre-amplifiers. These are presented in Figure 7-53 a through d for the four frequencies 2.2, 8.2, 13.7 and 21.6 GHz. Antenna diameters of 25.9m (85 ft) and 9.1m (30 ft) are used for 2.2 GHz and 8.2 GHz, and 9.1m (30 ft) and 3.8m (12.5 ft) for 13.7 and 21.6 GHz.



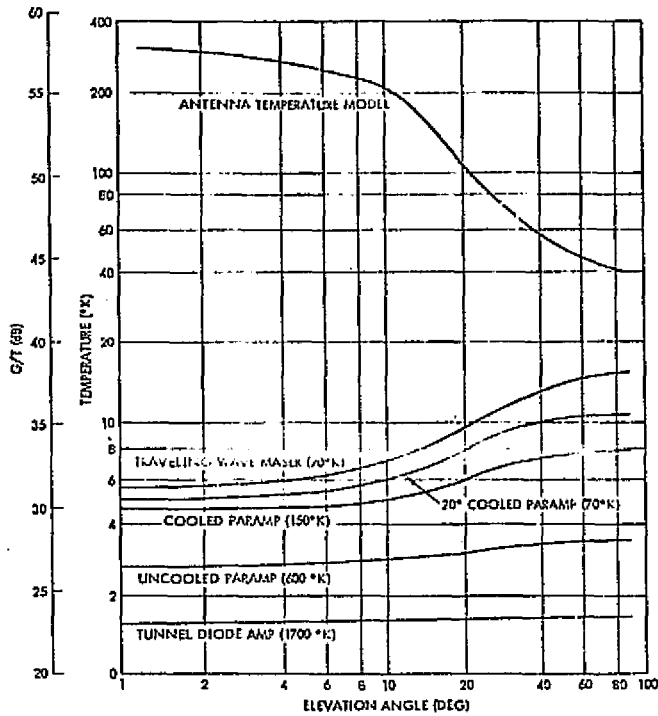
30 FOOT ANTENNA WITH A GAIN OF 43.9 dB
 85 FOOT ANTENNA WITH A GAIN OF 52.9 dB

Figure 7-53a. G/T for a 30-Foot and +85-Foot Parabolic Antenna at 2.2 GHz (add 9 db when using 85-foot antenna)



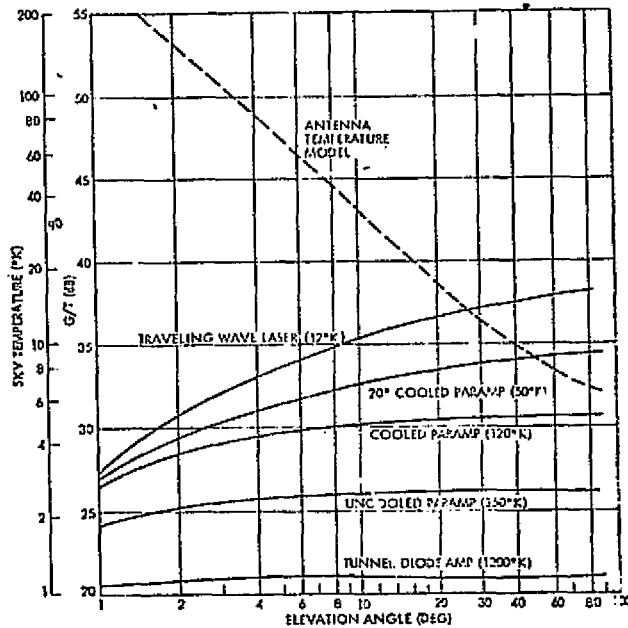
OPERATING FREQUENCY 8.2 GHz
 30 FOOT ANTENNA WITH A GAIN OF 55.3 dB
 +85 FOOT ANTENNA WITH A GAIN OF 64.3 dB

Figure 7-53b. G/T for a 30-Foot and +85-Foot Parabolic Antenna at 8.2 GHz (add 9 db when using 85-foot parabola)



OPERATING FREQUENCY 21.6 GHz
 12.5 FOOT (3.8M) ANTENNA WITH A GAIN OF 56.1 dB
 30.0 FOOT ANTENNA WITH A GAIN OF 63.7 dB

Figure 7-53c. G/T for a 12.5-Foot and +30.0-Foot Parabolic Antenna at 13.7 GHz (add 7.6 db when using 30-foot antenna)



12.5 FOOT (3.8M) ANTENNA GAIN IS 52.2 dB
 30.0 FOOT ANTENNA GAIN IS 59.0 dB

Figure 7-53d. G/T for a 12.5-Foot and 30.0-Foot Parabolic Antenna at 21.6 GHz (add 7.6 db when using 30-foot antenna)

7.3.6.4 Ground Receiving System Costs. Cost-oriented programs frequently must meet a system specification by a realistic determination of the cost effectiveness of the antenna system. There are numerous tradeoffs to be considered between the antenna costs, which relate to gain and antenna noise temperature, and the preamplifier costs, which relate to receiver noise temperature.

In the final analysis, the merit of the design of an earth station, will be how well it minimizes the cost of achieving a particular G/T. The problem of meeting a given G/T requirement at minimum cost, therefore, becomes one of selecting the minimum cost of an antenna and preamplifier.

Selecting the least-cost antenna preamplifier combination is accomplished by using the following: 1) cost curves for antennas, which vary with diameter and therefore with gain, 2) cost curves for preamplifiers, which vary with noise temperature, and 3) curves for feed cost, which also can vary with antenna size.

Antenna Cost Analysis. In any antenna system the antenna diameter is the principal parameter of cost. When it is greater than 30 feet, the cost of the structure increases rapidly so that the structure can withstand severe environmental conditions, and be movable by servo equipment on pedestals of practical design.

Potter of NASA/JPL related antenna costs to diameter according to the following equation

$$\text{cost } (\$000) = 4.37D^{2.78}$$

Where D is the antenna diameter in feet.

This equation is particularly applicable to antennas greater than 75 feet and also indicates that a small increase in antenna diameter can involve a very significant change in cost. For example, an increase of 14 feet for a 90-foot antenna can lead to a normal increase in cost between \$200,000 and \$300,000 over the cost of a 90-foot antenna.

Actually, no expression has ever been developed to represent antenna costs for the wide variety of types, cheap, commercial, military and for diameters as little as 5 feet.

The Philco-Ford curve, shown in Figure 7-54 represents antenna cost data made available through the POLFTS program, available in the GE Shared Computer Service.

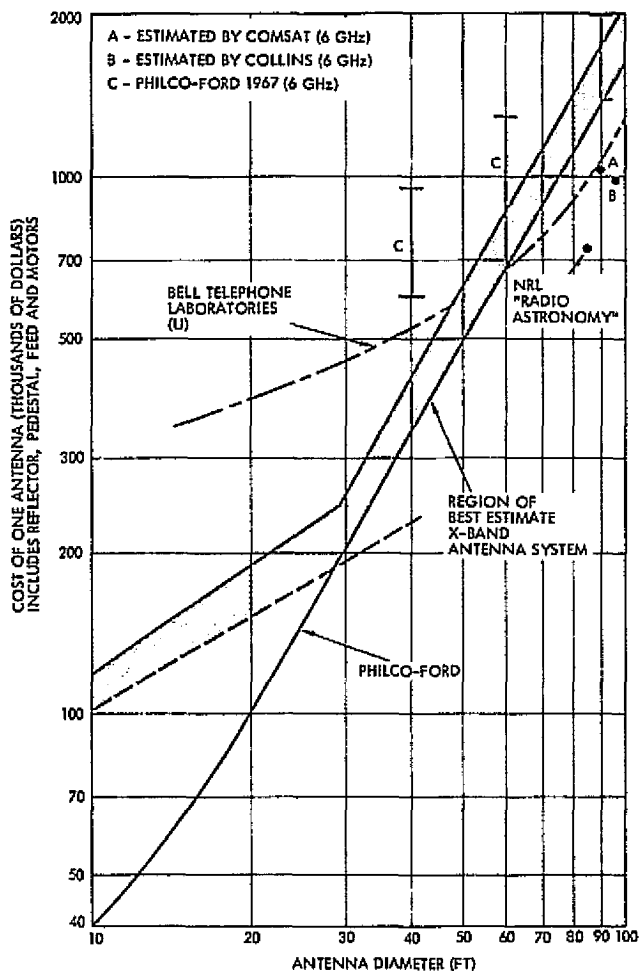


Figure 7-54. Ground Antenna System Costs

Preamplifier Cost Analysis. The choice of low-noise devices for a particular G/T depends not only on performance and noise temperature required in bandwidth, but very heavily upon cost. Many different cost levels are encountered, from the cost of a maser representing a cost in excess of a quarter of a million dollars, to the cost of a tunnel-diode amplifier, representing costs of less than \$3000. These costs are plotted in Figure 7-55 as a function of preamplifier noise temperature on a non-redundant per-channel basis. Costs are based on present figures reported by the various principal manufacturers of low-noise aerospace microwave amplifiers in the industry.

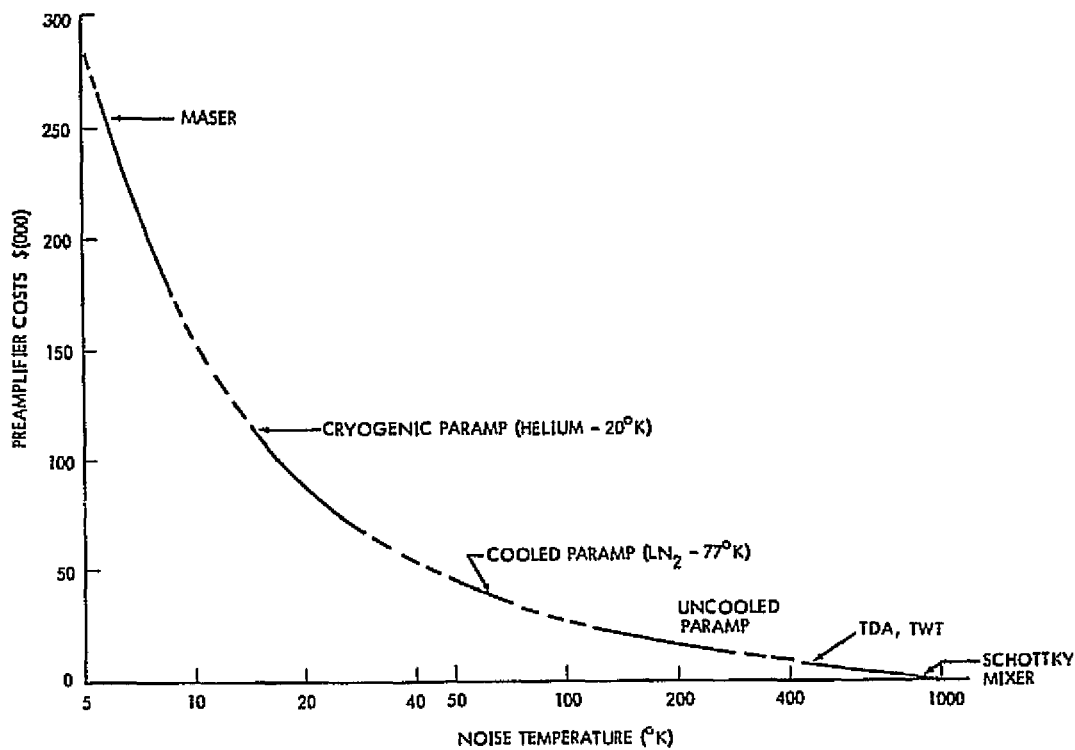


Figure 7-55. Preamplifier Costs

Cost Optimization Curves. G/T versus system costs for various antenna sizes may be developed from curves of G/T such as Figure 7-53 and costs of the antenna and preamplifiers cited above. An example is shown in Figure 7-56 for a low elevation angle of 7.5 degrees, which represents a near-to-worst case.

G/T versus antenna system costs were developed based on purchased or first costs for the frequencies 2.2, 8, 13, and 21 GHz, for antenna diameters for 5 up to 100 feet and G/T from 16 to 44 db where applicable.

Figures 7-57a through 7-57d show G/T cost curves as a function of antenna diameter for the above mentioned frequencies. The elevation chosen was 7.5 degrees representing a low elevation position close to the horizon, a near-to-worst case.

Each G/T curve has the basic curve form, following a small increment from the basic antenna and feed cost curve, and then passing through a minimum and rising to infinity in regions of sensitivity where cooled preamplifiers or masers are required to maintain sensitivity. The sharp minimum cost point reflects the domination of the antenna costs in the cost equation until the sensitivity can no longer be attained.

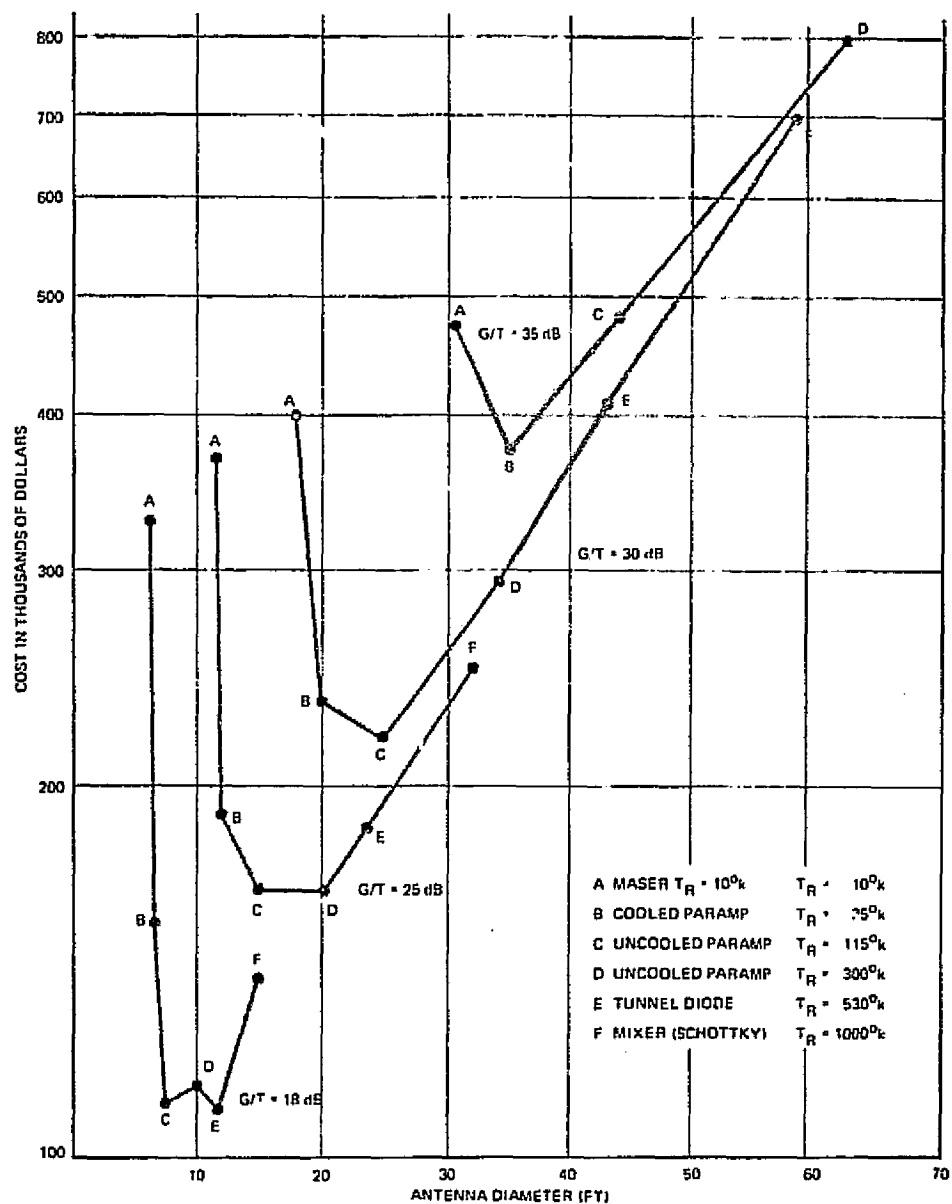
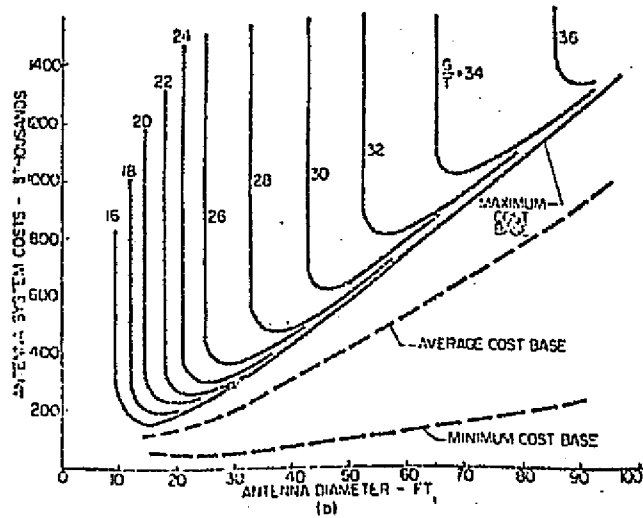
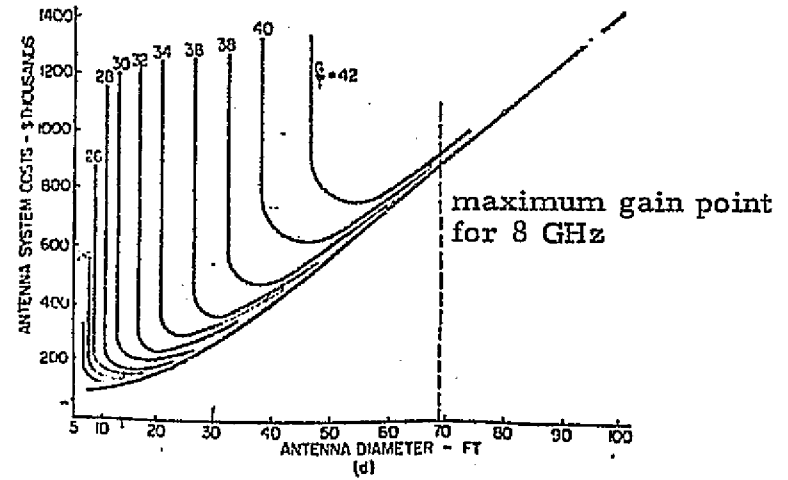


Figure 7-56. Estimated Minimum Cost Antenna System at Specified G/T Levels

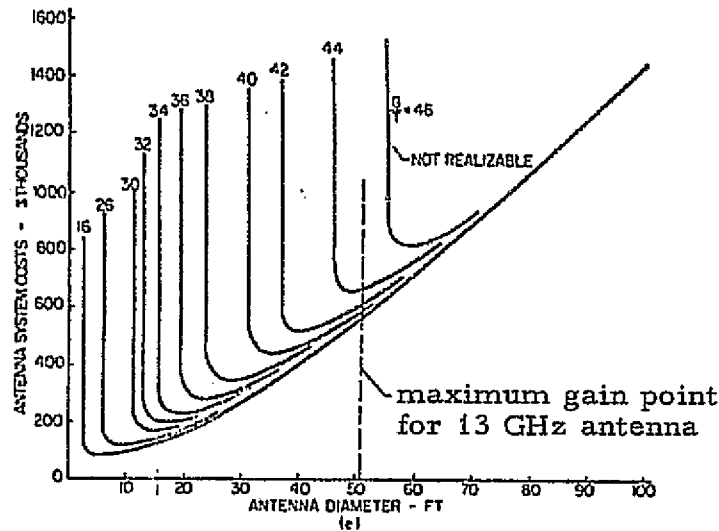
As the frequency is increased to 21 GHz, the maximum gain limitation providing a maximum diameter comes into effect sharply limiting antenna size. The curve for 21 GHz is semi-academic at points of maximum sensitivity since masers and cooled paramplifiers are not at the product status for these frequencies. Due to high atmospheric losses, the sensitivity of a space-to-earth link may not be economically served by a parametric amplifier due to the high noise level. Here a tunnel-diode amplifier at the 500°K noise temperature may provide the most practical approach to sensitivity that a typical link can provide.



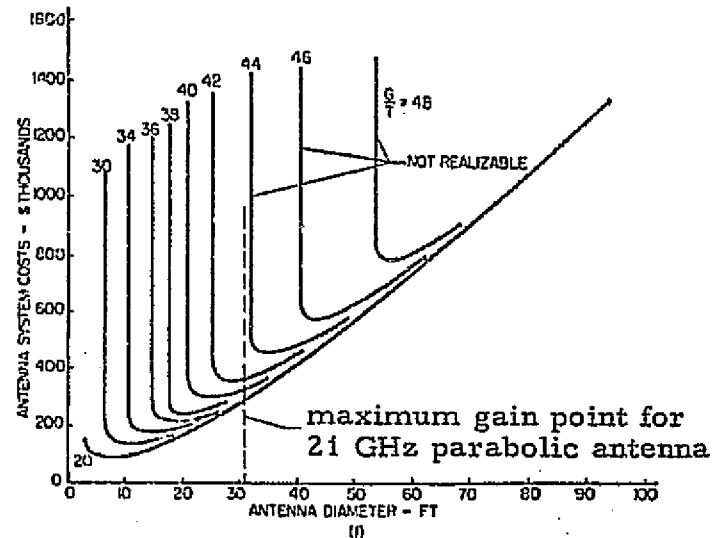
(a) Cost curves for "maximum cost base" antenna systems operating at 2.2 GHz and an elevation angle of 7.5 deg.



(b) Cost curves for "maximum cost base" antenna systems operating at 8 GHz and an elevation angle of 7.5 deg.



(c) Cost curves for "maximum cost base" antenna systems operating at 13 GHz and an elevation angle of 7.5 deg.



(d) Cost curves for "maximum cost base" antenna systems operating at 21 GHz and an elevation angle of 7.5 deg.

Figure 7-57. Cost Curves for "Maximum Cost Base" Antenna Systems

7.3.6.5 Minimum Cost for G/T and Frequency

An important aspect to economic antenna system design is the minimum cost point of a G/T curve where the optimum size of antenna is matched with the most economic value of amplifier noise temperature. Figure 7-58 shows a family of curves that represents the locus of lowest cost points at each frequency for each G/T versus antenna diameter curves of Figure 7-57a through 7-57d. The antenna cost range is for maximum cost or military antennas.

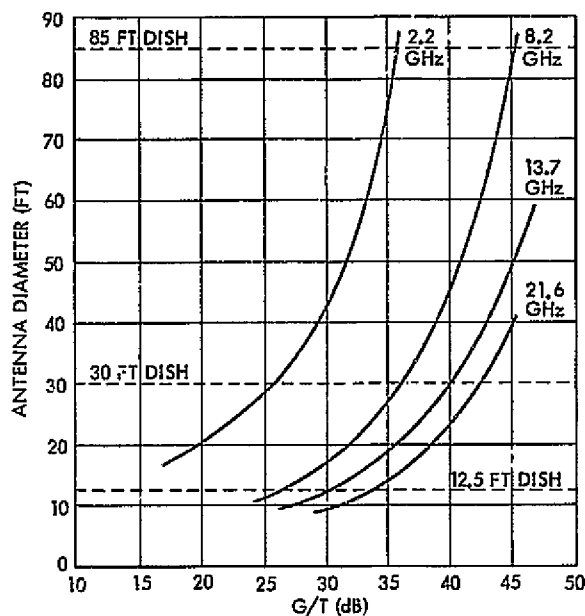


Figure 7-58. Minimum Cost Locus

7.4 ERS Power Budget Analysis

Section 7.1 summarizes projected requirements. Nine candidate missions are listed, with orbital altitudes ranging from 707 km to geosynchronous attitude. Parametric charts are presented here for five representative altitudes of 707, 852, 1146, 1852 and 34,880 km.

Section 7.2 reviews possible frequency allocations, and suggests six, ranging from 2.2 GHz to 65 GHz. Of these, parametric data is presented in this report for four; 2.2, 8.2, 13.7 and 21.6 GHz. Due to greater atmospheric absorption, the possibility of link operation at 51 or 65 GHz seems remote at this time.

A major concern regarding the higher frequencies, above 8.2 GHz is the increased attenuation at lower elevation angles, caused by atmospheric absorption and adverse weather. However, because of bandwidth requirements for projected data rates, and the STDN/TDRSS use of Ku-band, it is essential to consider these frequencies and to recognize the impact of excess attenuation on useful communications time during each orbit.

The following sections address the problem of synthesizing and selecting a suitable communication system for the missions developed earlier in this report.

7.4.1 Link Budget Technique

Section 7.3.1 presented an overview of the link power budget. Equation 7-18 is a variation of one form with parameters expressed in decibel form.

$$\frac{E_b}{N_c} = \underbrace{(P_t G_t)}_{(1)} + \underbrace{\frac{G_r}{T_{eq}}}_{(2)} - \underbrace{R_L}_{(3)} - \underbrace{k}_{(4)} - \underbrace{L_P}_{(5)} = \underbrace{\frac{E_b}{N_o}}_{(6)} \underbrace{+ M}_{(7)} \quad (7-18)$$

(1)
(2)
(3)
(4)
(5)
(6)
(7)

- (1) = Satellite ERP
- (2) = Ground receiving station figure of merit
- (3) = Information data rate
- (4) = Boltzman's constant = $-228 \text{ dbw}/\text{o}_K/\text{Hz}$
- (5) = Path loss
- (6) = Threshold $\frac{E_b}{N_o}$
- (7) = Link margin

Of these parameters, (1), (2), and (6) tend to be flexible, and subject to variation by the designer, who strives to select combinations leading to an effective low-cost system, subject to given constraints.

To establish a straightforward method of handling this reasonably complex communication synthesis problem, which requires evaluation at a set of communication frequencies and for a number of satellite orbits, a link power budget flow chart is provided in Figure 7-59. Successive steps are labeled and discussed below.

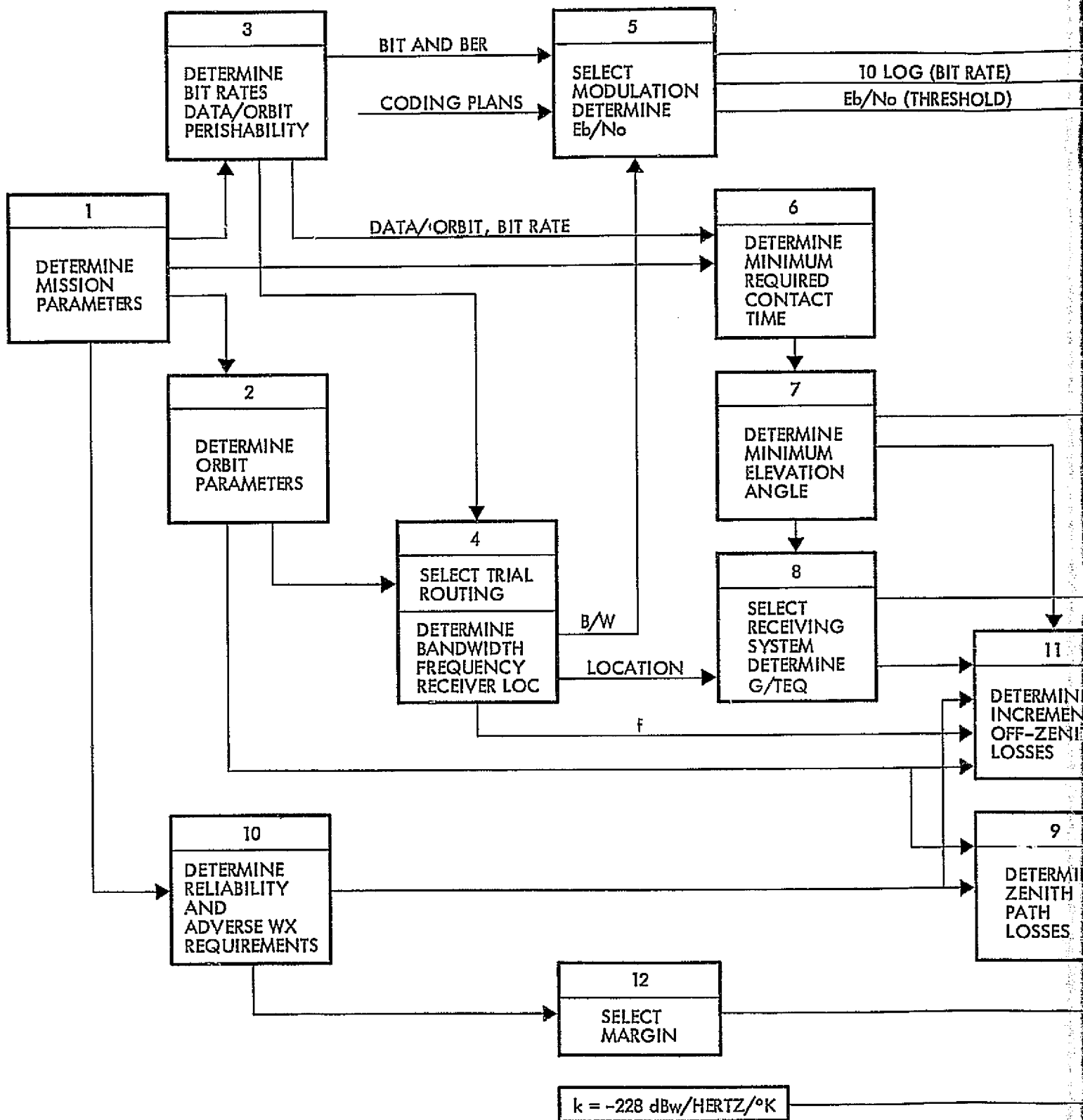
Step 1 and 2 gather the basic data necessary to define the mission, sensors, sensor data rates, on-board processing and/or storage, coding, reliability and orbit parameters. This information is addressed in previous sections of this report and is considered to be an input to the communication problem. Where inputs influence or constrain the system design, it would occasionally be desirable to influence specific parameters selected. An example would be the orbit selection problem which has important ramifications including available observation time and maximizing high-data rate flow before atmospheric loss occurs at low-elevation angles. An advantage of higher orbits includes increased contact time for circular orbits that do not pass directly overhead. Charts for the latter are included in Section 7.2.4.

Step 3. From Step 1, determine the sensor bit rates, the total amount of data to be accumulated per orbit, the data perishability, whether data is to be stored then retransmitted, the required bit transmission rates (which very likely will differ from the sensor data acquisition rates), and acceptable bit error rates.

Step 4. Based on Steps 1-3, review the constraints imposed by bit rates, orbital altitude, path and perishability and select a trial data routing. Candidates include the use of the STDN/TDRSS network in a direct or relay mode, and either real time or store and playback transmission to a ground terminal. (When STDN/TDRSS is to be used, it will ultimately be necessary to verify it's availability). The output of this step should include link frequency, the available bandwidth of the selected routing and the location of the receiving terminal (on the ground, or another spacecraft as in the TDRSS).

Step 5. Based on the results of Steps 1-4, including data rate, bandwidth limitations, required bit error rate, and whether coding will be employed, select a candidate modulation and establish the threshold E_b/N_0 for the required bit error rate. Bear in mind that coding will extend total transmission time for a fixed amount of data and fixed bandwidth.

An important cost consideration, also to be considered, is whether or not pre-established demodulation equipments already exist to handle



1960 OUT FRAME

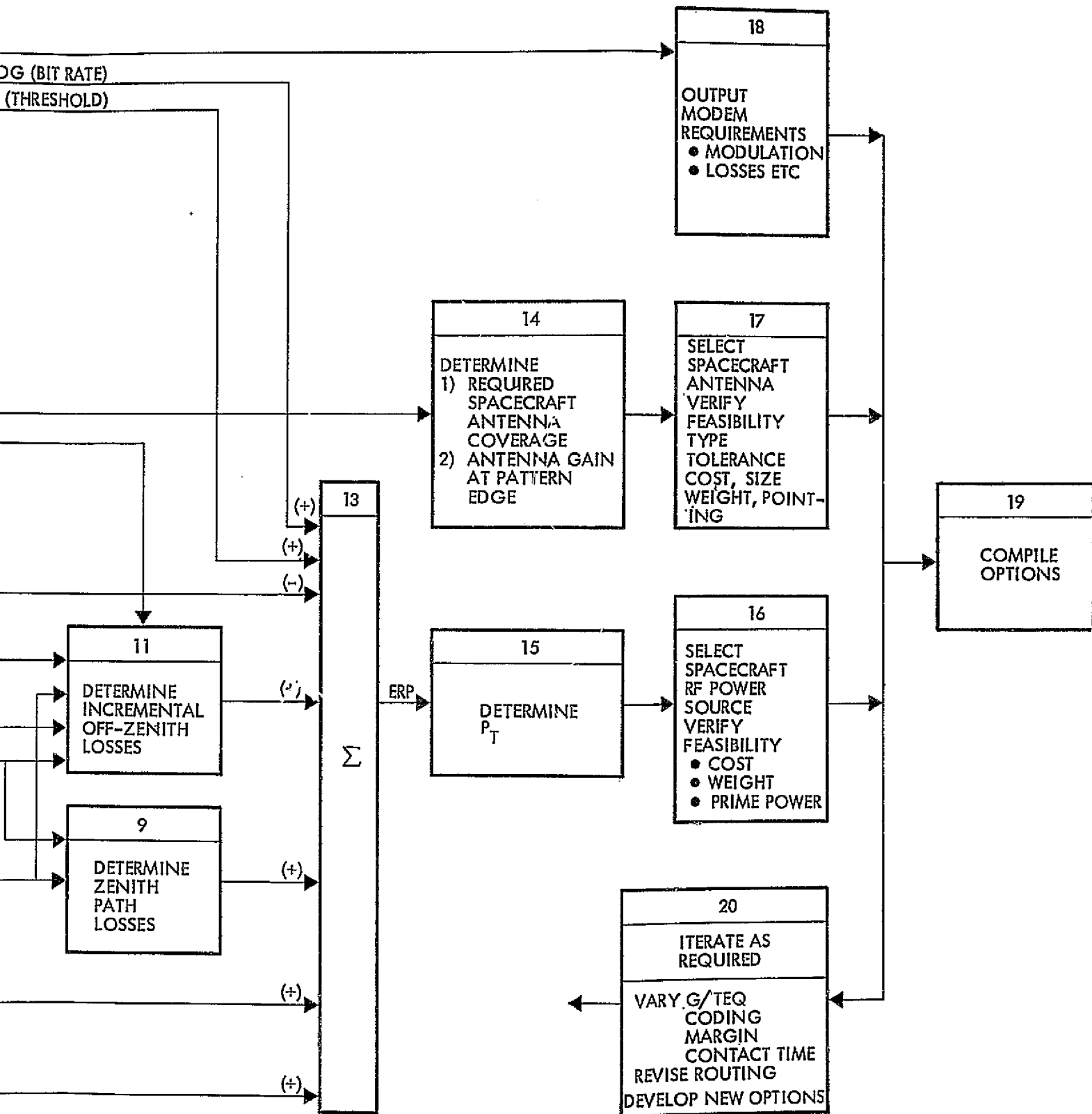


Figure 7-59. Link Power Budget Synthesis Sequence

data. For this case, many links are already operable using two- and four-state FSK transmission links. While these do not give the degree of bandwidth reduction that the higher order modulation techniques provide, hardware does exist for these modulation techniques and therefore is an important factor in the selection of the modulation technique chosen. Parametric curves to assist in selecting the modulation format and E_b/N_0 are presented in Figures 7-26, 28, 29 and 7-37 of Section 7.3.2. When the bit rate, after coding, exceeds the available bandwidth it will be necessary to use a multiple state modulation. Figure 7-30 relates bandwidth in Hertz/bit to the number of modulation states for FSK, QPSK, and for MSK. Final bandwidth may be computed by applying these ratios to the after-coding bit rate, which is the data bit rate divided by the coding ratio.

Figure 7-37 may be used to determine E_b/N_0 for various modulations for the particular case of a bit error rate of 10^{-4} . For other bit error rates, see Figure 7-26, 28 and 30 and Appendices B and C.

Coding gains, in decibels, may be inferred from Figure 6-13 or from Table 6-6. Required E_b/N_0 equals E_b^1/N_0 without coding, less the coding gain. For the particular case of a BER of 10^{-4} , rate 1/2 coding will reduce the threshold E_b/N_0 of Figure 7-37 by 5.2 db, whereas rate 1/3 coding will reduce it by 5.7 db. However, rate 1/2 and 1/3 will also double or triple the required R. F. bandwidth or transmission time.

Step 6. Based on the results of Step 3 through 5, determine the minimum time required during each orbit to transmit data to the receiver. This will be used to determine the minimum elevation angle, in Step 7 from which worst case path losses may be determined in Step 11.

Step 7. Based on receiver location, orbit parameters and minimum transmission time required, compute the minimum elevation angle to the spacecraft from the receiving station. This is facilitated by the charts in Figures 7-11 and 7-12 of Section 7.2.4. Since the spacecraft will seldom pass directly over the ground receiving site, worst-case off-zenith angles should be used when determining the minimum elevation angle.

If the receiver is in another spacecraft, such as the TDRSS relay, verify that the relay will be in view when required. The majority of the following sections relates to using ground receiving stations. Variations for the TDRSS are reviewed in Section 7.4.2.

Step 8. A major step in the link synthesis process is the selection of a ground station receiving system. To a certain extent this is dependent upon the routing being evaluated, thus if a STDN site location is under consideration, it very likely will have an in-place antenna and receiving system. If, on the other hand, a new station is to be erected at the ground receiving location, more options will be available.

To maximize the effectiveness of the link budgets presented here, three antenna sizes have been assumed. These include 30- and 85-foot dish antennas usable at 2.2 and 8.2 GHz. A 3.8-m (12.5-foot) antenna along with the 30-foot dish antenna has been selected for use at 13.7 and 21.6 GHz. After reviewing current STDN station capabilities and proposed plans for the stations through CONUS, these antenna selections seemed most reasonable. Selection of a receiver was more difficult to establish, so conservative models of six varieties have been considered. The six receiver types are: 1) transistor amplifier at 2.2 GHz only, 2) tunnel diode amplifier, 3) uncooled paramplifier, 4) 77°K cooled paramplifier, 5) 20°K cooled paramplifier, and 6) traveling wave maser. The very best device is a traveling wave maser and the most conventional and least costly device is the tunnel diode and/or transistor amplifier.

A part of this step is to determine the G/T_{eq} of the antenna/receiving system to be used. Figures 7-53a-d present parametric curves of likely G/T_{eq} for 85, 30 and 12.5 foot parabolic antennas with the selected amplifiers. This G/T_{eq} may be readily determined for the particular amplifier at the minimum elevation angle determined in Step 7.

If an existing site is to be used, the designer would use G/T_{eq} curves for that site. However, if a ground system is to be developed, some care should be given to the cost-aspects of selecting a receiver and pre-amplifier, with due attention given to the merit of selecting more sensitive preamplifiers in view of the elevation angles to be used. For example, between 10 degrees and zenith elevation angles, significant improvements can be realized by using the higher quality receivers. At

elevation angles of less than 10 degrees, the traveling wave maser and cooled parametric amplifiers coverge to about the same antenna gain to effective system temperature (G/T).

Step 9. Determine the free space zenith path losses from Figure 7-60 which is based on the equation

$$L_p = \left(\frac{4 \pi d}{\lambda} \right)^2$$

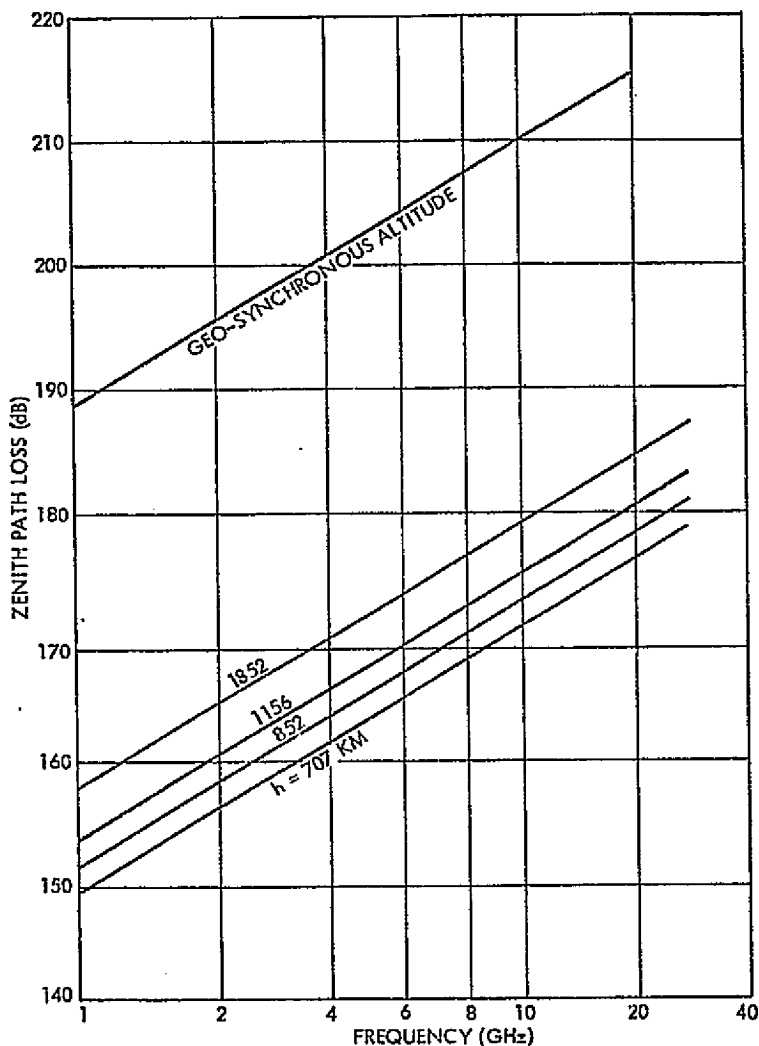


Figure 7-60. Zenith Path Losses

Step 10. It is next necessary to determine the incremental losses, at the minimum elevation angle, caused by atmospheric losses, weather, and increased path length due to off-zenith conditions. Before weather losses can be determined, however, it is necessary to review reliability and outage requirements from the mission requirement listing. This step therefore, involves checking link reliability and outage constraints from Step 1, and then determining the maximum rainfall rates that must be tolerated. This step, then, is to first determine the number of acceptable outage hours per year.

A portion of the acceptable outage hours can be allocated to adverse weather, with the remainder allocated to equipment failures.

Weather statistics are compiled in major meteorological stations and may be used, with varying success to determine atmospheric attenuation due to clouds and rain. Losses caused by clouds and weather is discussed in Section 7.2.6, and 7.3.5 and Appendix A. As an example, Figure 7-16 or Table A-1 present the average expected annual number of hours various rainfall rates occur at Washington, D.C., as well as attenuation for a 30 degree path. This table can be used to determine the worst-case acceptable rain rate in mm/hour, for use in Step 12. Similar data can be obtained for other sites of interest.

In view of the fact that the transmission time for some missions could be relatively short (see Table 7-1), repeat transmissions are worth considering for use when weather attenuation precludes successful data transmission on a particular pass. Retransmission could be on the same or on subsequent orbits. Thus, reliability and mission requirements should be reviewed to assess the need for automatic retransmission requests from the ground station. This possibility also needs to be assessed in terms of the total buildup of data from previous orbits, as well as on-board storage requirements and the number of orbits until the spacecraft is again within view of a ground station.

Step 11. Determine incremental losses caused by the atmosphere, clouds and weather, and by increased path length at off-zenith elevation angles. Atmospheric and weather losses will vary with the length of the path passing through the atmosphere or adverse weather, with frequency, and rainfall rates and cloud densities.

Considerable research has been invested on weather loss statistics, but there still is a great deal to be learned about the subject. Rain is by no means uniform, with heavier rainfalls occurring in smaller cells. Thus, there is concern about the true path lengths that pass through the heavier rain cells. For the purposes of this report, a conservative approach has been taken, leading to the atmospheric, cloud and rain losses presented in Figures 7-15a through d. A more precise statistical approach may be taken by those interested in doing so.

Based on the worst case rainfall rates from Step 10, and the minimum elevation angles of Step 7, one should next obtain excess transmission losses from Figures 7-15a through d.

Off-zenith path losses, due to increased path lengths may be determined from Figure 7-61, which is based on the equation

$$\text{loss (db)} = 20 \log \left[\frac{(r+h) \sin \left[\cos^{-1} \left(\frac{r \cos \delta}{r+h} \right) \right] - r \sin \delta}{h} \right] \quad (7-19)$$

where

- δ = the elevation angle
- h = orbit attitude
- r = the earth's radius, 6,378,388 km

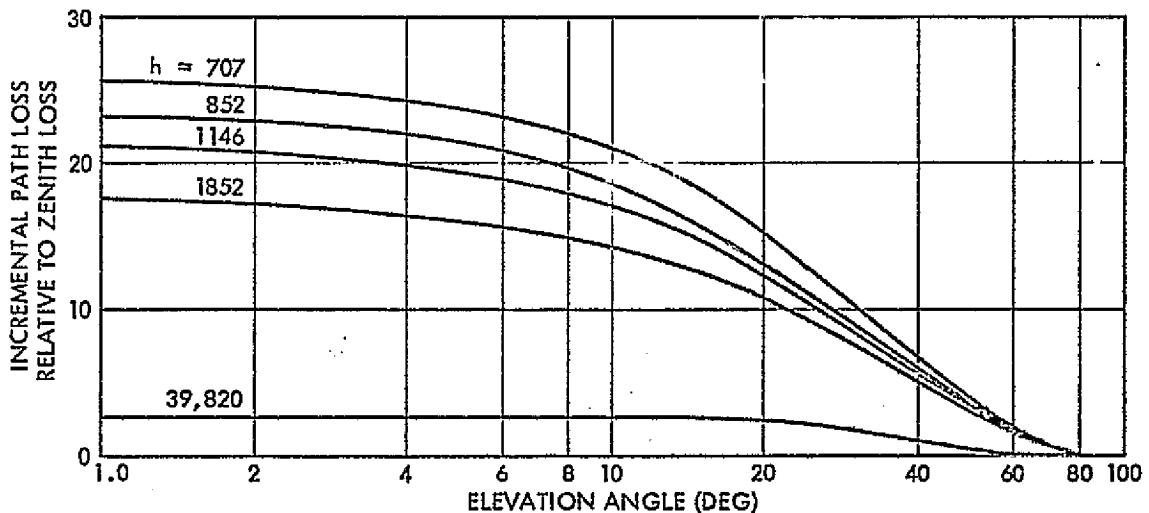


Figure 7-61. Off-Zenith Incremental Path Losses

Step 12. Select a system margin to allow for implementation losses, equipment degradations, additional path losses, or other factors. Reasonable values, sometimes used, vary from 3 to 6 db.

Step 13. Form the sum of parameters determined to date, in accordance with equation 7-18. The sum will yield the required spacecraft EIRP in the direction of the ground receiver at the minimum elevation angle. The remaining steps to be taken are to determine spacecraft antenna gain and rf power output, and to verify the feasibility of the design.

Step 14. Spacecraft antenna pattern and gain characteristics must next be determined. The EIRP of Step 13 applies to the direction of the ground receiver from the spacecraft. If the spacecraft antenna's bore-sight (direction of maximum gain) is not pointed at the ground terminal (or satellite relay), it is necessary to additionally compensate for pattern shape.

A major factor regarding spacecraft antenna gain limitations, is the mission constraint imposed by the possibility of requiring an antenna that illuminates the entire earth within view. If an earth-coverage antenna is required, it will not be possible to provide an arbitrarily high antenna gain to permit reducing the transmitted power.

If, on the other hand, earth coverage is not required, the spacecraft antenna pattern can be narrowed, and higher gain can be obtained.

Accordingly, it is necessary to review pattern coverage requirements and to then select an appropriate pattern and gain, bearing in mind that narrow beam antennas must also be pointed.

Figure 7-62 presents curves of parabolic antenna gain as a function of the diameter of the parabola, assuming 55 percent aperture efficiency. It also presents the resulting 3 db beamwidth versus gain, thus illustrating beam pointing requirements.

Step 15. The rf output power may next be determined, based on the EIRP computed in Step 13, and the antenna gain selected in Step 14.

Step 16 and 17 are feasibility check steps. At this point, one selects the antenna and rf power sources to be used, and verifies their feasibility. Factors influencing providing high EIRP's are illustrated

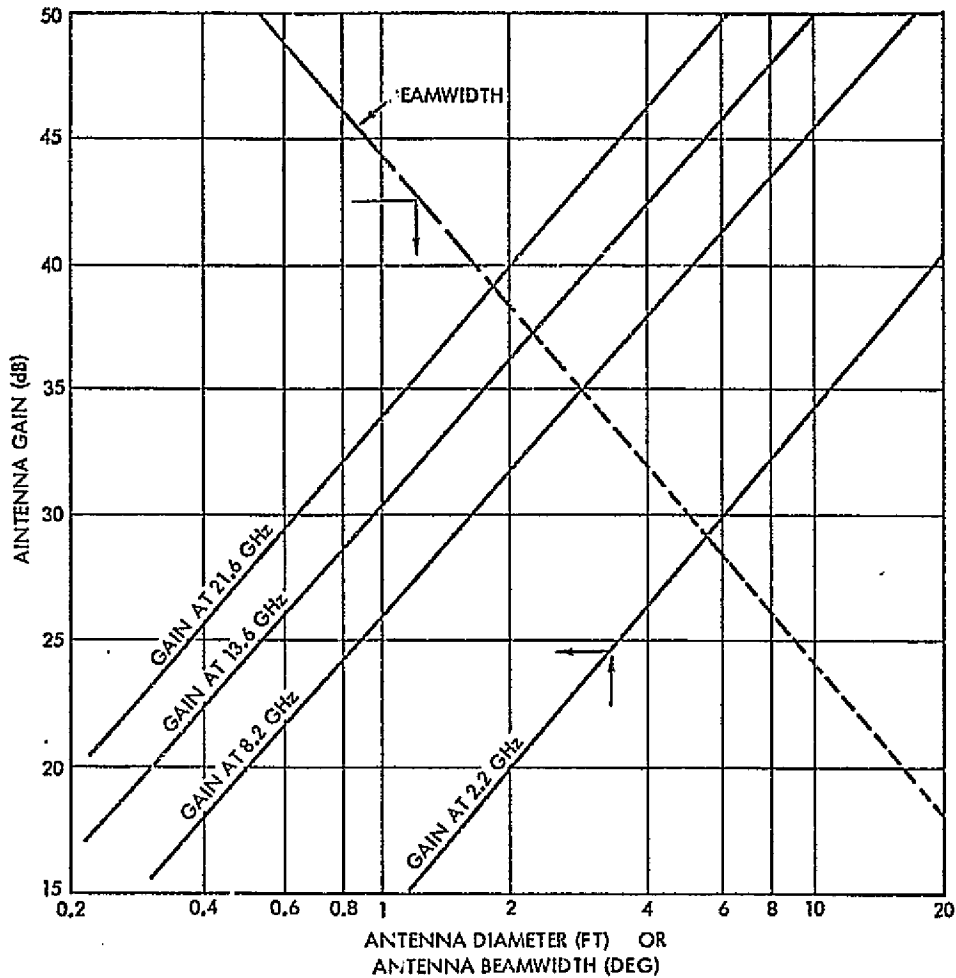


Figure 7-62. Spacecraft Antenna Gain and Beamwidth at 2.2, 8.2, 13.6 and 21.6 GHz

in Figure 7-63. Of these, prime power is a major factor that is directly influenced by rf power requirements as illustrated in Figure 7-64.

Step 18. Review modem requirements, including projected implementation losses, and development feasibility.

Step 19 and 20. Compile the basic parameters of this trial design, then consider iterating the design with input parameters adjusted in a direction anticipated to improve performance, lower cost or to simplify the design and improve feasibility.

7.4.2 Link Sizing for STDN and TDRSS

A process similar to that of the preceding section may be used to size a terminal to be used in conjunction with the STDN or TDRSS systems. These systems, however, will be designed for a specific modulation,

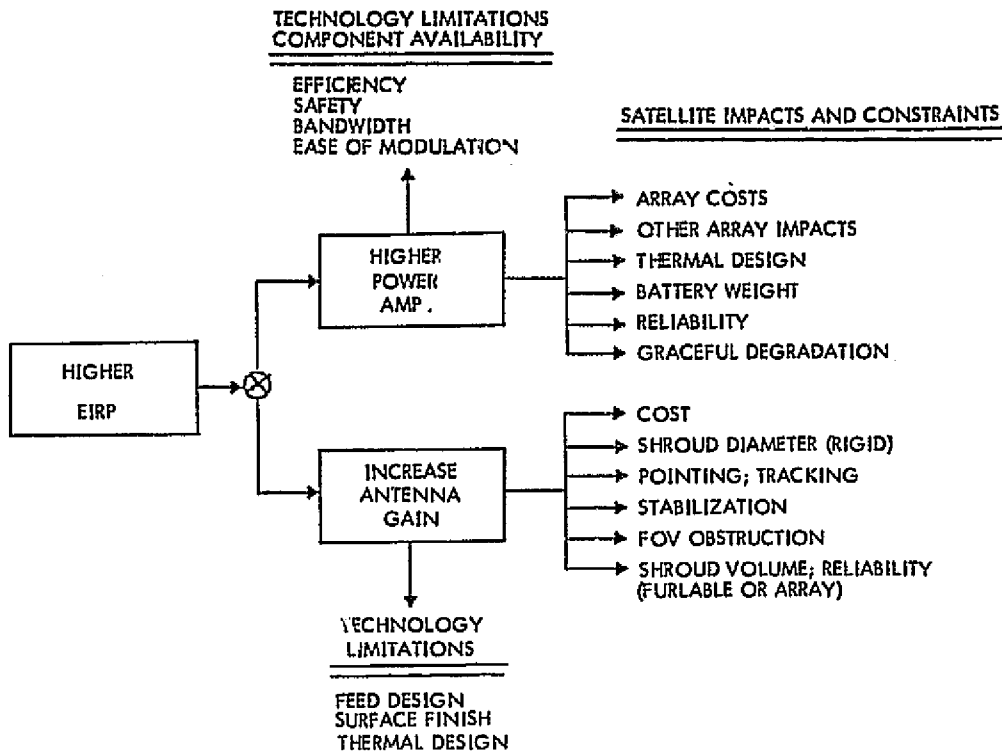


Figure 7-63. Tradeoff Factors Impacting Increase of EIRP

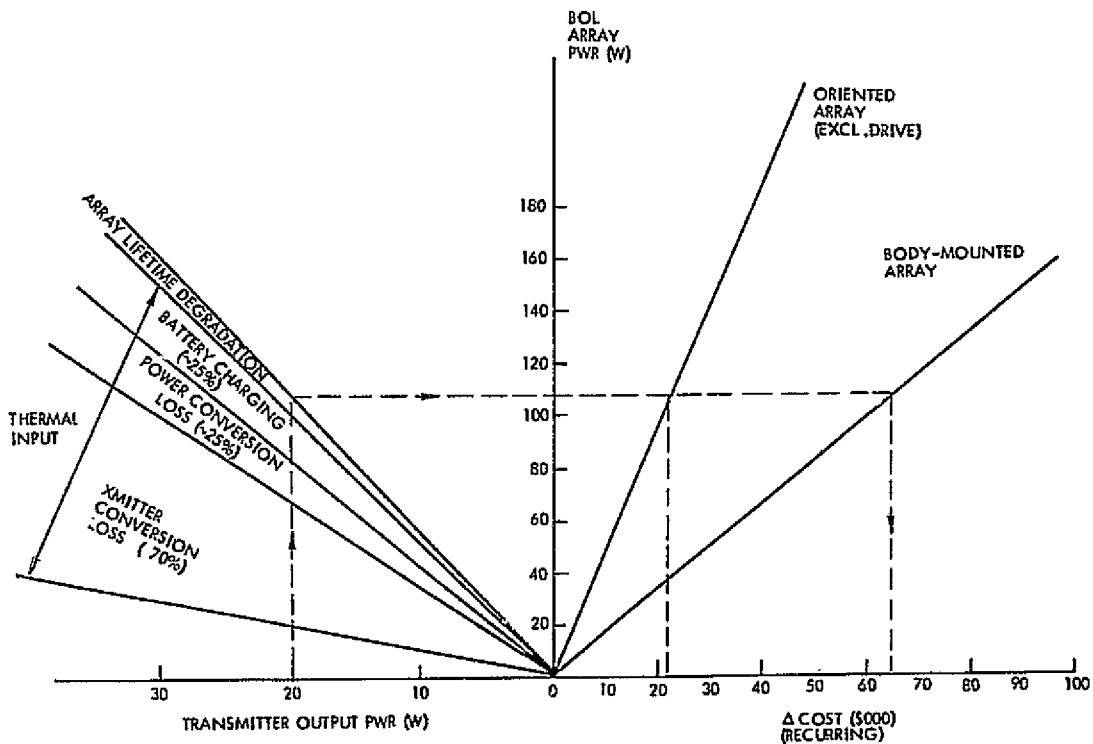


Figure 7-64. Impact of Increasing RF Power Output

(PSK), carrier frequency (S-and Ku-band) and will have receiving terminals in place. Accordingly, some of the steps of Figure 7-59 may be bypassed, since the only factors remaining to be determined is the required spacecraft EIRP and its allocation to antenna gain and rf power.

Figure 7-65 is a convenient nomogram to facilitate link sizing once the basic data rate has been selected. Three routings may be considered, two via the TDRSS relay at S-and Ku-band respectively, the third is via the STDN network at S-band. Spacecraft altitude for TDRSS may be anywhere below 5,000 km, with reduced availability below 1200 km. Spacecraft altitude for the STDN network is 4600 km, but may be adjusted by adding $20 \log (h/4600 \text{ km})$ to the EIRP requirements.

To use the chart, enter on the lower ordinate at the data rate and project left to the desired routing, then vertically to the required EIRP.

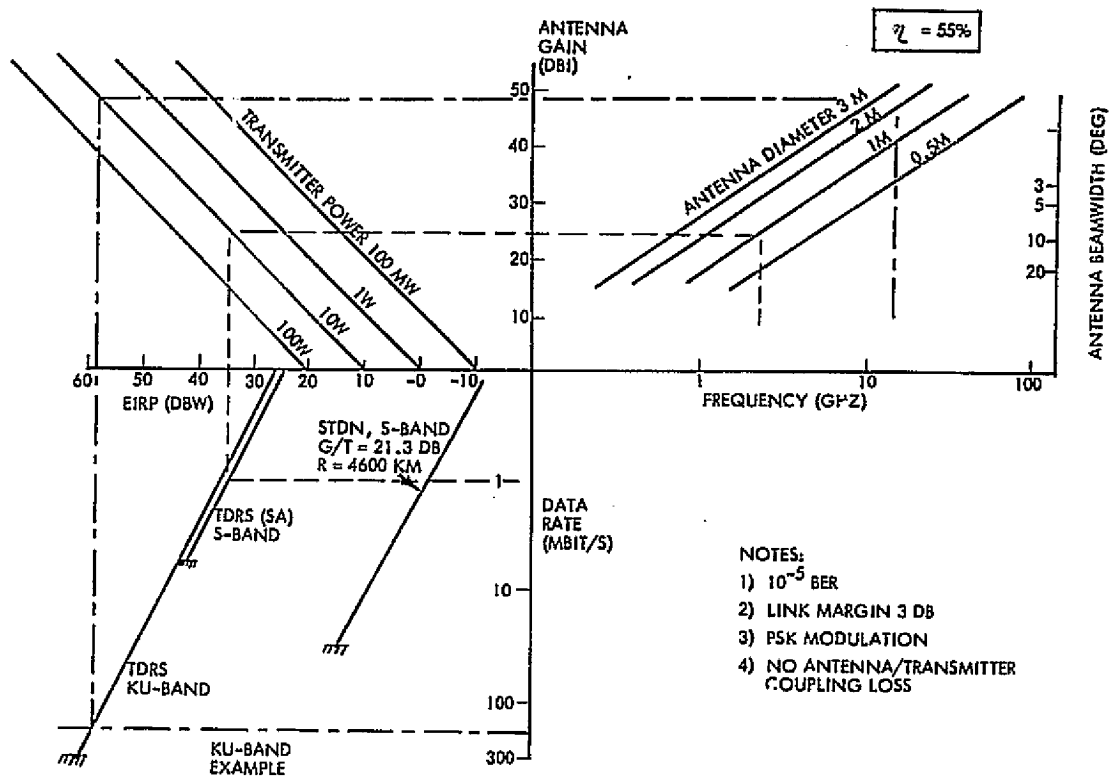


Figure 7-65. Communication Link Sizing Nomogram

The next step is to allocate EIRP to rf power and antenna size. Project vertically from required EIRP to a candidate rf power level, then horizontally to the correct frequency in the right quadrant to obtain

antenna size. Check the acceptability of the antenna size and the resulting beamwidth and iteratively adjust as necessary.

7.5 Optical Communication Systems

The use of visible or near-visible light frequencies for communication purposes differs from the use of microwave frequencies in some important ways. A laser can be considered as an oscillator that generates the energy used for the carrier of the information. Laser systems frequently, but not always, use a modulator separate from the oscillator. The modulator applies the information to the laser energy. An optical system consisting generally of a telescope used with the laser radiation projected out of the objective end is the counterpart of the microwave antenna. At the receiver another telescope collects the energy and focuses it onto a photodetector which converts the radiation onto an electrical output that represents the signal applied to the laser beam at the transmitter.

The most applicable types of lasers are listed in Table 7-14 and further described in Appendix E. The salient features of presently foreseeable lasers are:

- Low-power conversion efficiency
- Uncertain operational lifetime
- Unknown reliability.

Table 7-14. Applicable Lasers

Laser Type	Examples	Radiated Wavelength (μm)		Power Conversion Efficiency	Maximum Output Power for Nominal Space Applications
Atomic Gas	Helium - Neon	0.632		10^{-4} to 10^{-3}	50 m watt
	Helium - Cadmium	0.4416	0.3250 μm		50 m watt
	Argon	0.5145	0.4880 μm		10 m watt
Solid State Optically Pumped	Neodymium in YAG	1.06		5×10^{-3} to 10^{-2}	~ 1 watt
		0.53 (frequency doubles 1.06 output)			~ 0.4 watt
Solid State Electric Current Pump	Gallium Arsenide with various Dopants	0.9050		2×10^{-2}	150 watt peak
		0.8470			2×10^{-4} duty factor
Molecular Gas	Carbon Dioxide	10.6		0.08 to 0.20	~ 150 watts

Regular lasers are modulated by direct control of the output light beam using a birefringent material. Semiconductor diode lasers are an

exception; their output may be intensity modulated by control of the driving current. The critical performance parameters of the modulator are the modulation voltage sensitivity and the associated power needed to drive the modulator over the desired bandwidth. Not all modulation techniques used with microwave tubes can be applied to lasers.

Perhaps the most significant difference in the use of laser frequencies rather than microwave frequencies is in the area of detection. For laser systems, coherent detection is superior to detection of just the signal energy as in radar and is enormously superior to the alternative of detecting the temperature rise due to the incident energy. In the frequency region the energy of the photons is about 10^5 times greater than that in the microwave range. It is nearly as efficient to use an energy (incoherent) detector as opposed to a coherent (heterodyne) detector. At the wavelength corresponding to the CO_2 laser ($10.6 \mu\text{m}$) heterodyne detector is superior to energy detection because there are no detectors available that have internal gain producing mechanisms. This is probably not fundamental, and perhaps in the future such detector materials will be synthesized. The consideration of heterodyne versus noncoherent detection has important system tradeoffs associated with it, and is reviewed in a later paragraph. In the visible and near-visible frequency regions such detectors do exist in the form of photo-multiplier tubes and avalanche photodiodes.

The remaining major subsystem element is the collecting optics (antenna) required at both the transmitter and receiver. Applicable systems are in an acceptable state of development; however, improved materials and methods are needed to reduce the weight of large (>0.3 -meter diameter) systems while maintaining optical quality.

The first consideration is usually the choice of laser transmitter. If the particular communication problem is one with large relative velocities (as between a low-earth orbit satellite and a synchronous relay satellite) a CO_2 laser with its need for a heterodyne receiver burdens the relay satellite with the need for a tunable laser local oscillator, for a cryogenically cooled detector/photomixer and alignment tolerance at the receiver of a small fraction of a wavelength ($10.6 \mu\text{m}$) between the local oscillator beam and the received signal beam. This translates into a

stringent attitude control requirement on the receiving terminal. For application to a relay link between two synchronous satellites however, the use of a heterodyne detection system would be more attractive. This is in part because the power efficiency of the CO₂ laser is so favorable for spacecraft application. Other lasers operating at shorter wavelengths can employ incoherent or direct detection. The theoretical (photonnoise) limitation is only 3 dB worse for direct detection than for heterodyne detection. Beamwidths for such cases are in the range of about 5 μ radians to perhaps 100 μ radians. These are substantially smaller than satellite attitude control tolerances, so it is likely that the user of a laser communication subsystem on a spacecraft will call for special laser pointing and tracking. The use of such narrow beamwidth between communication terminals which have differing tangential velocities/earth-low orbit, or earth to synchronous requires that the transmitter beam be pointed ahead, to allow for the trans time of the radiation from say a low orbit satellite.

For ground terminal application many of the constraints are not applicable. A critical related area, however, is that of the earth's atmosphere and its ability to support laser frequency propagation. This problem is also of concern in the EHF region, particularly if ground stations located in areas of heavy rainfall. The tradeoff considerations include use of locations in high elevation dry climates, and geographical diversity. Optical ground stations may offer mobility, size, and cost benefits compared to microwave frequency terminals.

It is possible in some cases, that substantial radiant fluxes (>1 watt) will be transmitted by ground terminals. Such might be the case of a command transmitter to an earth synchronous satellite. At the present time there is considerable uncertainty to the hazard such beams might pose to personnel at the ground terminal or in over-flying aircraft.

7.6 Point-to-Point Ground Communications

7.6.1 Optical Ground Links

Another potential method of wideband transmission is to use optical carriers. Three transmission schemes have been demonstrated and are potentially applicable; they are:

- 1) Radiative — using laser beam
- 2) Periodic refocusing lens structure
- 3) Sheathed low-loss fiber optic guide.

The first approach uses a regular laser and remote photo detector in a manner entirely analogous to a microwave repeater. Its performance is highly dependent on local weather conditions. Infrared systems provide improved fog penetration. Potential eye damage should not be overlooked.

The periodic lensing method uses a succession of lens elements along a tube (pipe) to refocus the beam as it diverges and minimize loss. It does not necessarily require a laser.

The most interesting recent development is the sheathed glass fiber guide. This is a bundle of small diameter drawn glass fibers that exhibit low-signal attenuation by confining the radiation within the fiber walls by total internal reflection. The extreme flexibility and modest loss (<32 dB/mile) makes it an interesting transmission medium. The ultra-high carrier frequency makes any presently conceived modulation bandwidth (say 1 GHz) a small fraction, so there is no equivalent of equalization required; the band is essentially flat.

At present the cost is relatively high and the laser sources have far too short an operating life to consider such a system candidate. However, laser technology is rapidly maturing and the problems of radio spectrum congestion must lead to increased interest and emphasis on optical transmission.

The present state-of-the-art in fiber optic bundle attenuation, available in reasonable lengths (≈ 100 feet), is 6.15 dB+1000 foot (20 dB/km), which corresponds to 32.5 dB per statute mile.

The Corning Research Laboratories have drawn some ultra fine fibers of a few microns diameter, encased in a 100-micron glass sheath that exhibited even lower attenuation figures. The present loss performance has been found to be critically dependent on the interface between the core glass and the cladding and on the impurity levels in the glass.. Using very small diameter fibers, all but the simplest TE_{11} mode is suppressed, under these conditions, using high purity glass losses

equivalent to 5 to 7 dB/km were obtained. The key impurity elements are metal ions, most commonly iron and copper; these must be held to about 10 parts per billion to achieve the production material attenuation limits in the range of 5 dB/km.

The two most common classes of photon detection devices are the photomultiplier tube (PMT) and the Silicon Avalanche Diode (SAD). The sensitivity of a photon detection device is customarily expressed in terms of a noise equivalent power (NEP), defined as the radiant flux required to provide a unity SNR in unity bandwidth at the detector output. For either, the noise is dependent on the square root of the bandwidth. Representative performance figures are:

- a) For (visible range) PMT, $NEP \approx -160$ dBw/Hz
- b) For SAD $NEP \approx -120$ dBw/Hz.

The maximum permissible length of fiber optic guide between repeater locations is a function of the required SNR and the ratio of the source power to detector NEP. Present laser sources can provide outputs in the range 0.5 mW to 1000 watts.

There is a coupling loss associated with terminating the ends of the fiber guide material due to Fresnel reflection. The magnitude is a function of the ratio of refractive indices of the two materials at the interface.

The worst-case loss results if the guide interfaces with air, for which $N_2 = \text{unity}$, and an approximately 25 percent reflection coefficient would be realized for a fiber material of 1.62 refractive index.

The guide itself absorbs the light it conveys at a rate depending on its composition, purity, and condition, this loss is given by the expression:

$$\text{Loss} = e^{-\alpha L} \quad (7-20)$$

where

- e = base of natural logarithm
- α = a material dependent constant
- L = length of guide (in feet)

Additional space loss characteristics are included in Appendix F.

The limiting values that establish potential system performance are shown in Table 7-15.

Table 7-15. System Performance Limiting Values

	Maximum	Minimum
Source power (dBw)	30	-33
Detector NEP (dBw)	-160	-120
Assumed SNR (dB)	10	10
Net maximum loss (unit BW)	180 dB	77 dB

For the purpose of transmitting wideband data, we are interested in bandwidths in the range 10 to 1000 MHz for which we will have to trade the equivalent guide loss values (Table 7-16).

Table 7-16. Equivalent Guide Loss

Data Rate (MHz)	10	30	100	300	1000
Equivalent Guide Loss (dB)	35	37.3	40	42.3	45

The maximum permissible guide loss per repeater span is therefore between 180 to 35 or 145 dB best case, and 77 to 45 or 32 dB in the worst case. The several combinations possible are used in Table 7-17 to develop the maximum repeater spacing for a guide media having an attenuation of 10 dB/mile (≈ 6 dB/km).

The most important feature to notice is the modest reduction in repeater spacing for the very wide bandwidths, a most desirable characteristic for ERS applications (see Figure 7-66).

Table 7-17. Maximum Repeater Spacing (In Miles) for Optical Repeater Using 10 db/m Fiber Optic Guide

Data Rate	Equiv. Guide Loss	Guide Loss Margin	Photo Multiplier Tube			Silicon Avalanche Diode		
			Laser Power Used			Laser Power Used		
			1000W	1 Watt	1.0 MW	1000W	1 Watt	1.0 MW
10	35.0	145	14.5	11.5	8.5	10.5	7.5	4.5
30	37.3	142.7	14.27	11.27	8.27	10.27	7.27	4.27
100	40.0	140	14.0	11.0	8.0	10.0	7.0	4.0
300	42.3	137.7	13.77	10.77	7.77	9.77	6.77	3.77
1000	45.0	135	13.5	10.5	7.5	9.5	6.5	3.5

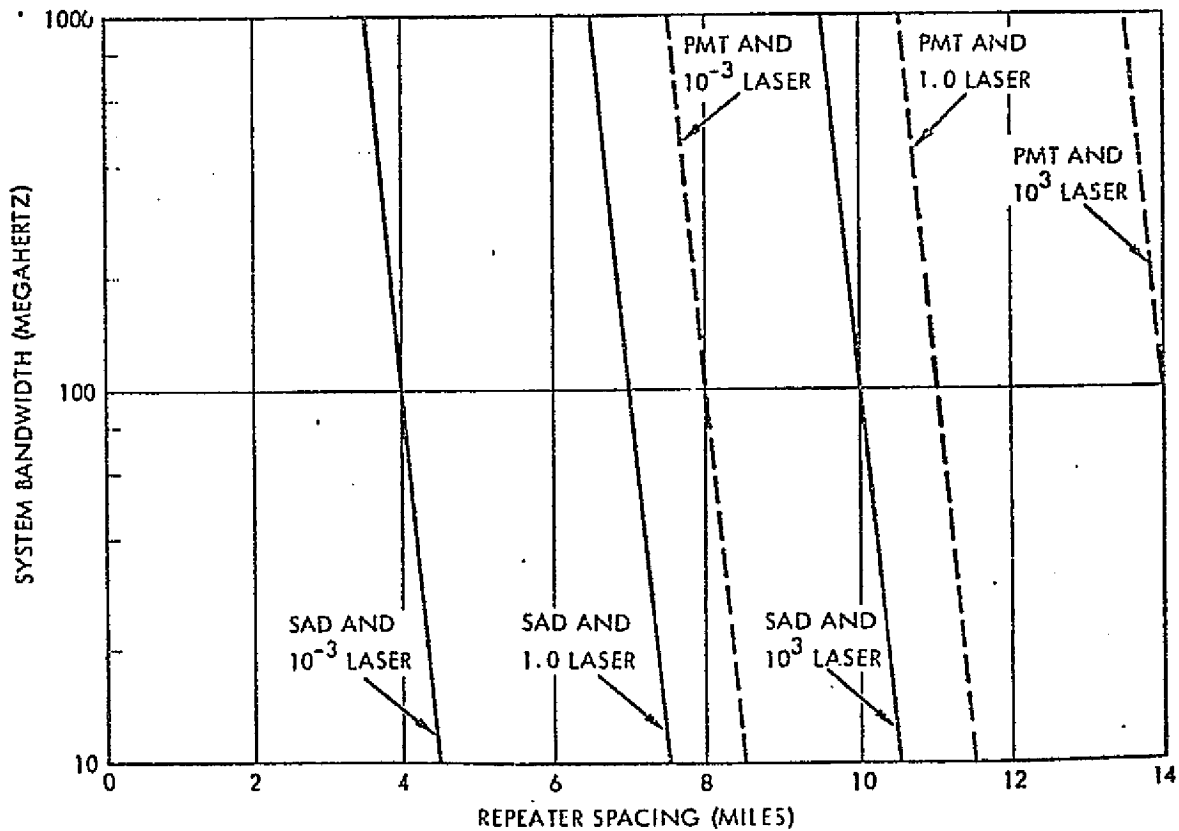


Figure 7-66. Maximum Repeater Spacings Anticipated for Fiber Optic Guide Ground Links Using 10 db/m Media

7.6.2 RF Ground Links

Point-to-point communications using standard rf techniques are reviewed in Task 5, Data Routing.

7.7 Summary and Conclusions

This section reviews data communications from the earth resources satellite to a ground terminal. Requirements and constraints are reviewed in Sections 7.1 and 7.2. The components of the link are reviewed individually in Section 7.3, including selecting the waveform modulation, the spacecraft rf power sources and antenna systems, ground terminal considerations relating to antenna sizing, pre-amplifier selection and combined cost economics. Path losses are reviewed as well, with more detail regarding atmospheric and weather losses provided in Appendix A. Link power budget considerations are presented in Section 7.4. Optical links are touched upon briefly in Sections 7.5 and 7.6.

Table 7-1 normalizes the data per orbit to the required transmission time per orbit, for data rates of 100, 300 or 728 Mbps. The first two rates correspond to the data rate of the S- and K-band TDRSS links; the third corresponds to the highest real-time data acquisition rate. Interestingly enough, the longest transmission of 30 minutes at 100 Mbps for mission seven corresponds to a relatively modest data acquisition rate of 32.3 Mbps. The next longest times do correspond to the highest acquisition rate, but even then, the total data/orbit can be transmitted in 7.25 minutes at 300 Mbps over the Ku-band TDRSS link.

The available time (Table 7.1) above 15 degree elevation, for direct overhead passes always exceeds the required transmission time per orbit at 300 Mbps, but not always at 100 Mbps. Available time falls off rapidly for orbits that do not pass directly over the ground station, particularly for the lower altitudes, such as Mission 3. For Mission 3 (the required transmission time per orbit must average 7.25 minutes at 300 Mbps) the time above 15 degrees vanishes when the orbit's sub-point misses the earth station by 15 degrees, or 900 nautical miles. Since there will be a large number of orbits that do not pass within view of a given ground station, the storage requirements for later transmission could be horrendous, or the TDRSS must be selected and used on every orbit, at the available 100 or 300 Mbps rate. Since recorder playback capabilities will be limited to approximately 300 Mbps, it will be difficult to play back the accumulated data from several orbits during the time available on the orbits within view of the ground station. Thus the TDRSS

or multiple ground stations appear to be the remaining options, with the TDRSS the more promising. Whether the TDRSS will be available to the ERS spacecraft, in view of the requirements of other spacecraft is subject to a traffic analysis not within the scope of this study.

It is appropriate to consider the consequences of the TDRSS not being available. If one is to maintain the same orbit altitude, and acquire the same sensor information, a great deal of data will have to be passed out over a number of candidate routings. For example, the high priority, highly perishable data could be passed to the TDRSS over a narrow band channel, with the balance recorded for playback when the spacecraft is in view of a candidate ground terminal. During this latter time, transmission data rates will be very high. The playback rate of on-board recorders, and the capacity of the data link, become limiting output factors. The initial data acquisition, and on-board processing and/or compression to reduce total data transmission requirements are the limiting input factors. On-board processing, including recording ramifications are reviewed in Section 6.

With respect to the data link capacity, there is pressure to move to the higher frequencies where available spectrum allocation provide increased bandwidth. However, atmospheric, and weather losses mitigate against moving upward, even though technology is beginning to make possible the necessary hardware such as stable oscillators and wideband modulators.

There is thus a considerable squeeze between bandwidth requirements and spectrum availability below the high loss regions beginning at X-band and getting progressively worse at Ku- and K-band.

Aside from limiting the data to be transmitted, or providing additional capability for storing and re-transmitting the data on a subsequent pass when weather becomes a problem, there are two principal alternate approaches - both of which ultimately require more ERP. The first approach is to move up in frequency to obtain wider bandwidth, and to provide additional ERP to make up for the losses. The second approach is to use higher order M-ary modulation to transmit more data in narrower bands at lower carrier frequencies. This, of course, will also

require a higher E_b/N_0 ratio, again leading to increased ERP requirements, although even here, CCIR regulations limit ERP in S- and X-bands.

We thus find that the system designer is constrained to operate within a region bounded by available bandwidth at various parts of the spectrum, atmospheric and weather losses that become progressively worse above 10 GHz, and ERP limits imposed by regulation or by spacecraft design and prime power constraints. To escape this bounded region requires minimizing the data to be transmitted, or improving the transmission duty cycle through the use of a system such as TDRSS.

Fortunately the capacity of the planned STDN/TDRSS system will be able to support the forecast communications needs of the ERS spacecraft, subject to the constraints of projected on-board recording and processing capability.

REFERENCES

1. Radio Frequency Allocations for Space and Satellite Requirements, Mission and Data Operations Directorate, Goddard Space Flight Center, Greenbelt, Maryland, 15 January 1973.
2. Technical Manual: Spaceflight Tracking and Data Network Ground Systems, MC-401, 15 May 1972.
3. Tracking and Data Relay Satellite System Configuration and Trade-off Study, Volume I, Study Summary, Goddard Space Flight Center, Contract No. NAS5-21705, April 1973.
4. C. Cuccia and R. Davies; Satellites in an Interference Environment, Microwave Journal, July 1970.
5. J. H. Davis and J. R. Cogdell, Pointing of the 16 Foot Antenna, Electronic Engineering Research Laboratory, University of Texas, Austin, Technical Memo NGL-006-69-3, November 1969.
6. C. W. Tolbert, A. W. Straiton, and L. C. Krause, A 16-Foot Diameter Millimeter Wavelength Antenna System, its Characteristics and its Applications, IEEE Trans. Antennas and Propagation, Volume AP-13, pp. 225-229, March 1965.
7. Space Communication Handbook, Philco, WDL-TR 1162, 1953.
8. S. J. Macko, Satellite Tracking; Publisher, John F. Rider, Inc. 1962.
9. Burington, Handbook of Mathematical Tables and Formulas; Third Edition, 1949, p. 22.
10. Microwave Semiconductor Power Generators, The Electronic Engineer Magazine, 1973, Microwave Journal International, 1974, p. 64.
11. Rosztorzy, Goldwasser and Rultan, GaSa Gunn Diodes, Microwave Journal, February 1973.
12. H. Wolkstein, Schindler and Puri, Miniature Broadband CW Travelling Wave Tubes, Microwave Journal, October 1973.
13. M. Schwartz, Information Transmission, Modulation and Noise, McGraw-Hill, Inc., 1959.
14. W. R. Bennett and J. R. Davey, Data Transmission, p. 227, Mc-Graw Hill Inc., 1965.
15. W. H. Kummer and A. T. Villeneuve, Study of Spacecraft Antenna Systems, Goddard Space Flight Center, Contract No. NAS5-3545.

REFERENCES - Continued

16. Jasik, H., ed. (1961), Antenna Engineering Handbook, McGraw-Hill, New York; (a) pp. 15-19 to 15-21; (b) pp. 10-4 to 10-5; (c) pp. 14-1 to 15-19; (d) p. 15-12; (e) pp. 14-12 to 14-15.
17. Ashmead, J., and A. B. Pippard (1964), The Use of Spherical Reflectors as Microwave Scanning Aerials, Journal IEE (London) 93, Pt. III-A, 627-632.
18. Drude, P. (1925), Theory of Optics, pp. 58-63, Longmans, Green, New York.
19. Friedlander, F. C. (1946), A Dielectric-lens Aerial for Wide Angle Beam Scanning, Journal IRR (London) 93, Pt. III-A, 653.
20. Ruze, J. (1950), Wide Angle Metal Plate Optics, Proc. IRE 38, 53-59.
21. White, W. D., and L. K. DeSize (1963), Electronically Steerable Antenna-Feed Techniques (ESAFT), 1963 PTGAP International Symposium Digest, 73-77.
22. Shapiro, S. S., ed. (1962), Mosaic Radar Study Program, Contract No. NORD-19179, Hughes Aircraft Company, Culver City, Calif.
 --- (a) Semiannual progress report, p. 57, Table III; (b) Semiannual Progress Report, p. 53, Figure 12; (c) Final Technical Report, pp. 7-8, Figure 2.
23. Silver, S. (1949), Microwave Antenna Theory and Design, MIT Rad. Lab. Series Vol. 12, McGraw-Hill, New York. (a) p. 195; (b) pp. 415-420; (c) pp. 497-502; (d) pp. 89-90.
24. Kay, A. F. (1959), Spherical Symmetric Lenses, IRE Trans. AP-7, 32-38.
25. Morgan, S. P. (1959), Generalizations of Spherically Symmetric Lenses, IRE Trans. AP-7, 342-345.
26. Chadwick, G. G., and J. C. Glass (1962), Investigation of a Multiple Beam Scanning Circular Array, Scientific Report No. 1 on Contract AF19(628)-367, Report No. AFCRL-63-136 TR31. Radiation Systems Inc., Alexandria, Virginia.
27. C. Louis Cuccia, The Economics of Antenna Receiving Systems, Microwaves, June 1969.
28. A Handbook for Data Collection and Position Location Using Satellites, Goddard Space Flight Center, Contract No. NAS5-21522, 1971.

REFERENCES - Continued

29. Earth Observatory Satellite System Definition Study, Final Report, Book 1, Design Cost Tradeoff Studies, Appendix A, Supporting Analysis and Tradeoffs, Goddard Space Flight Center, Contract No. NAS5-20519, October 1974.
30. STDN User's Guide, Baseline Document, STDN No. 101.1, Revision 2, Goddard Space Flight Center, May 1974.
31. Brief TDRSS User's Guide, Goddard Space Flight Center, October 1973.
32. Tracking and Data Relay Satellite System (TDRSS) Frequency Plan; Goddard Space Flight Center Document 16151/1-2.3/4.9.2 October 1973.
33. Space Flight Tracking and Data Network Support for Shuttle Payloads, Presentation by A. Grandi, NASA, Networks Directorate, Goddard Space Flight Center, August 1973.
34. W. Bennett and J.R. Davey, Data Transmission, McGraw Hill Inc., 1965.
35. S. Stein and J. Jones, Modern Communication Principles, McGraw Hill Inc., 1967.
36. E. D. Sunde, Ideal Binary Pulse Transmission by AM and FM, Bell Syst. Tech. J., Vol. 38, pp 1357-1426, Nov 1959.
37. H. Robert Mathwich, Member, IEEE, Joseph F. Balcewicz, Member, IEEE, and Martin Hecht, Member, IEEE, The Effect of Tandem Band and Amplitude Limiting on the E_b/N_0 Performance of Minimum (Frequency) Shift Keying (MSK), IEEE Transactions on Communications Techniques, October 1974, pg 1526-1540.
38. Rudi BeBuda, Coherent Demodulation of FSK with Low Deviation Radio, IEEE Trans. on Comm., pp 429-435, June 1972.
39. J. Jones, Filter Distortion and Intersymbol Interference Effects on PSK Signals, IEEE Trans. on Comm., April 1971, pp 120-132.
40. C. L. Cuccia, Phase Shift Keying: The Optimum Modulation Technique for DIGICOM, Microwave Systems News, Jan., 1973.
41. C. R. Cohn, Spread Spectrum Applications and State-of-the-Art Equipments; AGARD Lecture Series No. 50 Spread Spectrum Communications, AGARD-LSP-58; May 1973, pg 5-25.
42. K. S. Kelleher and H. P. Coleman, Off-Axis Characteristics of the Paraboloidal Reflector, Naval Research Lab Report 4088.

43. M. Y. Weidner, Coherent Digital Communication over a Gaussian Channel Corrupted by Linear Distortion of the Signal and/or Noise Process, TRW Systems 7323.4-85 and 7323.4-87, dated February 1968.
44. USAF Environmental Technical Applications Center Reports 7230: Estimates of One-way Cloud and Rain Attenuation of Ku-band Radio wave Transmission over a 200 Mile Slant Path in Central Europe, January 1974, Supplement A; Seasonal Distributions Concerning The X-band and C-band Transmissions
45. Reports 7230: One-Way Cloud and Rain Attenuation of Ku-band Radiowave Transmission over a 200 Mile Slant Path in the Khorat Plateau, Thailand, March 1974
46. Report 7044: Drone/RPV Automatic Landing Guidance System Climatology, June 1973.
47. J. P. Wargo, Moderately Worst One-Way Attenuation Statistics for Ku-band Radio Transmission in Central Europe, Office of the ASD/ Staff Meteorologist, Wright Patterson AFB, Ohio, October 1973.
48. Ruze, J. , Physical Limitations on Antennas, Tech. Report No. 248, Electronics Res. Lab., M.I.T.
49. Electronic Space Structures Corp. Antenna Specification to be met for Swedish Science Foundation.
50. Rohr Corp. Data Sheet, Kitt Peak National Observatory, Arizona.
51. C. L. Cuccia, Status Report, Modern Low Noise Amplifiers in Communications Systems, Missile and Space News, August/ September 1974.
52. Low Noise Paramps for Satellite Communication Earth Stations, Missile and Space News, August/September 1974, pg 27-32.
53. C. L. Cuccia and S. Teicher, The Economics of Antenna Receiving Systems, Microwaves, June 1969, pgs 86-95.
54. J. E. Eaton, An Extension of the Luneberg-Type Lenses, Naval Research Lab Report 4110, 1953.

APPENDIX 7A

7A.1 ATMOSPHERIC ABSORPTION AND SATELLITE-GROUND COMMUNICATIONS LINKS

Space-earth communications links are subject to attenuation due to oxygen, water vapor, rain and clouds. Over the years, numerous models have been used to determine the attenuation from each component. Statistical data of each meteorological parameter have been accumulated over a sufficient period of time to make a reasonable estimate on probability of future occurrence.

Figure 7A-1 shows attenuation for existing satellite frequencies between 1 and 100 GHz at an elevation angle of 30 degrees. This figure

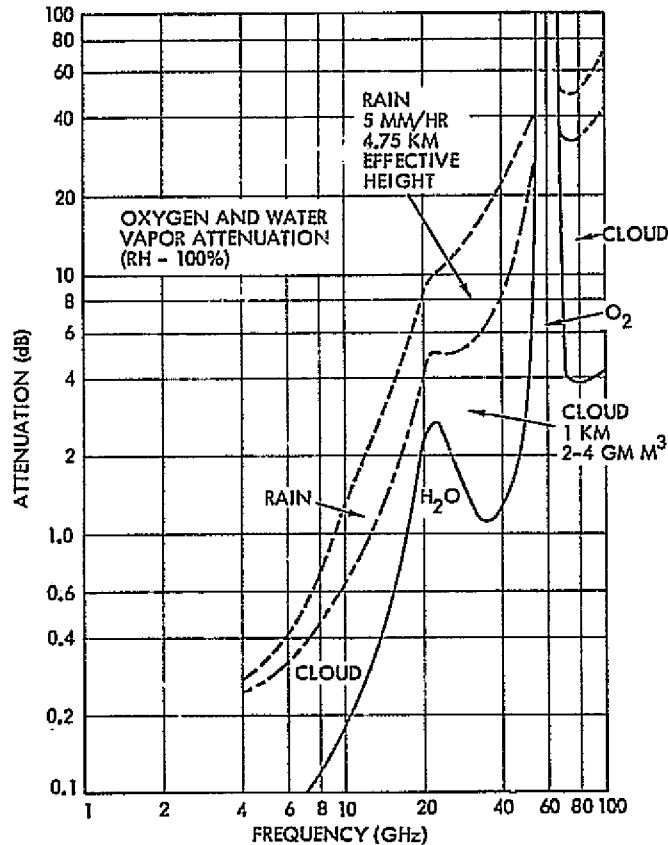


Figure 7A-1. Contributions of Rain, Cloud, Oxygen and Water Vapor Absorption to Total Attenuation at 30-Degree Elevation During Moderate Summer Rain.

also shows the relative importance of the various components of the attenuation. For example, the total attenuation at 30 degree elevation due to molecular absorption (O₂ and H₂O) at 10 GHz (0.2 db) is small compared

with the cloud (0.5 db) and rain (6.5 db) attenuation components. At the peak of the water vapor attenuation (22 GHz) it rises to over 2.5 db but is still less than the rain attenuation (5 db) and roughly equal to that of cloud. The effect of the peak oxygen absorption at about 60 GHz, however, is much greater than that of the rain or cloud. It should be noted that the so-called "windows" at 35 and 90 GHz can only be regarded as transparent under fine weather conditions and may suffer attenuation of 20 and 50 db, respectively, in moderately heavy rain.

7A.2 WEATHER MODELS

The major problem in the evaluation of tropospheric attenuation is in the synthesis of an adequate weather model from the components described above which can be correlated with a specific precipitation rate. In order to achieve a high confidence in the value of the maximum outage time per year, it is desirable to assume the worst credible weather model which can be associated with a specific precipitation rate. A number of temperate climate models with the maximum feasible attenuation values for oxygen, water vapor, rain, cloud, and melting snow have, therefore, been synthesized and evaluated to determine their effect on a space/ground link. Minimum values of tropospheric attenuation have also been obtained for clear, dry weather conditions for comparison. The results of the winter and summer models are shown by Figure 7A-2 and 7A-3. The cloud profiles for each case have been converted to an equivalent 1 km thickness for convenience. The actual freezing level heights vary with location and time. In order to make an allowance for the effect of wet snow in the melting region an equivalent height is used. Wet snow has an attenuation which is about 2.5 times that of rain for the same precipitation rate at 35 GHz. The melting region is therefore assumed to be about 2.5 times thicker than its actual value in the weather model, resulting in effective heights of about 4.8 km for the summer model.

In the winter the equivalent melting layer height may vary between 0 and about 2.4 km. An average value of 1.2 km is assumed.

For space/earth paths another meteorological parameter of importance is the height of the freezing layer since this directly affects the length of the path through the region of high attenuation. Systematic collection and publication of this information as a function of location and

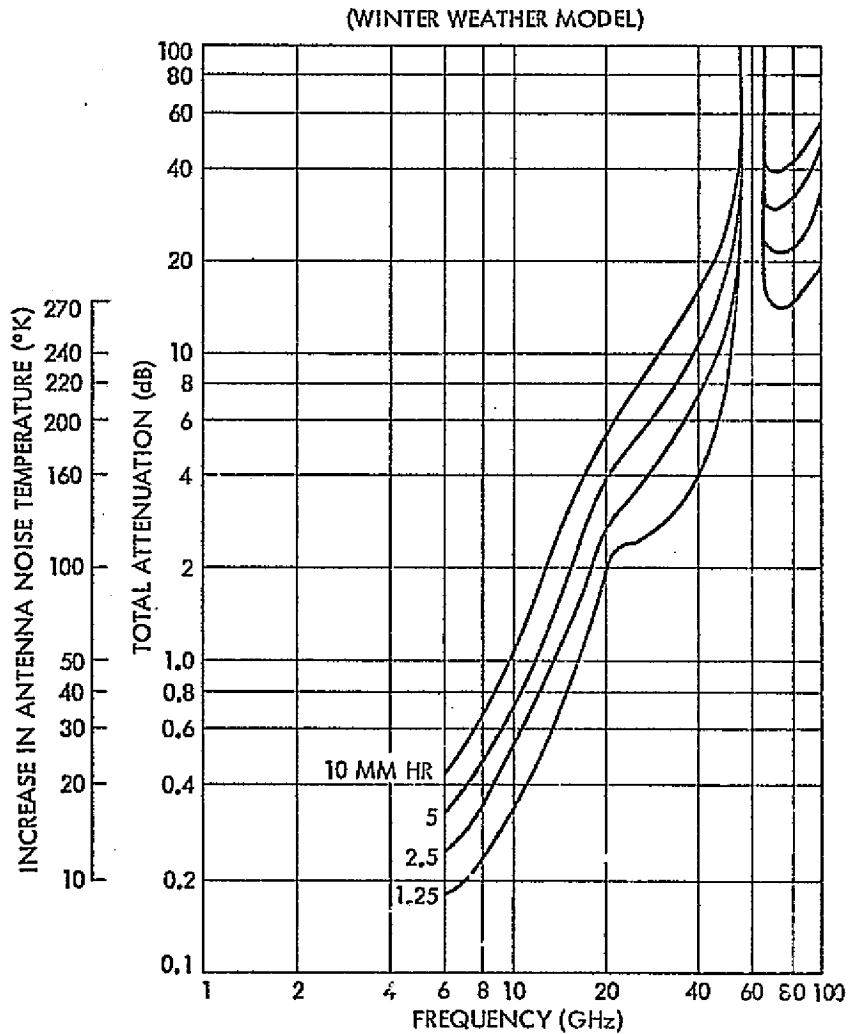


Figure 7A-2. Total Attenuation and Antenna Noise Temperature at 30-Degree Elevation (6 gm/M^3 water vapor 1.2 km freezing level)

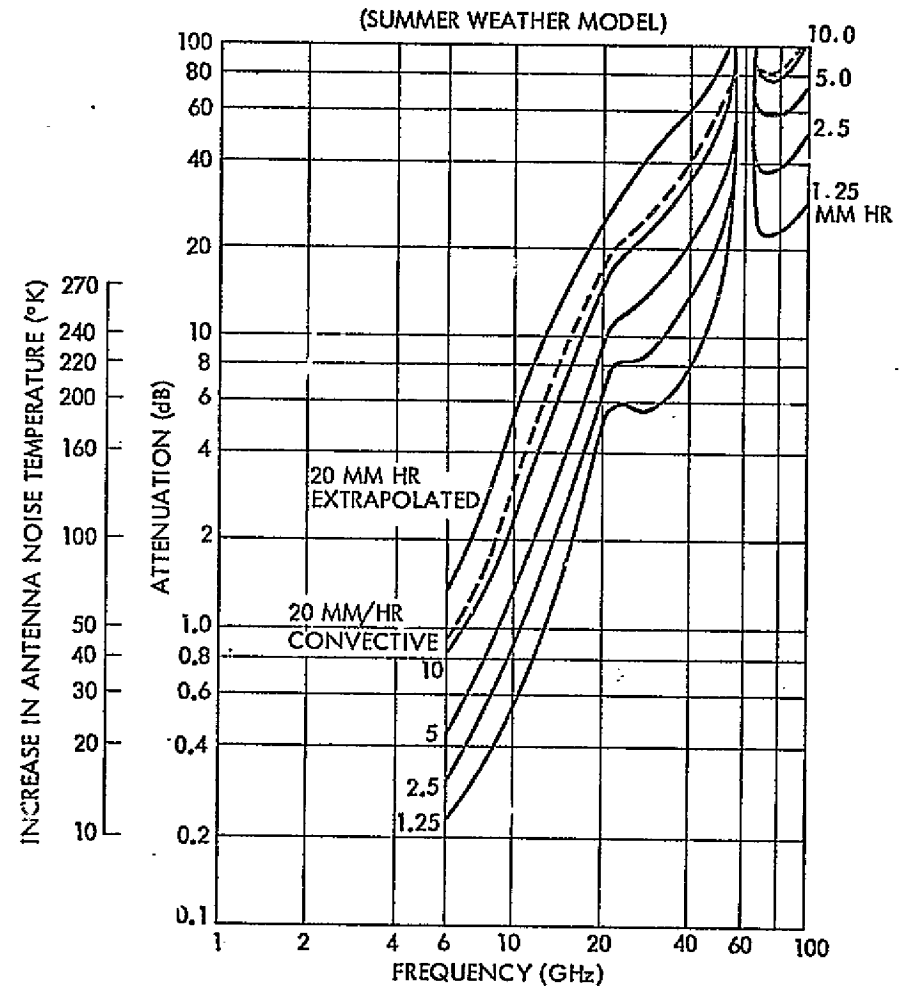


Figure 7A-3. Total Attenuation and Antenna Noise Temperature at 30-Degree Elevation (24 gm/M^3 water vapor 4.8 km freezing level)

time of the year enables better estimates to be made of the earth/space propagation losses at ground terminal locations.

7A.3 PRECIPITATION RATES

Data gathered over a period of several years are available from major meteorological stations which enable an estimate to be made as to the number of hours per month a certain median precipitation rate will occur within most regions within CONUS. The annual hours corresponding to the precipitation rates of a two season model of a ground station within the vicinity of Washington, D.C. is presented along with a annual attenuation experienced or exceeded for this area. (Figure 7A-4). This work can be done also for each of the possible CONUS site locations relating to ERS.

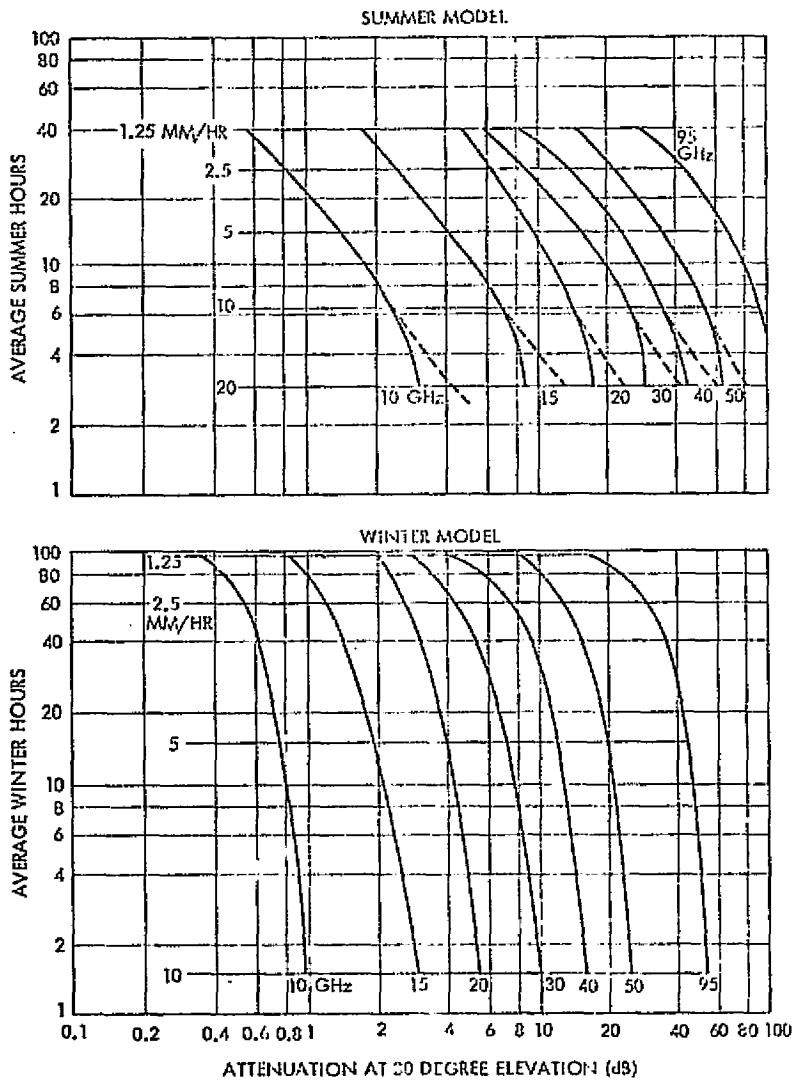
The total hours per year for a given attenuation can be anticipated are obtained by summing the hours per season for each model. The spring and models have been omitted here. The results that are presented in Table 7A-1 at 10, 15, 20, 30, 40, 50, and 95 GHz are for a ground station antenna with an elevation angle of 30 degrees. Value at other angles of elevation can be obtained by increasing the path length loss by the well known cosecant relationship. Thus the attenuation given should be multiplied by two for an angle of 14 degrees. It is apparent that very large excess capability may be required in certain frequency bands to be proposed at the 1971 Geneva conference if small outage times are required.

7A.4 SOME EFFECTS OF PROPAGATION LOSSES ON SYSTEM PERFORMANCE

In addition to the direct system loss due to attenuation under bad weather conditions there are additional losses due to increase of antenna effective noise temperature and to increase of radome losses when one is required.

The effect of bad weather conditions and attenuation due to the formation of a water film on the surface of a radome is detailed by Blevis. This relates the attenuation at a number of frequencies to the thickness of the water film and an empirical formula published by Gibble enables an estimate to be made of the thickness of a water film on a spherical radome by rain at a given precipitation rate. The curves in Figure 7A-5

7-132



ESTIMATED ANNUAL HOURS ATTENUATION IS EXPERIENCED OR EXCEEDED

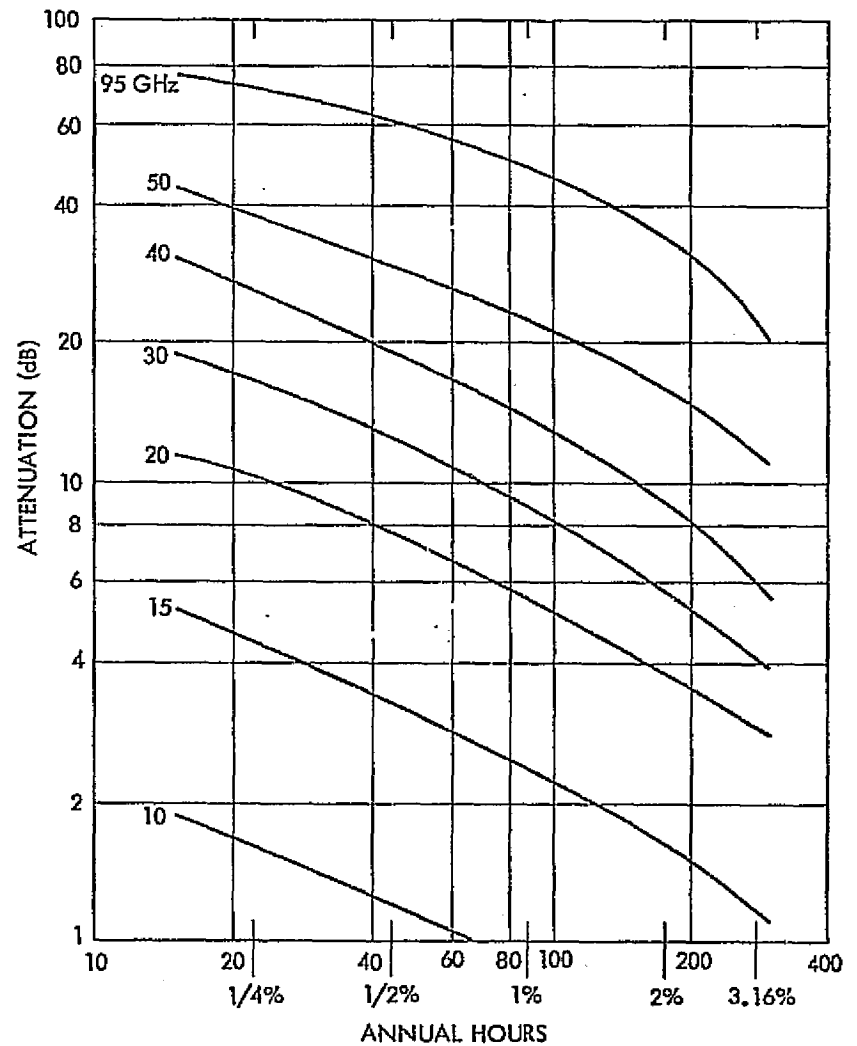


Figure 7A-4. Example of Ground Station in the Vicinity of Washington, D.C.

Table 7A-1. Summary of Attenuation (30° Elevation) for Three Temperate Regions with Stratiform Weather Models

Weather Model	Ground Level Precipitation Rate (mm/hr)	Cloud Water Density Normalized to 1 km (gm/cu meter)	Annual Hours (5 yr. avg) Washing-ton, D. C.	Attenuation in dB with Frequency in GHz							
				10	15	20	30	40	50	70	95
Summer model	Clear weather	-	N/A	0.26	0.8	3.2	7.0	1.7	3.8	5.9	4.2
Freezing level 4.8 km	1.25	1.0	40.0	0.54	1.7	4.8	5.6	8.0	15.0	23.0	27.0
Ground level water	2.50	1.7	27.0	0.82	2.5	6.0	9.0	14.0	22.0	37.0	43.0
Vapor content	5.0	2.4	14.0	1.3	4.0	9.0	15.0	22.0	33.0	58.0	66.0
24 gms/m ³ at 79°F	10.0	3.0	6.5	2.3	7.0	14.0	25.0	36.0	60.0	78.0	100.0
(100 percent RH)	20.0	3.65	2.8	5.0	4.0	25.0	42.0	55.0	82.0	112.0	143.0
Spring and fall model (Mediterranean year round)	Clear weather	-	N/A	0.2	.55	2.2	1.4	1.2	3.3	5.3	3.0
Freezing level 2.4 km	1.25	1.0	150.0	0.42	1.2	3.3	4.2	6.0	12.0	16.0	22.0
Ground level water vapor content 16 gms/m ³ at 65°F (100 percent RH)	2.50	1.7	92.0	0.6	1.8	4.2	6.4	9.5	17.0	25.0	35.0
	5.0	2.4	40.0	0.95	2.5	5.8	9.8	15.0	24.0	37.0	52.0
	10.0	3.0	13.0	1.5	4.2	8.8	16.0	25.0	37.0	54.0	70.0
	20.0	3.65	3.0	3.0	7.6	14.0	26.0	36.0	50.0	70.0	96.0
Winter model	Clear weather	-	N/A	0.11	0.25	0.83	0.6	.63	2.7	4.5	1.5
Freezing level 1.2 km	1.25	1.0	96.0	0.33	0.8	2.0	2.7	4.0	8.0	14.0	17.0
Ground level water	2.5	1.7	60.0	0.52	1.2	2.6	4.2	7.6	14.0	22.0	30.0
Vapor content 6 gms/m ³ (100 percent RH)	5.0	2.4	15.0	0.70	1.7	3.8	6.6	11.0	18.0	29.0	42.0
	10.0	3.0	1.5	1.1	3.0	5.4	10.0	16.0	25.0	40.0	55.0

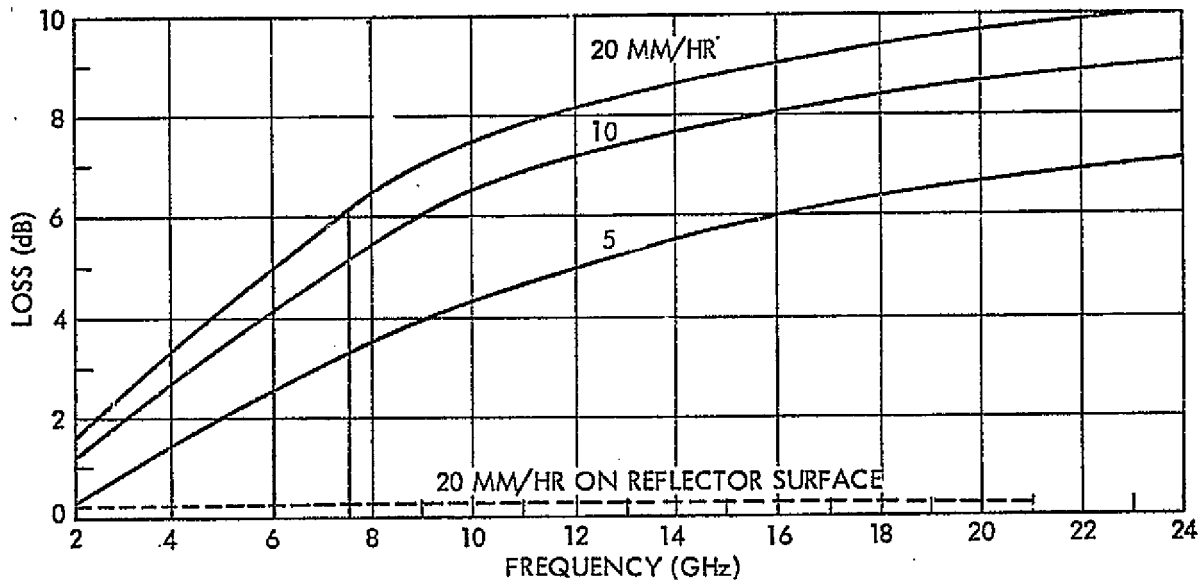


Figure A-5. Loss Due to Water Film on Radome for Various Rain Rates

are produced by a combination of these data and illustrate the severe attenuation which may be caused by a wet radome and is compared with the very small attenuation due to a similar water film on the surface of an antenna reflector. Thus the use of a radome should be avoided wherever possible but if a radome is mandatory a thorough investigation should be made of thermal or mechanical techniques to minimize the water film thickness in bad weather conditions.

APPENDIX 7A

REFERENCES

1. R. K. Crane, Scattering Parameters for New England Rain, Lincoln Laboratories Technical Report 426, October 1966.
2. Rosenblum, Atmospheric Absorption of 10-400 KMcps Radiation, Microwave Journal, Vol. 4, No. 3, 1961, p 91.
3. R.G. Medhurst, Rainfall Attenuation of Centimetre Waves, IEEE Trans. Antennas and Propagation, July 1965.
4. S. L. Godard, Propagation of Centimeter and Millimeter Wavelengths through Precipitation, IEEE Transaction on Antennas and Propagation, Vol. AP-15, No. 4, July 1970.
5. B. C. Blevis and R. M. Dohoo, Measurements of Rainfall Attenuation at 8 and 15 GHz III Transactions on Antennas and Propagation, Vol. AP-15, No. 3, May 1967.
6. J. I. Strickland and K.S. McCormick, Slant Path Attenuation due to Precipitation, 1968 IEE Conf. on Tropospheric Wave Propagation (London, England). p. 143.
7. U.S. Standard Atmosphere, prepared under sponsorship of NASA, USAF, and U.S. Weather Bureau. Washington, D. C., U.S. Government Printing Office, 1962.
8. McCormick, A Troposcatter Propagation Experiment at 15.7 GHz over a 500 km path, Proc. IEEE, Vol. 56, pp. 1729-1731, October 1968.
9. J. W. B. Day and K. S. McCormick, Propagation Measurements at 7 GHz on a Satellite to Earth Path, 1968 IEE Conf. on Tropospheric Wave Propagation (London, England), p. 138.
10. E. E. Reber, R. L. Mitchell, and C. J. Carter, Attenuation of the 5-mm wavelength Band in a Variable Atmosphere.
11. C. H. Reitan, Distribution of Precipitable Water Vapor over the Continental United States, Bull. Am. Meteorol. Soc., Vol. 41, No. 2, pp. 79-87, 1960.
12. E. E. Reber, R. L. Mitchell, and C. J. Carter, Oxygen Absorption in the Earth's Atmosphere, Aerospace Corp., Los Angeles, Calif., Tech. Report TR-0200 (4230-46) 3, November 1968.
13. B. C. Blevis, Rain Effects on Radomes and Antenna Reflectors, 1966 Proc. IEE Conf. on Large Steerable Aerials (London), pp. 148-152.

APPENDIX 7B

7B.1 APK SIGNAL TECHNIQUE

The increasing demands on the data transmission capacity of satellites has caused bandwidth efficiency of the signal modulation to become as important a consideration as its detection efficiency. Thus the poor bandwidth efficiency of the commonly employed biphasic and quadriphase PSK modulation can become a severe limitation on communication capacity. One way to increase the data capacity for a given bandwidth allocation is to increase the symbol alphabet size by using M-ary signal sets. M-ary PSK is a well-known example of this approach which is suitable for saturated TWT operation. The newer M-ary modulation technique which combines both amplitude and phase keying (APK), requires less peak or average power than M-ary PSK to achieve the same symbol error probability.

The performance of a number of candidate signal sets has been considered in terms of symbol error probability as a function of both average and peak signal-to-noise ratio (SNR). The tradeoff between the higher traffic capacity of the higher order alphabets and their increased signal energy requirements is presented by curves of $\log_2 M$, (information bits/symbol), versus peak and average bit energy-to-noise density ratio for a specified bit error probability. It is found that when signal sets such as in Figure 7B-1 are compared on an average SNR basis, the triangular design yields the best performance for $M \geq 32$. For 8-ary and 16-ary sets the (1, 7) and (1, 5, 10) circular* sets excel but the rectangular sets are very near optimum for all alphabet sizes. When compared on a peak SNR basis, circular designs are superior for all alphabet sizes.

PSK, because of its widespread use, is a natural standard of comparison for APK and this comparison has been made in each case. With an ideal channel, APK is superior to PSK on a average SNR basis for all $M \geq 8$, increasing from 1.8 db at $M=8$ to 13.1 db at $M=128$ for $P_e = 10^{-5}$. Based on peak SNR, APK has a 1.25 db advantage at $M=8$ which increases to 10.1 db at $M=128$.

*The circular set notation (a, b, c) means that there are three circles with "a" signals on the inner circle, "c" signals on the outer circle, etc..

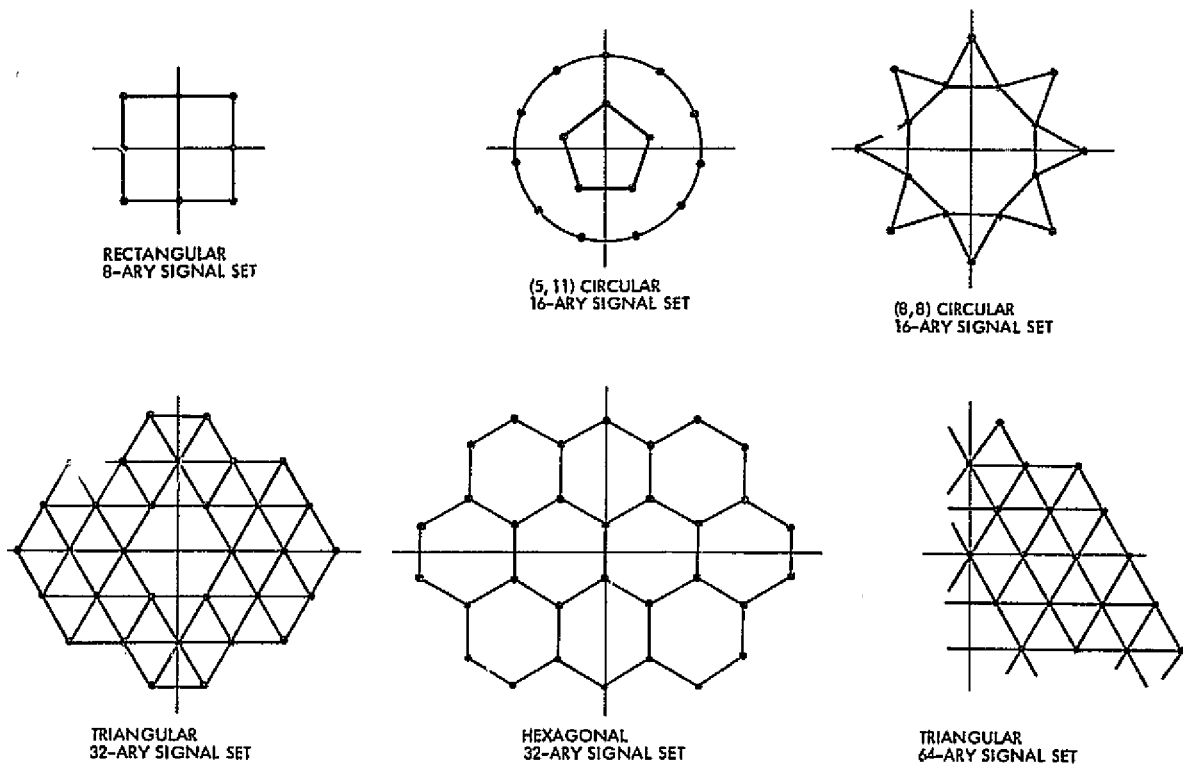


Figure 7B-1. Some Signal Set Candidates

Channel filtering affects PSK and APK in a nearly identical fashion. However, for high alphabet sizes PSK degrades somewhat more rapidly than APK for small bandwidths.

7B.2 CANDIDATE APK SIGNAL SETS

The purpose is to identify and describe those M-ary APK signal sets which appear to have performance and/or implementation advantages. The optimum APK signal set, in the sense of minimizing the average probability of symbol error in thermal noise under ideal conditions, is an unsolved problem.

Some theoretical guidance for very large signal sets is available from Shannon in consideration of the signal statistics of optimum analog AM and PM systems at high SNR. Shannon has shown that under an average power constraint the channel capacity is maximized with a signal that is uniformly distributed in phase and Rayleigh distributed in amplitude, i. e., two-dimensional Gaussian. Under a peak power constraint the capacity is maximized by a signal uniformly distributed in phase with an amplitude probability density which increases linearly with amplitude up to the peak amplitude constraint.

Candidate designs for each alphabet size are described and most of these designs fall into four categories: those with the signals arranged on concentric circles, and those with triangular, rectangular, or hexagonal grid arrangements. The circular and the rectangular sets are attractive because of their implementation convenience. The triangular sets yield high performance because, over an infinite plane, triangular packing is very efficient.

7B.2.1 8-ary Signal Sets

For 8-ary signal sets there are four candidate configurations as listed in Table 7B-1.

The first design is a 3×3 grid minus the center point and belongs to the rectangular-decision-region category. The second is a double circle with four signals per circle, denoted as a (4,4) design. Lucky and Hancock claim this second configuration to be the optimum 8-ary design under an average power constraint. The remaining two candidates are a (1,7) circular set and a triangular design. The rectangular 8-ary is shown in Figure 7B-1.

7B.2.2 16-ary Signal Sets

The five 16-ary candidate sets are listed in Table 7B-1 and are claimed to be acceptable for the reasons given. Two of the five are shown in Figure 7B-1. The rectangular set is a 4×4 square, while the triangular set is composed of alternating rows of 3 and 4 signals each, minus the center point. Four circular designs are included. The (8,8) arrangement is claimed by Lucky and Hancock to be optimum for both peak and average power constraints. The (5,11), (4,12), and (1,5,10) sets are considered because of their low peak power.

The (5,11), (4,12) and (1,5,10) circular sets were obtained by applying the Shannon criterion for peak power limited sets, i.e., that the signal distribution be uniform within the peak circle. This can be satisfied approximately with circular sets by making the number of signals per circle proportional to the circle radius.

7B.2.3 32-ary Signal Sets

There are five candidate configurations for 32-ary signal sets as listed in Table 7B-1. The first is a rectangular set sized to be 6×6 square

Table 7B-1. Candidate Signal Designs

Alphabet Size	Configuration	Reason for Selection
8	Rectangular (4,4) circular (1,7) circular Triangular	Ease of demodulation Peak power, Lucky and Hancock "optimum" Peak and average power Average power
16	Rectangular Triangular Hexagonal (5,11) circular (4,12) circular (8,8) circular (1,5,10) circular	Ease of demodulation, average power Packing efficiency, average power Regular polygonal structure Peak power, $d_{rm} = 0.87$ Peak power, $d_{rm} = 1.22$ Lucky and Hancock "optimum" Peak and average power, $d_{rm} = 0.84$
32	Rectangular Triangular Hexagonal (4,11,17) circular (5,11,16) circular	Ease of demod., average power Packing efficiency, average power Regular polygonal structure Peak power, $d_{rm} = 0.96$ Peak power, $d_{rm} = 0.84$
64	Rectangular Triangular Hexagonal (6,12,19,27) circular (6,13,19,26) circular	Ease of demodulation, average power Packing efficiency, average power Regular polygonal structure Peak power, $d_{rm} = 0.93$ Peak power, $d_{rm} = 0.96$
128	Rectangular Triangular (8,17,25,34,44) circular (6,12,18,24,30,38) circular	Ease of demodulation, average power Packing efficiency, average power Peak power, $d_{rm} = 0.84$ Peak power, $d_{rm} = 0.93$

minus the four corner points. The triangular and hexagonal design is shown in Figure 7B-1. The two circular designs are based on peak power considerations where again for uniform distribution the optimum number of signals/circle. This leads to the (5, 11, 16) design with the (4, 11, 17) design.

7B.2.4 64-ary Signal Sets

The triangular of the five candidate 64-ary designs are illustrated in Figure 7B-1 where only the basic symmetry region is shown. The rectangular configuration is an 8 x 8 square and the triangular set has a slightly diamond-like shape. Uniform distribution with circles leads to the (6, 12, 19, 27) and (6, 13, 19, 26) designs for two circles.

7B.2.5 128-ary Signal Sets

The four candidate designs selected for 128-ary signal sets, as illustrated in Table 7B-1 are the rectangular, triangular, five-circle (8, 17, 25, 34, 44), and six-circle (6, 12, 18, 24, 30, 38) configurations. The circles approximate a uniform signal distribution.

SUMMARY OF CANDIDATE SIGNAL SETS. The signal sets which were investigated are summarized in Table 7B-1 and the symbol d_{rm} is used to denote the distance between the two closest rings in a circular set; the smaller d_{rm} , the poorer the performance in general.

7B.3 APK THERMAL NOISE PERFORMANCE

To evaluate the thermal noise performance of the candidate APK signal sets selected in terms of symbol error probability versus both average and peak signal-signal-to-noise ratio (SNR), a tradeoff between the traffic capacity of higher order alphabets (2^k , $3 \leq k \leq 7$) and the increased signal energy requirements is required. This is presented by plotting $2k$ or m , the data rate per unit bandwidth, versus the peak and average bit energy-to-noise density ratio required to achieve a specified error probability.

The performance curves of Figures 7B-2 and 7B-3 are summarized in Table 7B-2, where the best circular design, the triangular, and the rectangular sets are compared for each alphabet size. The degradation incurred by using one of the nonoptimum sets is given for a symbol error

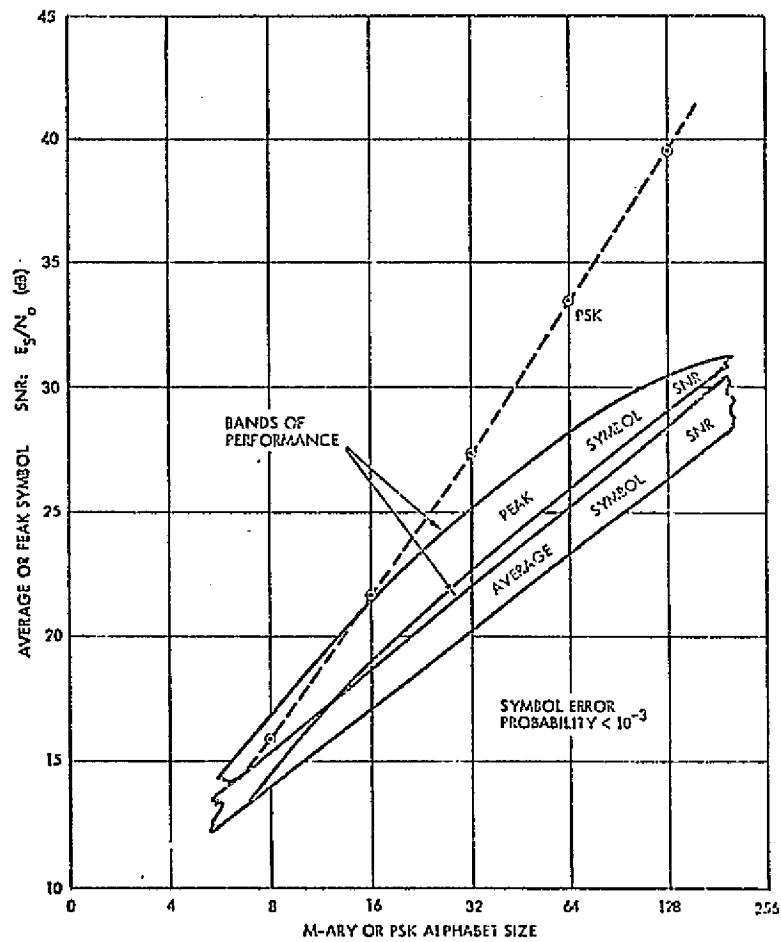


Figure 7B-2. APK Performance Curves

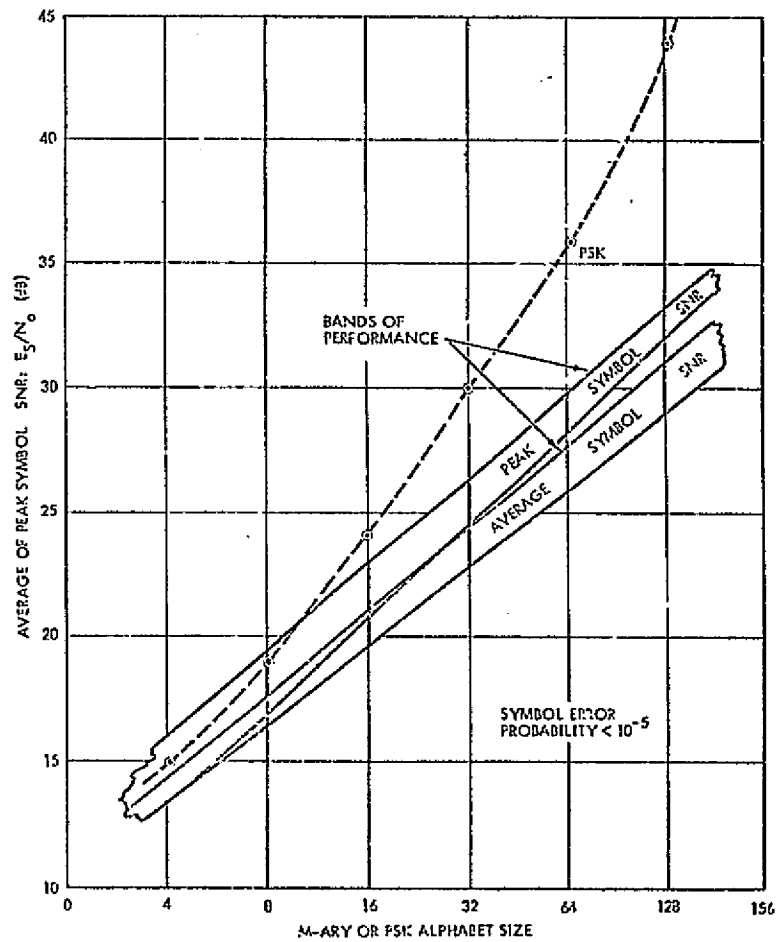


Figure 7B-3. APK Performance Curves

Table 7B-2. Comparison of Principal APK Sets

For Peak SNR				For Average SNR		
Alphabet Size	Best Set	Other Sets	Penalty With Respect To Best Set ($P_e=10^{-5}$)	Best Set	Other Sets	Penalty With Respect To Best Set ($P_e=10^{-5}$)
8	(1, 7)			(1, 7)	Triangular	0.1 db
		PSK	1.2 db		Rectangular	1.2
		Rectangular	1.7		PSK	1.8
16	(5, 11)			(1, 5, 10)	Rectangular	0.1 db
		Triangular	0.8 db		Triangular	0.2
		Rectangular	1.2		PSK	4.1
32	(4, 11, 17)			Triangular		
		Rectangular	0.5 db	Rectangular	0.2 db	
		Triangular	1.0	(4, 11, 17)	0.2	
64	(6, 13, 19, 26)			PSK	7.1	
		Triangular	0.7 db	Rectangular	0.4 db	
		Rectangular	0.9	(6, 13, 19, 26)	0.4	
128	(6, 12, 18, 24, 30, 38)			PSK	10.1	
		PSK	7.6	Rectangular	0.5 db	
		Triangular	0.2 db	(6, 12, 18, 24, 30, 38)	0.5	
		Rectangular	0.5	PSK	13.1	

of 10^{-5} but the value would change very little over the range 10^{-3} to 10^{-8} . The curve of Figure 7B-2 presents the average and peak symbol SNR required for each alphabet size investigated which will maintain a symbol error probability of 10^{-3} . The bands of performance indicate the range of SNR's found for near optimal to suboptimal signal set configurations. Probably the most important qualitative observation which can be made is that the bands of performance remain narrow in spite of the use of triangular, circular, rectangular or other more exotic signal constellations; so that one may expect at best, a two to 3 db improvement for a M-ary constellation over another M-ary constellation, assuming both have reasonable configurations to start with. The curve of Figure 7B-3 presents the same information required to maintain a symbol error probability of 10^{-5} .

Several important conclusions about APK signal selection and performance can be drawn from the results as summarized in Table 7B-2 and Figures 7B-2 and 7B-3.

The penalties and advantages of using M-ary alphabets are displayed in Figure 7B-2 and 7B-3 by plotting $k = \log_2 M$ versus the bit energy-to-noise density ratio for a given bit error probability. For an ideal band-limited channel which produces no distortion the capacity in bits/sec is proportional to k . As shown in Figures 7B-2 and 7B-3, however, the increased capacity is obtained at the expense of increased signal energy. To increase the capacity from 3 to 7 requires an increase of approximately 8 db in average power and 10 db in peak power. However, if the same capacity increase were attempted with PSK an increase of 20 db in signal power would be required.

On a peak SNR basis of comparison, the circular signal sets are optimum whether maximum likelihood detection or suboptimum pie-fan decision regions are employed. The rectangular set suffers a disadvantage of 0.5 to 1.7 db depending upon the alphabet size.

On an average SNR basis, the circular sets are best for $M=8$ and 16; for larger alphabets the high packing efficiency of the triangular structure gives it the best performance. The rectangular set, however, is within 0.5 db of optimum for $M \geq 16$.

Also, APK signal sets exhibit a striking advantage over PSK for all alphabet sizes ($M > 8$) on both a peak and an average SNR basis. For a peak SNR comparison the APK advantage increases from 1.2 db for $M=8$ to 10.1 db for $M=128$. For an average SNR comparison the advantage is even greater, increasing from 1.8 db for $M=8$ to 13.1 db for $M=128$.

APPENDIX 7B

REFERENCES

1. C. M. Thomas: Final Report on Amplitude - Phase Keying Techniques, TRW Systems Document No. 17699-6001-R0-00, August 1971.
2. Salz, Sheehan, and Paris, Data Transmission by Combined AM and PM. B.S.T.J. Vol. 50, No. 7, September 1971.
3. Foschini, Getlin and Weinstein. On the Selection of a Two-Dimensional Signal Constellation in the Presence of Phase Jitter and Gaussian Noise, BSTJ, Vol. 52, No. 6 July - August 1973.
4. Foschini, Getlin and Weinstein. Optimization of Two-Dimensional Signal Constellations in the Presence of Gaussian Noise, IEEE Transactions on Communications, Vol. COM-22, No. 1, January 1974.

APPENDIX 7C

7C.1 PAPM MODULATION TECHNIQUE

The increased satellite communication traffic density predicted for the 1975-1985 time period, makes it highly desirable to use available frequency band allotments more efficiently.

It is well known that single sideband, amplitude modulation (SSB/AM) attains a bandwidth ratio of unity and therefore permits the highest possible capacity for a system with no power constraint. There are many disadvantages to SSB for satellite operation, however. It is a linear modulation technique and hence has a SNR improvement factor, or process gain, of unity. It also has a high peak-to-average power ratio and high intelligible crosstalk when a reference carrier is transmitted to simplify demodulation. It is interesting to note that SSB/AM is actually a hybrid modulation because it consists of both AM and PM. Because linear SSB is so efficient in bandwidth one would expect an AM-PM modulation technique utilizing nonlinear or "twisted" modulation for SNR improvement to be a very appealing form of modulation, especially if the peak-to-average power ratio is not large.

One such hybrid technique extends pulse amplitude modulation (PAM) to two dimensions (amplitude-phase or inphase-quadrature) according to a specified mapping transformation to obtain a pulse-amplitude-phase modulation (PAPM). Because it is pulsed, its bandwidth exceeds SSB/AM by a factor of nearly 3. The nonlinearity of the modulation, however, yields an advantage of 5 to 12 db in terms of output SNR versus carrier-to-baseband noise power ratio. Compared to FM, the bandwidth improvement amounts to a factor of 2 for the same carrier-to-baseband noise power ratio. Thus PAPM achieves its SNR improvement without a corresponding increase in RF bandwidth and thus is much more attractive for channel-limited communication links.

This report evaluates PAPM performance under realistic transponder and transmitter/receiver equipment constraints. Two modulation mapping configurations are considered; 1) a linear, or rectangular, raster, and 2) a spiral.

The performance of three PAPM modulation schemes is evaluated in terms of output SNR versus peak and average carrier-to-noise ratio (CNR). Two types of errors affect the PAPM demodulator's estimate of the transmitted baseband signal. The first is an error that arises from interference parallel to the signal mapping locus; it is inversely proportional to CNR and predominates at high CNR. The second is due to interference normal to the mapping locus and causes large output errors, or "clicks," when these anomalous events occur. At low CNR anomalous errors predominate and produce a demodulator threshold. As in FM there is a tradeoff between SNR improvement and threshold level.

Since PAPM is both a coherent and a pulse modulation, its performance depends upon carrier phase and gain references and pulse sample timing. Errors in the carrier reference distort the locus of the received signal so that the inverse mapping produces an output signal error. A sync timing error reduces the energy in the desired pulse and increases the interpulse interference from adjacent pulse time slots.

Curves of SNR versus CNR as a function of synchronization error, (not given here) for the linear and spiral mapping indicate that PAPM is quite sensitive to all three types of error. A 5 db degradation in output SNR occurs with approximately 1 percent timing error or a 0.01-0.02 radian phase error for both linear and spiral mappings. A 2 percent gain error degrades the linear mapping 5 db, while the spiral can tolerate an 8 percent error for the same degradation. PAPM demodulators must be carefully designed to achieve such small gain, phase and timing reference error specifications. Hence very careful modem design will be required to achieve the high SNR improvement factors which make the PAM attractive a modulation technique.

Careful inspection of either linear, spiral, or still a third unmentioned variety of mapping called skewed linear mapping all results in the same basic performance characteristics and this is illustrated in Figure 7C-1.

A threshold is produced by a large, anomalous error which occurs when the noise is so large that the receiver selects the wrong RF locus segment for mapping back into the baseband domain. The probability of this anomalous error depends upon the distance between the locus segments.

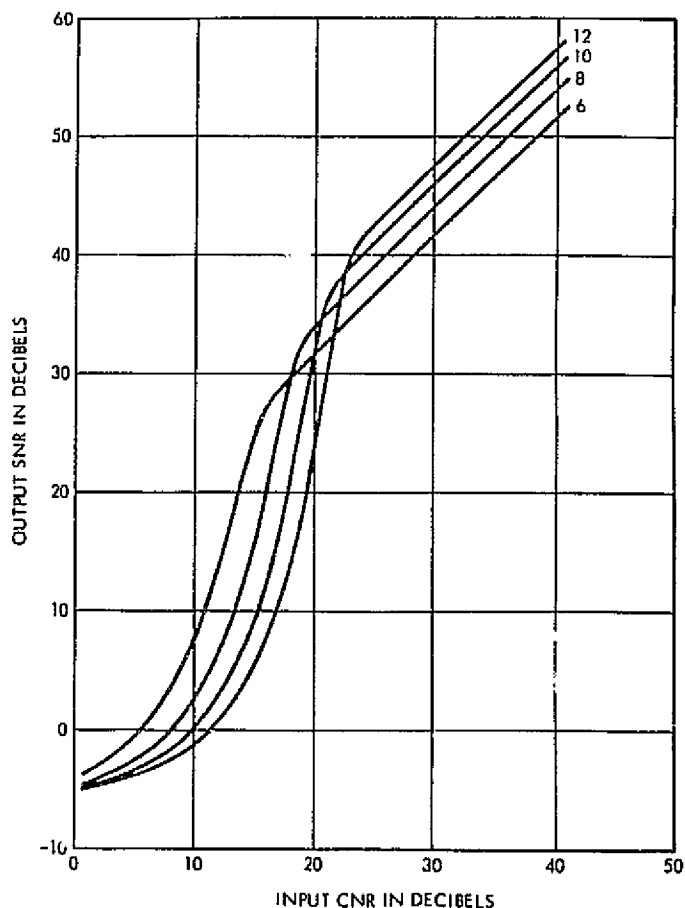


Figure 7C-1. PAPM Performance Characteristics (for 6, 8, 10, and 12 segment spirals)

7C.2 PAPM IMPLEMENTATION

PAPM is implemented by mapping the one dimensional locus of baseband sample values into a two-dimensional RF signal. Two such mappings are illustrated in Figure 7C-2 for a baseband signal constrained to ± 1 . The length of the resulting locus is $2L$ so that the locus has been "stretched" by a factor L . When the received RF signal-plus-noise is mapped back to the baseband domain the effective noise voltage is reduced by a factor of L .

Linear Mapping. For the linear loci, $L_i = 2L/N$ for all segments. As specified, the mappings for these loci map the point -1 to the bottom of the lefthand segment and $+1$ to the top of the righthand segment. The mapping on each segment is in an upward direction joining the top of a segment with the bottom of the next segment to the right. The segments for the linear locus extend from $-L/N$ to $+L/N$.

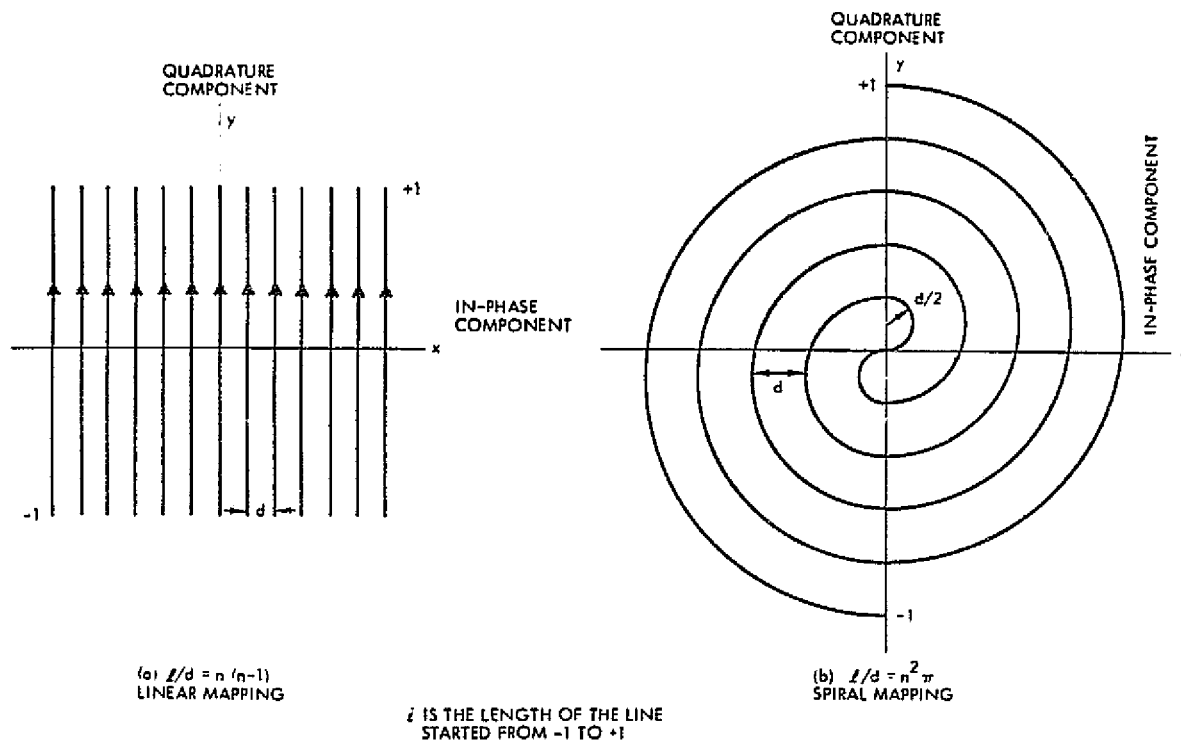


Figure 7C-2. Modulation Schemes

When the message pdf is uniform C_m the mean square carrier power is

$$C_m = \left(\frac{N-1}{3}\right) \left(\frac{d}{2}\right)^2 + \frac{(LN)^2}{3}$$

where L is the stretch factor.

Spiral Mapping. The spiral mapping is composed of semicircular segments of radius $(2k-1)d/2$, $k = 1, 2, \dots, N/2$. The locus is constructed so that each circular segment begins and ends on the y -axis. For N segments the stretch factor L is

$$L = \frac{\pi d}{2} \left(\frac{N}{2}\right)^2$$

when the message pdf is uniform.

The mean square carrier power is therefore

$$C_{ms} = \frac{2\pi}{L} \left(\frac{d}{2}\right)^3 \left(\frac{N}{2}\right)^4$$

APPENDIX 7C

REFERENCES

1. C. M. Thomas, Report on Hybrid Modulation TRW Systems Document No. 20531-6001-to -00, November 1972.

APPENDIX 7D

7D.1 ANTENNA PERFORMANCE

The performance characteristics of a set of parabolic antennas at each of the frequencies of interest has been evaluated for wavelength, diameter to wavelength ratio, gain at 54 percent efficiency, and beamwidth. Antenna tolerance has also been considered and less than 2 db will be lost as long as .010 inches surface deviation is maintained at 65 GHz. Surface accuracy problems will generally improve at the lower frequencies of interest.

The frequencies for the evaluations of Table 7D-1 to 7D-8 include:

- L-band (1.525 - 1.535 GHz) telemetering
- S-band (1.750 - 1.850 GHz) uplink, STDN
- S-band (2.025 - 2.125 GHz) user forward, STDN
- S-band (2.200 - 2.300 GHz) user return, STDN
- X-band (8.0 - 8.4 GHz) earth exploration
- Ku-band (13.4 - 14.0 GHz) user return, STDN
- Ku-band (14.6 - 15.2 GHz) user forward, STDN
- K-band (21.2 - 22.0 GHz) earth exploration
- V-band (51.0 - 52.0 GHz) earth exploration
- W-band (65.0 - 66.0 GHz) earth exploration

7D.2 ANTENNA TOLERANCE

The deviations of an antenna reflector from its ideal shape cause, in general, loss of gain and pattern degradation. These deviations may result from manufacturing and rigging tolerances and from thermal effects. The effects on surface deviations of manufacturing and rigging tolerances (including nondeterministic errors in the measuring instruments employed) are usually random in nature and can be estimated through stochastic analyses. Recently developed automated computation techniques permit structural engineers to predict accurately the deformations of the reflector surface caused by known temperature changes.

Table 7D-1. Parabolic Antenna Performance

L-Band; Space Operation and Telemetry Gain, 3 db Beamwidth 1.525-1.535 GHz

GAIN & 3 DB BEAMWIDTH AT FREQUENCY: 1.53 GHz : 1.535GHz : 1.54 GHz											
DISH DIAMETER: WAVELENGTH :DIA-WL:GAIN :BW-3 :GAIN :BW-3 :GAIN :BW-3											
FEET :METERS:INCHES: CM. :RATIO :DB. :DEG. :DB. :DEG. :DB. :DEG.											
2.83:	.86:	7.693:	19.54:	4.4:	20.1:	16.23:	20.1:	16.18:	20.2:	16.12	
3.36:	1.03:	7.743:	19.67:	5.2:	21.6:	13.65:	21.6:	13.60:	21.7:	13.56	
4.00:	1.22:	7.718:	19.61:	6.2:	23.1:	11.48:	23.1:	11.44:	23.2:	11.40	
4.76:	1.45:	7.693:	19.54:	7.4:	24.6:	9.65:	24.6:	9.62:	24.7:	9.59	
5.66:	1.72:	7.743:	19.67:	8.8:	26.1:	8.11:	26.2:	8.09:	26.2:	8.06	
6.73:	2.05:	7.718:	19.61:	10.5:	27.6:	6.82:	27.7:	6.80:	27.7:	6.79	
8.00:	2.44:	7.693:	19.54:	12.5:	29.1:	5.74:	29.2:	5.72:	29.2:	5.70	
9.51:	2.90:	7.743:	19.67:	14.7:	30.6:	4.82:	30.7:	4.81:	30.7:	4.79	
11.31:	3.45:	7.718:	19.61:	17.6:	32.1:	4.06:	32.2:	4.04:	32.2:	4.02	
13.45:	4.10:	7.693:	19.54:	21.0:	33.6:	3.41:	33.7:	3.40:	33.7:	3.39	
16.00:	4.88:	7.743:	19.67:	24.8:	35.2:	2.87:	35.2:	2.86:	35.2:	2.85	
19.03:	5.80:	7.718:	19.61:	29.6:	36.7:	2.41:	36.7:	2.40:	36.7:	2.40	
22.63:	6.90:	7.693:	19.54:	35.3:	38.2:	2.03:	38.2:	2.02:	38.2:	2.02	
26.91:	8.20:	7.743:	19.67:	41.7:	39.7:	1.71:	39.7:	1.70:	39.7:	1.69	
32.00:	9.75:	7.718:	19.61:	49.8:	41.2:	1.43:	41.2:	1.43:	41.2:	1.43	
38.05:	11.60:	7.693:	19.54:	59.4:	42.7:	1.21:	42.7:	1.20:	42.7:	1.20	
45.25:	13.79:	7.743:	19.67:	70.1:	44.2:	1.01:	44.2:	1.01:	44.2:	1.01	
53.82:	16.40:	7.718:	19.61:	83.7:	45.7:	.85:	45.7:	.85:	45.7:	.85	
64.00:	19.51:	7.693:	19.54:	99.8:	47.2:	.72:	47.2:	.71:	47.3:	.71	
76.11:	23.20:	7.743:	19.67:	118.0:	48.7:	.60:	48.7:	.60:	48.8:	.60	
90.51:	27.59:	7.718:	19.61:	140.7:	50.2:	.51:	50.2:	.51:	50.3:	.50	

S-Band; Uplink STDN Service Gain and 3 db Beamwidth 1.750-1.850 GHz

GAIN & 3 DB BEAMWIDTH AT FREQUENCY: 1.75 GHz : 1.80 GHz : 1.85 GHz											
DISH DIAMETER: WAVELENGTH :DIA-WL:GAIN :BW-3 :GAIN :BW-3 :GAIN :BW-3											
FEET :METERS:INCHES: CM. :RATIO :DB. :DEG. :DB. :DEG. :DB. :DEG.											
2.83:	.86:	6.383:	16.22:	5.3:	21.3:	14.14:	21.5:	13.75:	21.8:	13.38	
3.36:	1.03:	6.747:	17.14:	6.0:	22.8:	11.89:	23.0:	11.56:	23.3:	11.25	
4.00:	1.22:	6.560:	16.67:	7.3:	24.3:	10.00:	24.6:	9.72:	24.8:	9.46	
4.76:	1.45:	6.383:	16.22:	8.9:	25.8:	8.41:	26.1:	8.18:	26.3:	7.95	
5.66:	1.72:	6.747:	17.14:	10.1:	27.3:	7.07:	27.6:	6.87:	27.8:	6.69	
6.73:	2.05:	6.560:	16.67:	12.3:	28.8:	5.95:	29.1:	5.78:	29.3:	5.62	
8.00:	2.44:	6.383:	16.22:	15.0:	30.3:	5.00:	30.6:	4.86:	30.8:	4.73	
9.51:	2.90:	6.747:	17.14:	16.9:	31.8:	4.20:	32.1:	4.09:	32.3:	3.98	
11.31:	3.45:	6.560:	16.67:	20.7:	33.3:	3.54:	33.6:	3.44:	33.8:	3.34	
13.45:	4.10:	6.383:	16.22:	25.3:	34.8:	2.97:	35.1:	2.89:	35.3:	2.81	
16.00:	4.88:	6.747:	17.14:	28.5:	36.3:	2.50:	36.6:	2.43:	36.8:	2.36	
19.03:	5.80:	6.560:	16.67:	34.8:	37.9:	2.10:	38.1:	2.04:	38.3:	1.99	
22.63:	6.90:	6.383:	16.22:	42.5:	39.4:	1.77:	39.6:	1.72:	39.8:	1.67	
26.91:	8.20:	6.747:	17.14:	47.9:	40.9:	1.49:	41.1:	1.45:	41.3:	1.41	
32.00:	9.75:	6.560:	16.67:	58.5:	42.4:	1.25:	42.6:	1.22:	42.9:	1.18	
38.05:	11.60:	6.383:	16.22:	71.5:	43.9:	1.05:	44.1:	1.02:	44.4:	.99	
45.25:	13.79:	6.747:	17.14:	80.5:	45.4:	.88:	45.6:	.86:	45.9:	.84	
53.82:	16.40:	6.560:	16.67:	98.4:	46.9:	.74:	47.1:	.72:	47.4:	.70	
64.00:	19.51:	6.383:	16.22:	120.3:	48.4:	.63:	48.6:	.61:	48.9:	.59	
76.11:	23.20:	6.747:	17.14:	135.4:	49.9:	.53:	50.1:	.51:	50.4:	.50	
90.51:	27.59:	6.560:	16.67:	165.6:	51.4:	.44:	51.6:	.43:	51.9:	.42	

N_{ant} = 54 percent

ORIGINAL PAGE IS
OF POOR QUALITY

Table 7D-2. Parabolic Antenna Performance and STDN System Capabilities

S-Band; User Forward Link Gain and 3 db Beamwidth 2.025-2.125 GHz

GAIN & 3 DB BEAMWIDTH AT FREQUENCY: 2.025GHZ : 2.075GHZ : 2.125GHZ											
DISH DIAMETER: WAVELENGTH : DIA-WL:GAIN :BW-3 :GAIN :BW-3 :GAIN :BW-3											
FEET :METERS:INCHES: CM. :RATIO :DB. :DEG. :DB. :DEG. :DB. :DEG.											
2.38:	.72:	5.691:	14.46:	5.0:	21.1:	14.53:	21.3:	14.18:	21.5:	13.85	
2.83:	.86:	5.557:	14.12:	6.1:	22.6:	12.22:	22.8:	11.93:	23.0:	11.65	
3.36:	1.03:	5.831:	14.81:	6.9:	24.1:	10.28:	24.3:	10.03:	24.5:	9.79	
4.00:	1.22:	5.691:	14.46:	8.4:	25.6:	8.64:	25.8:	8.42:	26.0:	8.24	
4.76:	1.45:	5.557:	14.12:	10.3:	27.1:	7.27:	27.3:	7.09:	27.5:	6.93	
5.66:	1.72:	5.831:	14.81:	11.6:	28.6:	6.11:	28.8:	5.96:	29.0:	5.82	
6.73:	2.05:	5.691:	14.46:	14.2:	30.1:	5.14:	30.3:	5.01:	30.5:	4.90	
8.00:	2.44:	5.557:	14.12:	17.3:	31.6:	4.32:	31.8:	4.22:	32.0:	4.12	
9.51:	2.90:	5.831:	14.81:	19.6:	33.1:	3.63:	33.3:	3.55:	33.5:	3.46	
11.31:	3.45:	5.691:	14.46:	23.9:	34.6:	3.06:	34.8:	2.98:	35.0:	2.91	
13.45:	4.10:	5.557:	14.12:	29.1:	36.1:	2.57:	36.3:	2.51:	36.5:	2.45	
16.00:	4.88:	5.831:	14.81:	32.9:	37.6:	2.16:	37.8:	2.11:	38.0:	2.06	
19.03:	5.80:	5.691:	14.46:	40.1:	39.1:	1.82:	39.3:	1.77:	39.5:	1.73	
22.63:	6.90:	5.557:	14.12:	48.9:	40.6:	1.53:	40.8:	1.49:	41.0:	1.46	
26.91:	8.20:	5.831:	14.81:	55.4:	42.1:	1.28:	42.3:	1.25:	42.5:	1.22	
32.00:	9.75:	5.691:	14.46:	67.5:	43.6:	1.08:	43.8:	1.05:	44.1:	1.03	
38.05:	11.60:	5.557:	14.12:	82.2:	45.1:	.91:	45.4:	.89:	45.6:	.87	
45.25:	13.79:	5.831:	14.81:	95.1:	46.6:	.76:	46.9:	.75:	47.1:	.73	
53.82:	16.40:	5.691:	14.46:	113.5:	48.2:	.64:	48.4:	.63:	48.6:	.61	
64.00:	19.51:	5.557:	14.12:	138.2:	49.7:	.54:	49.9:	.53:	50.1:	.51	
76.11:	23.20:	5.831:	14.81:	156.6:	51.2:	.45:	51.4:	.44:	51.6:	.43	
90.51:	27.59:	5.691:	14.46:	190.9:	52.7:	.38:	52.9:	.37:	53.1:	.36	

S-Band; User Return Link Gain and 3 db Beamwidth 2.200-2.300 GHz

GAIN & 3 DB BEAMWIDTH AT FREQUENCY: 2.20 GHz : 2.25 GHz : 2.30 GHz											
DISH DIAMETER: WAVELENGTH : DIA-WL:GAIN :BW-3 :GAIN :BW-3 :GAIN :BW-3											
FEET :METERS:INCHES: CM. :RATIO :DB. :DEG. :DB. :DEG. :DB. :DEG.											
2.00:	.61:	5.367:	13.64:	4.5:	20.3:	15.91:	20.5:	15.56:	20.7:	15.22	
2.38:	.72:	5.248:	13.33:	5.4:	21.8:	13.38:	22.0:	13.08:	22.2:	12.80	
2.83:	.86:	5.134:	13.04:	6.6:	23.3:	11.25:	23.5:	11.00:	23.7:	10.76	
3.36:	1.03:	5.367:	13.64:	7.5:	24.8:	9.46:	25.0:	9.25:	25.2:	9.09	
4.00:	1.22:	5.248:	13.33:	9.1:	26.3:	7.95:	26.5:	7.78:	26.7:	7.61	
4.76:	1.45:	5.134:	13.04:	11.1:	27.8:	6.69:	28.0:	6.54:	28.2:	6.40	
5.66:	1.72:	5.367:	13.64:	12.6:	29.3:	5.62:	29.5:	5.50:	29.7:	5.38	
6.73:	2.05:	5.248:	13.33:	15.4:	30.8:	4.73:	31.0:	4.62:	31.2:	4.52	
8.00:	2.44:	5.134:	13.04:	18.7:	32.3:	3.98:	32.5:	3.89:	32.7:	3.80	
9.51:	2.90:	5.367:	13.64:	21.3:	33.8:	3.34:	34.0:	3.27:	34.2:	3.20	
11.31:	3.45:	5.248:	13.33:	25.9:	35.3:	2.81:	35.5:	2.75:	35.7:	2.69	
13.45:	4.10:	5.134:	13.04:	31.4:	36.8:	2.36:	37.0:	2.31:	37.2:	2.26	
16.00:	4.88:	5.367:	13.64:	35.8:	38.3:	1.99:	38.5:	1.94:	38.7:	1.90	
19.03:	5.80:	5.248:	13.33:	43.5:	39.8:	1.67:	40.0:	1.64:	40.2:	1.60	
22.63:	6.90:	5.134:	13.04:	52.9:	41.3:	1.41:	41.5:	1.37:	41.7:	1.35	
26.91:	8.20:	5.367:	13.64:	60.2:	42.9:	1.18:	43.0:	1.16:	43.2:	1.13	
32.00:	9.75:	5.248:	13.33:	73.2:	44.4:	.99:	44.5:	.97:	44.7:	.95	
38.05:	11.60:	5.134:	13.04:	88.9:	45.9:	.84:	46.1:	.82:	46.2:	.80	
45.25:	13.79:	5.367:	13.64:	101.2:	47.4:	.70:	47.6:	.69:	47.8:	.67	
53.82:	16.40:	5.248:	13.33:	123.1:	48.9:	.59:	49.1:	.58:	49.3:	.57	
64.00:	19.51:	5.134:	13.04:	149.6:	50.4:	.50:	50.6:	.49:	50.8:	.48	
76.11:	23.20:	5.367:	13.64:	170.2:	51.9:	.42:	52.1:	.41:	52.3:	.40	
90.51:	27.59:	5.248:	13.33:	207.0:	53.4:	.35:	53.6:	.34:	53.8:	.34	

N_{ant} = 54 percent

ORIGINAL PAGE IS
OF POOR QUALITY

Table 7D-3. Parabolic Antenna Performance for
Satellite Space Research and Earth Exploration

X-Band; Possible Satellite-Ground Data Link Gain and 3 db Beamwidth; 8.0-8.4 GHz

GAIN & 3 DB BEAMWIDTH AT FREQUENCY: 8.00 GHz : 8.20 GHz : 8.40 GHz											
DISH DIAMETER:		WAVELENGTH		DIA-WL:GAIN		BW-3		GAIN		BW-3	
FEET	METERS	INCHES	CM.	RATIO	DB.	DEG.	DB.	DEG.	DB.	DEG.	
.59:	.18:	1.406:	3.57:	5.1:	21.0:	14.72:	21.2:	14.36:	21.4:	14.01	
.71:	.22:	1.476:	3.75:	5.7:	22.5:	12.37:	22.7:	12.07:	22.9:	11.79	
.84:	.26:	1.440:	3.66:	7.0:	24.0:	10.41:	24.2:	10.15:	24.4:	9.91	
1.00:	.30:	1.406:	3.57:	8.5:	25.5:	8.75:	25.7:	8.54:	25.9:	8.33	
1.19:	.36:	1.476:	3.75:	9.7:	27.0:	7.36:	27.2:	7.18:	27.4:	7.01	
1.41:	.43:	1.440:	3.66:	11.8:	28.5:	6.19:	28.7:	6.04:	28.9:	5.89	
1.68:	.51:	1.406:	3.57:	14.4:	30.0:	5.20:	30.2:	5.08:	30.4:	4.96	
2.00:	.61:	1.476:	3.75:	16.3:	31.5:	4.38:	31.7:	4.27:	31.9:	4.17	
2.38:	.72:	1.440:	3.66:	19.8:	33.0:	3.68:	33.2:	3.59:	33.4:	3.50	
2.83:	.86:	1.406:	3.57:	24.1:	34.5:	3.09:	34.7:	3.02:	34.9:	2.95	
3.36:	1.03:	1.476:	3.75:	27.3:	36.0:	2.60:	36.2:	2.54:	36.4:	2.48	
4.00:	1.22:	1.440:	3.66:	33.3:	37.5:	2.19:	37.7:	2.13:	37.9:	2.08	
4.76:	1.45:	1.406:	3.57:	40.6:	39.0:	1.84:	39.2:	1.79:	39.4:	1.75	
5.66:	1.72:	1.476:	3.75:	46.0:	40.5:	1.55:	40.7:	1.51:	40.9:	1.47	
6.73:	2.05:	1.440:	3.66:	56.1:	42.0:	1.30:	42.2:	1.27:	42.4:	1.24	
8.00:	2.44:	1.406:	3.57:	68.3:	43.5:	1.09:	43.7:	1.07:	44.0:	1.04	
9.51:	2.90:	1.476:	3.75:	77.3:	45.0:	.92:	45.2:	.90:	45.5:	.88	
11.31:	3.45:	1.440:	3.66:	94.3:	46.5:	.77:	46.8:	.75:	47.0:	.74	
13.45:	4.10:	1.406:	3.57:	114.9:	48.0:	.65:	48.3:	.63:	48.5:	.62	
16.00:	4.88:	1.476:	3.75:	130.1:	49.5:	.55:	49.8:	.53:	50.0:	.52	
19.03:	5.80:	1.440:	3.66:	158.6:	51.1:	.46:	51.3:	.45:	51.5:	.44	
22.63:	6.90:	1.406:	3.57:	193.2:	52.6:	.39:	52.8:	.38:	53.0:	.37	
26.91:	8.20:	1.476:	3.75:	218.8:	54.1:	.33:	54.3:	.32:	54.5:	.31	
32.00:	9.75:	1.440:	3.66:	266.7:	55.6:	.27:	55.8:	.27:	56.0:	.26	
38.05:	11.60:	1.406:	3.57:	324.9:	57.1:	.23:	57.3:	.22:	57.5:	.22	
45.25:	13.79:	1.476:	3.75:	367.9:	58.6:	.19:	58.8:	.19:	59.0:	.18	
53.82:	16.40:	1.440:	3.66:	448.5:	60.1:	.16:	60.3:	.16:	60.5:	.15	
64.00:	19.51:	1.406:	3.57:	546.3:	61.6:	.14:	61.8:	.13:	62.0:	.13	
76.11:	23.20:	1.476:	3.75:	618.8:	63.1:	.11:	63.3:	.11:	63.5:	.11	
90.51:	27.59:	1.440:	3.66:	754.2:	64.6:	.10:	64.8:	.09:	65.0:	.09	

$N_{ant} = 54$ percent

ORIGINAL PAGE IS
OF POOR QUALITY.

Table 7D-4. Parabolic Antenna Performance and STDN System Capabilities

Ku-Band; User Return Link Gain and 3 db Beamwidth; 13.4-14.0 GHz

GAIN & 3 DB BEAMWIDTH AT FREQUENCY: 13.40 GHz : 13.70 GHz : 14.00 GHz													
DISH DIAMETER:		WAVELENGTH		DIA-WL:		GAIN		BW-3		GAIN		BW-3	
FEET	METERS	INCHES	CM.	RATIO	DB.	DEG.	DB.	DEG.	DB.	DEG.	DB.	DEG.	
.35:	.11:	.843:	2.14:	5.0:	20.9:	14.78:	21.1:	14.45:	21.3:	14.14			
.42:	.13:	.881:	2.24:	5.7:	22.4:	12.42:	22.6:	12.15:	22.8:	11.89			
.50:	.15:	.862:	2.19:	7.0:	23.9:	10.45:	24.1:	10.22:	24.3:	10.00			
.59:	.18:	.843:	2.14:	8.5:	25.4:	8.79:	25.6:	8.59:	25.8:	8.41			
.71:	.22:	.881:	2.24:	9.6:	26.9:	7.39:	27.1:	7.23:	27.3:	7.07			
.84:	.26:	.862:	2.19:	11.7:	28.4:	6.21:	28.6:	6.08:	28.8:	5.95			
1.00:	.30:	.843:	2.14:	14.2:	29.9:	5.22:	30.1:	5.11:	30.3:	5.00			
1.19:	.36:	.881:	2.24:	16.2:	31.5:	4.39:	31.6:	4.30:	31.8:	4.20			
1.41:	.43:	.862:	2.19:	19.7:	33.0:	3.69:	33.1:	3.61:	33.3:	3.54			
1.68:	.51:	.843:	2.14:	23.9:	34.5:	3.11:	34.7:	3.04:	34.8:	2.97			
2.00:	.61:	.881:	2.24:	27.2:	36.0:	2.61:	36.2:	2.55:	36.3:	2.50			
2.38:	.72:	.862:	2.19:	33.1:	37.5:	2.20:	37.7:	2.15:	37.9:	2.10			
2.83:	.86:	.843:	2.14:	40.2:	39.0:	1.85:	39.2:	1.81:	39.4:	1.77			
3.36:	1.03:	.881:	2.24:	45.9:	40.5:	1.55:	40.7:	1.52:	40.9:	1.49			
4.00:	1.22:	.862:	2.19:	55.7:	42.0:	1.31:	42.2:	1.28:	42.4:	1.25			
4.76:	1.45:	.843:	2.14:	67.7:	43.5:	1.10:	43.7:	1.07:	43.9:	1.05			
5.66:	1.72:	.881:	2.24:	77.0:	45.0:	.92:	45.2:	.90:	45.4:	.88			
6.73:	2.05:	.862:	2.19:	93.7:	46.5:	.78:	46.7:	.76:	46.9:	.74			
8.00:	2.44:	.843:	2.14:	113.8:	48.0:	.65:	48.2:	.64:	48.4:	.63			
9.51:	2.90:	.881:	2.24:	129.6:	49.5:	.55:	49.7:	.54:	49.9:	.53			
11.31:	3.45:	.862:	2.19:	157.5:	51.0:	.46:	51.2:	.45:	51.4:	.44			
13.45:	4.10:	.843:	2.14:	191.4:	52.5:	.39:	52.7:	.38:	52.9:	.37			
16.00:	4.88:	.881:	2.24:	217.9:	54.0:	.33:	54.2:	.32:	54.4:	.31			
19.03:	5.80:	.862:	2.19:	264.9:	55.5:	.27:	55.7:	.27:	55.9:	.26			
22.63:	6.90:	.843:	2.14:	321.9:	57.0:	.23:	57.2:	.23:	57.4:	.22			
26.91:	8.20:	.881:	2.24:	366.4:	58.5:	.19:	58.7:	.19:	58.9:	.19			
32.00:	9.75:	.862:	2.19:	445.5:	60.0:	.16:	60.2:	.16:	60.4:	.16			
38.05:	11.60:	.843:	2.14:	541.4:	61.5:	.14:	61.7:	.13:	61.9:	.13			
45.25:	13.79:	.881:	2.24:	616.3:	63.1:	.12:	63.3:	.11:	63.4:	.11			
53.82:	16.40:	.862:	2.19:	749.3:	64.6:	.10:	64.8:	.09:	64.9:	.09			
64.00:	19.51:	.843:	2.14:	910.6:	66.1:	.08:	66.3:	.08:	66.5:	.08			
76.11:	23.20:	.881:	2.24:	1036.4:	67.6:	.07:	67.8:	.07:	68.0:	.07			
90.51:	27.59:	.862:	2.19:	1260.1:	69.1:	.06:	69.3:	.06:	69.5:	.06			

ORIGINAL PAGE IS
OF POOR QUALITY

Table 7D-5. Parabolic Antenna Performance and STDN System Capabilities

Ku-Band; User Forward Link Gain and 3 db Beamwidth 14.6-15.2 GHz											
GAIN & 3 DB BEAMWIDTH AT FREQUENCY: 14.60 GHz : 14.90 GHz : 15.20 GHz											
DISH DIAMETER: WAVELENGTH : DIA-WL:GAIN :BW-3 :GAIN :BW-3 :GAIN :BW-3											
FEET : METERS: INCHES: CM. :RATIO :DB. :DEG. :DB. :DEG. :DB. :DEG.											
.30:	.09:	.792:	2.01:	4.5:	20.2:	16.13:	20.3:	15.80:	20.5:	15.49	
.35:	.11:	.777:	1.97:	5.5:	21.7:	13.56:	21.8:	13.29:	22.0:	13.03	
.42:	.13:	.809:	2.05:	6.2:	23.2:	11.40:	23.3:	11.17:	23.5:	10.95	
.50:	.15:	.792:	2.01:	7.6:	24.7:	9.59:	24.8:	9.40:	25.0:	9.21	
.59:	.18:	.777:	1.97:	9.2:	26.2:	8.06:	26.4:	7.90:	26.5:	7.75	
.71:	.22:	.809:	2.05:	10.5:	27.7:	6.78:	27.9:	6.64:	28.0:	6.51	
.84:	.26:	.792:	2.01:	12.7:	29.2:	5.70:	29.4:	5.59:	29.5:	5.48	
1.00:	.30:	.777:	1.97:	15.4:	30.7:	4.79:	30.9:	4.70:	31.0:	4.61	
1.19:	.36:	.809:	2.05:	17.6:	32.2:	4.03:	32.4:	3.95:	32.5:	3.87	
1.41:	.43:	.792:	2.01:	21.4:	33.7:	3.39:	33.9:	3.32:	34.1:	3.26	
1.68:	.51:	.777:	1.97:	26.0:	35.2:	2.85:	35.4:	2.79:	35.6:	2.74	
2.00:	.61:	.809:	2.05:	29.7:	36.7:	2.40:	36.9:	2.35:	37.1:	2.30	
2.38:	.72:	.792:	2.01:	36.0:	38.2:	2.02:	38.4:	1.98:	38.6:	1.94	
2.83:	.86:	.777:	1.97:	43.7:	39.7:	1.70:	39.9:	1.66:	40.1:	1.63	
3.36:	1.03:	.809:	2.05:	49.9:	41.2:	1.43:	41.4:	1.40:	41.6:	1.37	
4.00:	1.22:	.792:	2.01:	60.6:	42.7:	1.20:	42.9:	1.17:	43.1:	1.15	
4.76:	1.45:	.777:	1.97:	73.5:	44.2:	1.01:	44.4:	.99:	44.6:	.97	
5.66:	1.72:	.809:	2.05:	83.9:	45.7:	.85:	45.9:	.83:	46.1:	.81	
6.73:	2.05:	.792:	2.01:	101.9:	47.2:	.71:	47.4:	.70:	47.6:	.68	
8.00:	2.44:	.777:	1.97:	123.6:	48.8:	.60:	48.9:	.59:	49.1:	.58	
9.51:	2.90:	.809:	2.05:	141.2:	50.3:	.50:	50.4:	.49:	50.6:	.48	
11.31:	3.45:	.792:	2.01:	171.3:	51.8:	.42:	51.9:	.42:	52.1:	.41	
13.45:	4.10:	.777:	1.97:	207.8:	53.3:	.36:	53.4:	.35:	53.6:	.34	
16.00:	4.88:	.809:	2.05:	237.4:	54.8:	.30:	55.0:	.29:	55.1:	.29	
19.03:	5.80:	.792:	2.01:	288.1:	56.3:	.25:	56.5:	.25:	56.6:	.24	
22.63:	6.90:	.777:	1.97:	349.5:	57.8:	.21:	58.0:	.21:	58.1:	.20	
26.91:	8.20:	.809:	2.05:	399.3:	59.3:	.18:	59.5:	.17:	59.6:	.17	
32.00:	9.75:	.792:	2.01:	484.6:	60.8:	.15:	61.0:	.15:	61.1:	.14	
38.05:	11.60:	.777:	1.97:	587.8:	62.3:	.13:	62.5:	.12:	62.6:	.12	
45.25:	13.79:	.809:	2.05:	671.5:	63.8:	.11:	64.0:	.10:	64.2:	.10	
53.82:	16.40:	.792:	2.01:	814.9:	65.3:	.09:	65.5:	.09:	65.7:	.09	
64.00:	19.51:	.777:	1.97:	988.6:	66.8:	.07:	67.0:	.07:	67.2:	.07	
76.11:	23.20:	.809:	2.05:	1129.3:	68.3:	.06:	68.5:	.06:	68.7:	.06	
90.51:	27.59:	.792:	2.01:	1370.5:	69.8:	.05:	70.0:	.05:	70.2:	.05	

ORIGINAL PAGE IS
OF POOR QUALITY

Table 7D-6. Parabolic Antenna Performance for Satellite Space Research and Earth Exploration

K-Band; Possible Satellite-Ground Data Link Gain and 3 db Beamwidth;
21.2-22.0 GHz

GAIN & 3 DB BEAMWIDTH AT FREQUENCY: 21.20 GHz : 21.60 GHz : 22.00 GHz											
DISH DIAMETER		WAVELENGTH		DIA	WL	GAIN	BW-3	GAIN	BW-3	GAIN	BW-3
FEET	METERS	INCHES	CM.	RATIO	DB.	DEG.	DB.	DEG.	DB.	DEG.	DB.
.21:	.06:	.537:	1.36:	4.7:	20.4:	15.71:	20.5:	15.42:	20.7:	15.14	
.25:	.08:	.557:	1.42:	5.4:	21.9:	13.21:	22.1:	12.96:	22.2:	12.73	
.30:	.09:	.547:	1.39:	6.5:	23.4:	11.11:	23.6:	10.90:	23.7:	10.70	
.35:	.11:	.537:	1.36:	7.9:	24.9:	9.34:	25.1:	9.17:	25.2:	9.00	
.42:	.13:	.557:	1.42:	9.1:	26.4:	7.85:	26.6:	7.71:	26.7:	7.57	
.50:	.15:	.547:	1.39:	11.0:	27.9:	6.60:	28.1:	6.48:	28.2:	6.36	
.59:	.18:	.537:	1.36:	13.3:	29.4:	5.55:	29.6:	5.45:	29.7:	5.35	
.71:	.22:	.557:	1.42:	15.2:	30.9:	4.67:	31.1:	4.58:	31.2:	4.50	
.84:	.26:	.547:	1.39:	18.3:	32.4:	3.93:	32.6:	3.85:	32.7:	3.79	
1.00:	.30:	.537:	1.36:	22.4:	33.9:	3.30:	34.1:	3.24:	34.3:	3.18	
1.19:	.36:	.557:	1.42:	25.6:	35.4:	2.78:	35.6:	2.73:	35.8:	2.68	
1.41:	.43:	.547:	1.39:	31.0:	36.9:	2.33:	37.1:	2.29:	37.3:	2.25	
1.68:	.51:	.537:	1.36:	37.6:	38.4:	1.96:	38.6:	1.92:	38.8:	1.89	
2.00:	.61:	.557:	1.42:	43.1:	40.0:	1.65:	40.1:	1.62:	40.3:	1.59	
2.38:	.72:	.547:	1.39:	52.2:	41.5:	1.39:	41.6:	1.36:	41.8:	1.34	
2.83:	.86:	.537:	1.36:	63.2:	43.0:	1.17:	43.1:	1.15:	43.3:	1.12	
3.36:	1.03:	.557:	1.42:	72.5:	44.5:	.98:	44.6:	.96:	44.8:	.95	
4.00:	1.22:	.547:	1.39:	87.8:	46.0:	.83:	46.1:	.81:	46.3:	.80	
4.76:	1.43:	.537:	1.36:	106.4:	47.5:	.69:	47.6:	.68:	47.8:	.67	
5.66:	1.72:	.557:	1.42:	121.9:	49.0:	.58:	49.1:	.57:	49.3:	.56	
6.73:	2.05:	.547:	1.39:	147.7:	50.5:	.49:	50.7:	.48:	50.8:	.47	
8.00:	2.44:	.537:	1.36:	178.9:	52.0:	.41:	52.2:	.41:	52.3:	.40	
9.51:	2.90:	.557:	1.42:	205.0:	53.5:	.35:	53.7:	.34:	53.8:	.33	
11.31:	3.43:	.547:	1.39:	243.3:	55.0:	.29:	55.2:	.29:	55.3:	.28	
13.43:	4.10:	.537:	1.36:	300.8:	56.5:	.25:	56.7:	.24:	56.8:	.24	
16.00:	4.82:	.557:	1.42:	344.7:	58.0:	.21:	58.2:	.20:	58.3:	.20	
19.03:	5.80:	.547:	1.39:	417.7:	59.5:	.17:	59.7:	.17:	59.8:	.17	
22.63:	6.90:	.537:	1.36:	505.9:	61.0:	.15:	61.2:	.14:	61.3:	.14	
26.91:	8.20:	.557:	1.42:	579.7:	62.5:	.12:	62.7:	.12:	62.9:	.12	
32.00:	9.75:	.547:	1.39:	702.4:	64.0:	.10:	64.2:	.10:	64.4:	.10	
38.05:	11.60:	.537:	1.36:	850.8:	65.5:	.09:	65.7:	.09:	65.9:	.08	
45.25:	13.79:	.557:	1.42:	975.0:	67.0:	.07:	67.2:	.07:	67.4:	.07	
53.82:	16.40:	.547:	1.39:	1181.4:	68.5:	.06:	68.7:	.06:	68.9:	.06	

$N_{ant} = 54$ percent

ORIGINAL PAGE IS
OF POOR QUALITY

Table 7D-7. Parabolic Antenna Performance for Satellite Space Research and Earth Exploration

V-Band; Possible Satellite-Satellite Relay Return Link Gain and 3 db Beamwidth; 51.0-52.0 GHz

GAIN & 3 DB BEAMWIDTH AT FREQUENCY: 51.00 GHz : 51.50 GHz : 52.00 GHz											
DISH DIAMETER:		WAVELENGTH :		DIA-WL:		GAIN :BW-3 :		GAIN :BW-3 :		GAIN :BW-3 :	
FEET	METERS	INCHES	CM.	RATIO	DB.	DEG.	DB.	DEG.	DB.	DEG.	DB.
.09:	.03:	.232:	.59:	4.6:	20.5:	15.53:	20.6:	15.38:	20.7:	15.23:	
.11:	.03:	.229:	.58:	5.5:	22.0:	13.06:	22.1:	12.93:	22.2:	12.81:	
.13:	.04:	.227:	.58:	6.6:	23.5:	10.98:	23.6:	10.87:	23.7:	10.77:	
.15:	.05:	.232:	.59:	7.7:	25.0:	9.23:	25.1:	9.14:	25.2:	9.06:	
.18:	.05:	.229:	.58:	9.3:	26.5:	7.76:	26.6:	7.69:	26.7:	7.61:	
.21:	.06:	.227:	.58:	11.1:	28.0:	6.53:	28.1:	6.47:	28.2:	6.40:	
.25:	.08:	.232:	.59:	13.0:	29.5:	5.49:	29.6:	5.44:	29.7:	5.38:	
.30:	.09:	.229:	.58:	15.6:	31.0:	4.62:	31.1:	4.57:	31.2:	4.53:	
.35:	.11:	.227:	.58:	18.7:	32.5:	3.88:	32.6:	3.84:	32.7:	3.81:	
.42:	.13:	.232:	.59:	21.8:	34.0:	3.26:	34.1:	3.23:	34.2:	3.20:	
.50:	.15:	.229:	.58:	26.2:	35.5:	2.75:	35.6:	2.72:	35.7:	2.69:	
.59:	.18:	.227:	.58:	31.4:	37.0:	2.31:	37.1:	2.29:	37.2:	2.26:	
.71:	.22:	.232:	.59:	36.6:	38.5:	1.94:	38.6:	1.92:	38.7:	1.90:	
.84:	.26:	.229:	.58:	44.0:	40.1:	1.63:	40.1:	1.62:	40.2:	1.60:	
1.00:	.30:	.227:	.58:	52.8:	41.6:	1.37:	41.6:	1.36:	41.7:	1.35:	
1.19:	.36:	.232:	.59:	61.6:	43.1:	1.15:	43.1:	1.14:	43.2:	1.13:	
1.41:	.43:	.229:	.58:	74.0:	44.6:	.97:	44.7:	.96:	44.7:	.95:	
1.68:	.51:	.227:	.58:	88.9:	46.1:	.82:	46.2:	.81:	46.2:	.80:	
2.00:	.61:	.232:	.59:	103.7:	47.6:	.69:	47.7:	.68:	47.7:	.67:	
2.38:	.72:	.229:	.58:	124.5:	49.1:	.58:	49.2:	.57:	49.3:	.57:	
2.83:	.86:	.227:	.58:	149.5:	50.6:	.49:	50.7:	.48:	50.8:	.48:	
3.36:	1.03:	.232:	.59:	174.3:	52.1:	.41:	52.2:	.40:	52.3:	.40:	
4.00:	1.22:	.229:	.58:	209.3:	53.6:	.34:	53.7:	.34:	53.8:	.34:	
4.76:	1.45:	.227:	.58:	251.4:	55.1:	.29:	55.2:	.29:	55.3:	.28:	
5.66:	1.72:	.232:	.59:	293.2:	56.6:	.24:	56.7:	.24:	56.8:	.24:	
6.73:	2.05:	.229:	.58:	352.1:	58.1:	.20:	58.2:	.20:	58.3:	.20:	
8.00:	2.44:	.227:	.58:	422.8:	59.6:	.17:	59.7:	.17:	59.8:	.17:	
9.51:	2.90:	.232:	.59:	493.1:	61.1:	.14:	61.2:	.14:	61.3:	.14:	
11.31:	3.45:	.229:	.58:	582.1:	62.6:	.12:	62.7:	.12:	62.8:	.12:	
13.45:	4.10:	.227:	.58:	711.0:	64.1:	.10:	64.2:	.10:	64.3:	.10:	
16.00:	4.88:	.232:	.59:	829.3:	65.6:	.09:	65.7:	.08:	65.8:	.08:	
19.03:	5.80:	.229:	.58:	995.8:	67.1:	.07:	67.2:	.07:	67.3:	.07:	
22.63:	6.90:	.227:	.58:	1195.8:	68.6:	.06:	68.7:	.06:	68.8:	.06:	

$N_{ant} = 54$ percent

ORIGINAL PAGE IS
OF POOR QUALITY

Table 7D-8. Parabolic Antenna Performance for Satellite Space Research and Earth Exploration

W-Band; Possible Satellite-Satellite Relay Return Link Gain and 3 db Beamwidth; 65.0-66.0 GHz

GAIN & 3 DB BEAMWIDTH AT FREQUENCY: 65.00 GHz : 65.50 GHz : 66.00 GHz													
DISH DIAMETER		WAVELENGTH		DIA-WL	GAIN	BW-3	GAIN	BW-3	GAIN	BW-3			
FEET	METERS	INCHES	CM.	RATIO	DB.	DEG.	DB.	DEG.	DB.	DEG.	DB.	DEG.	DB.
.07:	.02:	.179:	.45:	5.0:	21.1:	14.49:	21.2:	14.38:	21.2:	14.27:			
.09:	.03:	.182:	.46:	5.8:	22.6:	12.18:	22.7:	12.09:	22.7:	12.00:			
.11:	.03:	.180:	.46:	7.0:	24.1:	10.25:	24.2:	10.17:	24.2:	10.09:			
.13:	.04:	.179:	.45:	8.4:	25.6:	8.62:	25.7:	8.55:	25.7:	8.48:			
.15:	.05:	.182:	.46:	9.8:	27.1:	7.24:	27.2:	7.19:	27.2:	7.13:			
.18:	.05:	.180:	.46:	11.8:	28.6:	6.09:	28.7:	6.05:	28.7:	6.00:			
.21:	.06:	.179:	.45:	14.1:	30.1:	5.12:	30.2:	5.08:	30.2:	5.05:			
.25:	.08:	.182:	.46:	16.5:	31.6:	4.31:	31.7:	4.27:	31.8:	4.24:			
.30:	.09:	.180:	.46:	19.8:	33.1:	3.62:	33.2:	3.59:	33.3:	3.57:			
.35:	.11:	.179:	.45:	23.7:	34.6:	3.05:	34.7:	3.02:	34.8:	3.00:			
.42:	.13:	.182:	.46:	27.8:	36.1:	2.56:	36.2:	2.54:	36.3:	2.52:			
.50:	.15:	.180:	.46:	33.3:	37.6:	2.15:	37.7:	2.14:	37.8:	2.12:			
.59:	.18:	.179:	.45:	39.9:	39.1:	1.81:	39.2:	1.80:	39.3:	1.78:			
.71:	.22:	.182:	.46:	46.7:	40.7:	1.52:	40.7:	1.51:	40.8:	1.50:			
.84:	.26:	.180:	.46:	56.0:	42.2:	1.28:	42.2:	1.27:	42.3:	1.26:			
1.00:	.30:	.179:	.45:	67.1:	43.7:	1.08:	43.7:	1.07:	43.8:	1.06:			
1.19:	.36:	.182:	.46:	78.6:	45.2:	.91:	45.2:	.90:	45.3:	.89:			
1.41:	.43:	.180:	.46:	94.1:	46.7:	.76:	46.7:	.76:	46.8:	.75:			
1.68:	.51:	.179:	.45:	112.8:	48.2:	.64:	48.2:	.64:	48.3:	.63:			
2.00:	.61:	.182:	.46:	132.1:	49.7:	.54:	49.8:	.53:	49.8:	.53:			
2.38:	.72:	.180:	.46:	158.3:	51.2:	.45:	51.3:	.45:	51.3:	.45:			
2.83:	.86:	.179:	.45:	189.7:	52.7:	.38:	52.8:	.38:	52.8:	.37:			
3.36:	1.03:	.182:	.46:	222.2:	54.2:	.32:	54.3:	.32:	54.3:	.32:			
4.00:	1.22:	.180:	.46:	266.3:	55.7:	.27:	55.8:	.27:	55.8:	.27:			
4.76:	1.45:	.179:	.45:	319.1:	57.2:	.23:	57.3:	.22:	57.3:	.22:			
5.66:	1.72:	.182:	.46:	373.7:	58.7:	.19:	58.8:	.19:	58.8:	.19:			
6.73:	2.05:	.180:	.46:	447.8:	60.2:	.16:	60.3:	.16:	60.4:	.16:			
8.00:	2.44:	.179:	.45:	536.6:	61.7:	.13:	61.8:	.13:	61.9:	.13:			
9.51:	2.90:	.182:	.46:	628.4:	63.2:	.11:	63.3:	.11:	63.4:	.11:			
11.31:	3.45:	.180:	.46:	753.1:	64.7:	.10:	64.8:	.09:	64.9:	.09:			
13.45:	4.10:	.179:	.45:	902.4:	66.2:	.08:	66.3:	.08:	66.4:	.08:			
16.00:	4.88:	.182:	.46:	1056.9:	67.7:	.07:	67.8:	.07:	67.9:	.07:			
19.02:	5.80:	.180:	.46:	1266.6:	69.3:	.06:	69.3:	.06:	69.4:	.06:			

N_{ant} = 54 percent

ORIGINAL PAGE IS
OF POOR QUALITY

To show the accuracy of the usual tolerance theory in predicting the loss of gain of antennas due to surface deviations, the axial loss of a uniformly-illuminated paraboloidal reflector with various radially-linear distributions of surface deviations is calculated and the results are compared with the corresponding values obtained assuming uniform error distribution.

Four cases are considered for this purpose, as follows:

Case I: The function σ vanishes at the outer edge of the reflector.

Case II: The function σ vanishes at the center of the reflector.

Case III: An intermediate condition in which the rate of change of σ with radius is one half that for Case I.

Case IV: An intermediate condition in which the rate of change of σ with radius is one half that for Case II.

σ_0 = standard deviation of phase error over the aperture.

The results are shown in Figure 7D-1 and indicate that the assumption of uniform distribution of surface deviations over the aperture involves errors that become significant for high-tolerance losses.

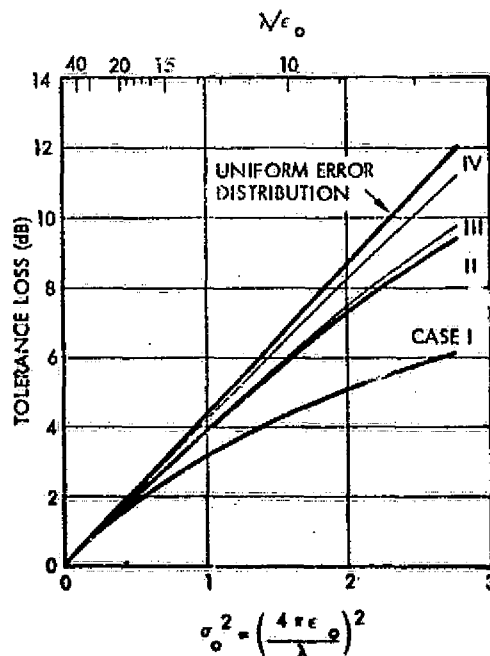


Figure 7D-1. Tolerance Loss for Various Distributions of Surface Deviations

APPENDIX D
REFERENCES

1. M. S. Zarghamu, On Antenna Tolerance Theory, IEEE Transactions on Antennas and Propagation, Vol. AP-15, No. 6, November 1967.
2. J.R. Cogdell and G. McCu, High Resolution Millimeter Reflector Antennas, IEEE Transactions on Antennas and Propagation, Vol. AP 18, No. 4, July 1970.
3. J. Ruze, The Effect of Aperture Errors on the Antenna Radiation Pattern, Suppl. Nuove Cimento, Vol. 9, pp. 364-380, 1952.
4. J. Ruze, Antenna Tolerance Theory - A Review, Proc. IEEE, Vol. 54, pp. 633-640, April 1966.

APPENDIX 7E

7E.1 NEUTRAL GAS LASERS

Since the first report in 1961 of population inversion and oscillation in a gas discharge in a helium-neon mixture, oscillation in 29 elements on more than 450 identified transitions in neutral species has been reported. Oscillation in neutral species has been observed in all atomic groups.

Neutral gas lasers fit into three broad classifications depending on the types of electrical excitation used. These types of excitation are:

1. Weakly ionized dc and rf-excited discharges
2. Pulsed afterglow discharges
3. Short rise-time pulsed discharges.

The most commonly used CW laser medium for neutral species is the weakly ionized plasma of the positive column of the glow discharge. The current densities involved in such discharges in which CW-oscillation has been reported are typically 100-200 mA/cm². The properties of the plasma of the positive column are determined by the electric field existing along the column. In a steady, unstriated, uniform positive column the longitudinal electric field has such a value that the number of electrons and ions produced is equal to the diffusion loss of charged particles to the walls of the discharge tube. The electron temperature in the plasma adjusts itself to that value required to maintain the flow of positive ions and the loss of electrons to the walls. A theoretical treatment of the positive column in gases and gas-mixtures, where volume-ionization and electron-metastable collisions are not significant, leads to the important result that the average electron temperature is determined primarily by the pressure and tube-diameter product (pD). A low pD results in a high electron temperature, and a high pD in a low electron temperature. To produce given discharge conditions in a discharge in a single gas, all that is necessary is that the pD be maintained constant (at constant electron concentration). In the weakly ionized plasma of the positive column the electron concentration is directly proportional to the current density.

The basic importance of the pD-product in laser discharges in single gases or mixtures of gases, include values of the optimum pD for giving population inversion on a large number of transitions.

7E.2 IONIZED GAS LASERS

This category includes all known laser lines originating from transitions between energy levels of the ionized states of atoms in gas discharges. Not surprisingly, the elements are those that occur as gases at room temperature or are easily vaporized. Many other elements doubtless would exhibit ion laser action if they were studied. Of those elements already found to exhibit laser action, 29 in total, more than 450 identified transitions have been reported. Surprisingly enough, the transitions identified for the ionized gas lasers are not the same as those identified for neutral gas lasers. Within the ionized gas laser regime, gain, power CW and superradiant operation has been observed.

7E.3 MOLECULAR GAS LASERS

Molecular gas lasers have been operated using a variety of excitation methods, including electrical, optical and chemical pumping. In some pumping methods, a mixture of gases is added to the laser gas to modify relaxation rates and gas cooling, or to provide collisional energy transfer. An example of this is the addition of He and N₂ to CO₂ gas lasers.

Frequently, the excited laser molecule itself is produced in the discharge or reaction tube as a result of excitation of one or more different molecules. The reaction of CS₂ and O₂, excited by either flash photolysis or an electric discharge, to produce excited CO molecules in the CO laser is representative of this case. Some 25 varieties of molecular gas lasers have been identified.

7E.4 DYE LASERS

The properties of close to 200 varieties of dye lasers have been investigated and are summarized in Table 7E-1.

A number of workers have noted the role of various additives to the dye solution. Molecular oxygen quenches the lifetime of the triplet state and usually increases the duration of lasing,³⁷ but since it can also enhance singlet-triplet transitions, in some cases it decreases the

laser output. The effect of oxygen addition has been studied for a number of dyes. ³⁸

Table 7E-1. Summary of Dye Laser Properties

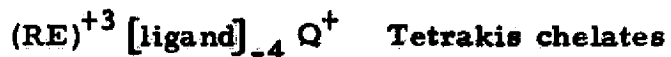
Property	Typical values	Conditions	Comments	
Wavelength	3400-11,750 Å	Flashlamp and/or laser pumped	A variety of dye-solvent combinations are available to span the entire wavelength range nearly continuously	
Tuning	Up to 1760 Å	Prism, filter, grating, Q-switch in cavity	Length, concentration, and temperature of active medium also provide tuning. Solvent pH affects tuning range.	
Spectral Width	15-150 Å ~ 0.5 Å ~ 0.01 Å	Broadband mirrors Grating in cavity Grating plus etalon		
Beam Divergence	2-5 mrad 0.5 mrad	Flashlamp and/or laser pumped Etalon in cavity	Dependent on uniformity of pumping	
Efficiency	Up to 25 percent ~ 0.4 percent	Laser pumped Flashlamp pumped	Measured optical efficiency Electrical energy input to laser energy output	
Output	Energy	2J (high)- 0.1J (typical)	Flashlamp pumped	
	Power	~ 2 MW 0.75-2.0 MW	20 MW pump Flashlamp pumped	Rhodamine 6G
	Repetition Rate	Up to 200 pps	Laser pumped	Pump laser rate limits
		20-50 pps	Linear flashlamp	System cooling and component failure are limits
Temporal		1 pps continuous	Annular flashlamp (Laser pumped) (small cavity)	Dye liquid flow transversely through cavity
	Pulse Duration	~ 20 nsec	Laser pumped	Follows pump pulse
		0.5 μsec typical; up to 500 μsec achieved	Flashlamp pumped	Shorter than pump duration
	Mode-Locked		Mode-locked pump	Pump cavity length integral multiple of dye cavity
			Pulses - 10 ⁻⁹ sec	Flashlamp pumped with intracavity saturable absorber
	Pulses < 10 ⁻¹¹ sec	Mode-locked pump	Observed by two-photon fluorescence	

7E.5 RARE EARTH LIQUID LASERS

Rare earth lasers use rare earth ions in solution. All of these lasers have been operated only in a pulsed mode, using xenon-filled flashlamps for optical excitation.

The Chelates in solution are a class of laser materials in which the active ion is a trivalent rare earth (RE) bonded to several organic groups or ligands. Most chelates are soluble in a number of organic solvents and are historically important because a Eu-chelate dissolved in alcohol was the first liquid material to exhibit laser action.

Two general types of compounds can be distinguished:



where Q^{+} is a cation. The efficiency of chelate lasers is limited by excessive absorption in pump band regions: output energy is limited by the very small volume of active material that can be effectively pumped. Extensive search for different [ligand] and Q combinations has not yielded materials of significantly higher efficiency. Small changes in wavelength (for a particular ion) can be achieved by changing the ligand or the cation.

7E.6 COMMERCIAL LASER GLASSES

The following examples illustrate the extremes in performance that have been achieved with glass laser systems. Thresholds for laser action as low as 0.9 joules have been obtained for clad laser rods 3.0 cm long with a 0.1 mm diameter core. Efficiencies up to 9 percent have been reported for rods 20 mm in diameter by 92.4 cm long, and efficiencies of 12 percent have been predicted. In the millisecond time domain, output energies as high as 5000 joules in a 10 milliradian beam angle have been obtained from a clad glass laser rod 1 meter long with a 30 mm active core diameter. In the picosecond time domain, 51 joule pulses with power densities of 17×10^{12} watts have been reported.

Diffraction limited, lowest order mode glass laser systems have produced high radiance outputs of 2×10^{17} watts/cm² steradian from an oscillator-amplifier system in which the output from the last amplifier rod (38 mm diameter by 1 meter long) was 90 joules in a 40 microradian beam angle.

Damage in laser glass is currently receiving much attention and has been the subject of two symposia, June 1969 and June 1970, sponsored by

the American Society for Testing and Materials, and a study by the National Materials Advisory Board of the National Academy of Sciences and the National Academy of Engineering. In a report by the latter, it is concluded that the three main causes of laser damage in glass laser material are:

1. Absorption of light by metallic and nonmetallic inclusions followed by thermally induced fracture around the inclusion.
2. Intrinsic bulk damage initiated by a self-focusing mechanism resulting in plasma formation and filamentary damage tracks.
3. Surface damage accompanied by plasma formation at the surface.

At the time at which the above report was issued, it was felt that inclusions were the most serious cause of damage, but that glass with a low absorption loss and a damage threshold of 20 joules/cm² in a 3×10^{-8} second pulse was being produced with a reasonable yield in both platinum and ceramic crucibles.

The threshold for intrinsic damage in bulk glass is over 1000 joules/cm² in a 3×10^{-8} second pulse. These intensities can be reached by a self-focusing mechanism, which has a threshold of formation in the range of 50 to 100 joules/cm² for a 3×10^{-8} pulse.

The mechanism for surface damage is only partially understood. Surface preparation appears to play the major role in determining the threshold for surface damage. By appropriate surface treatment, surface damage thresholds of 100 joules/cm² should be possible in a 3×10^{-8} second pulse.

The threshold for laser damage appears to vary with the duration of the laser pulse. The threshold for inclusion-induced damage varies, in a complex manner, with both pulse duration and particle size. The threshold for surface damage appears to decrease with decreasing pulse duration. Self focusing not only depends on the pulse duration, but also on beam uniformity and the length of the sample being tested.

APPENDIX 7F

7F.1 ATMOSPHERIC ATTENUATION AT VISIBLE AND INFRARED FREQUENCIES

Optical transmission of energy is most usually expressed by:

$$T = \exp(-\sigma R),$$

where σ is the attenuation coefficient or extinction coefficient and R is the result of two processes--scattering and absorption. The scattering portion of the attenuation coefficient may be further broken down into scattering from air molecules and from aerosols. Scattering from air molecules is called Rayleigh scattering and varies as the altitude. Scattering from aerosols is a function among other things, of atmospheric pressure and geographic location--distinction often being made on the basis of maritime and continental aerosols. The data presented here does not reflect this distinction and therefore must be considered as qualitative. The majority of the existing experimental and theoretical work in atmospheric transmission has been involved with incoherent, broad-band sources and must be evaluated with care, since the absorption bands consist of a multiplicity of lines, whose width and strength depend upon the pressure and concentration of the particular absorbing constituent. Figure 7F-1 displays the broad-band transmission for various atmospheric conditions. Figures 7F-2 and 7F-3 provide a convenient method of evaluating the slant path attenuation at a wavelength of 10.59 for a model standard clear atmosphere. Also, in general, Table 7F-1 indicates those lasers that are strongly and weakly affected by the atmospheric absorption.

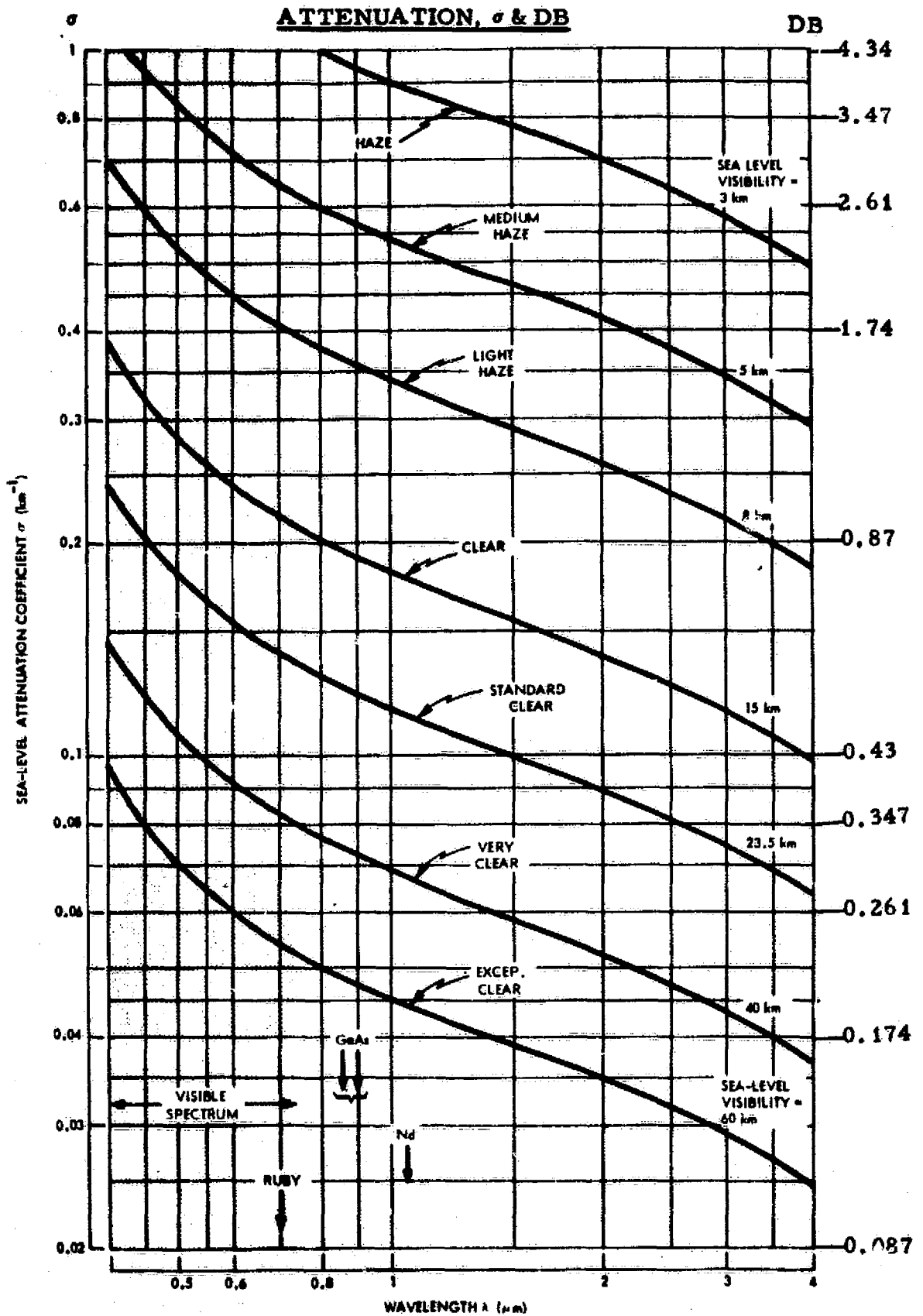


Figure 7F-1. Approximate Variation of Attenuation Coefficients with Wavelength at Sea Level for Various Atmospheric Conditions (Neglects Absorption by Water Vapor and Carbon Dioxide)

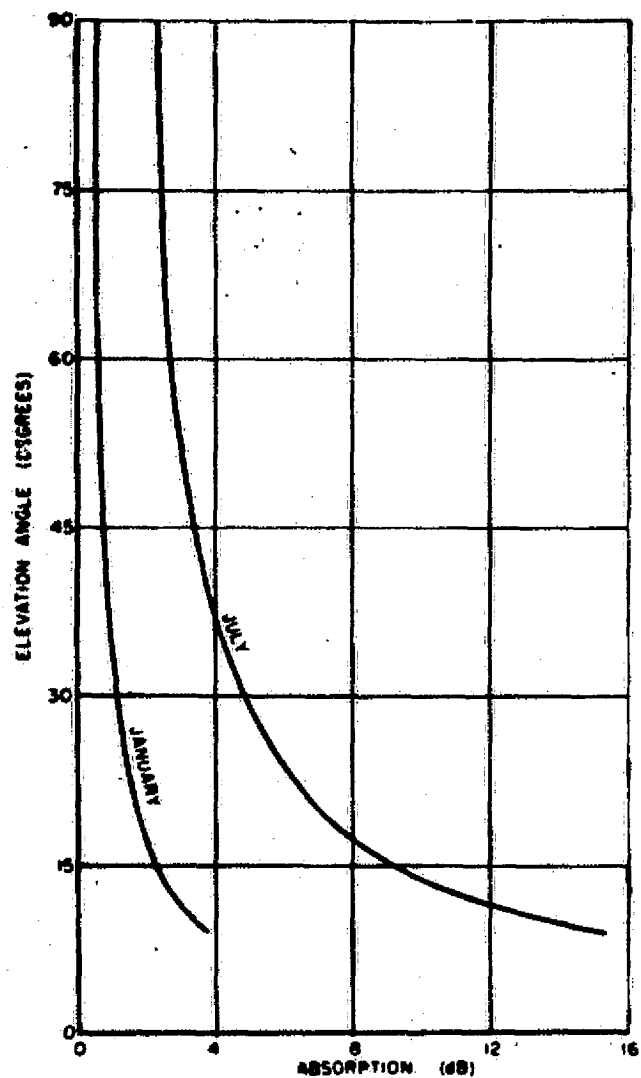


Figure 7F-2. Calculated Water Vapor Absorption at 10.59μ vs. the Elevation Angle for Propagation Paths Traversing the Entire Atmosphere

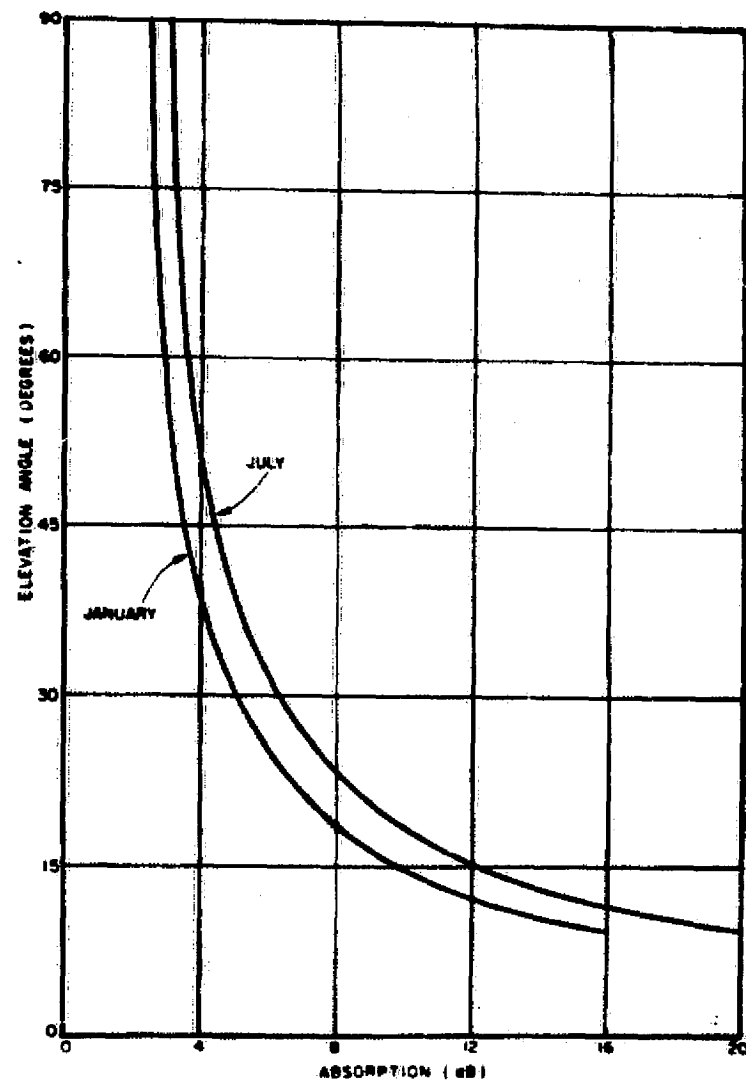


Figure 7F-3. Calculated Carbon Dioxide Absorption at 10.59μ vs. the Elevation Angle for Propagation Paths Traversing the Entire Atmosphere.

Table 7F-1. Laser Lines Absorbed by the Atmosphere

STRONGLY ABSORBED			WEAK TO MODERATE ABSORPTION			
Laser	λ , microns	Absorber	Laser	λ	Comment	
Atomic krypton	1.7843	H ₂ O	Ionized argon	4880 Å, 5145 Å	Close attention must be paid to temperature of operation; increased absorption occurs from approx. 8600 Å to 9250 Å	
Atomic krypton	1.9211	H ₂ O	Atomic neon (He-Ne)	6328 Å		
Tm ³⁺ -CaWO ₄	1.911	H ₂ O	GaAs	8300 Å, 9200 Å		
Tm ³⁺ -CaWO ₄	1.916	H ₂ O				
U ³⁺ -SrF ₂	2.472	H ₂ O				
U ³⁺ -CaF ₂	2.511	H ₂ O				
Atomic krypton	2.5234	H ₂ O	Ruby	6934 - 6945 Å		
U ³⁺ -BaF ₂	2.556	H ₂ O	Nd ³⁺	≈ 1.06 μ		
U ³⁺ -CaF ₂	2.613	H ₂ O	Atomic neon (He-Ne)	1.1523 μ		
				5 lines		
Atomic neon	3.391317	CH ₄	CH ₄ Raman shift of 1.06 μ	1.53 μ	Strong H ₂ O absorptions can occur. Very low absorption Moderate H ₂ O absorption	
Carbon monoxide	5.2 to 7	H ₂ O	Er ³⁺ (CaF ₂) (glass)	1.55 - 1.65 μ		
Cesium	7.1821	H ₂ O	Ho ³⁺ -CaWO ₄	2.04 μ		
Atomic neon	18.3040	H ₂ O	Ho ³⁺ -YAG	to		
Atomic neon	20.351	H ₂ O	Ho ³⁺ -CaF ₂	2.128 μ		
			Atomic Xe	3.50704 μ		
			DF	3.8 μ		
			CO ₂	10.6 μ		
						CO ₂
						Water absorption

8. GROUND DATA HANDLING SUBSYSTEM (GDHS) CONSIDERATIONS

The objective of this section is to investigate ground data handling for Earth Resource Systems (ERS) in the 1978 to 1988 time-frame, identify technologies involved, develop a parametric model for the ground data handling system (GDHS), and summarize significant trade-offs and problem areas. The results of this effort will be used in conjunction with results from related Phase B studies addressed to 1) data routing analysis, 2) on-board data processing, and 3) communication link considerations to synthesize potential data management systems.

This section is divided into four parts. The first part presents an overview of the GDHS structure and illustrates how it interfaces with the system components used for data handling in the Earth Resources System. This section also identifies modes of data handling used in the GDHS. It further identifies dominant technologies associated with the GDHS and discusses each of the areas and their relationship to ERS ground data handling problems. A parametric model of the ERS GDHS is also presented.

The parametric model relates ERS data processing requirements to the costs of implementing the GDHS for ERS. The methodology is new and evolves from TRW's past experience in processing ERTS data. The estimated hardware costs were derived, for the most part, by using engineering judgment to extrapolate present knowledge.

Conclusions are presented for the ERS GDHS data handling considerations, these identify the dominant tradeoffs, and required development areas, as well as other critical considerations necessary to ensure smooth progress in the design of GDHS for future NASA Earth Resource Systems.

8.1 System Analysis of GDHS Structure

The ERS GDHS has been evaluated on the basis of the overall system, including spacecraft, to define functional interfaces for allocation of requirements among the ERS elements. This yields an understanding of the GDHS design elements, which in turn, can be evaluated using the supplied parametric model.

The user community has identified a list of various output data products for ERS. NASA will orbit a sensor payload that can best service the list while providing the best data quality. It is expected that NASA will retain responsibility for, and control of, all system-induced errors associated with the output data from the sensors. The four major components of the system include the information generation and transmission function, the data capturing function, the system error correction function, and the information extraction function. Figure 8-1 illustrates the system.

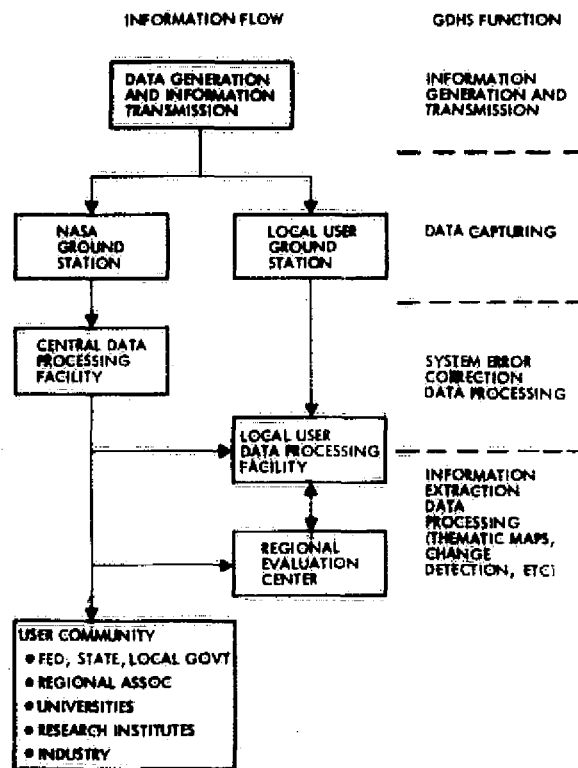


Figure 8-1. GDHS Structure

System-induced errors from the first three functions are assumed to be under NASA's responsibility and control. Certain elements of the fourth function may also be within NASA's purview. Consequently, GDHS requirements will result from NASA tradeoffs between error control and error measurement/correction for each function.

8.1.1 Information Generation

There are several ways in which information is formulated for the ERS GDHS. Figure 8-2 provides a structure for this process and indicates

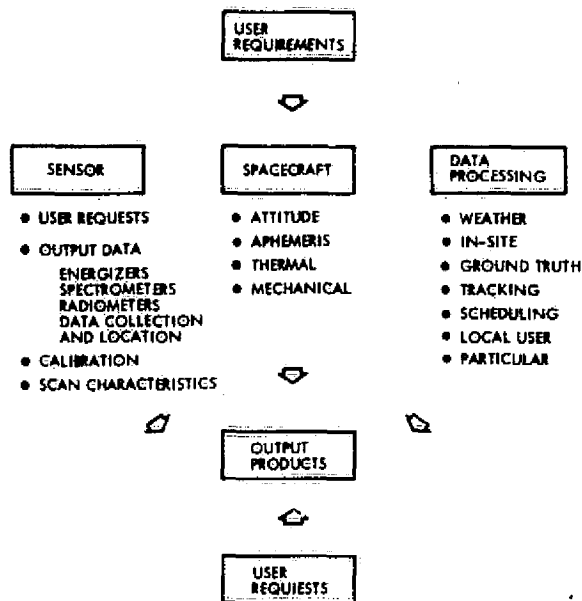


Figure 8-2. Information Flow for ERS GDHS

the different types of information. These sources of information are determined by the ERS user community requirements for useful output products.

The ERS sensors can be categorized into four general classes: 1) imagers, 2) spectrometers, 3) radiometers, and 4) data collection and location units. Each class contributes specialized information for producing output products. In addition to the sensor's output data, information must be obtained from the sensor for calibration and scan characteristics. To process this sensor data, spacecraft information (attitude, ephemeris, thermal, and mechanical data) must be obtained to estimate distortions with the imager class of sensors particularly demanding. Finally, information must be obtained to satisfy data processing requirements for the specific output products. Examples of these types of information are weather, in situ data, and ground truth. There is also a requirement for information on the mission operation of the spacecraft to schedule sensor operation and provide tracking and processing data inputs to local user ground stations.

8.1.2 Data Capturing Function

The data capturing function transforms spacecraft-transmitted energy into a data format suitable for processing sensor information. Figure 8-3 is a functional block diagram of the principal components

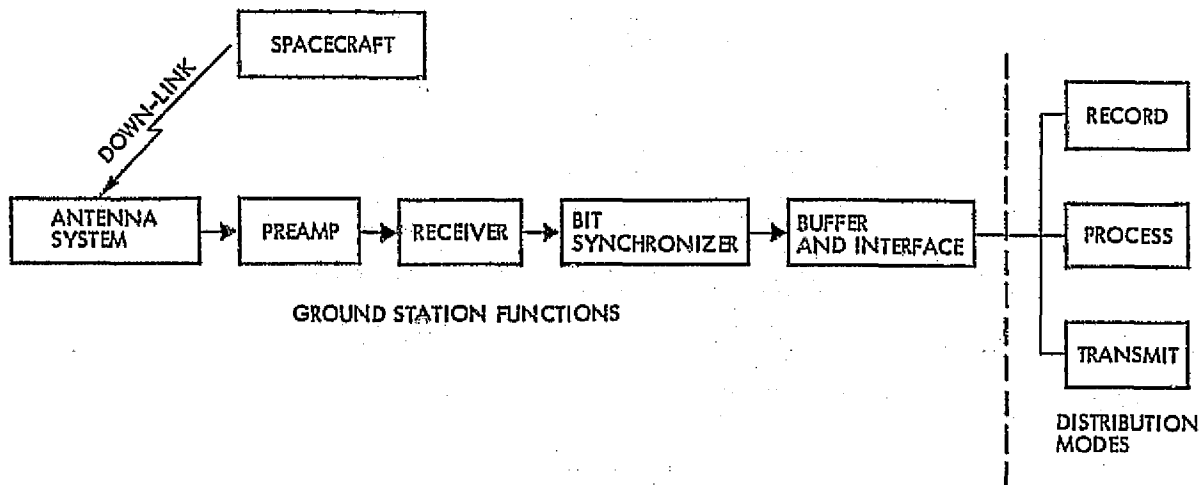


Figure 8-3. Principle Components of the Data Capturing Function

of data capturing function for ERS, covering anticipated ERS configurations from the low-cost user station through the NASA ground station concepts.

The downlink data stream from the spacecraft is received by the antenna system. This requires an antenna and associated RF electronics matched to the transmission characteristics of the data stream, and a tracking system matched to the mission operational characteristics of the spacecraft and receiving station site. The antenna system interfaces with a preamplifier, and the antenna gain and preamplifier noise figure determine the essential RF characteristics of the data capturing function. The receiver demodulates the RF signal into a bit stream which is conditioned, synchronized, and timed for subsequent processing in the buffer and interface function.

The buffer and interface function matches the serial bit stream to the three basic distribution modes for the data: 1) record for further processing, 2) process in real time, and 3) transmit over a data link. All three modes have a required format and any processing not performed on the spacecraft to obtain these formats must be accomplished by the buffer and interface function.

8.1.3 Central Data Processing Facility (CDPF)

Figure 8-4 shows a system functional flow which is basically a sequential processing structure that may incorporate parallel processes for certain functions which would otherwise limit throughput performance.

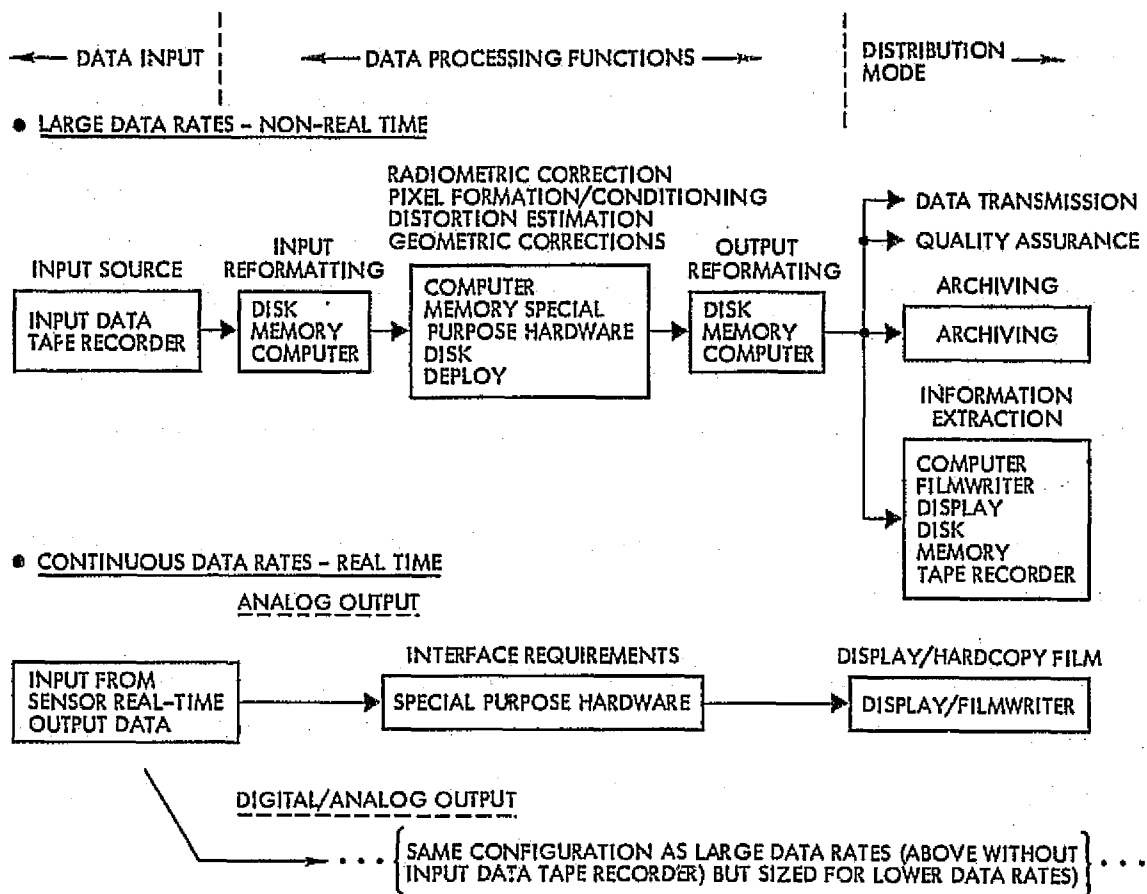


Figure 8-4. Ground Data Handling Functional Block Diagram

Also shown are configurations for different modes of sensor data processing: nonreal-time and real-time with the various technologies of each function. There are three essential steps associated with each configuration: input reformatting, correction of sensor output data, and output data reformatting. Within each step exists the possibility of parallel as well as pipeline processing.

The input data stream is from one of the distribution modes of the data capturing function. Reformatting of the data may be necessary. If the data from several sensors are multiplexed to form the data stream, demultiplexing may also be required. The use of common data formats for all interfaces is certainly an issue that can simplify data handling and data processing requirements.

Correction of sensor output data for system errors will initially require the formation and conditioning of pixel values. This process could be rather simple or very demanding, e.g., radar imagery data

can require azimuthal as well as range compression. Distortion estimation, including registration control point (RCP) location, is also performed early in this step. The output from the estimation routines may be required for the pixel formation/conditioning process if demanded by the particular sensor type. Radiometric calibration of the data is required; this function can be incorporated at any time before the detector outputs are transformed. The last function is the process of geometrically correcting the data. This process generally requires resampling the data to obtain an output that has been corrected for system-induced errors.

If a uniform data format is not possible for the several modes of output data distribution, the processed data will have to be reformatted. The output data reformatting is the last of the three essential steps comprising the functions of the CDPF. One of the output distribution modes is the quality assurance rejection mode. In addition to this mode, there may be quality control checks incorporated into the system error correction process which will reject certain data. Consideration must be given to incorporating this data into the quality assurance rejection mode.

Certain GDHS data management functions such as scheduling will be automated, probably on general-purpose computers. Time-sharing communication will probably be incorporated to handle user requests and special-processing requirements. While these aspects cannot be addressed here, consideration must be given to the data management problems.

User community requirements for ERS data increasingly demand the usage of digital data. Therefore, an all digital implementation of the data processing functions is indicated to preserve the quality of sensor data. This does not preclude the possibility of analog implementations of various processes for ERS GDHS designs. However, for purposes of this study, an all digital approach will be used for sizing the CDPF hardware architecture.

Figure 8-5 presents a CDPF architecture. This configuration will be used for sizing the hardware requirements and costs of the GDHS.

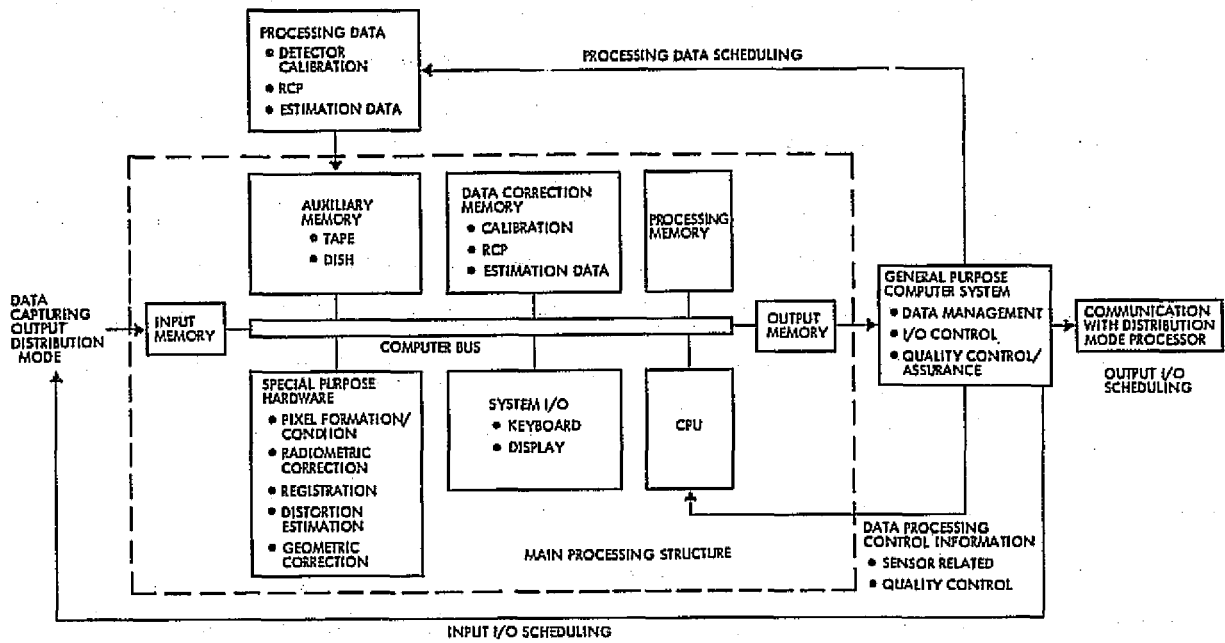


Figure 8-5. Central Data Processing Facility Sizing Architecture

It is an extrapolation of present hardware configurations and is presented for modelling purposes only. The main processing structure is a computer-based system, probably mini- or midi-implemented, which performs the three essential steps of the CDPF. The processing is performed in a pipeline fashion with parallel processing used to obtain the necessary throughput. In fact, this main processing structure itself could be an element in a parallel processing configuration. For example, data from each sensor could be corrected using its own dedicated main processing structure. A general-purpose computer system is used to supervise the generation of corrected output data and distribute this data to the various output modes. It is envisioned that this computer could communicate directly with the processors associated with each distribution mode.

8.1.4 Local User Data Processing Facility (LUDPF)

The local user data processing facility and the CDPF perform the same functional sequence. It receives input sensor data from one of the three distribution modes of the data capturing function. In fact, the data capturing function and local user data processing might be implemented in one facility for some ERS GDHS configurations. Three considerations differentiate the implementation of the LUDPF from the

CDPF: lower data rates, smaller data volume, and user specific data processing. Because of these differences, the implementation of LUDPF will be assumed to be just the main processing structure of the CDPF architecture as presented in Figure 8-5.

In addition to the above considerations, the dominant LUDPF design consideration will be achieving low cost and providing fast turnaround time for processing data. The output products of the LUDPF will combine all the distribution modes of the CDPF as part of its implementation, but the products will be tailored to the needs of the local user community.

8.1.5 ERS Information Distribution Modes

There are four basic modes for distributing ERS information which has been corrected for all system errors: archiving, generation of output data products, transmission over a data link, and quality assurance processing. Figure 8-6 presents a diagram of these modes and lists the dominant characteristics of each mode.

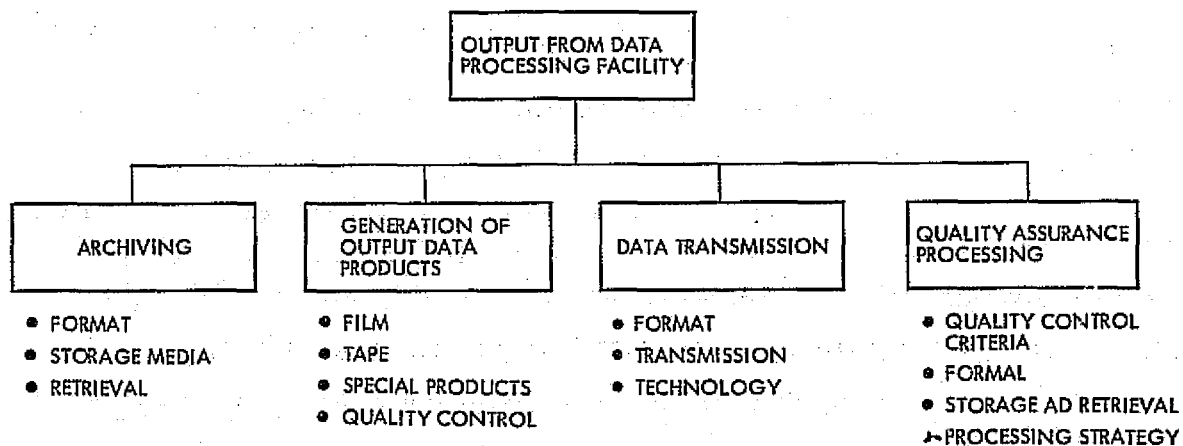


Figure 8-6. Distribution Modes from Data Processing Facility

Archiving ERS data requires careful consideration of the formats and storage media used, data retrieval requirements to satisfy the anticipated needs of the user community, and data volume requirements. Generation of output data products requires the use of filmwriter and photographic technology to produce film copy, additional data processing to produce the output tape formats to perform the information extraction necessary to obtain the special products desired by users, and the use of quality control techniques to assure data quality.

The output of the data processing facility can also be transmitted over a data link to regional evaluation centers, local users, and other processing centers of the ERS user community. Concern must be given to the data format and transmission technology used for this process. Lastly, ERS data which does not meet the quality control criteria will have to be processed. To perform this quality assurance processing, consideration must be given to the format used for the rejected data, how data are stored and retrieved, and the degree of processing necessary to make its data quality acceptable.

8.2 Dominant Technology Areas of the ERS GDHS

The following sections present a discussion and evaluation of the dominant areas of technology associated with the ERS GDHS. Pursuant to the level of effort, no claim is made that an in-depth study has been performed within each area. Rather, the value of the following sections is in identifying dominant technology areas involved with the GDHS and presenting a brief discussion of the issues faced by each area.

8.2.1 ERS Data Formats

Data formats (structure), issues of minor consequence in the past, become an important issue of automated, high-throughput, flexible ERS ground data handling systems. Indeed, one of the tradeoffs is system flexibility and data format. The highly flexible system will use common data formats but have the penalty of a higher initial cost. The initial design must allow for a wide range of sensors, but reduce data handling at interfaces. The first question to be asked is where to introduce format commonality — at the sensor, at the data capture point, or at the ground data processing facility.

Sensor designs typically do not produce data streams in a format amenable for direct data processing. Moreover, if data compression is required to meet the communication link capabilities, the compressed format may not be amenable for direct data processing. The first logical point to establish commonality is at the data capturing point. Spacecraft preprocessing could alleviate the capturing ground station's data handling load if the downlink data stream were structured to be close to the common format.

Data handling at the data capture point implies data processing hardware collocated with the data capturing equipment and a consequent increase of ground station costs as the handling capability increases. The mode of data transmission to the processing facility (either central or local) will also determine if significant reformatting should be done at the data capture point. The reformatted data volume may produce an unmanageable number of tapes or choke a high-speed ground communications link.

It is desirable, however, that common data formats be used from the point of input to processing through the final distribution modes. Consequently, the easiest design, but perhaps least optimum for ERS, would be to follow the traditional approach and reformat at the processing facility prior to the actual data processing function. However, this choice limits ERS data handling flexibility (e. g., the use of a data link network to disseminate input data from the data capture point to the various processing facilities).

8.2.2 Ground Station Tape Recorder and Interface

It is inevitable that the high data rate sensors used by the ERS program will require recording and subsequent non-real-time processing of their data to produce corrected data. (Albeit, the requirement may be nothing more than a back-up for a high-speed data link.) Furthermore, it is generally true that any processing performed on the spacecraft can also be performed on the ground, i. e., if the sensor data can be multiplexed and transmitted from the spacecraft, then technology should exist to receive and demultiplex the data on the ground. These two concepts indicate that the tape recorder and interface technology will probably be the driving consideration for implementation of the data capturing function.

There appears to be an upper bound to the transmitted data; a 300 Mbit/s channel rate for the TDRS data link. Of course, this rate could be for data compressed information, allowing higher total sensor data rates, and requiring decompression of the data on the ground. Nevertheless, the 300 Mbit/s can be established as an upper bound to the required rate. The actual recording rate may be lower since each of the large data rate sensors could have its data recorded separately after

demultiplexing on the ground. Conceptually, multitrack tape recorder technology could handle a 300 Mbit/s data rate; see Figure 8-7.* A 240-Mbit/s tape recorder (HDMR-240G) has been developed by RCA using high density multitrack recording (MDMR) technology.* This technology allows 80 tracks/inch for lower linear packing densities, on the order of 25,000 bits per inch (BPI), which result in bit error rates (BER) less than 10^{-5} .

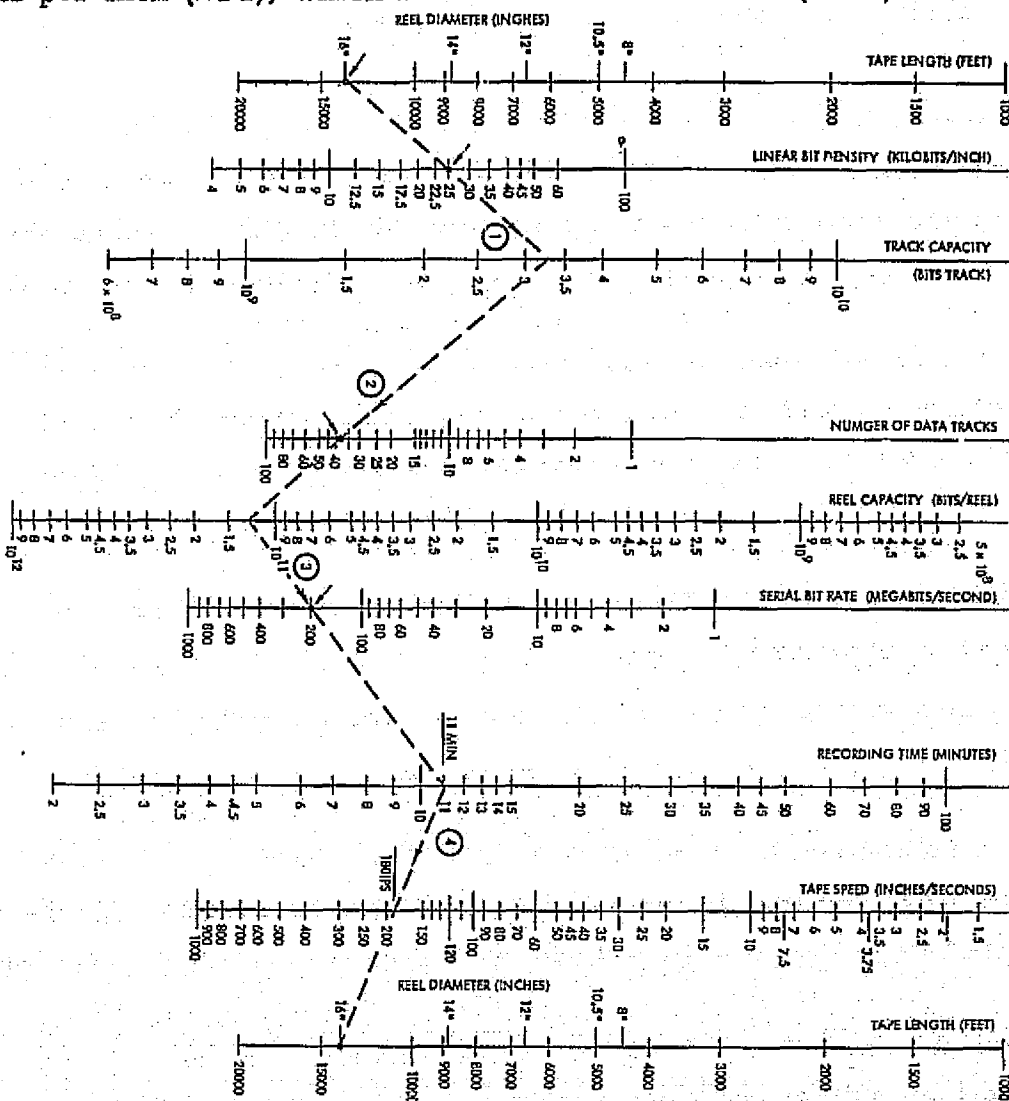


Figure 8-7. Design Chart for Space Division Multiplex Recording

*Charles F. Spitzer (Ampex), "Digital Recording of Video Signals up to 50 MHz" presented at Society of Photo-Optical Instrumentation Engineers Technology Utilization Program on Military Airborne Video Recording: Requirements Utilization and Techniques, April 3-5, 1974, Dayton, Ohio.

*O. E. Bessette (RCA), "A High Capacity, High Data Rate Instrumentation Tape Recorder System," presented at International Telemetry Conference, October 9-11, 1973, Washington, D. C.

It appears the maximum packing density (an order of 10^6 bits/in.²) for magnetic tape recorders is being approached by both the multitrack fixed-head and rotating-head recording technologies. The speeds used by these technologies should cover the maximum data rate of 300 Mbit/s. This estimate assumes, however, that the present rate of research and development funding in the recording industry continues as there are significant problems to overcome in achieving this recording rate and reproducing the data.

Multitrack recorder technology is concerned with the deskew/interchannel flutter problem. This problem is a result of the tape being reproduced with multichannel data being demultiplexed into a serial data stream (or at least when some of the tracks are combined into one data stream). Skew, relative to time or distance, across the tape (with respect to the center track) develops due to gap scatter, misalignment of the heads, track circuit timing variations, and stretching and rotation of the tape. Flutter problems are time or distance instabilities resulting in the reference track and, hence, cause relative errors in the other data tracks. There are a number of approaches to solving these problems and advances in digital circuit technology speeds should provide the means to accomplish this task.

The other approach to high-data capacity and recording speed is the rotating head technology. A number of machines using this technology has been converted from television applications into digital recorders. To achieve the high packing densities, the head is rotated across the tape as the tape is moved in a longitudinal direction. Transverse and helical scans have been used. The data are recorded serially, eliminating the skew problem and requirement for multiplexing and demultiplexing electronics. There are timing problems in reproducing the data and longitudinal tracks are used to provide control signals to solve this problem.

Regardless of which recording technology is used, the ground station recorder must present the capability to reproduce data at a substantially lower rate than the recorded rate, e. g., ratios of 10 through 100 to 1. The reduced playback capability and need for reproducing the

data on a different machine than recorded, will be a significant factor in determining technology used for the ground station tape recorder and its required interface.

8.2.3 Processing Algorithm Development

A recent study by TRW for NASA* has shown that high-order algorithms are required to produce imagery of high-precision (mean error less than one pixel). Moreover, all digital processing is possible with these algorithms with little decrease in processing speed compared to low-order algorithm implementations. Indeed, special-purpose or microcoded processor implementations would speed up the higher order image correction process.

The nature of algorithms used in the ground data handling of image data is well understood. For example, the fast Fourier transform (FFT) is well known and speed of operation is not the major point, but the opportunity for parallelism and pipelining the data through the FFT. So rather than the nature of the algorithms dominating ERS image processing system design, it is the data structure and hardware/software implementation of the algorithms that demand attention.

Above and beyond image processing considerations, there are the myriad of GDHS management algorithms to consider. For example, ERS application of the elegant scheduling algorithms developed for transportation problems should be considered for managing data requests and data flow through the system. The proper design/implementation of the management algorithms will ensure effective functioning of the GDHS.

8.2.4 Filmwriter/Display

Filmwriter/display technology is concerned with presenting sensor output data in a visual format, either as a display or film products. There are two basic modes for presenting the data. The first is generating film products at the CDPE or regional evaluation centers under conditions of large data throughput. The second usage of this technology is in real-time processing applications either for continuous rate sensors or at the

* TRW Report No. 20634-6003-Ur-00, "Evaluation of Digital Correction Techniques for ERS Images, Final Report," March 1974.

lower data rates processed at local user processing facilities. This second mode also includes display capability for visual analysis of the sensor data.

Generating film output products from the sensor output data is a problem that has been faced by ERTS NDPF. Because of throughput and desired output film product sizes and quality, two approaches to producing film products have evolved. One uses laser beam recorders (LBR) and the other electron beam recorders (EBR). Both approaches can accommodate very large input data rates far exceeding 100 Mbit/s. CBS Laboratory's ERTS Electron Beam Recorder, Type 70c and Type 70f, are examples of EBR's that are presently being used to generate ERTS film products. While the EBR's can be used to geometrically and photo-metrically correct an image, they are limited by their technology to a maximum scan width on the order of 8 cm. On the other hand, LBR's can accommodate relatively large film widths (as large as 40 cm). A great deal of discussion has transpired regarding the relative merits of each approach to film generation, most of the discussions centered around the ERTS application. These film recording systems are fairly expensive, running in excess of \$100 K.

The second method of presenting sensor output data in a visual format is a new application area derived from the earth resources system modes of sensor data distribution. It is envisioned there will be a need for real-time monitoring of continuous rate sensors as well as visual presentation of processed data. Furthermore, a need for hard copy of the sensor output data is anticipated. Low-cost local user facilities can be configured with filmwriter/display systems as their means of processing ERS data and generating output products. In addition, filmwriter/display units can be used in facsimile systems to transmit sensor data directly to the user community in real-time or with a relatively small time lag. Maximum data rates should be on the order of 20 Mbit/s for the local ground station/processing facility application and 2 Mbit/s for other applications.

Cost is a driving consideration for the design of a filmwriter/display system. The present technology of the LBR's and EBR's certainly will satisfy the rate specifications. Flying-spot scanners such as

the Optronics Model 5619 cost around \$35 K but have low data rates (on the order of 60 kbit/s). High-resolution CRT technology systems can be obtained for on the order of \$60 K at recording rates around 1 Mbit/s; a new example of such technology is the DICOMED Model D47, which can provide color products as well as black and white. A new solution is a relatively low-cost LBR being developed by Goodyear Aerospace for commercial applications. It should meet the ERS requirements for this mode, and is estimated to cost on the order of \$50 K; a cost which includes a general-purpose buffer/interface. This represents a new direction and should be closely monitored.

A need also exists for computer compatible displays with quick-look and interactive processing capabilities. For these applications, smaller frame sizes (~500 x 500 pixels) and lower data rates (~10 usec/pixel) will probably be sufficient. Displays with these capabilities are presently available in the \$20 to \$60K price range. This cost is determined by the precision, rate, and color requirements desired.

8.2.5 Computer Hardware Technology

Computer hardware technology is slowly changing focus from the general-purpose sequential von Neumann machines to architectures oriented toward solving a particular class of problems. The architecture used to size processing requirements of the CDPF is an example of this new focus. Because of the level of support for this study it is not feasible to investigate the new technologies that are expected to provide design elements for future computing systems. Rather, as indicated in Figure 8-5, an existing approach to the implementation of computing processes will be used. Therefore, present computer technology will be used to size the data processing requirements and estimated costs for the ERS GDHS. Wherever appropriate, existing technology performance characteristics will be extrapolated to cover the ERS time frame.

It should be noted this is a very conservative approach. The advantage of this approach results from the fact that if the present technical approach (with the improved performance specifications anticipated in the future) can meet the requirements, then the incorporation of

unanticipated new technologies in the actual ERS GDHS implementation does not invalidate the conclusion that the requirements can be satisfied.

Some general trends in computer hardware should be mentioned. Memory costs in the future, as now, will exceed processor costs. There is a great deal of activity in memory technology and most will be applicable to the ERS GDHS data processing requirements. Processor speeds continue to increase at a rapid rate, and this also is applicable to present problems. New computing elements are evolving; microprocessors and hard-wired processors are well established in the field. Computing architectures with multiple CPU configurations are now commonplace. Peripheral technology also continues to develop rapidly. In summary, all the trends appear to favor an optimistic view of possibilities for the future.

However, one concept will become increasingly important as the data processing tasks become more automated and higher throughputs are demanded. That concept is structure, or format, of the data. The format of the incoming data stream, word length optimized to data content, will have a significant impact on the choice of computer hardware used. The data structure must be tailored to facilitate storage, ease data partitioning, and minimize data handling requirements. Commonality of formats across system interfaces is a desirable, if not necessary, design goal.

8.2.6 Archiving Technology

A significant problem facing the ERS GDHS is storage and retrieval of collected sensor data. The storage volume will have to be measured in units of terabits, 10^{12} bits of data. The storage problem will be at least one magnitude greater than the present ERTS situation. Fortunately, a new technology has developed, called mass memory systems. These are systems that can store on-line the order of one terabit of data and efficiently retrieve these data with very little degradation of quality.

There are essentially three approaches at this time for storing large amounts of digital data: 1) tape recording systems, 2) print

writing systems, and 3) holographic memory systems. Table 8-1 illustrates a comparison for some characteristics of each. The tape recording systems are basically derived from the television video tape recorder technology, especially the cartridge approach. Data are stored on magnetic tape (an erasable medium) and retrieved in most applications with the assistance of a minicomputer data processing subsystem. Examples of such systems as the Ampex Terabit Memory System and System Development Corporation Mass Storage System MMSS-1 and MMSS-2 incorporating the International Video IVC-1000 recorder. The RCA TCR-100 would be a candidate (using 11 units) to develop a terabit system incorporating tape cartridges.

Table 8-1. Brief Characteristics of Terabit Archiving Technologies

Table 8-1. Brief Characteristics of Terabit Archiving Technologies

	Storage Media	Estimated Terabit Storage Size	Estimated Maximum Access Time (sec)	Recording/Reading Rate (Mbit/s)	BER	~ Cost (\$M)
Tape recorder	Magnetic tape cartridge or reel	220 6 x 8 x 9 cm cartridges or 11 40 cm (16 in.) reels	25	Both 1 to 10	10^{-8}	1.5
Point writing	Metal or thermoplastic strip	500 thin strips: 8 x 25 cm	10	5/3	10^{-8}	1.5
Holographic	Photographic film	5 kg of film	20	10/10	10^{-10}	1

A well-publicized example of the point writing system is the Precision Instrument UNICON 690-212 laser recording system installed at NASA/Ames. Further developments in this approach are anticipated. The remaining approach is the relatively new area of laser holography. A holographic storage system has been developed by TRW and its use demonstrated over the past year. Improvements in the holographic memory approach should make this a particularly attractive possibility for solving the ERS GDHS archival and storage problem.

In addition to the actual storage and retrieval technology factors, the entire issue of data formats to be used for archiving and data management aspects of storage and retrieval present considerations for the ERS GDHS system. The latter are nontrivial and deserve as much attention as technologies investigated for archiving and storage.

8.2.7 Output Data Quality Specifications and Quality Assurance

The most meaningful way to specify output data quality is to consider the data's ultimate use or its output from the information extraction processing function. For example, precise geodetic accuracy of image data is required to produce maps whereas high precision is not required to produce thematic maps for land management analysis. It is therefore important to understand the nature of the final products derived from sensor output data. That nature must then be specified in quantitative terms that lead to meaningful output quality specifications for the system error corrected data.

As parts of the ERS system evolve from a research objective into an operational mode, efforts must be continued to ascertain the nature of the final products. These efforts must provide the basis for determining quality control criteria and output data quality assurance.

8.2.8 ERS GDHS Management Considerations

It is easy when concentrating on the implementation of complex data processing systems to overlook the management aspects. This observation applies to the ERS GDHS system. Under the guise of management considerations, a number of items should be addressed including: overall administration (e.g., personnel, procurement, budget, and maintenance), information systems organization (e.g., scheduling, distribution, and allocation of resources), output product generation, and further development of the NASA/user community interface.

8.3 Parametric Model for ERS GDHS Requirements and Estimated Costs

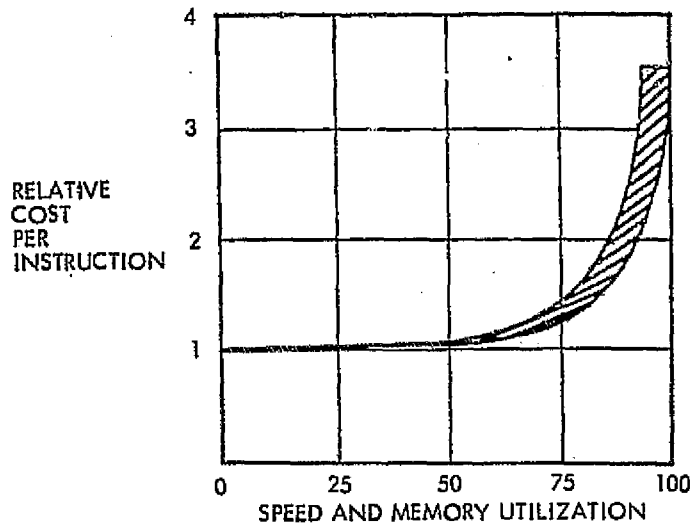
Reliance has been placed on TRW's accumulated experience in processing ERTS images for the development of the parametric model for the ERS GDHS during the 1978 to 1988 time-frame. The thrust of the model is the hardware implementation requirements and costs for data handling functions performed by the ERS GDHS. The model is sufficient to indicate the technological requirements for processing the data to perform system error correction of the sensor output data and ascertain the hardware cost of implementing the data processing. Because of the technical requirements of the ERS output data rates and volume, filmwriter/display technology also has been included. For

purposes of sizing this model, it is assumed that only sensor data obtained over the United States, its territories, and other areas relevant to its interest will be processed by the ERS GDHS configuration. The tape recorder and interface requirements are the only consideration addressed within the data capturing function. Furthermore, present data processing schemes and algorithms are assumed, where applicable, for sizing purposes.

Because of the level of effort supported; manpower, facilities, maintenance and costs for processing system error corrected output data as well as overall consideration of the information extraction data processing requirements and implementation have not been included. The latter is difficult to define at this time because of the research nature of the present usage of earth resource data by the user community. The former considerations are important for ascertaining the actual cost of implementing the ERS GDHS; it is a truism that the operating expenses eventually lead to a greater cost than the cost of purchasing capital equipment. Hence, for assessing total implementation cost of the ERS GDHS it will be necessary to provide additional information covering these considerations.

It should be noted that in sizing a problem for a GDHS there are striking cost implications associated with the sizing. This is particularly true if the computer(s) is so selected that almost all of its resources are used by the problem or by the software situated thereon. Note in particular Figure 8-8 showing data developed by Dr. Barry Boehm of the Rand Corporation. This figure shows software development costs rising dramatically as either the memory capacity or the machine throughput limits are approached. The figure strongly suggests that for a relatively small increase in hardware costs, a major savings in software costs may be realized. Such a savings would occur if the machine were significantly larger than needed to handle the problem for which the machine was selected. To realize the potential savings in selecting an oversized computer, however, it is necessary to exercise good control in management over the software so that a Parkinsonian effect does not predominate over the effect shown in this figure.

SOFTWARE DEVELOPMENT COSTS VARY AS THE THROUGHPUT LIMIT OF THE MACHINE IS APPROACHED.



(REFERENCE: BARRY BOEHM,
RAND CORPORATION)

Minimum software development cost is incurred if design point is below 50 percent of computer capacity.

Figure 8-8. Software Development Costs

The model begins with a definition of the input data and its characterization. Hardware technology areas used in the ERS GDHS system are then characterized in terms sufficient to ascertain the requirements to correct system errors and produce output data products for the modes of distribution. Estimated costs of the hardware technology in terms of this characterization are then presented. Next a model is presented for sizing the data processing configuration for correcting system errors. The model commences with the tape recorder and interface requirements of the data capturing function through the data processing facility requirements and terminating with film-writer/display and archiving technology requirements. This sizing model is then used to estimate hardware technology requirements and implementation costs. Finally, some examples are presented to illustrate use of the parametric model.

8.3.1 Data Processing Requirements

For data processing modeling purposes, the sensor data types were divided into two classes: 1) data characterized by daily data

volume in units of Mbits, 2) data characterized by data rate in units of Mbit/s. The first class can represent large data rate sensors, which operate a relatively short period of time, as well as lower data rate sensors, which operate for longer periods of time. The second class represents continuously operating sensors as well as sensors whose data are processed in real-time. These two classes are then characterized by their required processing throughput rate in units of $\mu\text{sec}/\text{pixel}$, processing memory requirements in units of Mbits, and data volume for archiving requirements in units of terabits (10^{12} bits). The encoding level of the digital data in units of bits/pixel is parameterized for these considerations.

The processing throughput and yearly volume, as determined by the sensor output daily volume, for the first class is presented in Figure 8-9. The figure and subsequent figures shows annotation is

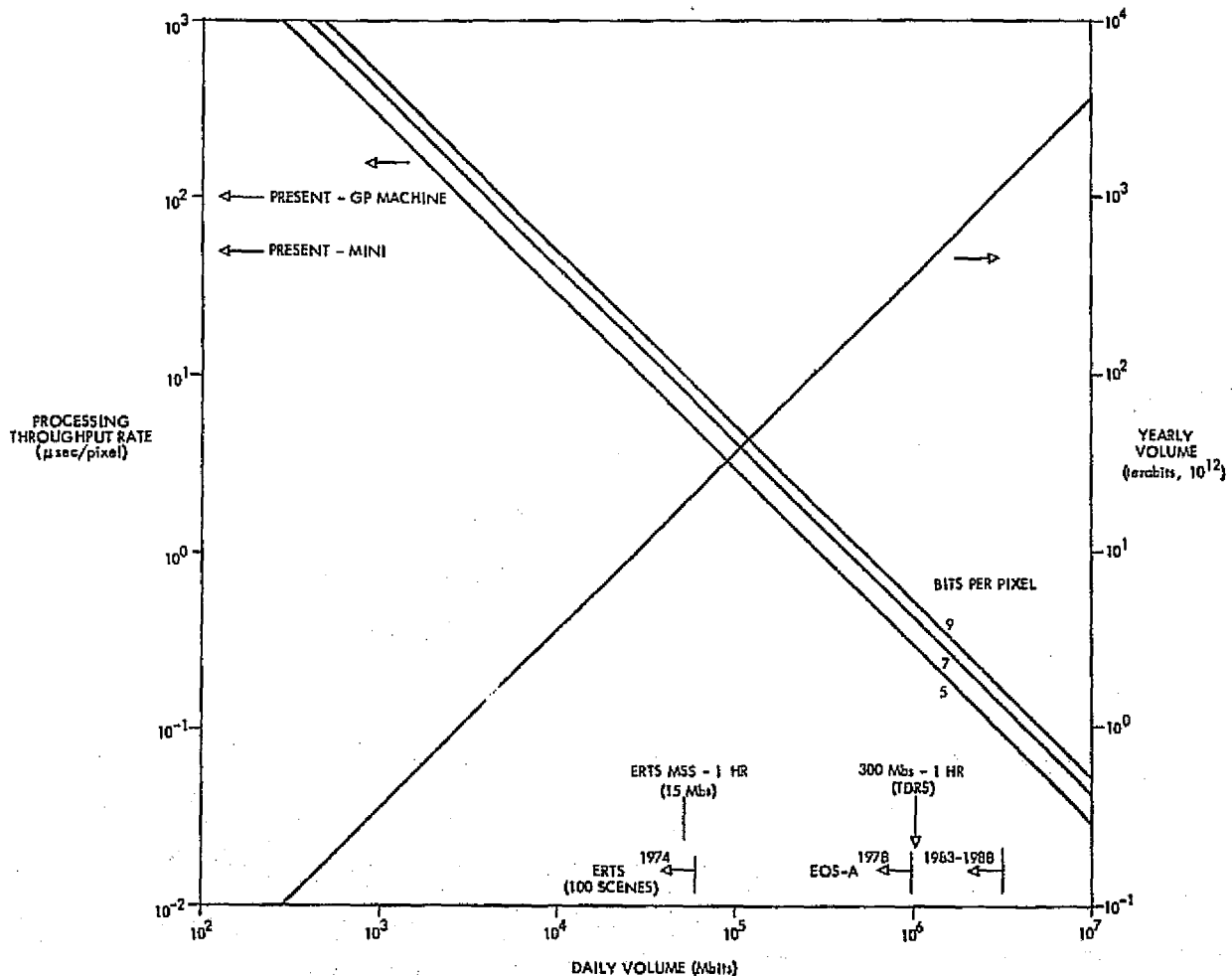


Figure 8-9. Large Data Rate Sensor Characterization

provided to establish benchmarks for performance and yield perspective for the values presented. Note that the throughput and volume data are parameterized with respect to the number of bits/pixel. The processing throughput rate is calculated on the basis of two shifts (16 hours per day) for the processing. Note that no allowance has been made for overhead time; however, overhead can be easily incorporated into the model by suitably adjusting the daily volume or, in the case of the second data class, adjusting the continuous rate.

Figure 8-10 presents the required processing throughput rate for the second class of sensors and the daily and yearly data volume for this class are presented in Figure 8-11.

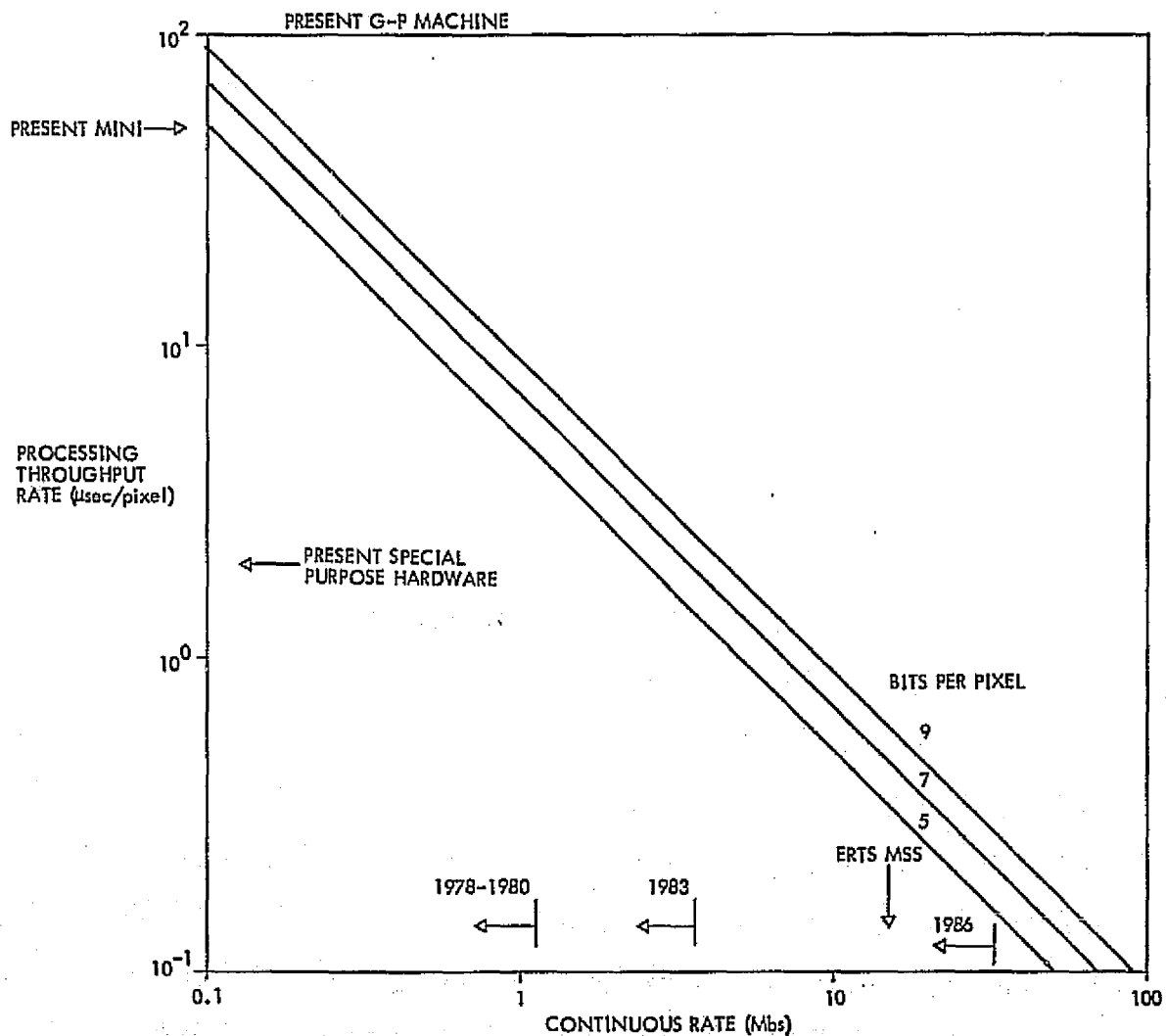


Figure 8-10. Required Throughput for Continuous Sensors

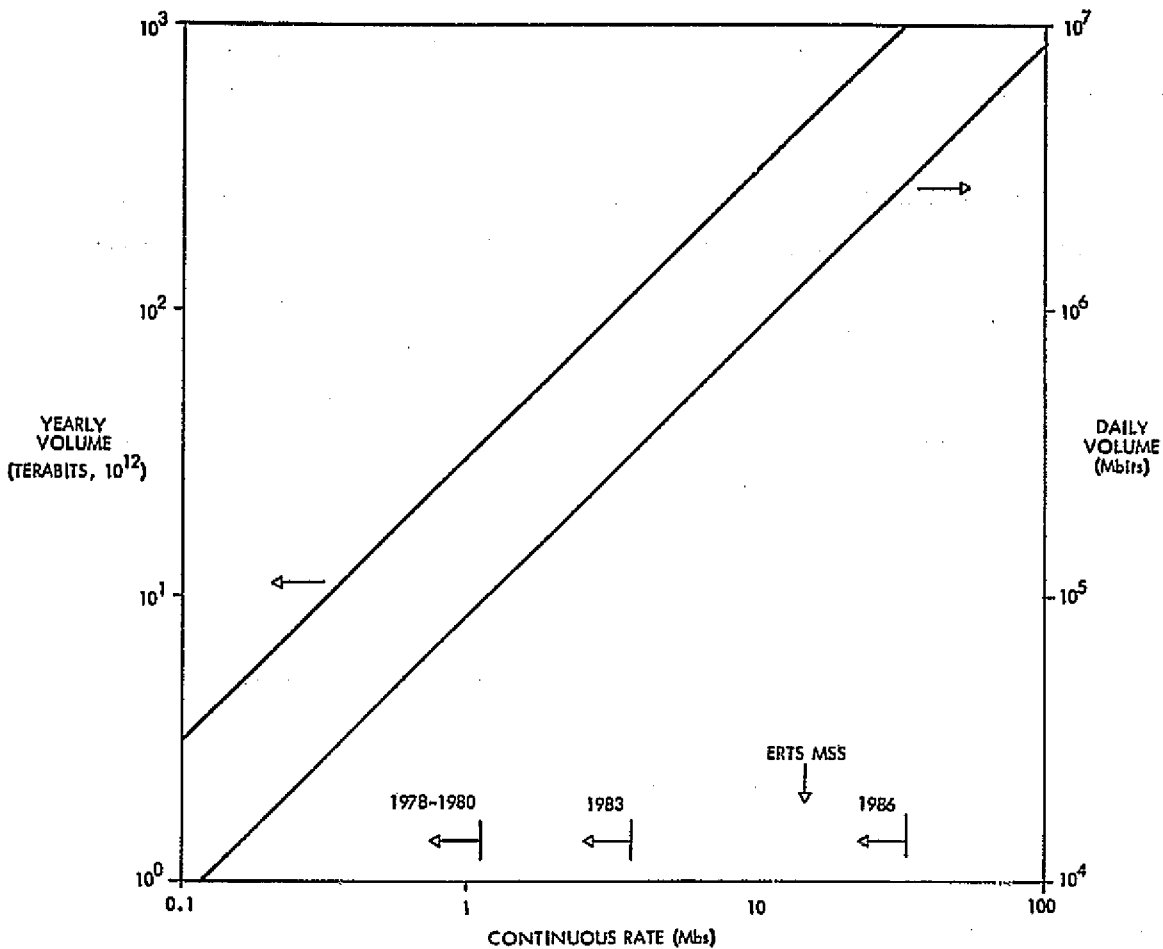


Figure 8-11. Required Volume for Continuous Sensors

Processing memory requirements for the sensor data are modeled in the following manner. For the purposes of input data formatting it is assumed that a full frame worth of data (including all spectral bands) must be stored. To unscramble the data it is assumed that a scan's width of lines must be stored for reformatting. For example, if each sensor scan produced data for 10^2 detectors and the line length was 10^4 pixels, then 10^6 pixels would have to be stored to separate the spectral bands for subsequent processing. This factor also should model any conical to linear scan transformations. Implicit in these considerations is the assumption that data are processed in a band sequential format, certainly a conservative assumption. Finally, detector calibration correction using table look-up, or possible modifications of this approach, will place a requirement on at least a ROM capability. This memory requirement is determined by the number of detectors and encoding

levels. These three generic memory requirements will be referred to as the sensor frame volume, sensor scan volume, and calibration data volume, respectively.

These three sensor related volumes are related to the data processing memory requirements by Figures 8-12, 8-13, and 8-14. Figure 8-12 relates the sensor frame volume in pixels to the input data frame volume in Mbits. The processing data volume memory requirement in Mbits is related to the sensor scan volume in pixels in Figure 8-13. The detector calibration requirement leads to the calibration data volume requirement in Mbits as shown in Figure 8-14. Some additional comment is necessary about the results in Figure 8-14. These requirements are very conservative; it will become more cost-effective for the larger volumes to store piecewise linear models and calculate corrected sensor output pixel values. Nevertheless, this presentation will expose the problem.

As a convenience, the next two figures, 8-15 and 8-16, have been included to relate the sensor output data characterizations to the sensor coverage. Figure 8-15 relates the sensor daily operation time to the daily volume using the sensor data rate as a parameter. Once the daily operation time is known, Figure 8-16 can be used to calculate the coverage area given the spacecraft altitude and sensor swathwidth. Figure 8-16 presents the nadir ground spread of the spacecraft for the range of orbits (other than geostationary) considered for the ERS missions. Conversely, the sensor coverage can be used with the aid of Figures 8-15 and 8-16 to obtain the daily volume and, hence, enter the parametric model.

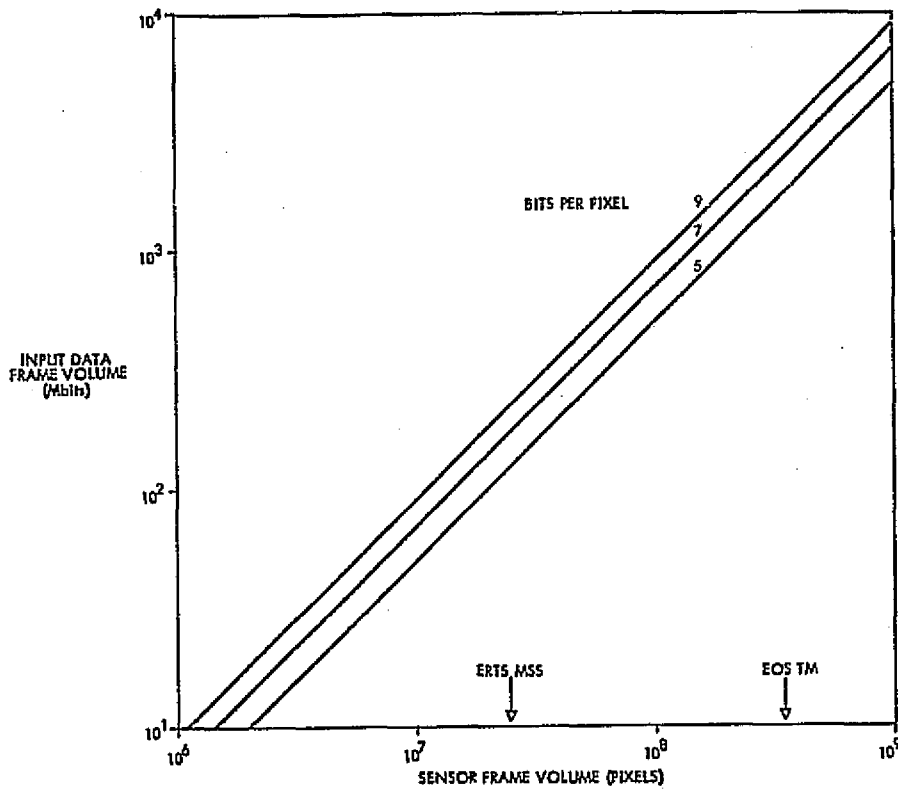


Figure 8-12. Input Data Frame Volume Requirements

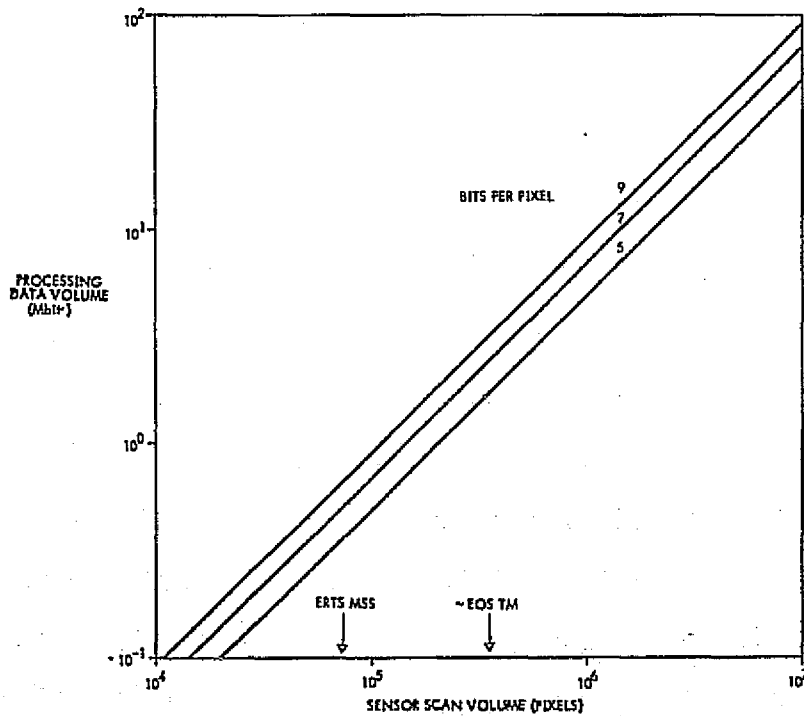


Figure 8-13. Processing Data Volume Requirements

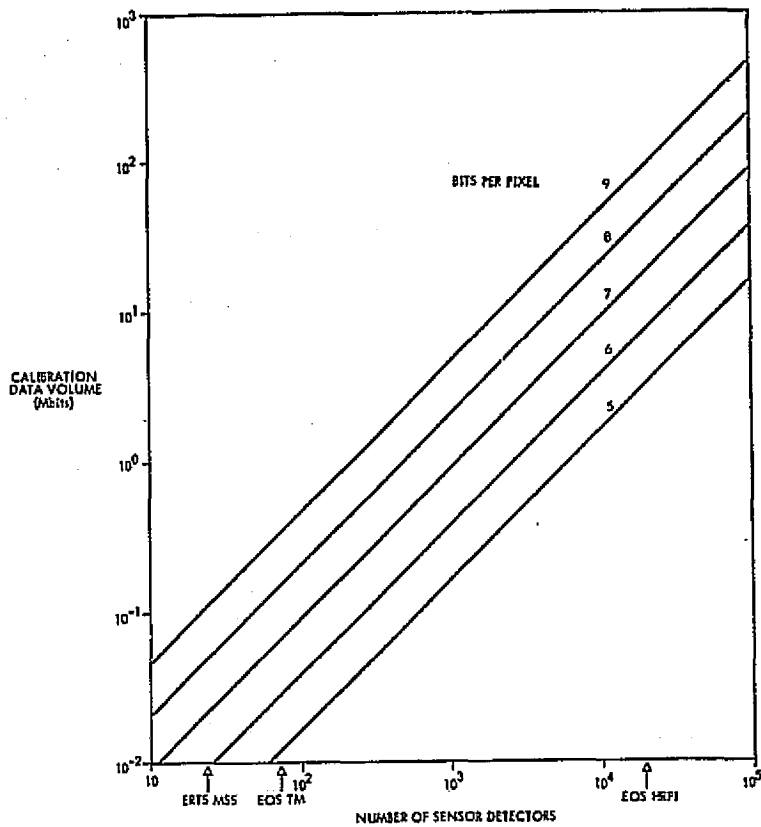


Figure 8-14. Calibration Data Volume Requirements

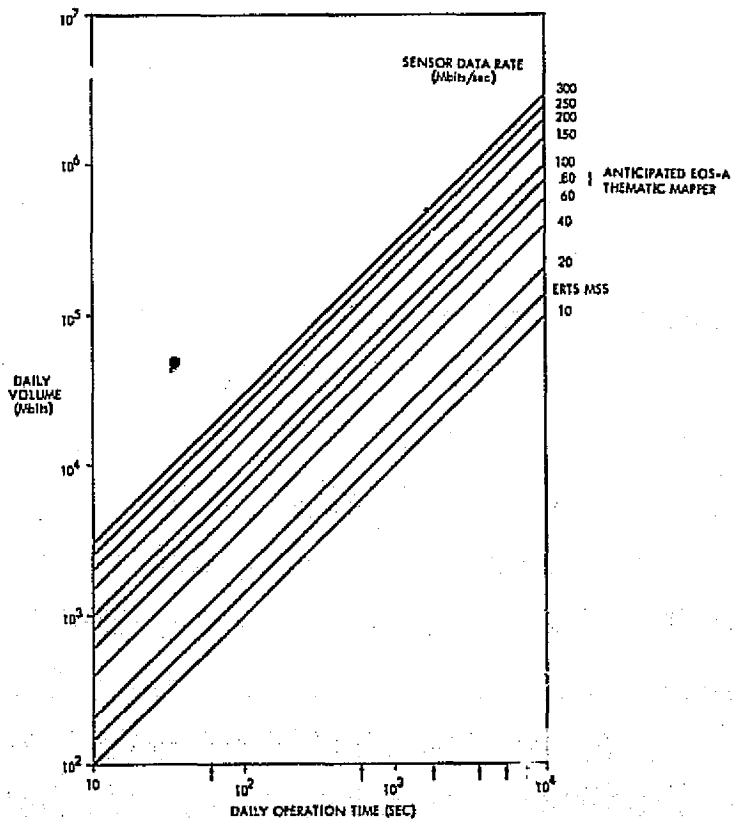


Figure 8-15. Daily Volume as Determined by Sensor Operation

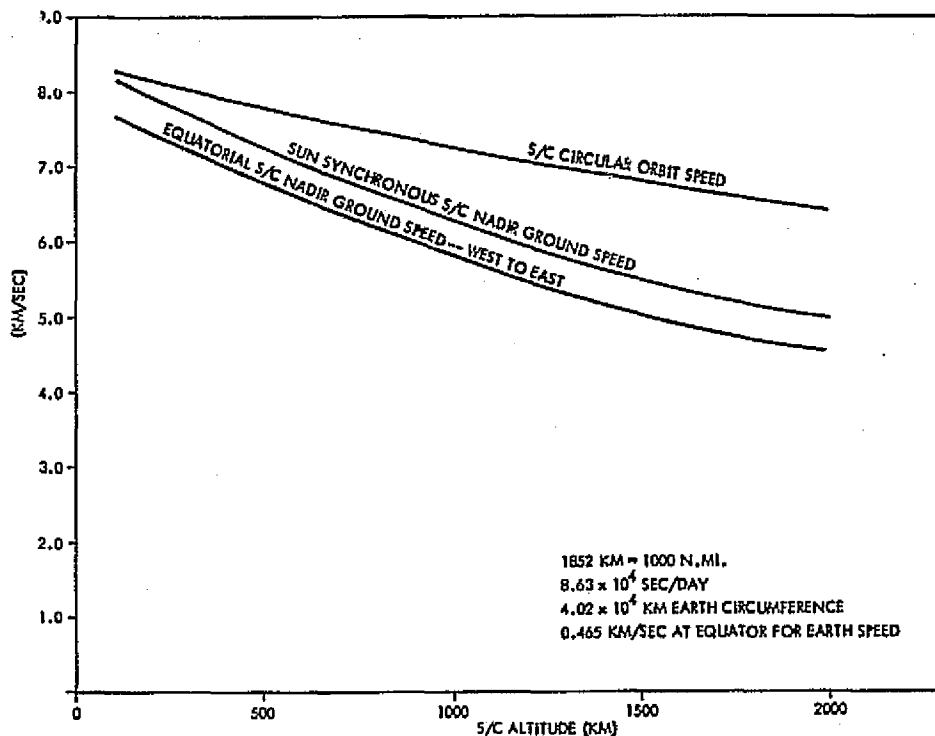


Figure 8-16. Nadir Ground Speed as a Function of Spacecraft Altitude and Orbit

8.3.2 Hardware Technology Area Requirements and Estimated Costs

The hardware technology areas associated with the ERS GDHS are discussed in this section and estimates of implementation cost are presented. It is important to recognize that the estimated costs should be evaluated with a critical eye and be open for further study. While the estimates made are the best possible, they are not necessarily best estimates, especially given the time-frame over which they apply.

It is appropriate to summarize again the assumptions used. Basically, the approach is to use existing technology to construct a model for the ERS GDHS data preprocessing requirements. Estimates are then made for the future performance of the technological areas used in the ERS GDHS and predictions are made for the costs of implementation. The following data processing functions are investigated with respect to their hardware implementation: the ground station tape recorder and interface for the data capturing function, the data processing facility using the sizing architecture presented in Figure 8-5 for the system error correction function, and the archiving and filmwriter/display technologies relevant to the output distribution modes used in the information extraction function.

Figure 8-17 presents the estimated range of cost for the ground station tape recorder and interface as a function of input rate. Figure 8-17 and those following show that annotation is included on the figure to provide perspective and enhance the presentation. Also, the dashed lines represent "weak" estimates and the solid lines represent "strong" estimates. There appears to be a gap between the 10 and 100 Mbit/s recorder technology. However, 100 Mbit/s multitrack technology exists and is shown by cost estimates. A significant aspect of the recorder problem is the reproduce serial bit rate slow-down on playback necessary to process the data. Figure 8-18 presents this requirement as a function of daily volume. It appears that development is proceeding in this area.

The data processing facility hardware requirements are evaluated in the context of the sizing architecture presented in Figure 8-5. The following parts are incorporated into the concept of a minicomputer system for implementation and cost requirements: CPU, computer bus, system I/O, and auxiliary memory. The input and output memories, data correction memory, processing memory, and the special-purpose hardware components will be discussed separately as well as the general-purpose computer system.

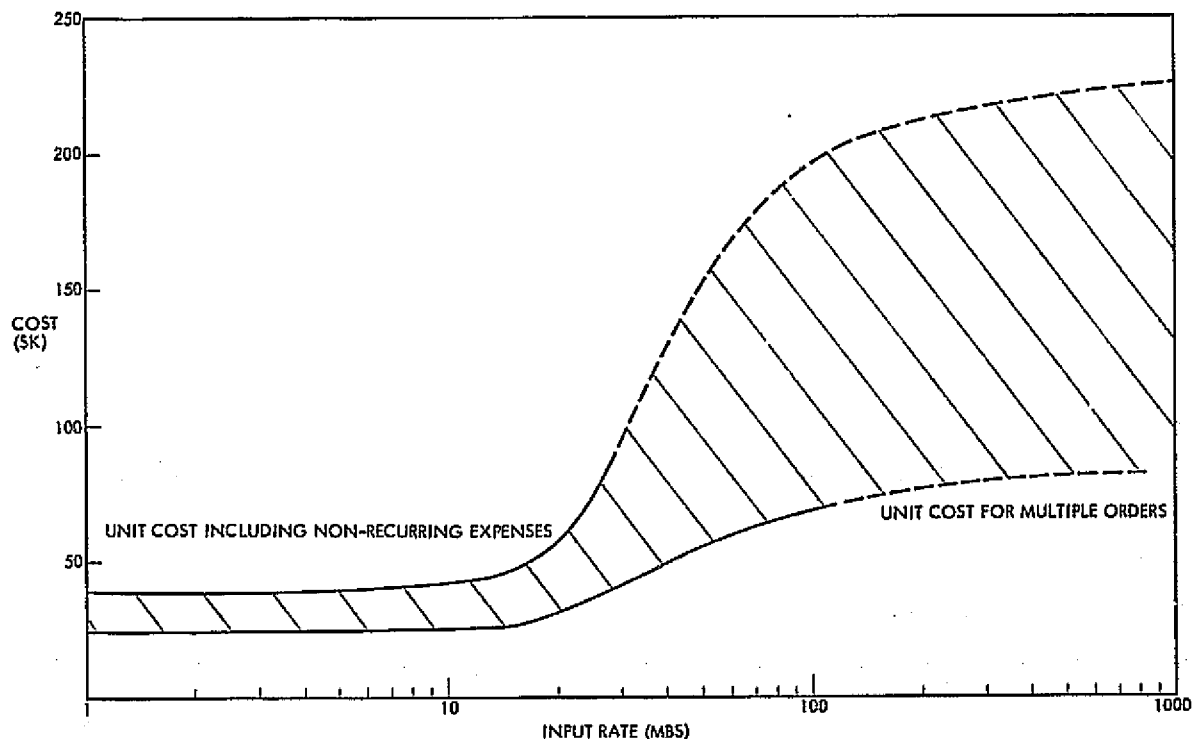


Figure 8-17. Estimated Range of Cost for Ground Station Tape Recorder and Interface

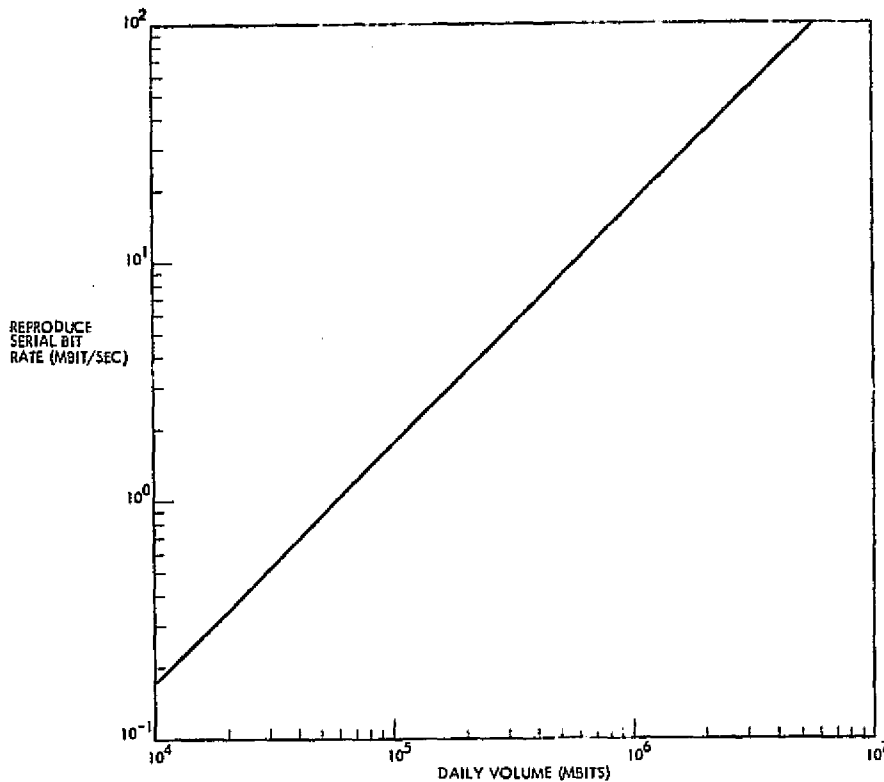


Figure 8-18. Input Data Tape Recorder Requirements - Two Shifts

Figure 8-19 presents the CPU/data bus processing rate requirements for the minicomputer system as a function of throughput rate. Indicated along the ordinate are the ranges of processing rates at present and those estimated for 1980 and 1980; these estimates are based upon speed predictions given for LSI technology, technology used in fabricating minicomputer components. The estimated range of cost for the minicomputer system is 50 to 100 thousand dollars.

The input and output data memory requirements are demanding on both volume and transfer rate. To satisfy the throughput requirements, it probably will be necessary to double buffer both the input and output. The estimated range of cost values presented in Figure 8-20, includes the double buffering requirement; the costs shown are also sum of both input and output memory costs.

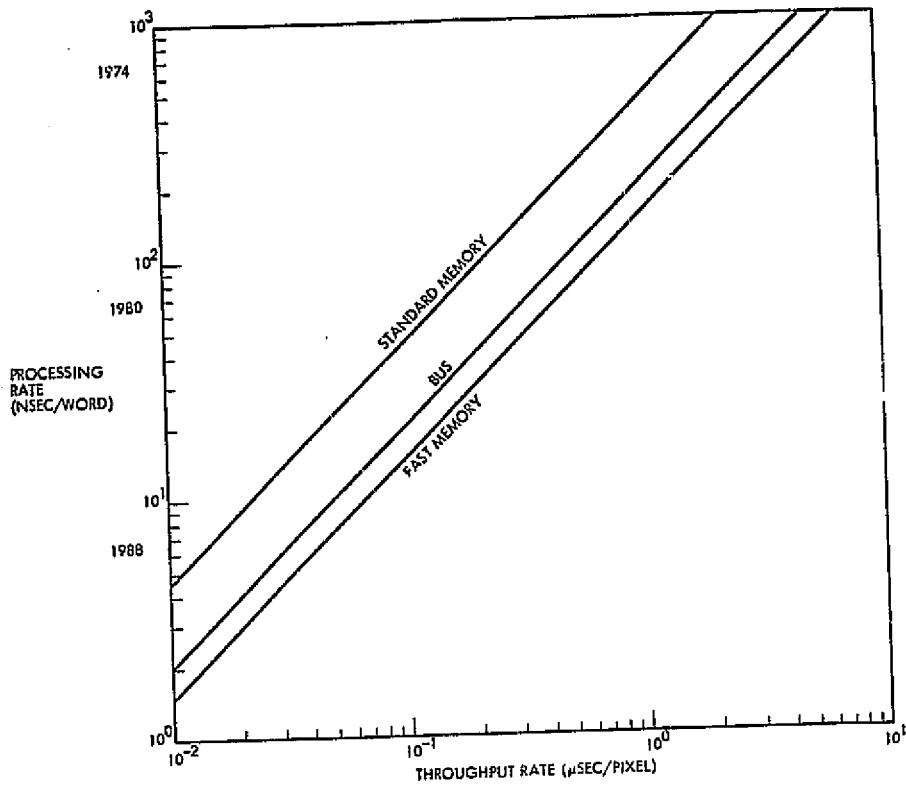


Figure 8-19. CPU/Data Bus Processing Rate Requirements

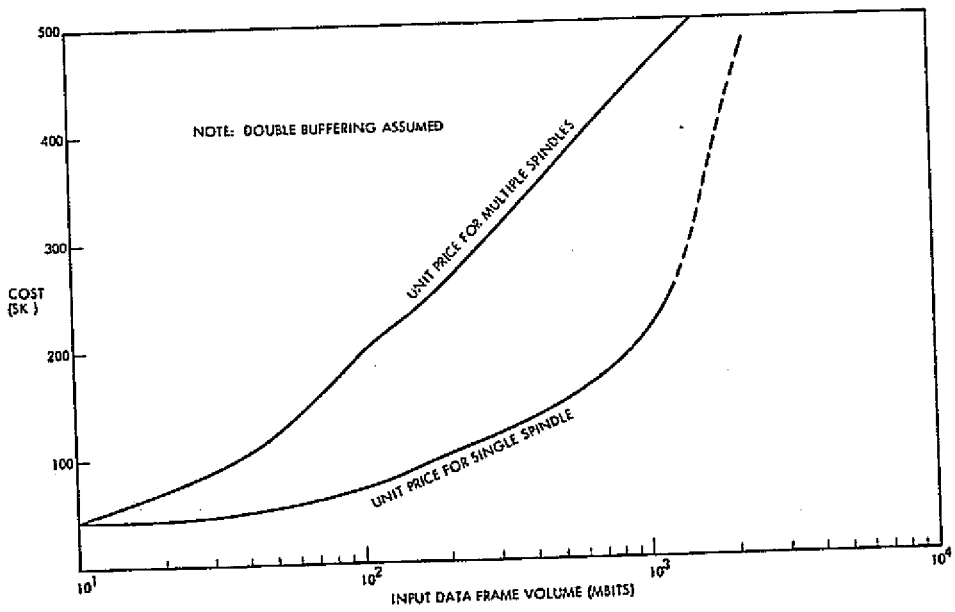


Figure 8-20. Estimated Range of Cost for Input/Output Data Reformatting Memories

The estimated range of costs for the other two memories associated with the main processing structure are presented in Figure 8-21. As noted, one Mbit should be added to the calibration data volume requirement to size the RCP and estimation data storage. This range is more optimistic than the other costs as it is felt that LSI technology is moving rapidly in this area towards reducing costs.

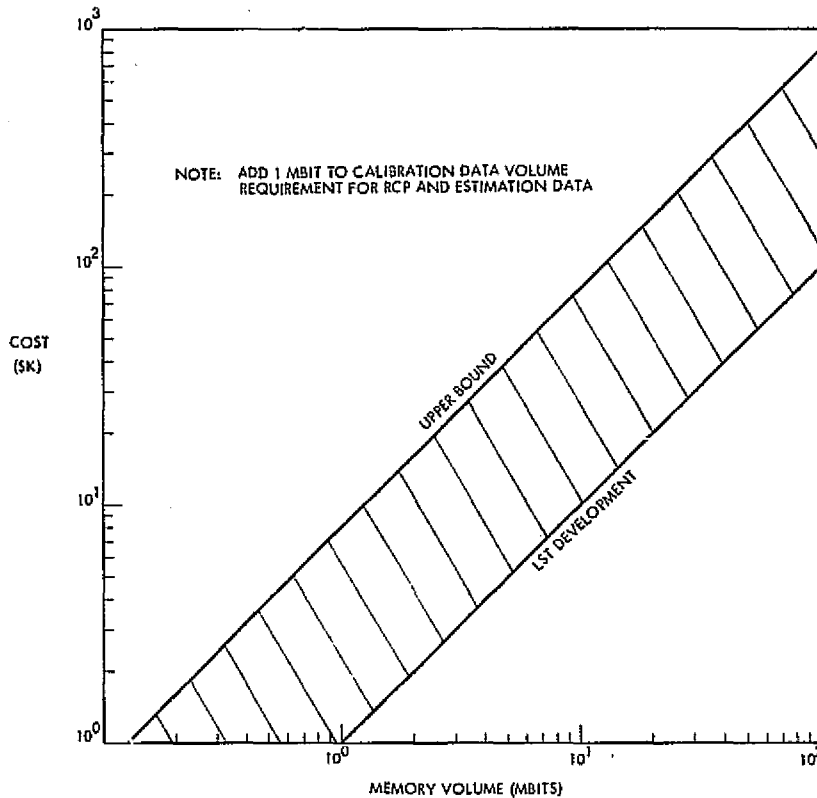


Figure 8-21. Estimated Range of Cost for Data Correction and Processing Data Memories

The processing rate requirements sized to the throughput rate are presented in Figure 8-22. This graphical relationship is based upon TRW's experience and an extrapolation of that experience. Also shown are typical ranges for time periods. The estimated range of costs for special-purpose hardware is presented in Figure 8-23; the upper values are determined by the development costs. The basic concept is that the special-purpose hardware is used to implement a particular processing algorithm. A number of units may be necessary for a data processing scheme and they could be pipelined. The type of functions performed are listed in Figure 8-5.

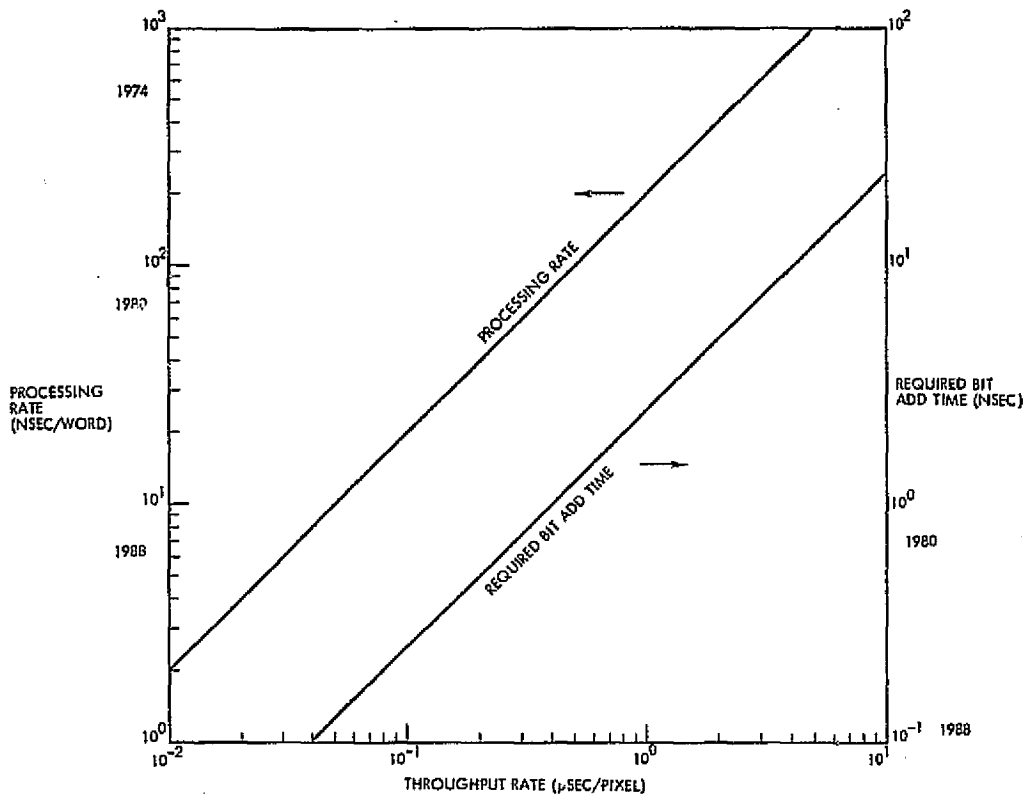


Figure 8-22. Special Purpose Hardware Processing Rate Requirements

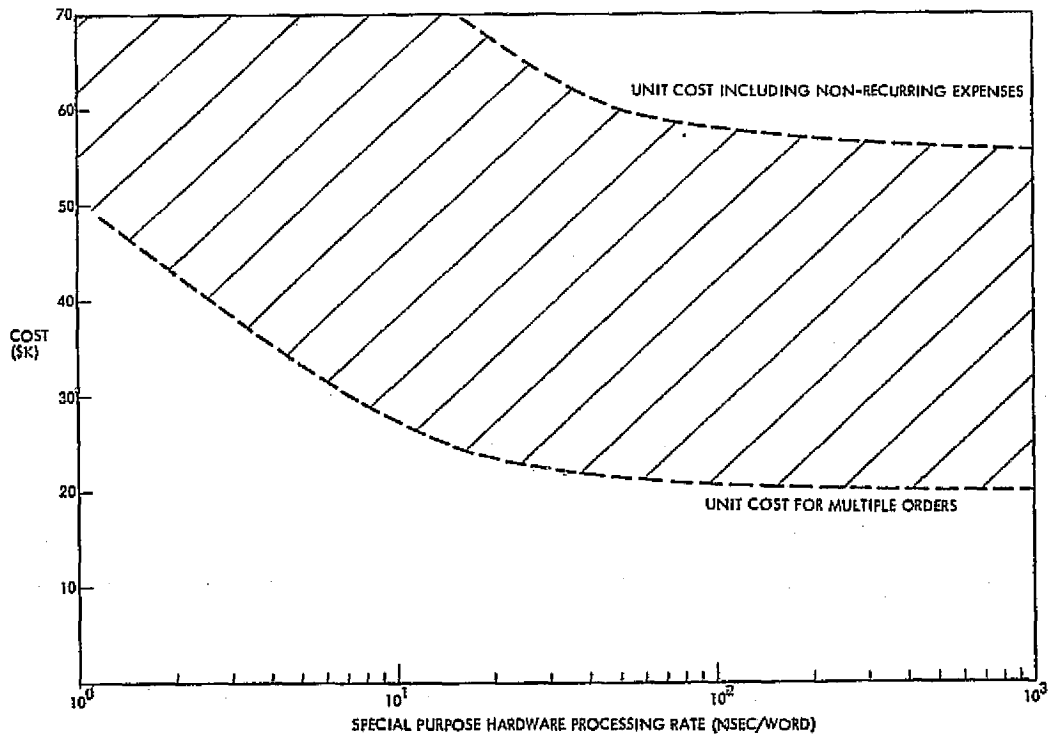


Figure 8-23. Estimated Range of Cost for Special Purpose Hardware

The last item considered for the data processing facility is the general-purpose computer. This computer will handle the scheduling, control, and I/O processing. It is envisioned to be a medium-to-large scale computer in the 500 thousand to one million dollar range. Technology to perform the anticipated functions exist today, but the systems integration function must be carefully planned.

The two technologies in the information extraction function will now be considered. Figure 8-24 presents the estimated range of cost for filmwriter technology. There is quite a range because of the availability of very high-precision LBR and RBR recorders. However, there is much activity centered around reducing the cost of this technology and, hence, the lower bound on the range.

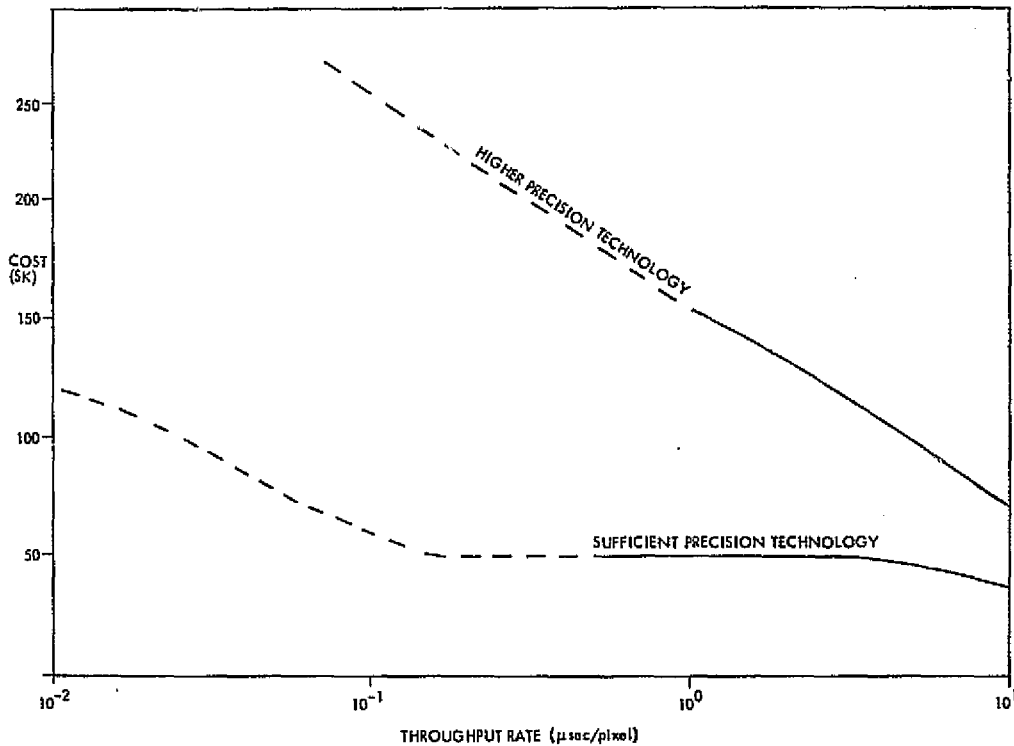


Figure 8-24. Estimated Range of Cost for Filmwriter Technology

Figure 8-25 presents an estimated range of cost of capital expense for archiving. The lower bound is essentially the high-density digital tape recorder approach and the upper bound is the mass memory systems being developed. Unfortunately, there is some uncertainty as to the estimated cost at volumes around 10⁶ Mbit and above — definitely an area for

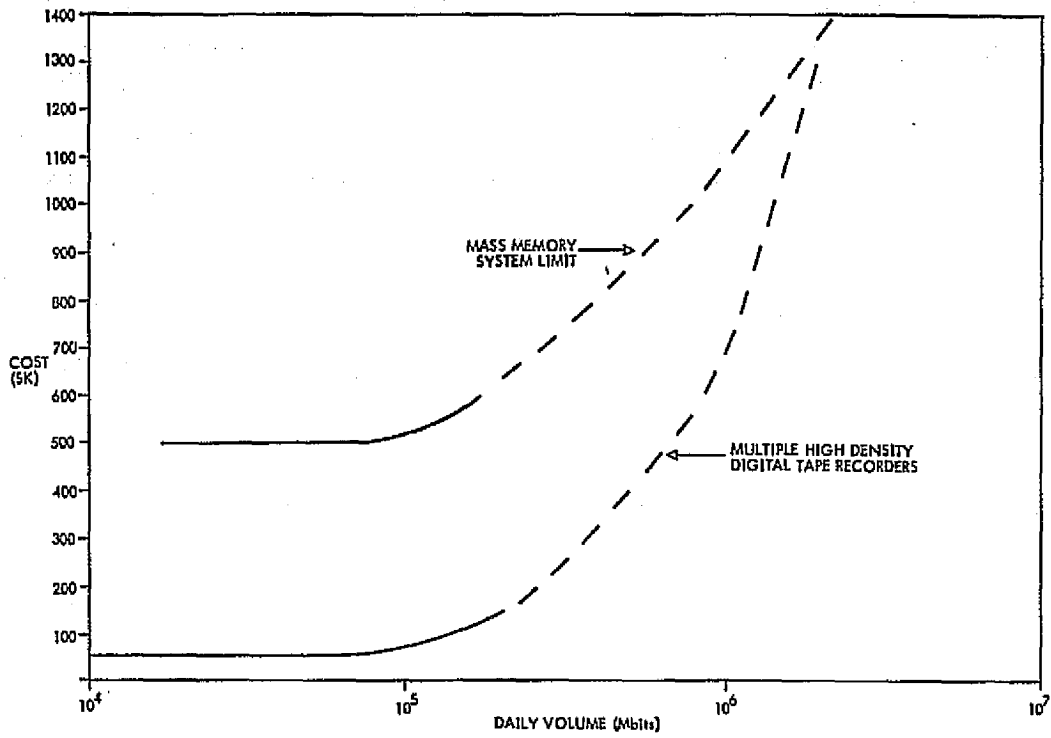


Figure 8-25. Estimated Archiving Capital Expense further study. The required archiving read data rates are presented in Figure 8-26. This figure is included to stress the throughput requirements.

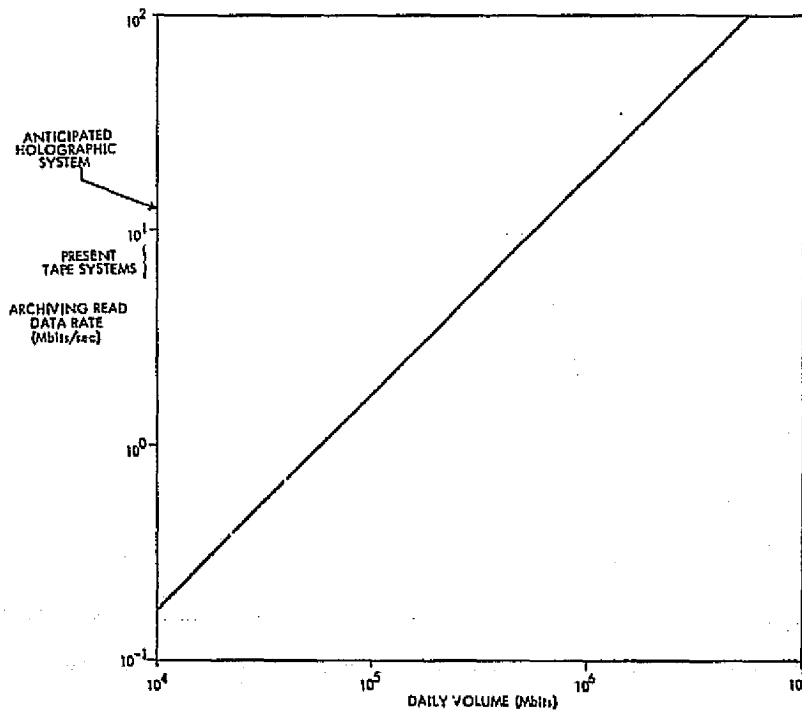


Figure 8-26. Archiving Read Data Rate Replacement - Two Shifts

Finally, the filmwriter/display and interface requirements for the continuous rate -- real-time configuration is anticipated to be satisfied by extensions of existing technology. The price range for this hardware implementation is estimated to range between 50 and 100 thousand dollars. Table 8-2 summarizes this fact and the computer cost estimates.

Table 8-2. Summary of Computer and Filmwriter/Display Estimated Costs

Minicomputer system	50 - 100 thousand dollars
General purpose computer	0.5 - 1.0 million dollars
Filmwriter/displayed interface	50 - 100 thousand dollars

8.3.3 Applications of the Parametric Model

This section presents eight steps that can be followed and an example to illustrate their use for the parametric model. They are:

- 1) Obtain Data Processing Requirements. With the aid of Figures 8-15 and 8-16, determine the throughput rate, daily volume, and memory requirements using Figures 8-9 and 8-14 for each sensor used in the spacecraft payload
- 2) Determine Ground Station Tape Recorder Requirements. Using Figures 8-17 and 8-18, the tape recorder requirements for non real-time processing can be determined. A decision must be made to ascertain whether single or multiple recorders (sensor dependent, perhaps) are to be used. The higher estimates of cost for the multiple case should be used to compensate for the multiplex requirements.
- 3) Determine the Degree of Major Parallelism in the Data Processing Facilities. The degree of major parallelism in the data processing facility for the main processing structure and for the input/output data memory requirements are determined by the use of Figures 8-19 and 8-20. For purposes of sizing the requirements, the higher cost estimates should be used to compensate for the system integration costs. The procedure is described below.
 - Determine the Main Processing Structure Requirements. Figure 8-19 is used to determine the number of main processing structures needed. If the total throughput cannot be processed, then parallel structures must be incorporated. A main processing structure can be used for one sensor's output or part of one sensor's output depending on the throughput required. Note that this approach can duplicate some common processing, e.g., distortion estimation, so they will be on the conservative side.

- Determine Input/ Output Requirements. The use of Figure 8-20 will indicate the degree of difficulty in meeting the frame volume requirements. If the volume requirements are too large, then parallel structure will have to be used; the degree of parallelism is based upon a single or partial sensor output.
- 4) Determine Special Purpose Hardware Requirements. Figure 8-22 and 8-23 are used to determine the special-purpose hardware requirements. Candidates for special-purpose hardware implementation are any definable data processing algorithm. Figure 8-22 determines the degree of parallelism necessary; as stated before, use the larger estimates for parallel structures to compensate for the system integration costs.
 - 5) Determine Data Correction and Processing Data Memory Requirements. Use Figure 8-21 to estimate the memory requirements; do not forget to include the basic memory volume in the estimate for the data correction memory.
 - 6) Determine Film Writer and Archiving Requirements. Use Figures 8-24 and 8-25 to estimate the cost and requirements of the film writer and archiving technologies. Figure 8-25 should be used to determine the degree of parallelism necessary for the archiving technology.
 - 7) Considerations of Continuous or Real-Time Sensor Data Processing and LUDPF Requirements. If the processing is to be analog only (see Figure 8-4), use Step 1 above and the lower valued estimates in Figure 8-24 to determine hardware technology requirements. If digital processing is used, skip Step 2, tape recorder considerations. The sensor input characteristics for the LUDPF determine the data processing requirements; just follow the same steps as before.
 - 8) Determine Estimated Hardware Cost. Taking into account all the parallelisms, add up the estimated hardware costs. For the CDPF, add the costs of the minicomputer systems and general-purpose computer; for the LUDPF with digital processing, use only the high estimates for the minicomputer system.

CAUTION: Be sure all assumptions are understood when interpreting the estimated hardware costs.

It is appropriate to present an example of use of the parametric model to illustrate the application of the eight steps. To enhance the illustration, a hypothetical example is chosen. Two sensors are assumed to be used within a year from now; 1) a large data volume sensor consisting of 8 spectral bands of data using 20 detectors for each band (a total of 160 detectors to be calibrated), 7-bit encoding, a line length of

4000 pixels with a 4000 by 4000 pixel frame size, and a daily volume of 5×10^5 Mbits at an sensor rate of 80 Mbits, and a continuous rate sensor with a data rate of 1 Mbit/s, 10 spectral bands with 4 detectors each band with 5-bit encoding, and a frame size of 1000 x 1000 pixels.

Starting at Step 1, the large data volume sensor has a throughput rate of $\sim 0.9 \mu\text{sec}/\text{pixel}$ and the continuous sensor is $5 \mu\text{sec}/\text{pixel}$. The daily volumes are 5×10^5 and $\sim 9 \times 10^4$ Mbit/s, the sensor frame volumes are 1.28×10^8 and 1.0×10^7 pixels yielding 900 and 50 Mbits, respectively, for the input data frame volumes. The sensor scan volumes are 6.4×10^5 and 4.0×10^4 pixels yielding 4.5 and 0.2 Mbit/s, respectively for the processing data volumes. The calibration data volumes are, respectively, ~ 0.15 and less than 0.01 Mbit/s.

For the large data volume sensor, Step 2 is used to obtain an estimate of \$70K for each ground station recorder, assuming multiple unit purchases; the playback rate is ~ 9 Mbit/s. Step 3 shows there should not be a problem with implementing the minicomputer system for the continuous rate sensor ($15 \mu\text{sec}/\text{pixel}$). however, for the large data volume sensor ($0.9 \mu\text{sec}/\text{pixel}$), two main processing structures will have to be used. The input data frame volume for the larger data rate sensor is near the border for the estimated input/output memory costs, therefore, a conservative estimate of \$220K is used. An estimate of \$70K is used for the continuous rate sensor for the same costs.

Step 4 is addressed for the special-purpose hardware requirements. The continuous rate sensor is well within the capabilities of present technology; nevertheless, assume two pieces will be used to implement the distortion estimation and geometric correction algorithm for a total estimated cost of \$60K. Two main processing structures are already assumed for the large data volume sensor; this implies only $1.8 \mu\text{sec}/\text{pixel}$ are needed, which is in the neighborhood of present technology. The same two algorithms are assumed implemented in special-purpose hardware for this sensor yielding an estimate of \$120K (two each).

The data correction memory costs for each are estimated to be \$10K, adding the 1 Mbit to the calibration data volumes. The processing memory costs are estimated to be 30 and \$10K respectively, taking the upper limit because of the present time assumption. This completes Step 5.

Step 6 is followed next. The lower estimates are used for the filmwriter costs because it is assumed two are used, one for each, yielding a total cost of \$100K. The archiving requirements are estimated for the combination of both sensors yielding a conservative estimate for the $\sim 5.9 \times 10^5$ Mbit/s of \$700K. Step 7 has implicitly been followed and, hence, Step 8 completes the example. The total estimated hardware costs using the lower estimates for the minicomputer system and the general purpose computer comes to \$2.05M. Table 8-3 summarizes the costs.

Table 8-3. Example of Use of Parametric Model for Estimated Hardware Costs

	Large Data Volume (\$K)	Continuous Rate (\$K)
Ground station tape recorder*	70	0
Input/Output memory	220	70
Special-purpose hardware	120	60
Data correction memory	10	10
Processing memory	30	10
Minicomputer systems	<u>100</u>	<u>50</u>
Subtotal	550	200
	Additional Estimated Hardware Costs (\$K)	
General-purpose computer		500
Filmwriter		100
Archiving		<u>700</u>
Subtotal		1300
Total Estimated Hardware Cost	$\$2.05 \times 10^6$	
*Cost for only one unit		

Care must be taken in interpreting this estimate. It does not include, for example, the programming effort, facilities, manpower and maintenance costs, nor the RF portion of the data capturing function. Nevertheless, it does indicate the relative proportions of the different

hardware costs to implement the data processing for system error correction. But it is not the total estimated cost for the ERS GDHS data handling.

This example indicates the flexibility intrinsic to the parametric model. It also illustrates engineering judgment must be exercised for application of predicting costs. It is fair to state that this parametric model is a beginning, and future work must be performed to extend and refine its substance.

8.4 Conclusions of this Study of ERS GDHS Data Handling Considerations

The most important contribution of this study is the definition of a structure for the ERS GDHS data handling considerations and development of a parametric model for its data processing requirements. While readily admitting limitations in this parametric model, it represents a beginning for the development of a strong, quantitative understanding of future ERS ground data processing requirements.

Some preliminary conclusions can be stated on the basis of this study with respect to the ERS GDHS. They are:

- Proceeding from the ERTS to the EOS data processing requirements is more significant than consideration of the post-EOS requirements; therefore, solving the technical problems associated with EOS-A essentially will establish the feasibility of meeting future ERS GDHS requirements.
- The state of each of the eight dominant technology areas specified should be determined in sufficient depth to confidently predict future developments.
- Data format is a significant consideration: where common data formats are formed (on-board, ground station, CDPF or LUDPF), the word length/encoding level, and archiving formats to be used are just some of the issues involved.
- Archiving technology at the higher data volumes needs more detailed effort to determine the most cost-effective technology.
- Output data quality specifications need more study. Cognizance must be taken of the fact that present systems are research-oriented; therefore, operational systems may have less demanding requirements. Hence, data quality requirements necessary for the user community needs should be used in future specifications. Also, quality control and assurance will become increasingly important in the future.

- There is a definite tradeoff between single and multiple unit ground station tape recorders.
- Operating costs generally exceed capital expenses; therefore, it is essential that the management aspects of the ERS GDHS be thoroughly examined.
- Low-cost filmwriter/display units for real-time processing and high data rate facsimile applications of ERS data have been established as a future need; more detailed study of this particular area of technology is necessary.

9. POTENTIAL DATA MANAGEMENT SYSTEMS

9.1 Introduction

The objectives of this task were twofold: first, to use the parametric data generated in Tasks 4 through 8 to synthesize optimum ERS data management systems and second, to generate a list of technological advances needed to make each approach feasible.

The study plan proposed carrying out the synthesis of three of the missions identified in Task 3. Selection of the three missions was coordinated and approved by NASA prior to the start of Task 9. The criteria use in selecting these three missions are listed below:

- 1) Launch date; coverage of the time span of interest to the study (1978-1988) was desirable.
- 2) Orbit type; non-geostationary orbit types were of primary interest.
- 3) Both research and operational mission types should be represented.
- 4) A variety of mission disciplines should be included.
- 5) Medium and high bit rates and data perishability should be covered.

Based on these criteria, the following three missions were selected for the Task 9 effort:

- Mission 2, a 1980 launch in a sun-synchronous orbit for ocean and meteorological research.
- Mission 6, a 1984 sun-synchronous launch with an operational mission in terrestrial survey/environmental quality.
- Mission 9, an equatorial orbit launch in 1987 with meteorological research as the principal function .

The reader is cautioned not to interpret these missions as representing approved NASA missions. They were structured with a minimum of coordination with NASA planning groups and their performance parameters were specifically chosen to maximize the demand for technology development.

Carrying out the mission synthesis proved to be more difficult than we had originally anticipated. We underestimated the amount of iteration that would be required between mission synthesis and development of the data base. Thus our original plan of directly applying the data base to derive the desired systems was modified to allow for considerable judgment as synthesis progressed.

Specifically, we discovered that the interrelationships between sensor design, frequency of coverage and data readout led to orbit choices different than those postulated in Sections 2, 3, and 4 and these in turn impacted sensor design and data handling approach.

In addition, it was necessary to use judgment to balance the relative importance of performance and cost. In research missions we typically deemed validating a conjecture very important while perishability and completeness of coverage were of secondary importance compared to cost. Operational missions, however, received an inverse emphasis. In Mission 6 (an operational mission), for example we proposed a constellation of three satellites to ensure that needs for relatively frequent coverage at high resolution were met. The data taking among these three has been staggered so that a degree of redundancy occurs. Should one satellite fail, full data collection still continues but at a reduced coverage frequency. This reflects our view that in an operational system it is mandatory to provide a high probability of data continuity.

9.2 Mission 2

9.2.1 Mission Requirements

Mission 2 is a research and development mission which addresses the user needs for synoptic oceanographic and meteorological data. It is the first in a series of three missions: two R&D precursors plus an operational mission. The research and development nature of this mission applies to both the use of a space platform for the development of sensors and the means for conducting oceanographic and meteorological studies.

The launch data for Mission 2 is FY 1980. It will have the following sensor complement:

- Pointable imager

- Oceanic scanning spectrophotometer
- Sea surface temperature imaging radiometer
- Advanced atmospheric sounder
- Data collection and location system.

The instruments are described in Table 9-1. The selection of swath width, IFOV, pointing capability and resolution are computed as part of the mission design (see Sections 9.2.2 and 9.2.3).

The mission must be optimized for routine surveillance of dynamic coastal oceanic and meteorological phenomena in the vicinity of CONUS and territories. It should provide enough coverage of phenomena of interest for potential users to converge on data handling techniques which are optimal for their specific individual program objectives. Therefore, near-raw data (i. e., data corrected for geometric and photometric/radiometric errors) should be disseminated to the users at a rate which matches their perishability requirements.

Table 9-2 summarizes the data requirements, in terms of observation frequency, perishability and data format requirements, for each data use and indicates which instruments are used to gather the data. Three data use categories are not addressed by the mission sensor complement: earth radiation budget, snow/ice survey and soil moisture.

9.2.2 Orbit/Satellite - Constellation Design

Mission 2 is characterized by relatively low data rates, rapid perishability of data and its relatively early initiation so that largely existing technology must be employed. Because the mission is for research purposes, only one satellite can be justified. Reviewing the mission requirements reveals that three of the seven instruments can employ very wide swaths and require daily to twice daily coverage, that a third instrument (the PI) has a narrow swath width but must be able to point selectively at any spot once daily and that the fourth instrument (the OSS) must make observations in a much narrower swath every three to five days.

These requirements suggest an orbit Q whose fractional part is $1/4$. To minimize obliquity and ease data communication, a fairly small (12)

Table 9-1. Sensor Complement for Mission 2

INSTRUMENT	DISCIPLINE	APPLICATION	TYPE OF SCAN	SPECTRUM/BANDWIDTH (MICRONS)	ERROR SOURCES	UNIQUE DATA PROCESSING REQUIREMENTS
POINTABLE IMAGER	EARTH RESOURCES	GEOLOGY, AGRONOMY, FORESTRY, COASTAL	PUSH BROOM SOLID STATE ARRAY	0.5 TO 0.6 0.6 TO 0.7 0.7 TO 0.8 0.8 TO 1.1 1.35 TO 1.75	<p>GEOMETRIC:</p> <ul style="list-style-type: none"> SPACECRAFT ATTITUDE AND EPHEMERIS ERRORS LOCAL SURFACE ALTITUDE VARIATIONS <p>RADIOMETRIC:</p> <ul style="list-style-type: none"> CALIBRATION DARK CURRENT NONUNIFORMITY IN DETECTOR RESPONSE ATMOSPHERIC EFFECT 	<p>RADIOMETRIC CORRECTION FOR DARK CURRENT AND NONUNIFORMITY OF DETECTOR RESPONSIVITIES</p> <p>CORRECTION FOR EFFECTS OF EARTH ROTATION</p>
SYNTHETIC APERTURE RADAR	EARTH RESOURCES	GEOLOGICAL SURVEY, LAND USE MONITORING, WATER, ICE MONITORING	ALONG TRACK - SPACECRAFT MOTION ACROSS TRACK-RANGE DISCRIMINATION	X-BAND/15MHz, DUAL POLARIZATION L-BAND/15MHz, DUAL POLARIZATION	<p>GEOMETRIC:</p> <ul style="list-style-type: none"> SPACECRAFT ATTITUDE EARTH ROTATION EFFECTS SLANT RANGE DISTORTION 	<p>AZIMUTH DATA PROCESSING REQUIRED TO ACHIEVE AZIMUTH RESOLUTION.</p> <p>COMPENSATION FOR EARTH ROTATION AND GEOMETRIC EFFECTS</p>
ADVANCED ATMOSPHERIC SOUNDER	METEOROLOGY	TEMPERATURE PROFILES FOR NUMERICAL MODELS AND LOCAL AREA FORECASTS OF POLLUTION TURBULENCE, FOG ETC.	+40°, CROSS TRACK, SAMPLES 400 KM APART	8 CHANNELS - 15 BAND 4 CHANNELS - 4.3 1 CHANNEL - 9.6 1 CHANNEL - 11.1 2 CHANNELS - 3.8 3 CHANNELS - 18 TO 30 2 CHANNELS - MICRO-WAVE	<p>RADIOMETRIC:</p> <ul style="list-style-type: none"> CALIBRATION DETECTORS, NOISE EQUIVALENT POWER ATMOSPHERIC ABSORPTION COEFFICIENCES 	
HIGH RESOLUTION MULTISPECTRAL POINT SCANNER	EARTH RESOURCES	TERRESTRIAL THEMATIC MAPPING (GEOLOGY, HYDROLOGY, AGRONOMY, FORESTRY, ETC.)	BIDIRECTIONAL BUDGET BAND SCANNING USING OSCILLATING MIRROR DUTY CYCLE POINT 8	9 CHANNELS: 6 IN VISIBLE 0.43 TO 0.8	<p>GEOMETRIC:</p> <ul style="list-style-type: none"> SCAN VARIATIONS SPACECRAFT ATTITUDE AND EPHEMERIS ERRORS LOCAL SURFACE ALTITUDE VARIATIONS <p>RADIOMETRIC:</p> <ul style="list-style-type: none"> CALIBRATION ATMOSPHERIC EFFECTS 	<p>ACCOUNT FOR 14 SCAN LINES/MIRROR SCAN. ALTERNATE SCAN DIRECTIONS. VARYING SCAN LENGTHS EFFECTS OF EARTH ROTATION.</p>

Table 9-2. Summary of the Data Requirements and Applicable Instruments for Each Data Use in Mission 2

DATA USE	INSTRUMENTS				DATA REQUIREMENTS SUMMARY								
	POINTABLE IMAGER	OCEAN SCANNING SPECTROPHOTOMETER	SEA SURFACE TEMPERATURE IMAGING RADIOMETER	ADVANCED ATMOSPHERIC SOUNDER	OBSERVATION FREQUENCY (DAYS BETWEEN)	DATA PERISHABILITY (DAYS)	BASIC FORMAT REQUIREMENTS						
				OVERLAY			SPECIAL MEASUREMENTS	PHOTOMAPS	THEMATIC MAPS	AUTOMATED INVENTORY	GEOMET. REF. SPAT. MEAS.	STATISTICAL SUMMARIES	AUTO. CHANGE DISCRIM.
SHOAL AND COASTAL MAPPING	P	P	S		30-180	365	•	•	•	•	•	•	•
SEA SURFACE CURRENTS	P	P	P		*	2-5	•	•	•	•	•	•	•
SEA SURFACE COMPOSITION	P	P	P		4-7	7	•	•	•	•	•	•	•
SEA SURFACE TEMPERATURE	P	P	S		1	1-4	•	•	•	•	•	•	•
SEA SURFACE ROUGHNESS	P	P			1/3-1	1-1	•	•	•	•	•	•	•
SEA SURFACE PHASE	P	P	P		3-14	7-14	•	•	•	•	•	•	•
CLOUD COVER	P	P	S		1/2	1-1/6	•	•	•	•	•	•	•
PRECIPITATION	P	P			1/2-1	1-1/6	•	•	•	•	•	•	•
OCEANIC RADIATION BUDGET	S	S	P		1	-	•	•	•	•	•	•	•
EARTH RADIATION BUDGET					1	-	•	•	•	•	•	•	•
CLOUD PHYSICS	S	S	S	S	1	-	•	•	•	•	•	•	•
UPPER ATM. TEMPERATURE				P	2	1	•	•	•	•	•	•	•
UPPER ATM. COMPOSITION	P	P	P	S	2	1	•	•	•	•	•	•	•
SNOW/ICE SURVEY					7-90	17	•	•	•	•	•	•	•
SOIL MOISTURE					14-60	14	•	•	•	•	•	•	•
SEA SURFACE POLLUTION	P	P	P		1/4-14	1-14	•	•	•	•	•	•	•
ATMOSPHERIC POLLUTION	P	P	P		1/5-1	1	•	•	•	•	•	•	•
SEVERE STORM WARNING	P	P	P		1/2-1	1-1/6	•	•	•	•	•	•	•

NOT ADDRESSED BY INSTRUMENTS

P = PRIMARY APPLICATION
S = SECONDARY APPLICATION

*RANGE COVERING TIDAL CYCLE - COASTAL

integer part of Q has been selected. After establishing the inclination to give sun synchronism, we have:

$$Q = 12-1/4 \quad \text{Orbit to orbit swath} = 3265.6 \text{ km}$$

$$h = 1652.2 \text{ km} \quad \text{Adjacent daily swath} = 816 \text{ km}$$

$$i = 102.28 \text{ degree} \quad \text{Ground velocity} = 5.677 \text{ km/sec}$$

The coverage pattern is depicted in Figure 9-1.

9.2.3 Sensor Design

9.2.3.1 OSS Design

The ocean scanning spectrophotometer has 20 spectral bands each encoded to 8 bits and achieving a ground resolution of 2 km. Assuming a 1.4 kell factor and a swath of 900 km (to allow for overlap), we obtain the number of samples per line to be:

$$900 \times 1.4/2 = 630$$

The rate at which lines are generated is:

$$5.677/2 = 2.8385 \text{ line/sec}$$

ONE SATELLITE
 Q = 12 1/4 ORBITS/DAY

SENSORS	COVERAGE FREQUENCY
OSS-OCEAN SCANNING SPECTROPHOTOMETER	4 DAYS
SSTIR-SEA SURFACE TEMPERATURE IMAGING RADIOMETER	1/2 DAY
PI-POINTABLE IMAGER	DAILY

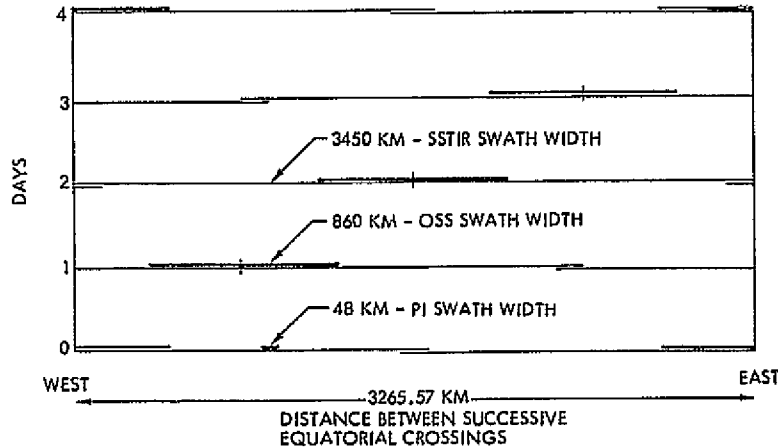


Figure 9-1. Mission 2 Coverage Geometry

Thus for each spectral band the sample rate is:

$$630 \times 2.8385 = 1788 \text{ samples/sec}$$

Converting to bit rate for all the bands gives:

$$286 \text{ kilobits/sec}$$

9.2.3.2 Pointable Imager Design

The pointable imager has a 48 km swath width achieving a 10 meter resolution in each of four spectral bands. The number of samples per line is thus

$$48 \times 10^3 / 10 = 4800$$

The rate of line generation is:

$$5.677 \times 10^3 / 10 = 567.7 \text{ lines per sec}$$

Thus $567.7 \times 4800 = 2.725$ mega samples per second per channel are generated. Encoding at a 7 bit level for each of the bands yields a data rate of 76.3 megabits/sec.

9.2.3.3 Sea Surface Temperature Imagery Radiometer Design

The sea surface temperature imaging radiometer obtains 2 km cell measurements at 10 bit accuracy in each of five spectral bands over

a 3600 km swath. Thus the number of cells per line is:

$$3600/2 = 1800 \text{ cells}$$

The line rate is:

$$5,677/2 = 2,838 \text{ lines/sec}$$

The sample rate per spectral band is:

$$2,838 \times 1800 = 5108 \text{ samples per sec}$$

Converting to bits for all spectral bands gives 256 k bits/sec.

The performance of Mission 2 with the orbital and sensor characteristics mentioned above is evaluated in Figure 9-2 in terms of observation frequency requirements. Cloud cover is the only data use not addressed by at least one primary sensor.

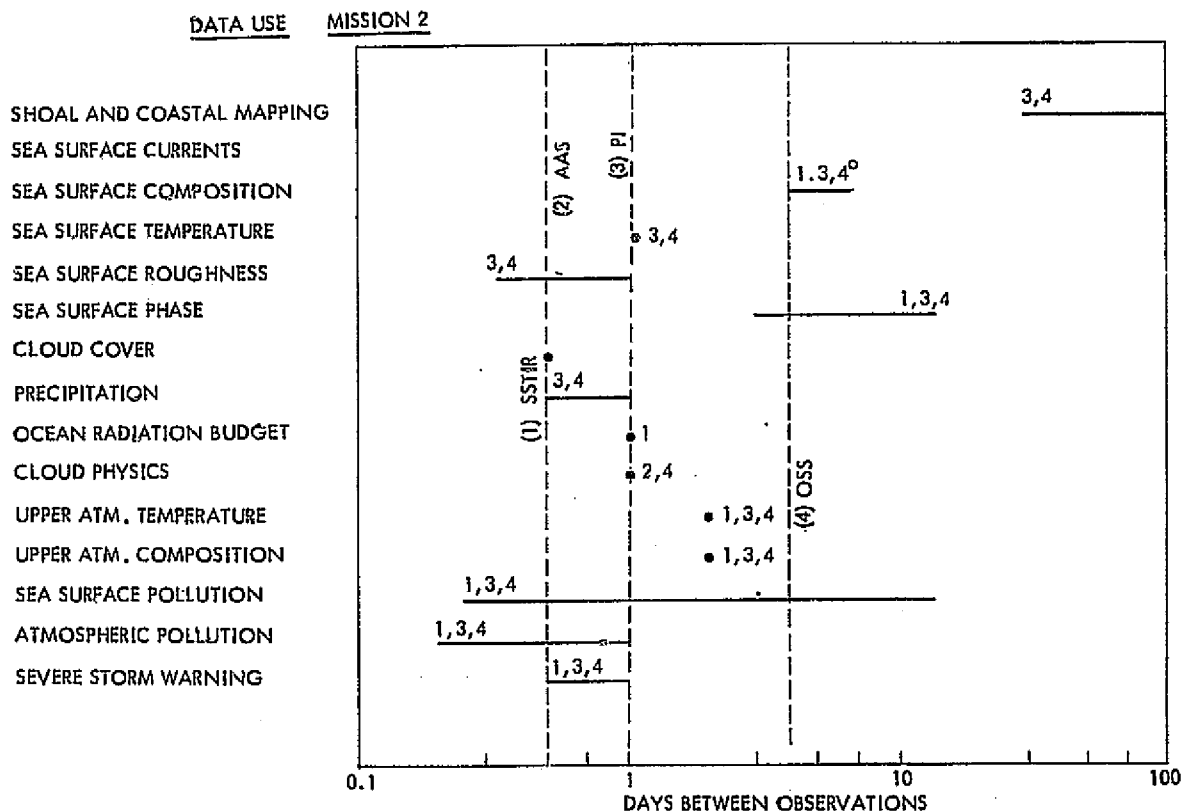


Figure 9-2. A Comparison of the Coverage Frequency of Mission 2 Sensors in a 1562.2 km, 102.3° Orbit and the Observation Frequency Requirements

9.2.4 Communication System Design

Getting high bit rate data from the satellite to the ground may be accomplished by direct transmission to the STDN or via TDRSS. The 76.7×10^6 bit per second data rate plus the wide areal coverage of Mission 2 make transmission via TDRSS mandatory. The high data rate of the P. I. instrument compared to the other suggests that two different communication channels be employed; one at about 80 megabits and the other at about 600 Kb/sec. The wideband link would employ the single access KU-band and the other the single access S-band link. EIRP requirements for these links are displayed in Figures 9-3 and 9-4, respectively. Based

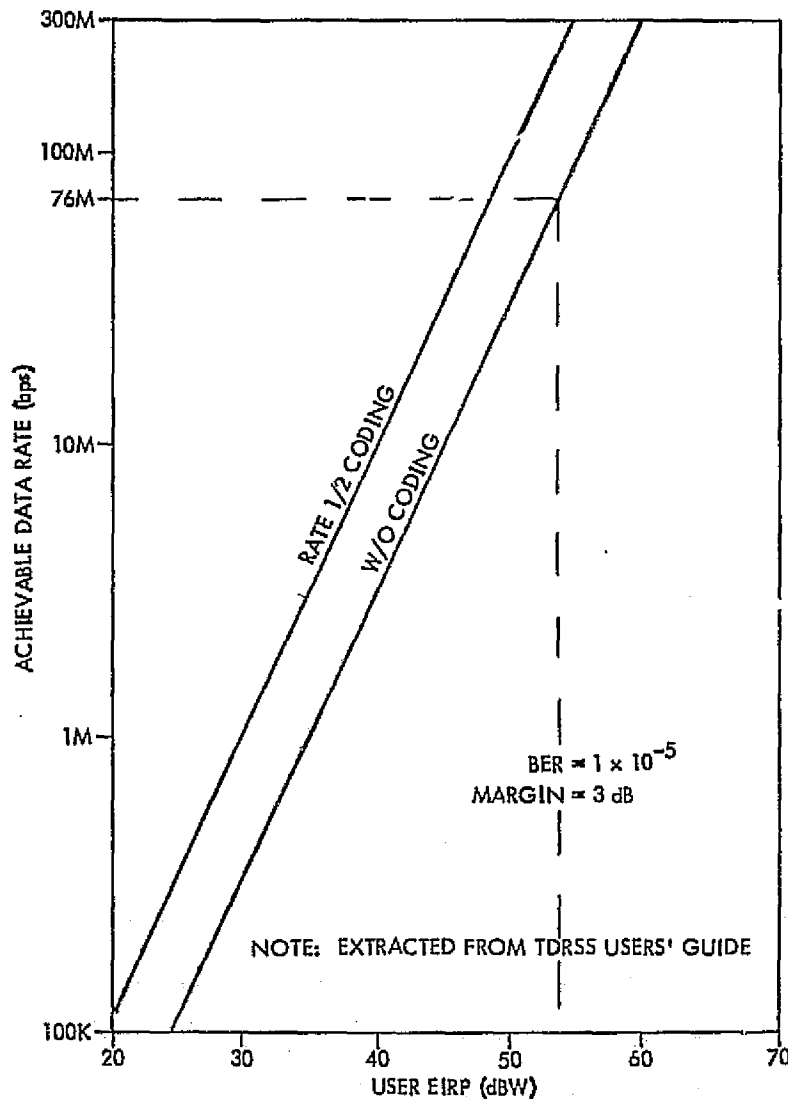


Figure 9-3. Mission 2 Ku-Band Link Requirements

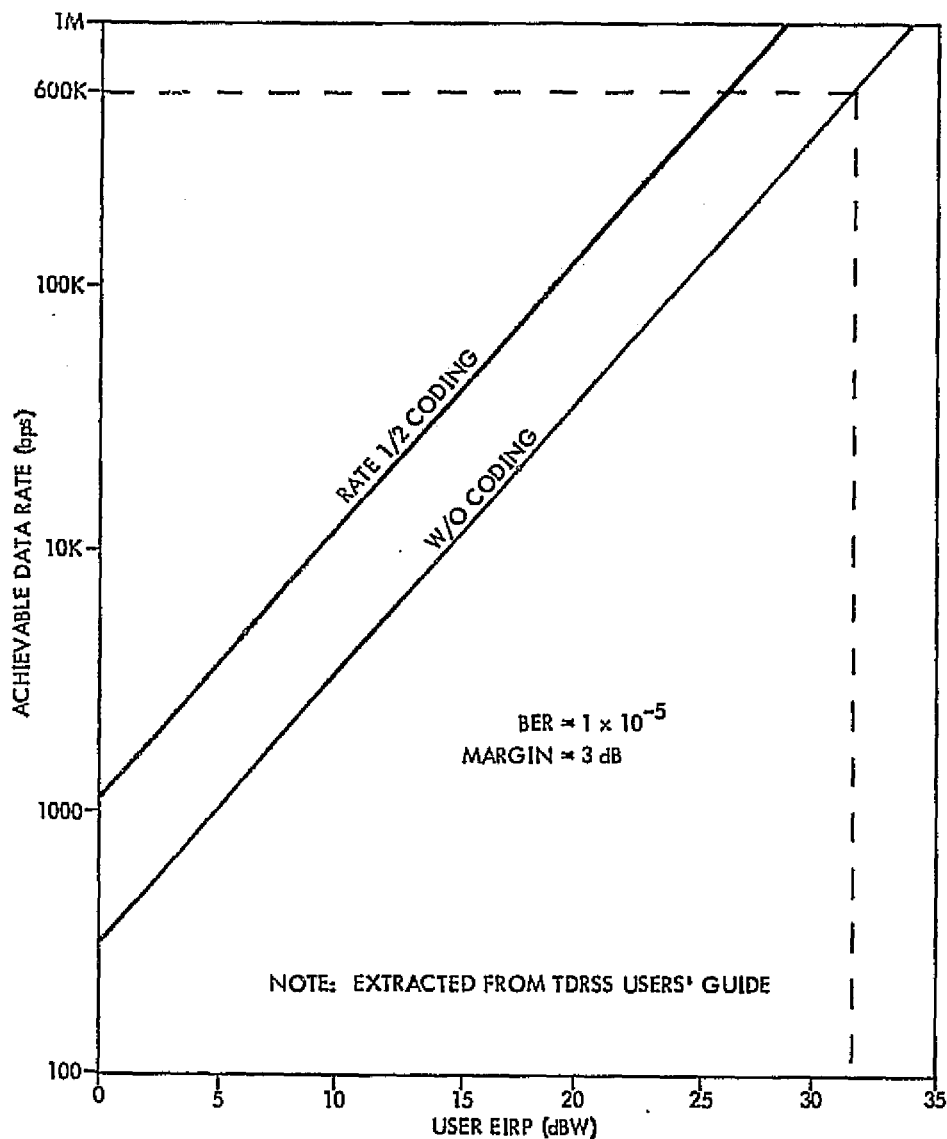


Figure 9-4. Mission 2 S-Band Link Requirements

on these requirements it is possible to structure the two links. One configuration for each link is derived below:

	<u>S-Band</u>	<u>Ku-Band</u>
EIRP Required	31 dB (without encoding)	54 dB (without encoding)
Antenna Gain	20.5 dB	43 dB
Antenna Size	1.5 ft dish	4 ft dish
Transmitter Losses	2.5 dB	2 dB
Power	13 dB = 20 watts	13 dB = 20 watts

Supporting and pointing these antennas, and particularly the 4-foot diameter Ku-band dish, may be a severe design problem. Gimbal design, clear field of view, plus the narrow 1 degree beamwidth of the Ku-band dish all tend to increase the complexity of this system element.

9.2.5 Ground Data Handling System Design

As discussed in Section 8.3, TRW has developed a parametric model for the ERS GDHS during the 1978 to 1988 time-frame which determines the hardware implementation requirements and costs for data handling functions. In this section the model will be applied to Mission 2. Costs will be derived for:

- Data station - mainprocessing structure
- Land line (if required) - tariff and terminals
- Filmwriter, archiving and computer.

The analysis is based upon a routing scheme in which error processing is performed at the data station and output product generation is performed in a separate facility at NASA/GSFC (see Figure 9-5).

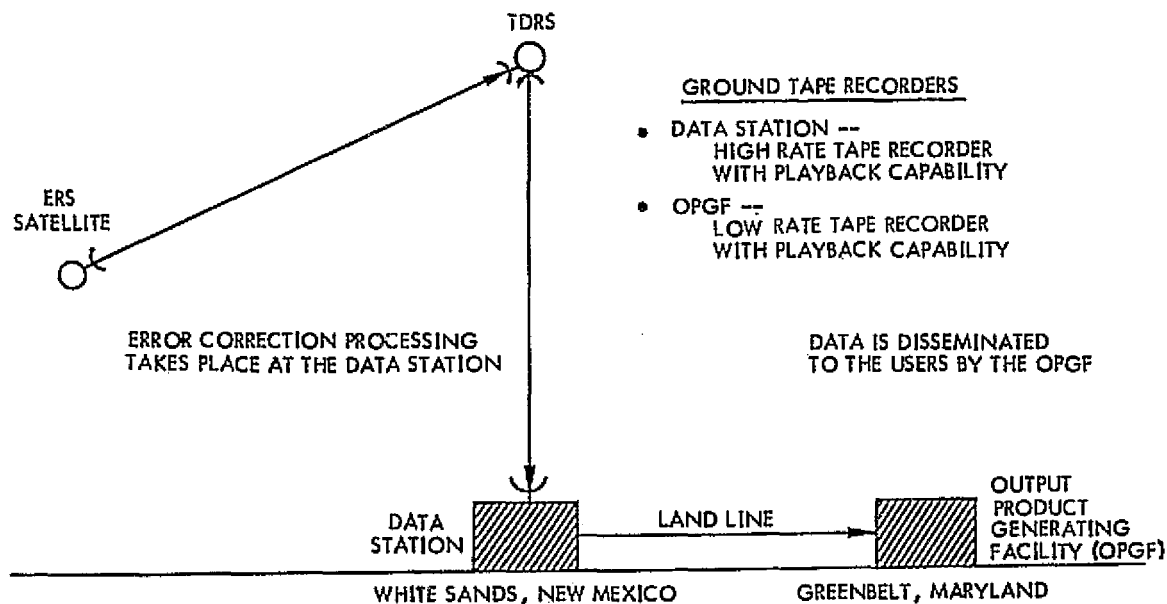


Figure 9-5. Data Routing for Mission 2

The sensor characteristics of interest, in terms of sizing the ground data handling system, are shown in Table 9-3. The duty cycle for all three instruments is continuous coverage over United States coastal areas (see Section 4.1).

Table 9-3. Sensor Characteristics Considered in the Ground Data Handling System Parametric Model

PARAMETER	SENSOR		
	OSS	PI	SSTIR
DATA RATE (MBPS)	0.25	76.20	0.29
NUMBER OF DETECTORS	9000	19200	8500
ENCODING LEVEL (BITS/PIXEL)	7	10	8
SWATH WIDTH (KM)	900	48	3400
RESOLUTION (KM)	2	.01	2

Beginning at Step 1 in the parametric model analysis, the data volume was computed for each sensor by multiplying the daily coverage times the data rate. The calculations are depicted in Table 4-2 and the resulting volumes are listed in Table 9-2. Using the data volumes and encoding levels and Figure 8-8, the processing throughput rates were derived: OSS - $1.4 \times 10^3 \mu\text{sec/pixel}$, PI - $1.4 \times 10^2 \mu\text{sec/pixel}$ and SSTIR - $7.9 \times 10^2 \mu\text{sec/pixel}$. These rates were based on a two shift throughput. The number of detectors were used in Figure 8-13 to determine the calibration memory requirements (see Table 9-3). The data frame volume in pixels was converted to bits using Figure 8-11. Before the processing volume could be determined, a decision had to be made with respect to the image volume required to correct for attitude uncertainties. For the ERTS-MSS and the EOS-TM the frame volume required was less than 0.1 percent. For this analysis, 0.5 percent was used. The processing memories were computed using this percentage, the data volumes, and using Figure 8-12 (see Table 9-4).

Step 2 was used to determine the ground station tape recorder requirements. An input rate of ~76.7 Mbps implied a unit cost of \$75K-182K (see Figure 8-17). Since present technology is adequate, a recorder in the late 70's would cost \$75K. Adding an additional unit for redundancy, the total cost for recorders would be \$150K. Step 3 shows that Mission 2 throughput rates could easily be handled with FY74 technology (Figure 8-19) and one main processing structure was adequate.

The input/output memory cost for a total frame volume of 892 Mbits would be \$186K since this frame volume was well within state of the art (see Figure 8-20).

Table 9-4. Ground Data Handling Volume Requirements for the Mission 2 Design Driving Sensors

PARAMETER	SENSOR		
	OSS	PI	SSTIR
DATA VOLUME (Mb/DAY)	3.29×10^2	2.90×10^3	7.75×10^2
CALIBRATION DATA VOLUME (MBITS/DAY)	19	30	18
DATA FRAME VOLUME (MPIXELS/FRAME/DAY) (MBITS/FRAME/DAY)	4.05 (32.0)	9.22 (750)	1.45 (110)
PROCESSING DATA VOLUME (MBITS/DAY)	0.16	3.20	0.72

Special purpose hardware requirements are determined in Step 4. A throughput rate of $1.4 \times 10^2 \mu\text{sec}/\text{pixel}$ is equivalent to a processing rate on the order of $10^4 \text{ nsec}/\text{word}$ which is well within FY74 technology as shown in Figure 8-22. The cost per unit is ~50K assuming a single unit purchase.

Step 5 determines the data correction and processing data memory requirements. Using the throughput rates calculated in Step 1, the processing memory costs were estimated (see Figure 8-21):

- OSS - 1K
- PI - 15K
- SSTIR - 3K

Data correction memory costs were computed using the calibration data volumes derived in Step 1:

- OSS - 110K
- PI - 140K
- HRMPS - 82K

Steps 1 through 5 were used to derive the cost of the main processing structure in the data station. A cost summary is shown in Table 9-5.

Table 9-5. Cost Summary for the Error Processing System at the Data Station (\$Thousands)

ITEM	UNIT COST	QUANTITY	TOTAL COST
TAPE RECORDERS	75	2	150
MAIN PROCESSOR	186	1	186
SPECIAL PURPOSE HARDWARE	50	1	50
PROCESSING DATA MEMORY	19	-	19
CALIBRATION DATA MEMORY	332	-	332
MINICOMPUTER SYSTEM	100	2	100
TOTAL			837

The filmwriter and archiving requirements for the OPGF were determined in Step 6. For the throughput rates being considered a filmwriter would cost on the order of 50K (see Figure 8-24). A daily volume of 2.9×10^3 Mbits/day resulted in an archiving cost range of 50K for multiple high-density recorders to 500K for mass memory; as shown in Figure 8-25 300K was selected as a representative value. A general purpose computer would cost 500K (see Table 8-2). The degree to which the OPGF would satisfy the user format requirements is shown in Table 9-6.

The total ground data handling system costs are shown in Table 9-7. They do not include programming effort, facilities, manpower and maintenance costs.

Table 9-7. GDHS Cost Summary

ITEM	COST
DATA STATION	837K
OPGF	850K

Table 9-6. Satisfaction of User Format Requirements by the Output Product Generation Facility in Mission 2

FORMAT	DESCRIPTION	FUNCTION OF OUTPUT PRODUCT GENERATION FACILITY
PHOTOMAP	PHOTOGRAPH WHICH MAY INCLUDE SUPERIMPOSED GRIDGING AND ANNOTATION	SUPPLIES BY THE OUTPUT PRODUCT GENERATION FACILITY (OPGF) FILMWRITER.
OVERLAY	ONE OR MORE IMAGES ADJUSTED IN SCALE AND ORIENTATION	SUPPLIES BY THE OUTPUT PRODUCT GENERATION FACILITY (OPGF) FILMWRITER. OVERLAYS CONSIST OF PRINTS AND/OR TRANSPARENCIES.
THEMATIC MAP	MAPS UPON WHICH GEOGRAPHICALLY DISTRIBUTED ATTRIBUTES ARE DESCRIBED BY VISUAL AIDS SUCH AS CONTOUR AND COLOR DIFFERENTIATION	SINCE THE OUTPUT REQUIRES CLASSIFICATION ALGORITHMS AND THIS IS AN RESEARCH AND DEVELOPMENT MISSION, THIS FORMAT WILL NOT BE SUPPLIED BY THE OPGF.
GEOMETRICALLY REFERENCED SPATIAL MEASUREMENTS	GEOMETRICALLY CORRECTED IMAGERY	PRECISION PROCESSED DATA WITH SUB-PIXEL REGISTERABILITY WILL BE SUPPLIED TO THE USER VIA THE OPGF. HOWEVER ALL CORRECTIONS WILL HAVE BEEN MADE AT THE CDPF.
INPUT TO MATHEMATICAL MODELS	GENERATION OF MODEL PARAMETER INPUTS IN A COMPUTER COMPATIBLE FORMAT	PRECISION PROCESSED DATA WITH SUB-PIXEL REGISTERABILITY WILL BE SUPPLIED TO THE USER VIA THE OPGF. HOWEVER ALL CORRECTIONS WILL HAVE BEEN MADE AT THE CDPF. THIS FORMAT WILL NOT BE SUPPLIED BY THE OPGF.
STATISTICAL SUMMARIES	DATA SUMMARIES (E.G., AVERAGING ON PIXELS)	PRECISION PROCESSED DATA WITH SUB-PIXEL REGISTERABILITY WILL BE SUPPLIED TO THE USER VIA THE OPGF. HOWEVER ALL CORRECTIONS WILL HAVE BEEN MADE AT THE CDPF. THIS FORMAT WILL NOT BE SUPPLIED BY THE OPGF.
AUTOMATED INVENTORY	APPLICATION OF SIGNATURE RECOGNITION ALGORITHMS	PRECISION PROCESSED DATA WITH SUB-PIXEL REGISTERABILITY WILL BE SUPPLIED TO THE USER VIA THE OPGF. HOWEVER ALL CORRECTIONS WILL HAVE BEEN MADE AT THE CDPF. THIS FORMAT WILL NOT BE SUPPLIED BY THE OPGF.
AUTOMATED CHANGE DISCRIMINATION	APPLICATION OF SIGNATURE RECOGNITION ALGORITHMS	PRECISION PROCESSED DATA WITH SUB-PIXEL REGISTERABILITY WILL BE SUPPLIED TO THE USER VIA THE OPGF. HOWEVER ALL CORRECTIONS WILL HAVE BEEN MADE AT THE CDPF. THIS FORMAT WILL NOT BE SUPPLIED BY THE OPGF.
SPECIAL MEASUREMENTS	APPLICATION OF COMPUTATIONAL ALGORITHMS	PRECISION PROCESSED DATA WITH SUB-PIXEL REGISTERABILITY WILL BE SUPPLIED TO THE USER VIA THE OPGF. HOWEVER ALL CORRECTIONS WILL HAVE BEEN MADE AT THE CDPF. THIS FORMAT WILL NOT BE SUPPLIED BY THE OPGF.

9.2.6 Data Dissemination System

Since Mission 2 is a research mission, distribution of the satellite data will be limited. Data will arrive at the White Sands terminal and must be routed to the Output Products Generating Facility (OPGF) at Goddard. Dissemination of these data will be limited by the facilities which are projected for the 1980 time frame of this mission. Thus, the options available for data distribution are limited to the following:

- 1) Hard copy via mail or courier.
- 2) Error corrected tapes via mail or courier.
- 3) Digital data via commercial leased lines.

In addition, unprocessed data could be made available via land line from the White Sands facility.

Construction of a domestic data distribution satellite (i. e., DOMSAT) could significantly improve the timeliness and the scope of data dissemination. However it does not appear that such a satellite system will be operational in time to support Mission 2.

9.2.7 System Summary

Figure 9-6 shows the proposed Mission 2 system in simplified block diagram form. The system configuration is conventional but there are several elements which merit further comment.

The most serious problem with this system involves the TDRS antennas. As noted in Section 9.2.4, providing a two axis drive for a 4 foot dish which is not affected by blockage from the earth or from the spacecraft body and which also meets the Ku-band pointing requirements is a challenging design problem.

A family of miniature TWT's (now under development) which use samarium-cobalt magnets is proposed as the candidate Ku-band power amplifier. Should this development be delayed, some alternate configuration for this device would have to be found.

A similar situation exists relative to the 70-80 MBPS recorder required at the TDRS ground station. Such a recorder appears to be feasible with current technology, but such a device will require development. For Mission 2, an additional complication is added by the input/output ratio imposed by the TDRS-OPGF landline data rate limitation.

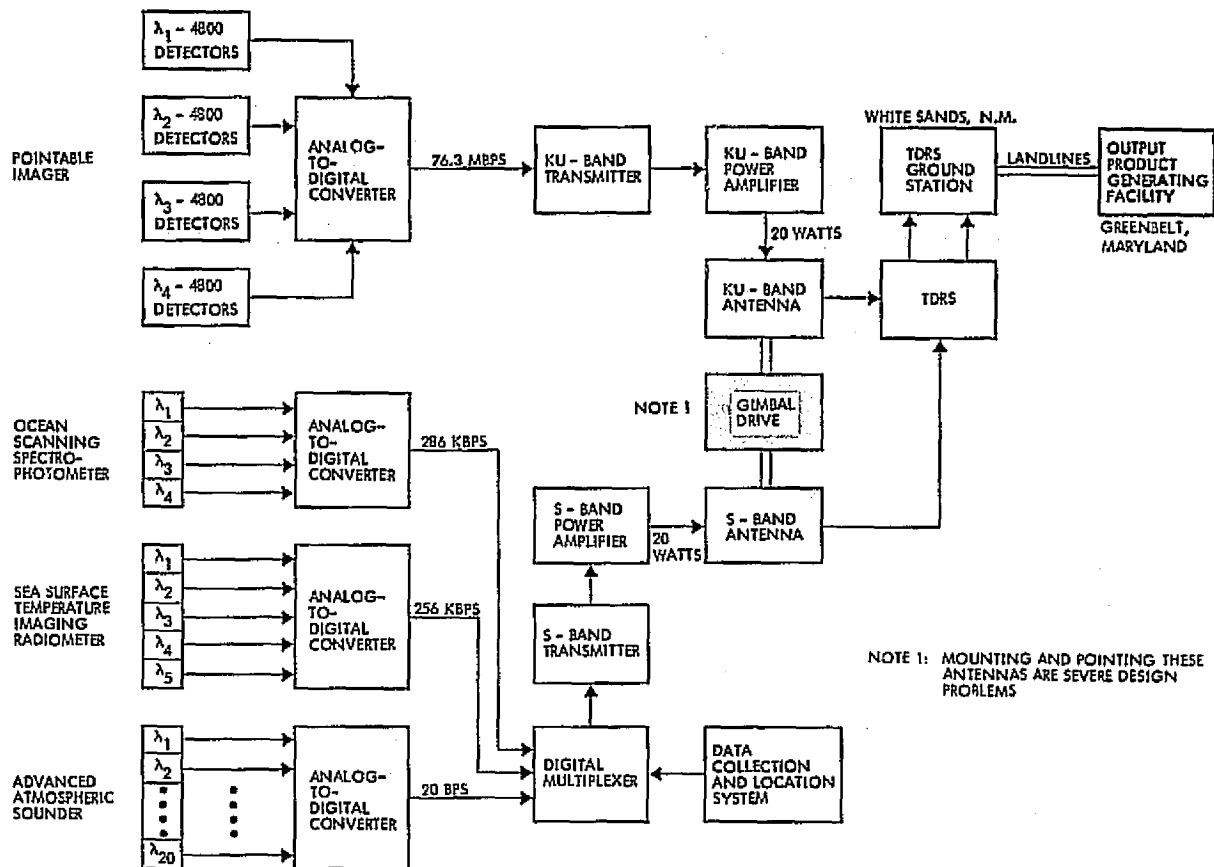


Figure 9-0. Mission 3 Data System Block Diagram

The data enter the ground station at 76.3 Mbps and leave at 57 Kbps. This 1340:1 data rate reduction may be accomplished through a combination of the following techniques:

- 1) Demultiplexing the incoming signal into the original 4 spectral bands (4:1).
- 2) Speed reduction of the recorder for playback (20:1).
- 3) Buffering of data into the processor at the ground station and/or into the landline terminal.

In summary, the proposed system configuration will satisfy mission requirements and is technologically feasible for a 1980 mission.

9.3 Mission 6

9.3.1 Mission Requirements

Mission 6 is the final operational system in a mission series dedicated to terrestrial survey and environmental quality monitoring. As such, it will generate the largest data load in the mission series and data handling considerations become most critical.

The launch date for Mission 6 is FY 1984. Its sensor complement consists of four instruments:

- Synthetic aperture radar
- Combined scanning spectroradiometer/pointable imager
- Advanced atmospheric sounder
- Data location and collection system.

The second instrument will be considered as two separate sensors because of insufficient data on the combined version; the high resolution multispectral point scanner (which represents the spectrophotometer) and the pointable imager. The sensor complement is described in Table 9-8. For a more detailed description see Section 2.0. As in Mission 2, the swathwidth, IFOV, pointing capability and resolution of the instruments are determined as part of the mission design. (See Section 9.3.2).

The research and development precursory to Mission 6 (i.e., Missions 1 and 3) were sensor testbeds and collection, processing and dissemination systems used to accomplish terrestrial and environmental research. Each contributed to the development of data handling technology that would be adequate to deal effectively with data from an operational mission. Consequently, near raw data or partially processed data were sent to the users in these early R&D missions so they could perform the appropriate data processing and analysis to decide on optimal approaches tailored to their specific needs. These selected approaches were transformed into special processing and formatting requirements. The central data processing facility in Mission 6 should meet these requirements and provide final format data directly to the users for analysis and interpretation in a manner which meets their perishability requirements.

Mission 6 is basically an "operational ERTS" with special emphasis on environmental quality monitoring. As discussed in Section 3.3, the major application areas include:

- Agriculture, forestry and rangelands
- Geography

ORIGINAL PAGE IS
OF POOR QUALITY

Table 9-8. Sensor Complement for Mission 6

9-18

INSTRUMENT	DISCIPLINE	APPLICATION	TYPE OF SCAN	SPECTRUM/BANDWIDTH (MICRONS)	ERROR SOURCES	UNIQUE DATA PROCESSING REQUIREMENTS
POINTABLE IMAGER	EARTH RESOURCES	GEOLOGY, AGRONOMY, FORESTRY, COASTAL	PUSH BROOM SOLID STATE ARRAY	0.5 TO 0.6 0.6 TO 0.7 0.7 TO 0.8 0.8 TO 1.1	GEOMETRIC: <ul style="list-style-type: none"> SPACECRAFT ATTITUDE AND EPHEMERIS ERRORS LOCAL SURFACE ALTITUDE VARIATIONS RADIOMETRIC: <ul style="list-style-type: none"> CALIBRATION DARK CURRENT NONUNIFORMITY DETECTOR RESPONSE ATMOSPHERIC EFFECT 	RADIOMETRIC CORRECTION FOR DARK CURRENT AND NONUNIFORMITY OF DETECTOR RESPONSIVITIES CORRECTION FOR EFFECTS OF EARTH ROTATION
OCEANIC SCANNING SPECTROPHOTOMETER	OCEANOGRAPHY	CHLOROPHYLL CONTENT; POLLUTION UPWELLING; OCEAN CURRENTS	CROSS TRACK, ELECTRICAL OR MECHANICAL	0.4 TO 0.7 μ /150 ANGSTROMS, 20 BANDS	GEOMETRIC: <ul style="list-style-type: none"> SPACECRAFT ATTITUDE EARTH ROTATION SCAN DISTORTION RADIOMETRIC: <ul style="list-style-type: none"> CALIBRATION SUN ANGLE ATMOSPHERIC SCATTERING 	RADIOMETRIC CORRECTIONS FOR SHADING, SUN ANGLE, SCAN ANGLE GEOMETRIC CORRECTIONS FOR SPACECRAFT ATTITUDE, SCAN ANGLE, OFFSET ANGLE
SEA SURFACE TEMPERATURE IMAGING RADAR	OCEANOGRAPHY AND METEOROLOGY	SEA SURFACE TEMPERATURE, CLOUD COVER, RADIATION BUDGET OF OCEAN	CROSS TRACK LINE SCAN	0.2 TO 4.0 CLOUD TAG (DAY) 3.6 TO 4.1 CLOUD TAG (NIGHT) 6.5 TO 7.0 H ₂ O ABSORPTION ² 8.9 TO 9.4 H ₂ O CONTINUUM ² 10.5 TO 11.5 SEA SURFACE TEMPERATURE	GEOMETRIC: <ul style="list-style-type: none"> SPACECRAFT ATTITUDE VARIABLE RESOLUTION RADIOMETRIC: <ul style="list-style-type: none"> CLOUD INTERFERENCE ATMOSPHERIC TURBIDITY 	CALIBRATION OF DATA FROM FIVE CHANNELS TO DETERMINE TEMPERATURE
ADVANCED ATMOSPHERIC SOUNDER	METEOROLOGY	TEMPERATURE PROFILES FOR NUMERICAL MODELS AND LOCAL AREA FORECASTS OF POLLUTION TURBULENCE	440 $^{\circ}$, CROSS TRACK, SAMPLES 400 KM APART	8 CHANNELS - 15 BAND 4 CHANNELS - 4.3 1 CHANNEL - 9.6 1 CHANNEL - 11.1 2 CHANNELS - 3.8 3 CHANNELS - 18 TO 30 2 CHANNELS - MICRO-WAVE	RADIOMETRIC: <ul style="list-style-type: none"> CALIBRATION DETECTORS, NOISE EQUIVALENT POWER ATMOSPHERIC ABSORPTION COEFFICIENTS 	

- Geology
- Hydrology
- Environmental pollution

The data requirements for each data use category and the instruments used to gather the data are depicted in Table 9-9. All of the data use categories were addressed by at least one instrument.

Table 9-9. Summary of the Data Requirements and Applicable Instruments for Each Data Use in Mission 6

DATA USE	INSTRUMENTS				DATA REQUIREMENT SUMMARY										
	SYNTHETIC APERTURE RADAR	HIGH RESOLUTION MULTISPECTRAL POINT SCANNER	POINTABLE IMAGER	ADVANCED ATMOSPHERIC SOUNDER	OBSERVATION FREQUENCY (DAYS BETWEEN LOOKS)	PERISHABILITY OF DATA (DAYS)	OVERLAY	SPECIAL MEASUREMENTS	PHOTOMAPS	THEMATIC MAPS	AUTOMATED INVENTORY	GEOMET. REF. SPAT. MEAS.	STATISTICAL SUMMARIES	AUTO. CHANGE DISCRIMINATION	INPUT TO MATH MODELS
SHOAL AND COASTAL MAPPING	S	S	S		30-180	365	•	•	•	•	•	•	•	•	•
PRECIPITATION	S				1/2-1	1/6	•	•	•	•	•	•	•	•	•
SNOW/ICE SURVEY	P	P	P		7-90	7	•	•	•	•	•	•	•	•	•
SOIL MOISTURE		P	P		14-60	14	•	•	•	•	•	•	•	•	•
TERRAIN MAPPING	P	P	P		1-30	1-30	•	•	•	•	•	•	•	•	•
EARTH SURFACE COMPOSITION	P	P	P		1-30	365	•	•	•	•	•	•	•	•	•
ATMOSPHERIC POLLUTION		P	P		1/5-1	1	•	•	•	•	•	•	•	•	•
SEA SURFACE POLLUTION		S	S		1/4-14	1-14	•	•	•	•	•	•	•	•	•
WATER QUALITY		P	P		7-30	30	•	•	•	•	•	•	•	•	•
SURFACE WATER MAPPING	P	P	P		90	30	•	•	•	•	•	•	•	•	•
SEVERE STORM WARNING	S				1/2-1	1/6	•	•	•	•	•	•	•	•	•
CLOUD COVER		S	S	S	1/2	1/6	•	•	•	•	•	•	•	•	•
EARTH RADIATION BUDGETS		P	P		1		•	•	•	•	•	•	•	•	•
CLOUD PHYSICS				S	1		•	•	•	•	•	•	•	•	•
UPPER ATM. TEMPERATURE		S	S	S	2	1	•	•	•	•	•	•	•	•	•
UPPER ATM. COMPOSITION				S	2	1	•	•	•	•	•	•	•	•	•

S = SECONDARY APPLICATION

P = PRIMARY APPLICATION

9.3.2 Orbit/Satellite-Constellation Design

The requirements for this mission indicate that three primary instruments (HRMPS, SAR, PI) are involved and that repetition frequency for HRMPS images must be in the order of two or three days, for SAR

images less than a week, for PI images daily at selected small regions. Furthermore, preliminary HRMPS design considerations which include viewing obliquities, optical field of view, design of detector clusters in the image plane, and total data rate suggest a maximum swath width of about 400 km. Preliminary SAR design considerations including transmitter power, PRF, and data rate limit SAR swath widths to about 100 km. If, for a starting point, we assume an equatorial orbit-to-orbit separation of about 3000 km we find that $3000/400 = 7.5$ satellite passes (at one per day per satellite) are required before repeated viewing with the HRMPS is possible. Similarly for the SAR, $3000/100 = 30$ satellite passes are required between repetitions. Both repetition times miss by several times over the mission requirements for frequency of repetition. The obvious way to meet the HRMPS requirements is to employ three satellites phased such that they interlace at $1/3$ the original coverage interval. In this case coverage is reduced to about 2.5 days (figures at this point are only approximate). For a three satellite constellation, repeated coverage by the SAR would reduce to 10 days which is still in excess of the weekly repetition desired. Here, however, it is possible to employ two SAR's, one looking out each side of the spacecraft and effectively increase the swath width (though not contiguous) to 200 km and reduce the interval between passes of the three satellite system to about five days.

Using the above analysis as a first step one would select an orbital Q such that its fractional denominator was 5. Each satellite would interlace such that the orbit-to-orbit separation would be divided into 15 pass positions. With this orbital configuration, however, the failure of a sensor on any satellite would leave a permanent series of gaps in the ground coverage. By selecting an orbital Q whose denominator is 15 rather than 5, each satellite will cover each ground region during the 15 day repeat pattern and failure of any single instrument will merely cause an occasional delay in coverage repetition but will not cause permanent deletion of any ground region.

Because the swath width of the HRMPS will be twice the width of the 15 sections the orbit-to-orbit distance is divided into, it is appropriate that adjacent swaths on succeeding days advance (or lag) by two units. This says the numerator of the fractional part of Q should be 2 or D-2.

That is, Q should be $N \frac{2}{15}$ or $N \frac{13}{15}$ where N is an integer about 13 and still to be determined. Table 9-10 presents some consequences of selecting Q within the guidelines given above. Not only have the (non-overlapping) swath widths for the HRMPS and SAR been presented, but also the ground distance from satellite nadir over which direct communication can take place. For reasons discussed in Section 9.3.5, communication will take place directly to Sioux Falls for this mission. Since the PI and the SAR look off to the side, it is important that communication can take place when Nadir is hundreds of kilometers off shore. For this reason we have selected $Q = 13 \frac{2}{15}$ which leads to an altitude of 1203.6 km and an inclination of 100.4 degrees. A summary of the orbits considered is shown in Table 9-10. At this altitude, communication directly to Sioux Falls can occur

Table 9-10. Summary of the Orbits Considered for Mission 6

PARAMETERS	Q (ORBITS/DAY)									
	11 13/15		12 2/15		12 13/15		13 2/15		13 13/15	
	NM	KM	NM	KM	NM	KM	NM	KM	NM	KM
ORBIT TO ORBIT SWATH	1820.2	3371.0	1780.2	3297.0	1678.8	3109.0	1644.7	3045.9	1557.7	2884.8
HRMPS SWATH	242.7	449.5	237.4	439.6	223.8	414.5	219.3	406.1	207.7	384.6
SAR SWATH	60.7	112.4	59.3	109.9	56.0	103.6	54.8	101.5	51.9	96.2
ALTITUDE	935.2	1143.6	870.9	1614.7	705.5	1308.0	649.2	1203.6	503.7	933.9
VISIBILITY CIRCLE RADIUS*	2007.7	3718.4	1942.3	3597.0	1755.0	3251.6	1687.0	3124.0	1482.9	2746.3

SELECTED ORBIT

*SIOUX FALLS

at distances exceeding 400 km off the coast of Continental U.S. The coverage pattern is described in Figure 9-7. The performance of Mission 6 with the orbital characteristics mentioned above is evaluated in Figure 9-8 for the user observation requirements two data use observation requirements were not satisfied by at least one primary instrument.

9.3.3 Sensor Design

9.3.3.1 SAR Design

Mission requirements suggest a 15 meter ground resolution for the SAR in each of two received polarizations at both X- and L-band.

Q = 13 2/15 ORBITS/DAY
 THREE SATELLITES = A, B, C

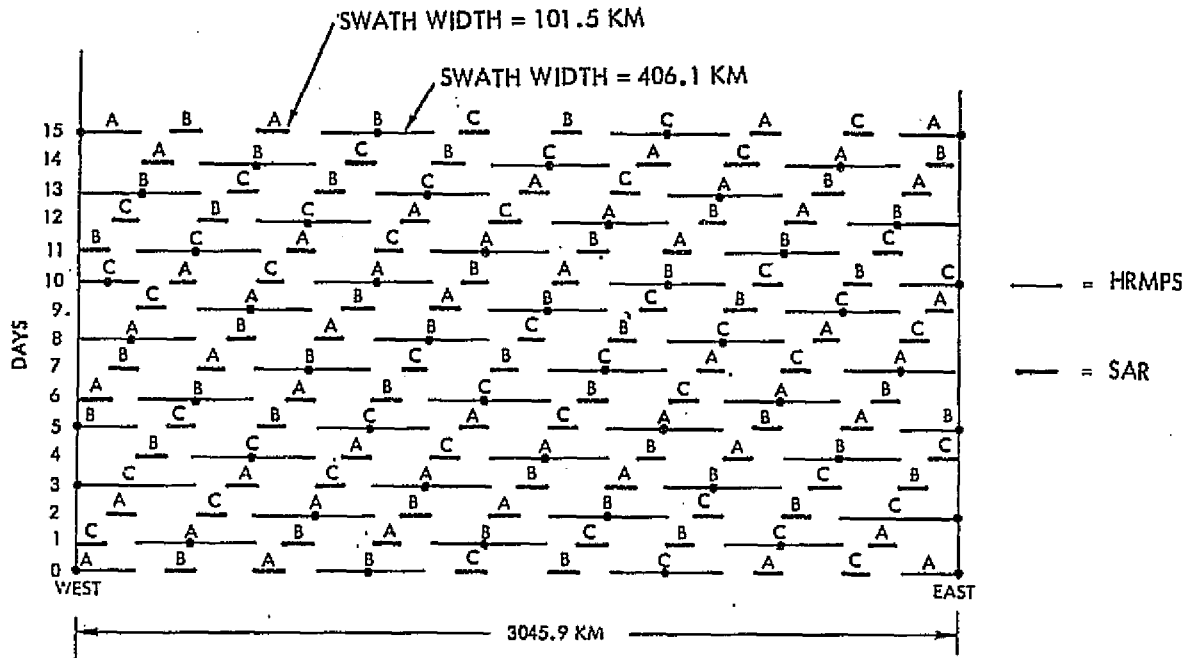


Figure 9-7. Coverage Pattern for Mission 6

DATA USE

- SHOAL AND COASTAL MAPPING
- PRECIPITATION
- SNOW/ICE SURVEY
- SOIL MOISTURE
- TERRAIN MAPPING
- EARTH SURFACE COMPOSITION
- ATM. POLLUTION
- SEA SURFACE POLLUTION
- WATER QUALITY
- SURFACE WATER MAPPING
- SEVERE STORM WARNING
- CLOUD COVER
- EARTH RADIATION BUDGET
- CLOUD PHYSICS
- UPPER ATM. TEMPERATURE
- UPPER ATM. COMPOSITION

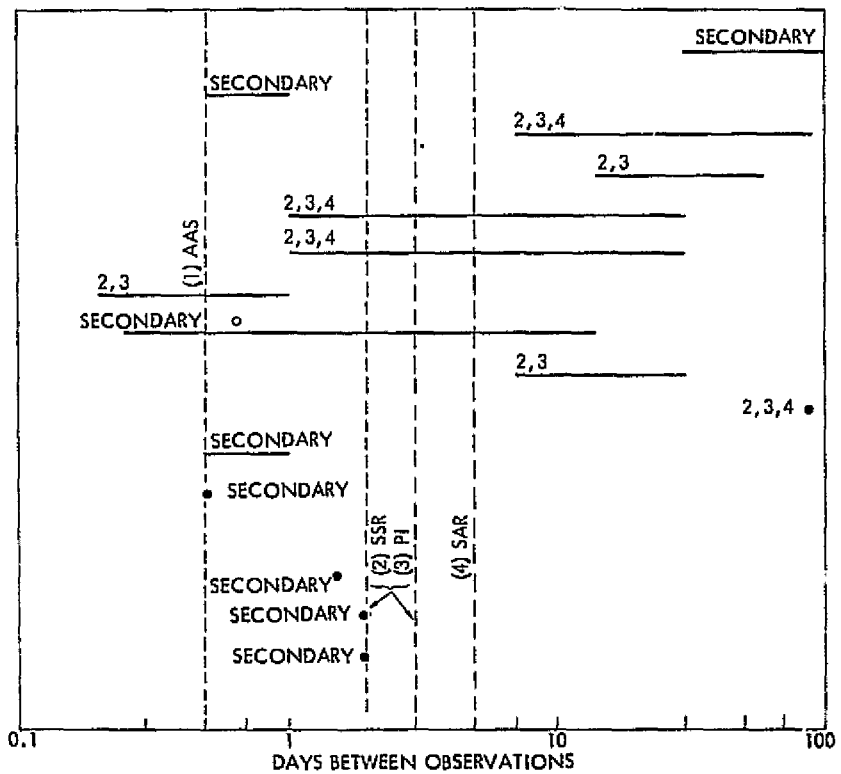


Figure 9-8. A Comparison of the Coverage Frequency of the Mission 6 Sensors in a 1203.6 km, 102.3° Orbit and the Observation Frequency Requirements

The orbit analysis previously concluded indicates a swath on each of two SAR's looking out opposite sides of the spacecraft should be 101.5 km. A depression angle of about 60 degrees where the beginning and end of a swath are multiples of 101.5 km from nadir extends from 609 km to 711.5 km. To provide overlap between adjacent swaths, we have designed the swath to extend an additional 4 km toward nadir and an additional 4.5 km away from nadir yielding actual swath of 110 km. These relationships are shown in Figure 9-9. Using the Range to inner and outer swath edges, we can calculate the round trip time to be 9149.3 and 9558.7 μ sec respectively. All the information desired is conveyed in the echoes received between these times; that is in a 409.4 μ sec interval.

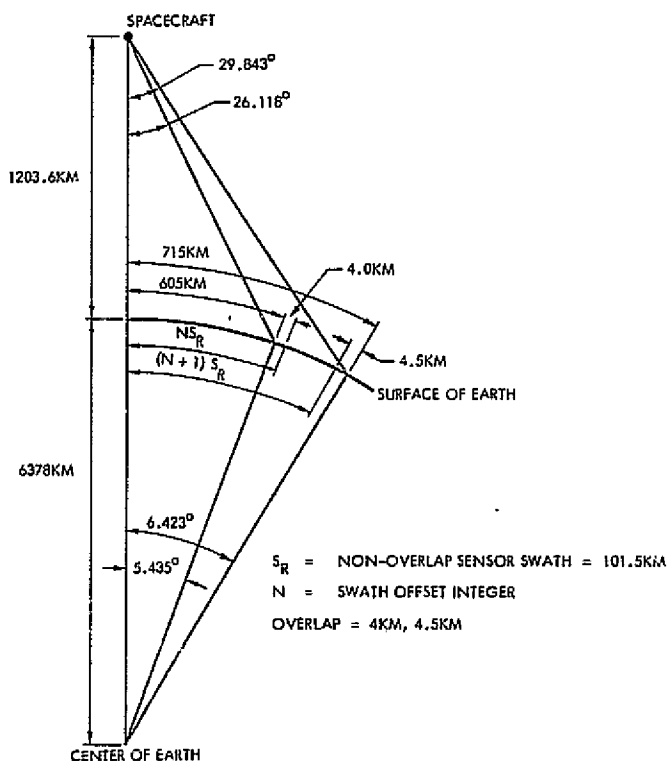


Figure 9-9. Synthetic Aperture Radar Geometry

In SAR design one tries to employ an antenna whose along track length equals the desired along track resolution. Furthermore, the SAR design requires that two pulses be transmitted during the time the antenna moves its length. Using the orbital velocity of the spacecraft for the $Q = 13 \frac{2}{15}$ ($v = 7.2285$ km/sec) and the desired resolution of 15 meters we calculate the interval between transmitted pulses as approximately 1038

μ sec, which is slightly over twice the observation time required per pulse. This suggests that the radars on opposite sides of the spacecraft can transmit alternately yielding a time between pulses of about 500μ sec which is still adequate if properly phased to permit the desired echo to fall entirely between transmitted pulses. It must be noted that the observation of the echo from a given pulse occurs many (about 9) transmitted pulses later. In fact, we have selected the PRF of each radar to be 940 pps or the combined PRF to be 1880 PPS. Figure 9-10 illustrates the timing relationships and shows that the wanted portion of an echo from a given pulse falls

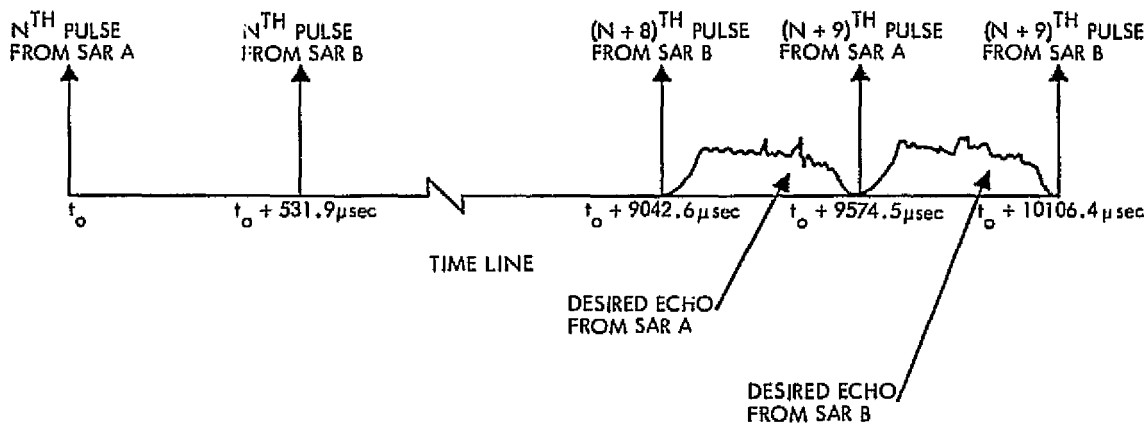


Figure 9-10. Timing Relationship Between the Transmitted Pulses and Echo Returns for the Synthetic Aperture Radars in Mission 6

squarely between transmission of the 9th following pulse of the same SAR and the 9th following pulse of the SAR on the opposite side. To accommodate both X- and L-band systems it is suggested that pulses from each system be transmitted nearly simultaneously, so that the listening periods are silent for both systems. Range gating is used to exclude reception except during the intervals of interest. Given that the PRF is 940 the antenna length is chosen to be $2 \sqrt{940} = 15.4$ meters. This also is used to establish the ground resolution. The width of the X- and L-band antennas can be established using the desired beamwidth from Figure 9-10 and the respective wavelengths. For X-band the width perpendicular to the line to the center of the swath is .46 meter and for L-band this is 3.54 meter. Some system simplification can result from using a single horizontally oriented antenna to transmit alternately on each side of the spacecraft. This requires broadening the antenna from .46m to .52m for X-band and from 3.54m to 4.0m for L-band.

The data rate can now be computed as follows:

- The PRF for each system is 940 PPS.
 $940 \times 7150 \times 6 \times 4 = 161.3$ megabits/sec
- There are $110\text{km}/15.4\text{m} = 7150$ range bins
- Each sample is quantized to 6 bits
- Four modes of data are conveyed (two polarizations in each of two bands)

The average transmitted power per polarization required to achieve adequate dynamic range for the X-band system is about 200 watts while for L-band the corresponding value is 25 watts. Thus for all four systems, 450 watts is required. The peak pulse power will depend on the transmitted pulse length. The required time resolution is $409.4 \text{ sec}/7150 = 0.057 \mu\text{sec}$. This corresponds to a duty cycle of 1 in 18,580. Clearly pulse compression is required, and at a compression ratio of 300 to 1 the peak transmitted power would be 12.4 kw for X-band and 1550 watts for L-band.

9.3.3.2 Pointable Imager

The pointable imager uses push broom detectors to achieve a 7.5 meter resolution in a 48 km swath for each of five spectral bands. Basic design is straightforward assuming a 6 bit quantization and 5 percent overhead for synchronization and housekeeping data. There will be $48 \times 10^3/7.5 = 6400$ detectors for each spectral band. Each will be sampled once each time the spacecraft moves 7.5m; that is, $6081/7.5 = 810$ lines per second. Thus the data rate will be $6400 \times 810 \times 5 \times 6 \times 1.05 = 163.5$ megabits.

Since viewing of any selected region once per day is required, offset pointing must be provided. Figure 9-11 shows the geometry of this situation. The greatest surface distance a target can be from a sub-orbital point is half the orbit-to-orbit distance, i. e., 1523 km at the orbital altitude of 1204 km this corresponds to an offset pointing angle of 47.45 degrees. Scenes viewed from this angle are seen quite obliquely (61.1°) and resolution across track is reduced to about 15 meters. Fortunately this is an extreme case and on the succeeding day pointing offset and obliquity will reduce to 40.5 degrees and 50.5 degrees respectively.

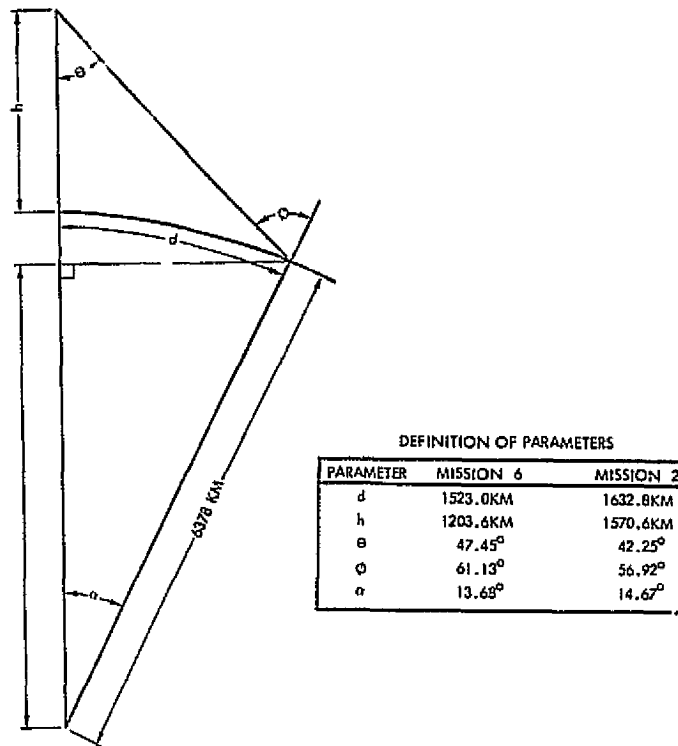


Figure 9-11. Geometry for Determining Pointable Imager Offset Angle Θ , and Ground Obliquity ϕ

9.3.3.3 HRMPS Design

Mission requirements dictate a 30 meter resolution for the HRMPS in eight spectral bands. The technique for communicating the satellite data which is discussed in Section 9.3.5 permits a reduction in resolution to 27.5 meters and it is this latter value which is used in the following discussion.

The orbital swath identified for the HRMPS in Section 9.3.2 was 406 km. To allow for overlap at the sides the sensor design swath has been set at 425 km. The number of across track cells is thus $425 \times 10^3 \times 1.4 \times 27.5 = 21636$ cells, where the 1.4 is the over sampling factor commonly required in this type sensor. Lines are collected at a rate of $6081/27.5 = 221.1$ lines per second. Combining these numbers with the number of bits/pixel, (7), the number of spectral bands, (8), and a 20 percent retrace inefficiency factor yields a total data rate of $21636 \times 221.1 \times 7 \times 8 \times 1.2 = 321.5$ megabits/sec.

For each spectral band multiple detectors scanning in parallel will be used to reduce the scanning frequency and to reduce the optical aperture through the ability to dwell longer on each pixel. The image on the ground of the line of detectors will however tend to elongate at the edges of the scan due to the increase in scanning radius. For this sensor and altitude the elongation will be 1.0184. Thus if we desire to eliminate overlap at the outer detectors at the swath edge to about 10 percent we cannot use more than six detectors scanning in parallel. (This actually produces 11 percent overlap). This occurs in each of the eight spectral bands so that in total 48 detectors are employed.

9.3.4 Onboard Data Handling System Design

The proposed implementation of Mission 6 data processing on board the spacecraft involves the following:

- 1) Analog-to-digital conversion of a variety of sensor data.
- 2) Recording and playback of data acquired over territorial or other remote locations.
- 3) Storing commands for use throughout the mission.

Configuring a data system to meet these requirements is straightforward and a typical block diagram is given in Figure 9-12.

The typical analog multiplexer frequency is 165/4 or approximately 41 mbps, and the largest number of encoding levels is 7. Reference to Figure 9-13 shows that these units are within range of current technology and should represent no significant SRT concern.

Tape recorders to support the proposed configuration are projected to be available in the 1980's as illustrated in Table 9-11.

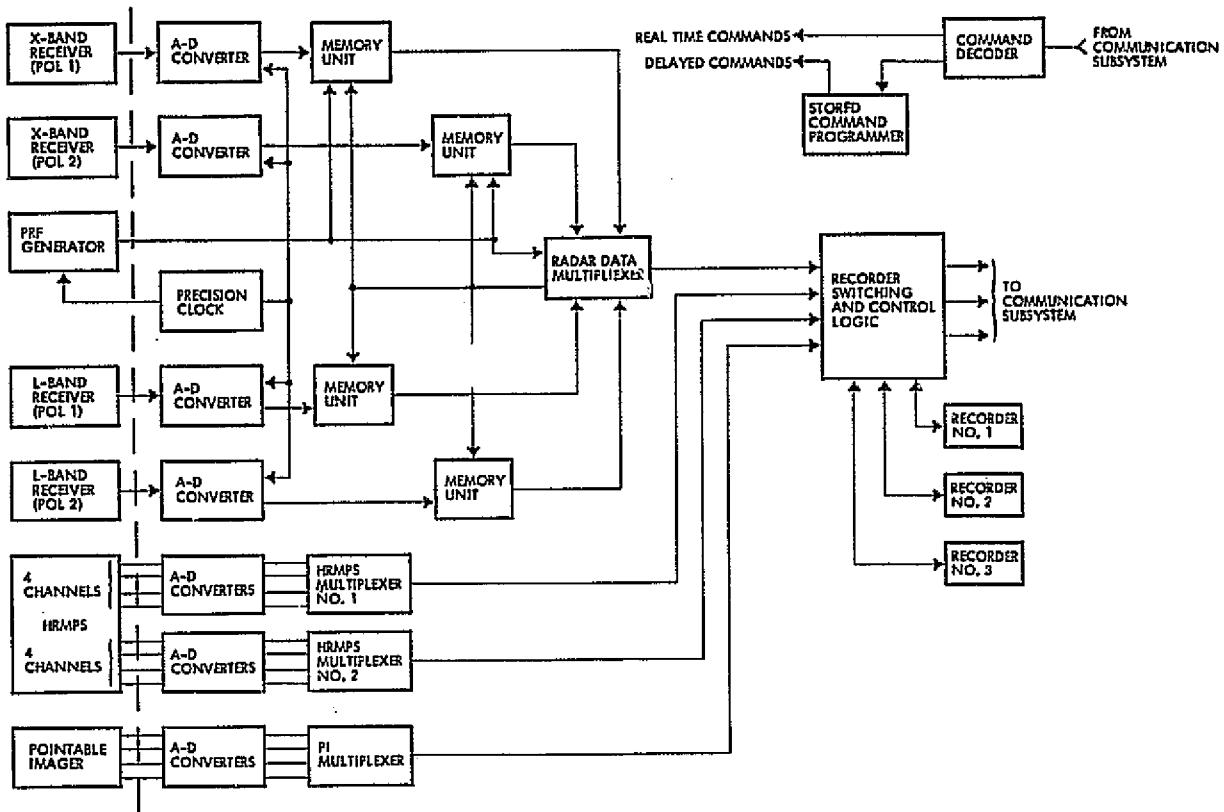


Figure 9-12. On-Board Data Handling Subsystem

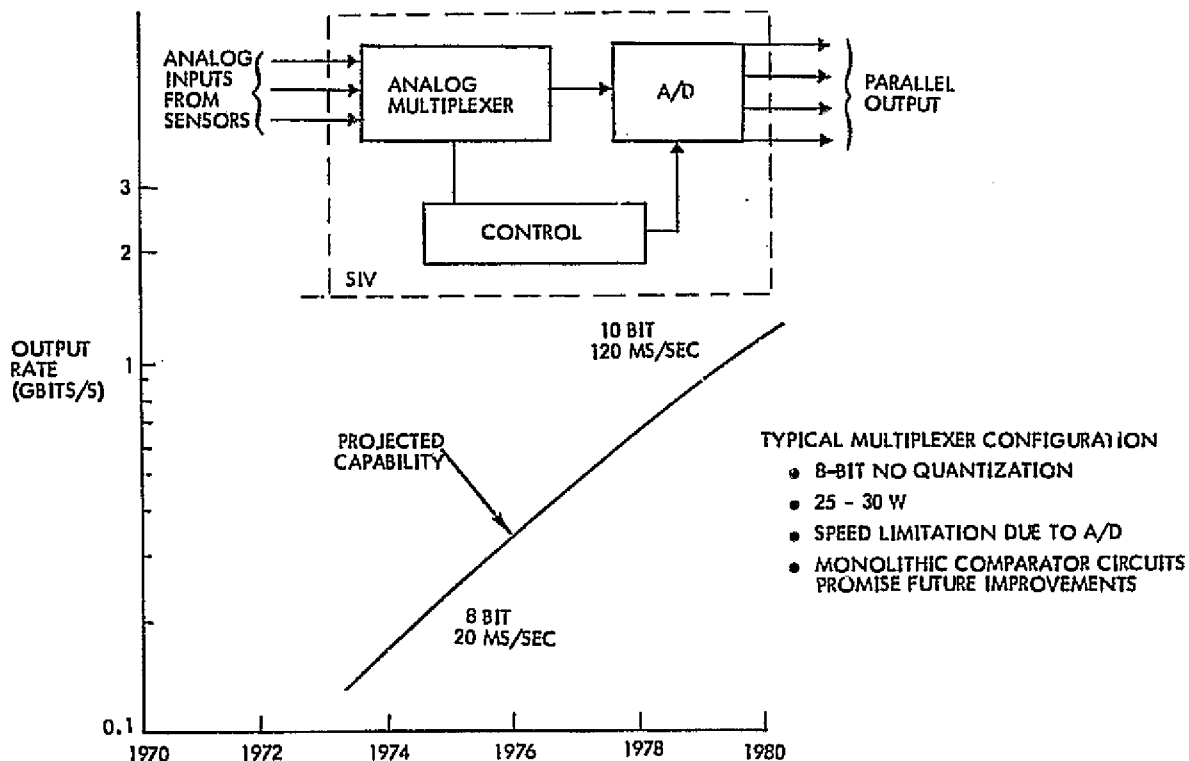


Figure 9-13. Sensor Interface Unit - Key Technology Item

Table 9-11. Projected Characteristics of Data Storage Devices

DATA STORAGE TECHNOLOGY	PARAMETER PRESENT ('74-75)/PROJECTED ('80)									
	CAPACITY (BITS)	PACKING DENSITY	DATA RATE (MBPS)	WEIGHT (KG)	POWER (W)	MTBF (HR)	ENVIRONMENTAL RESPONSE			
							TEMP	SHOCK	VIB	RAD
TAPE RECORDER	$10^9/10^{11}-10^{13}$	25/50	56/300	4/6	200	4×10^4	A	A	A	G
CCD	$10^7/10^9$	0.9/2 ($\times 10^6$ BITS/IN ²)	10/50-100	3/6	3/20	10^6-10^7	G	G	G	A
BUBBLE MEMORY ^①	$10^8/10^{10}$	1.5/100 ($\times 10^6$ BITS/IN ²)	0.6/10	4.5/7	4/5	10^{10}	A	G	G	G
PLATED WIRE	$10^6/10^7-10^8$	50/1000 ($\times 10^3$ BITS/IN ³)	0.5/1	15/70	20/40	②	A	A	A	C

① LABORATORY MODEL - 10^7 BITS

② DEPENDENT ON ELECTRICAL CONNECTION.

LEGEND:

G = GOOD
 A = ADEQUATE
 P = POOR

9.3.5 Communication System Design

The technique which shows the greatest benefit for transferring data collected at the satellite to the central processing facility at Sioux Falls is direct transmission over the Continental U.S. and relay via wide band tape recorder for Alaska, Hawaii and our island possessions. Analysis shows that such an approach minimizes cost because a TDRSS link is not required for the bulk of data anyway, and a tape recorder will cost less than separate ground stations for the two non-contiguous states and each possession.

The transmission link from satellite to Sioux Falls consists of three identical but independent channels each capable of supporting a 165 megabit data stream (Figure 9-14). Cross-strapping permits working around any multiple failures that may occur. The HRMPS data output is grouped such that four channels are delivered on one line and the remaining four on another line. The outputs from these lines can occupy two of the three transmission channels during daylight passes of the U.S. The PI output would normally occupy the third output. During night time passes the SAR would occupy one channel and two of the three tape recorders could be dumped. Since the data volume which must be recorded is much less than that sent real time, no data backup is anticipated.

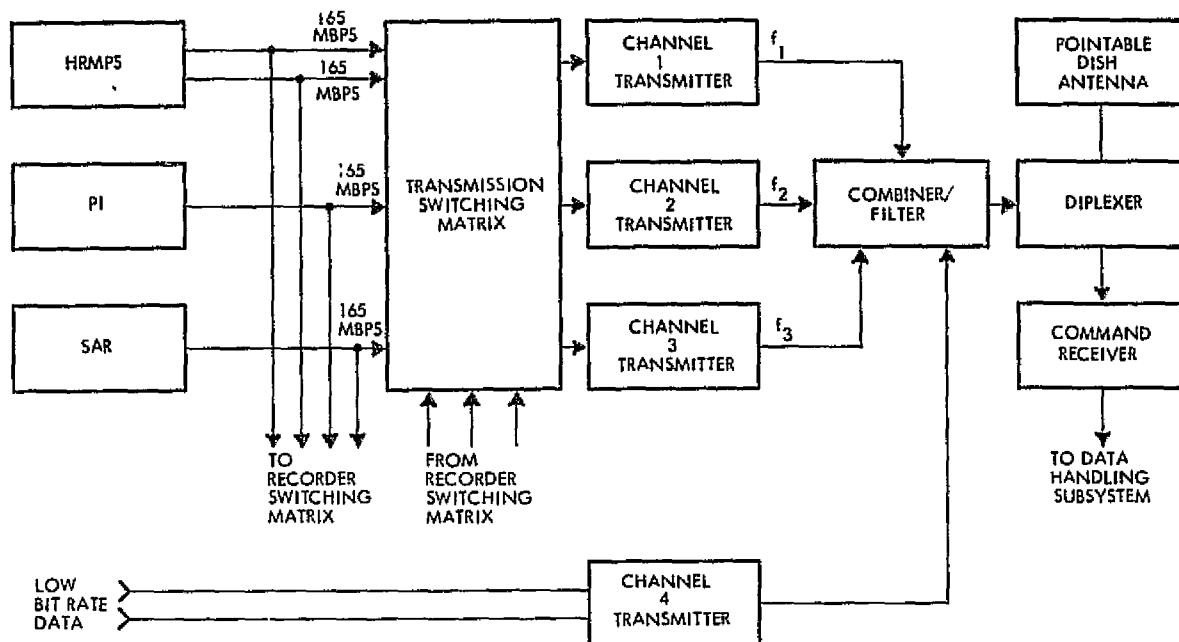


Figure 9-14. Mission 6 Communication System Configuration

A power budget which is representative of any of the three channels is given in Table 9-12. Assuming that a 30-foot antenna and a low noise parametric preamplifier are employed at Sioux Falls, a spacecraft transmitter power of 0.5 watt transmitting into a 1.7 foot pointable dish maintains reliable communication at the channel data rate.

Table 9-12. Mission 6 Power Budget (Each of Three Channels)

TRANSMITTER POWER (.5W)	- 3 DBW
TRANSMITTER LOSSES	- 2 DB
SPACECRAFT ANTENNA GAIN (1.7' DISH)	30 DB
EIRP	25 DBW
SPACE LOSS (3581.3 KM, X-BAND)	- 180.2 DB
ATMOSPHERIC LOSS	- 3 DB
RECEIVING ANTENNA GAIN (30' DISH)	53.7
RECEIVED SIGNAL POWER	- 104.5 DBW
BIT RATE (1 CHANNEL) (165 MBPS)	82.17
RECEIVED ENERGY/BIT (E_b)	- 186.67 DBW/HZ
RECEIVER NOISE SPECTRAL DENSITY (AT 184°K)	- 206. DBW/HZ
E_b/N_o	+ 19.33 DB
E_b/N_o FOR $P_E = 10^{-5}$ (PSK)	9.5 DB
RECEIVED $\frac{E_b}{N_o}$ - REQUIRED $\frac{E_b}{N_o}$	+ 9.83 DB
DEMOD. LOSSES	2 DB
TRUNCATION LOSSES	1 DB
SYSTEM MARGIN	6.83 DB

9.3.6 Ground Data Handling System

As discussed earlier, Mission 6 is an operational terrestrial survey-environmental quality mission with a constellation of three satellites. The data obtained by each collection platform is sent directly to a central data processing facility (CDFP) at Sioux Falls from distances exceeding 400 km off the coast of CONUS (see Figure 9-15). Territorial data re stored on tape recorders and dumped at night when the satellite is within view of CDFP. Processed data re transmitted to the users via a data dissemination satellite.

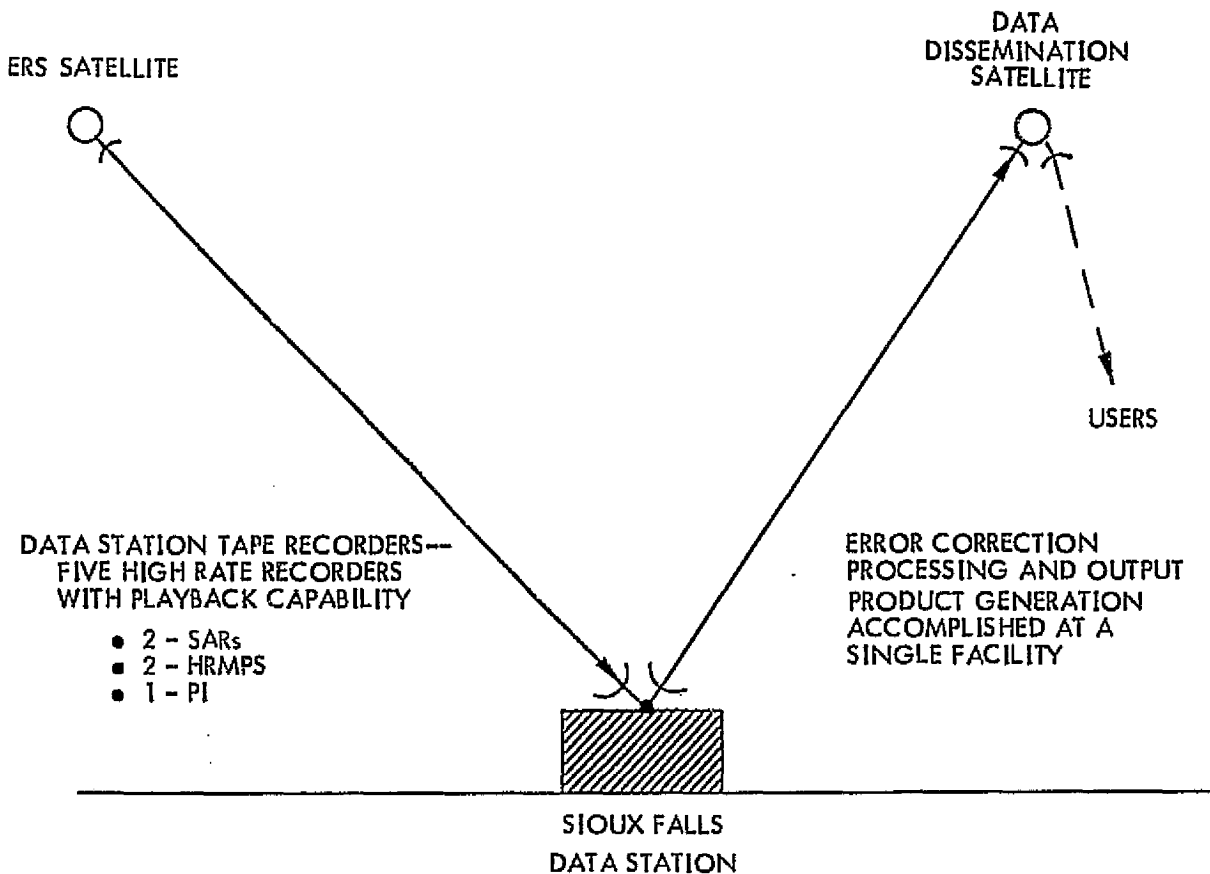


Figure 9-15. Data Routing for Mission 6

The characteristics of interest for the ground data handling system design driving sensors are listed in Table 9-13. The duty cycle for the SAR's is different than for the imagers. The SAR's gathers data over the United States at night and periodically may be used during daylight in place of an imager. HRMPS and PI maintain continuous daylight coverage over the United States.

Table 9-13. Sensor Characteristics Considered in the Ground Data Handling System Parametric Model

PARAMETERS	SENSORS		
	SAR	PI	HRMPS
DATA RATE (MBPS)	161.3	163.5	321.5
NUMBER OF DETECTORS	N/A	32000	48
ENCODING LEVEL (BITS/PIXEL)	6	6	7
SWATH WIDTH (KM)	110	48	425
RESOLUTION (M)	15.0	7.5	30.0

In Step 1 of the parametric model, the data volume, processing throughput, detector calibration memory, data frame volume and processing data volume were computed. Data volumes were based on the information in Figure 4-6. The resulting throughput rates were: SAR - $0.7 \mu\text{sec/pixel}$, PI - $2.0 \mu\text{sec/pixel}$, and HRMPS - $0.7 \mu\text{sec/pixel}$. In calculating the data frame volumes, the SARs were assumed to be sequentially processed. The image storage requirement used in determining the processing data volume was assumed to be the same as Mission 2, 0.5 percent. The resulting data handling volume requirements are summarized in Table 9-14.

Table 9-14. Data Handling Volume Requirements for Mission 6 Design Driving Sensors

PARAMETERS	SENSORS		
	SAR	PI	HRMPS
DATA VOLUME (Mb/DAY)	5.13×10^4	2.60×10^4	5.11×10^4
CALIBRATION DATA VOLUME (MBITS/DAY)	N/A	12.00	0.04
DATA FRAME VOLUME (MPIXELS/FRAME/DAY) (MBITS/FRAME/DAY)	2.16×10^2 (1.30×10^3)	2.05×10^2 (1.23×10^3)	1.74×10^3 (1.22×10^4)
PROCESSING DATA VOLUME (MBITS/DAY)	6.6	6.0	61.0

In Step 2, the assumption was made that one tape recorder was required for each 165 Mbps band of data. Five tape recorders are therefore required (see Figure 9-15) at a cost per unit of \$200K.

Three main processing structures, one for each instrument, were required to handle the throughput rate in Step 3. The input/output data memory costs were estimated to be:

- SAR 400K
- PI 400K
- HRMPS 500K

Step 4 determined the special purpose hardware requirements. As a result of this analysis two pieces of hardware were required for each sensor. The imagers would use one for along-line interpolation and one for across-line interpolation. The SAR also required two pieces, one for fast fourier transforms and one for convolutions or filtering. The cost for each piece was estimated to be 60K.

Step 5 determined the data correction and processing data memory requirements. The estimated costs were

	<u>Processing Memory</u>	<u>Calibration Memory</u>
• SAR	20K	
• PI	20K	10K
• HRMPS	200K	1K

The filmwriter and archiving requirements determined in Step 6 resulted in a cost of 2000K. Based on Table 8-2, a general purpose computer would cost 500K.

The costs for the CDPF are summarized in Table 9-15. The most significant cost drivers are tape recorders, input/output memory and archiving (~61 percent of the total cost).

9.3.7 Data Dissemination System Design

Distribution of the satellite data received at the Sioux Falls terminal may involve many routes and many data formats. To adequately define a distribution system will require specification of the following variables:

Table 9-15. Cost Summary for the Ground Data Handling System (\$ Thousands)

ITEM	UNIT COST	QUANTITY	TOTAL COST
TAPE RECORDERS	200	5	1000
INPUT/OUTPUT MEMORY	1300	-	1300
SPECIAL PURPOSE HARDWARE	60	6	360
PROCESSING DATA MEMORY	240	-	240
CALIBRATION DATA MEMORY	100	-	100
MINICOMPUTER SYSTEMS	100	3	300
FILMWRIER	200	1	200
ARCHIVING	1800	-	1800
GENERAL PURPOSE COMPUTER	500	1	500
TOTAL			5800

- 1) The average data rate received by the Sioux Falls station.
- 2) The number of formats and the percentage of the total data required by the various users.
- 3) The location of all users and their specific data needs (format, frequency, coverage, etc.).
- 4) Possible reduction of total data throughput due to cloud cover or the use of compression techniques.

The maximum possible data input from the Mission 6 satellite may be computed as follows (see Figure 9-16):

$$\begin{aligned}
 D_{\max} &= \text{Bit Rate} \times \frac{\text{Time}}{\text{Pass}} \times \frac{\text{Passes}}{\text{Day}} \\
 &= (495 \times 10^6) \times (6.09 \times 60) \times 12 \\
 &= 2.1705 \times 10^{12} \text{ bits/day}
 \end{aligned}$$

which yield an average data rate from Conus data of approximately 25 Mbps. Alternatively, the total area of interest represents approximately 2 percent of the earth's surface. Hence the data can be stretched by a

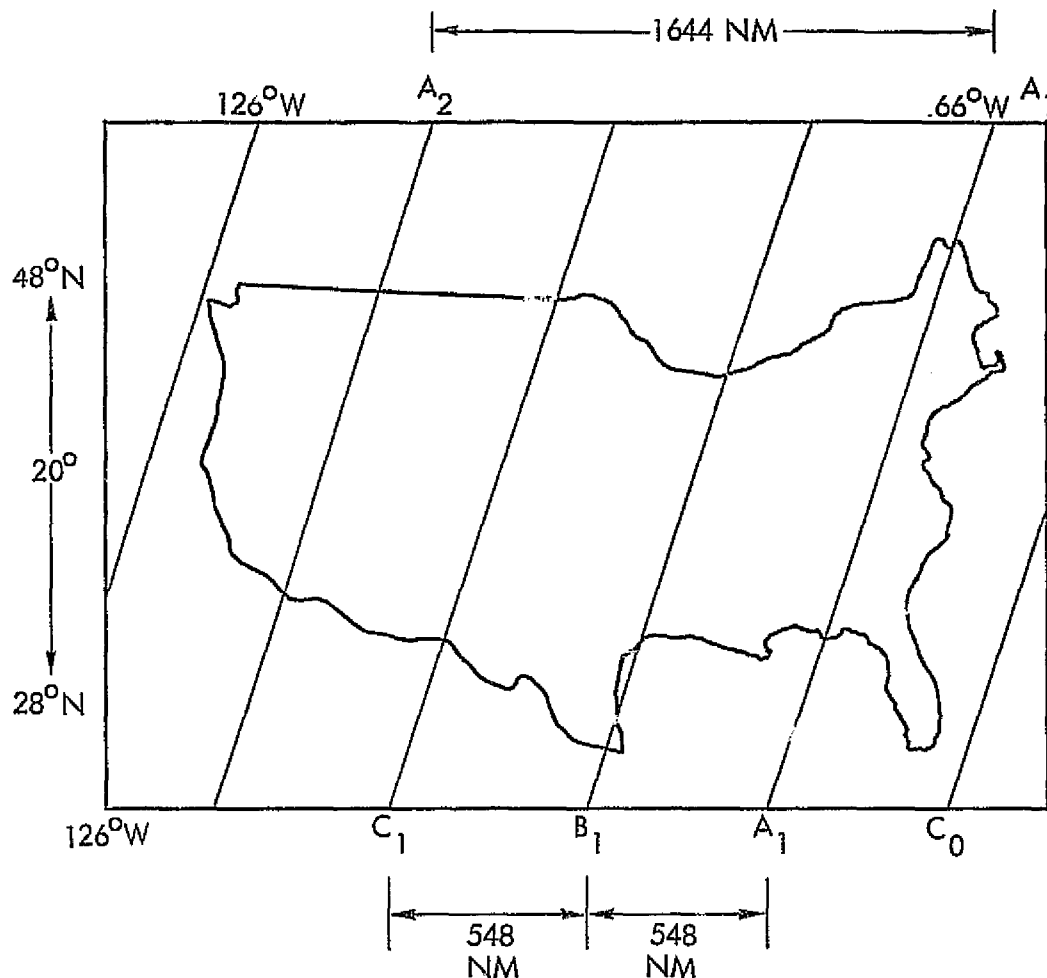


Figure 9-16. Coverage of CONUS Per Day

factor $98/2$ or 49 and the stretched data rate would be $\frac{495}{49} = 10.1$ Mbps. A compromise value of 15 Mbps will be taken to represent the average data rate.

Modelling the users and their specific data needs is a difficult task. There are several types of users which have been identified:

- 1) Large archiving and processing centers of various agencies in the Washington, D.C. area. Presumably these centers will want all of the data received either in raw form or in a multiplicity of formats.
- 2) Moderate regional centers of the various government agencies which will want regional data, processed and in a multiplicity of formats.
- 3) Small users (counties, cities, etc.) which will want a very small amount of data but also in a multiplicity of formats.

User locations include all of Conus, Alaska, Hawaii, and U.S. territories. To distribute high bit rate data over such a wide geographic area suggests the use of a synchronous data dissemination satellite. Figure 9-17 shows the possible coverage of such a satellite when located at 120°W. Assuming that this coverage includes all potential users, this

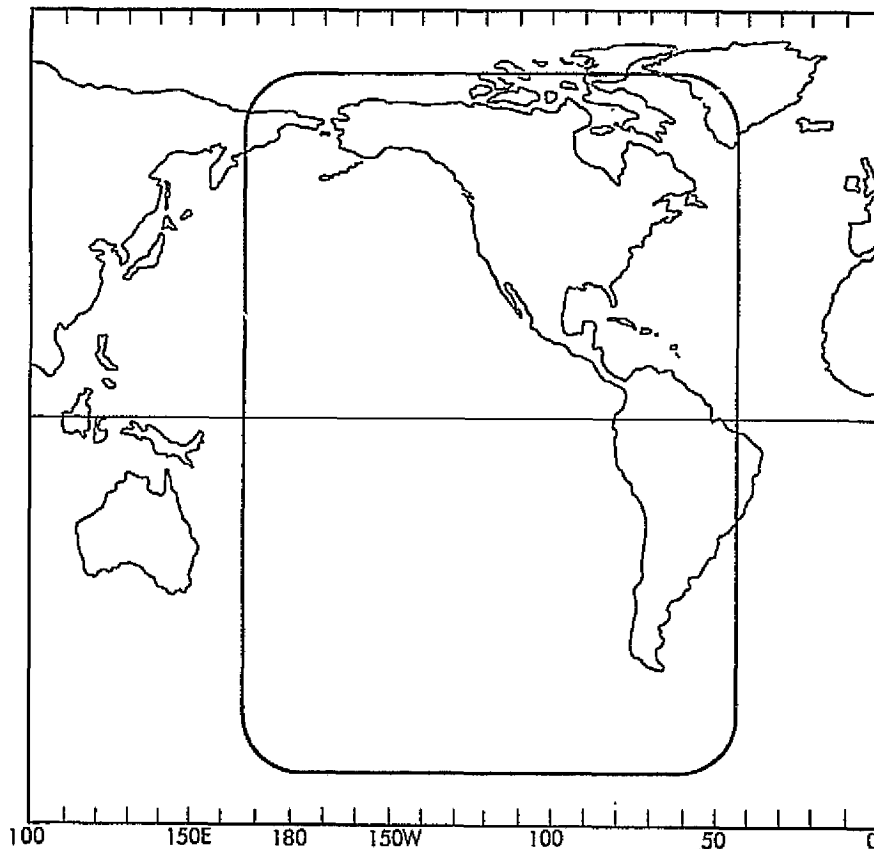


Figure 9-17. Data Dissemination Satellite Coverage

method of distributing data will be analyzed further. The small and moderate data users will be the limiting cases. For these users, the following assumptions apply:

- 1) Divide Conus into 10 regions (Figure 9-18) plus two additional for Alaska and Hawaii plus eight additional for territories (total of 20 regions).
- 2) Limit small user antenna diameter to 15 feet (fixed pointing).
- 3) All regional data transmitted in a maximum of six different formats.

With these assumptions it is possible to proceed with the description of a data dissemination system.

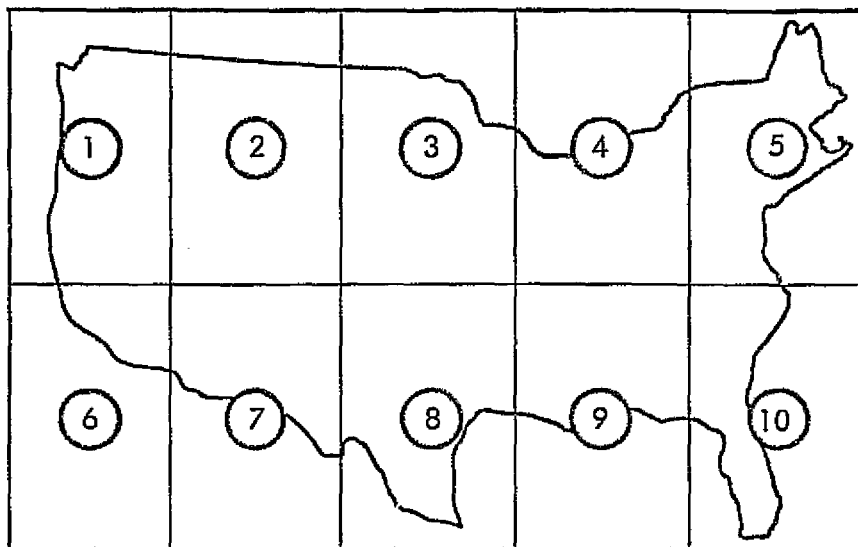


Figure 9-18. CONUS Data User Regions

Figure 9-19 shows one approach to the configuration of a data distribution satellite. Here it is assumed that all data leaving Sioux Falls will be processed and formatted to satisfy the various users. The EIRP required to transmit $6 \times 15 = 90$ Mbps from synchronous altitude is

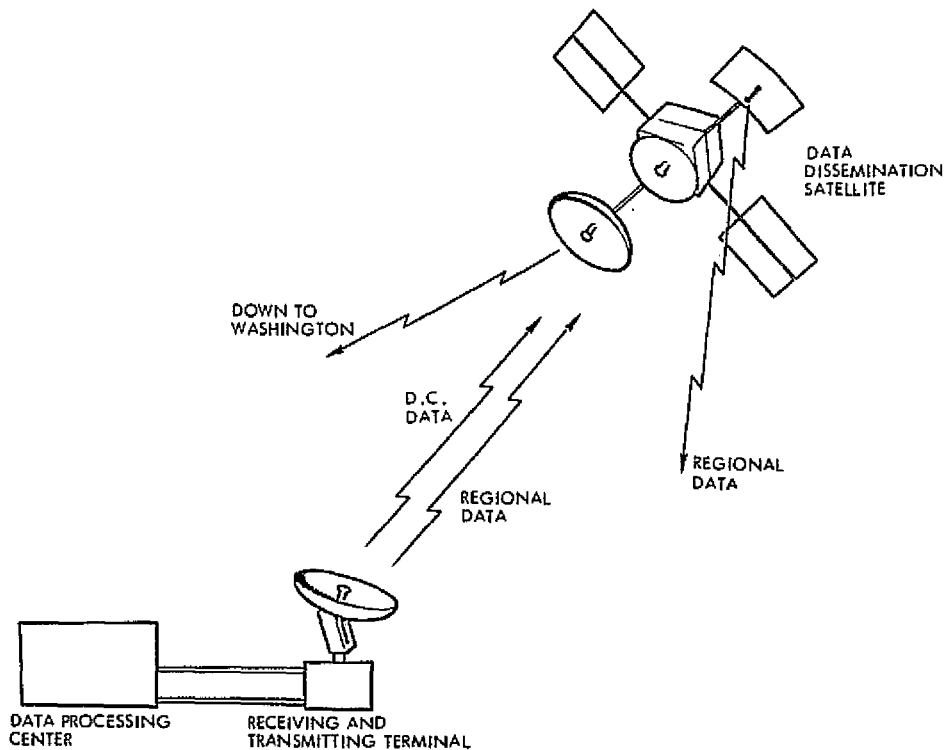


Figure 9-19. Data Dissemination Satellite Configuration

42 dbw (see Table 9-16) when operating at X-band into a 15-foot dish, but with no system margin. With 4 db system margin, the EIRP required is 46 dbw. The gain of an antenna (see Figure 9-20) which approximately

Table 9-16. Small Data User - Link Power Budget

1. DEMODULATOR LOSS	1.0 DB
2. SPECTRAL TRUNCATION LOSS	2.0 DB
3. E_b/N_0 REQUIRED FOR $P_E = 10^{-5}$	9.5 DB
4. E_b/N_0 REQUIRED	12.5 DB
5. RECEIVER NOISE DENSITY (N_0) FOR $T = 184^{\circ}K$	-206 DBW/Hz
6. REQUIRED ENERGY/BIT (E_b)	-193.5 DBW/Hz
7. BIT RATE (90 MBPS)	79.5 DBW - Hz
8. RECEIVED SIGNAL POWER REQUIRED	-114.0 DBW
9. RECEIVER ANTENNA GAIN (15 FOOT-DISH)	+ 51 DB
10. ATMOSPHERIC LOSSES	- 3 DB
11. SPACE LOSS (19,323 N.M. and 10 GHz)	-204 DB
12. REQUIRED EIRP (NO MARGIN)	41 DBW
13. TRANSMITTER LOSSES	- 2 DB
14. GAIN x POWER	43 DBW
15. SYSTEM MARGIN	4 DB
16. NEW $G_T \times P_T$	47 DBW
17. SHAPED ANTENNA GAIN (G_T)	42 DB
18. REQUIRED POWER (3.2 WATTS)	5 DBW

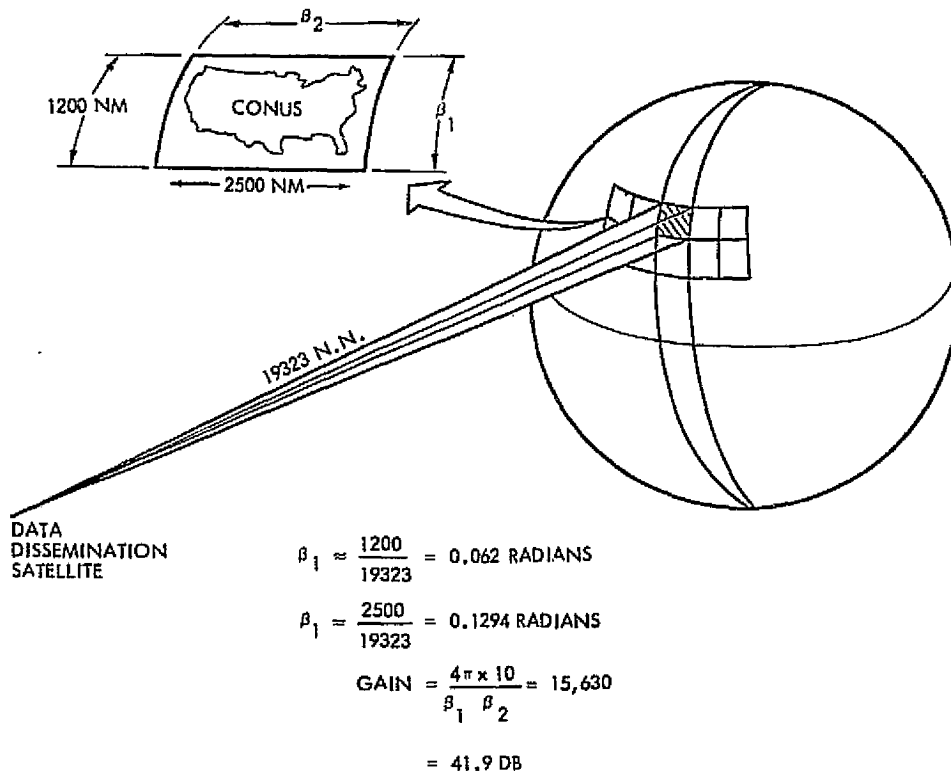


Figure 9-20. Regional Coverage Antenna Gain

covers one of the 10 regions of Conus is 42 db. Hence with 3.2 watt of transmitter power it is possible to provide six data formats to each of the regions of interest.

To recap the capabilities of the data dissemination satellite:

- All data will be transmitted from Sioux Falls in processed, formatted form
- All data will be transmitted via a dedicated link to Washington, D.C.
- Any user within view of the satellite can receive all of his regional data in six different formats with a 15-foot fixed dish.

Figure 9-21 is an abbreviated block diagram of the Mission 6 end-to-end data system. Details of the on-board data handling and communication subsystems may be found on Figures 9-17 and 9-19, respectively. Although this spacecraft is scheduled to fly in 1984, the proposed design reflects a minimal use of new/advanced technology items. This is due in part to the operational character of the mission which dictates the use of flight-proven hardware where possible.

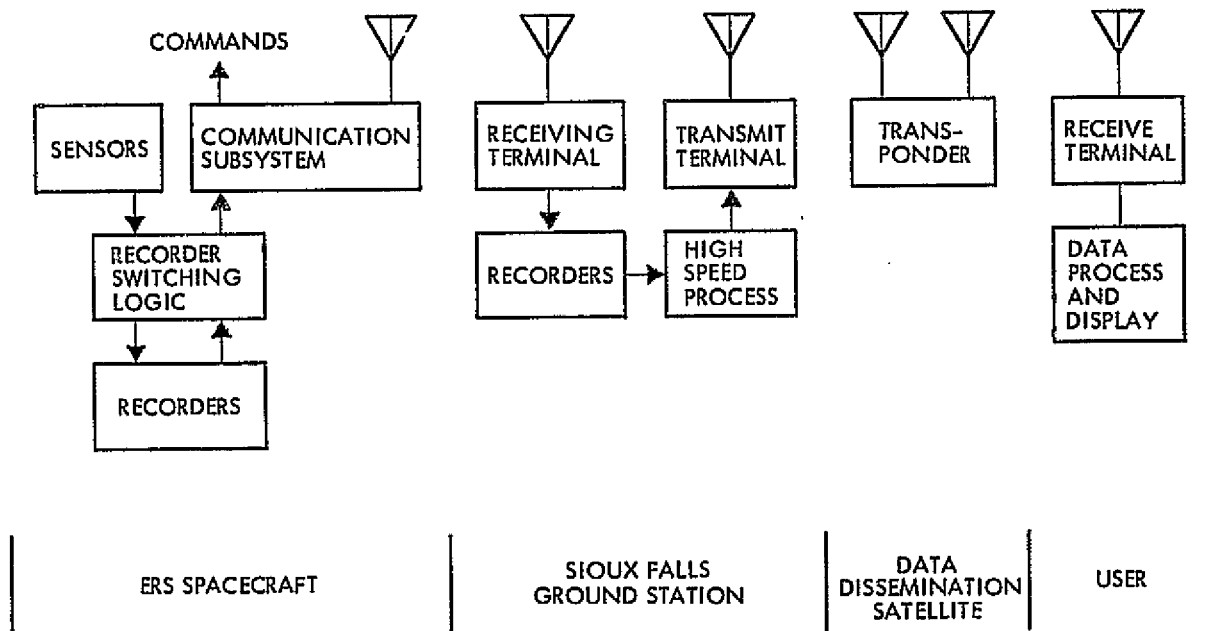


Figure 9-21. Mission 6 System Block Diagram

Recording data acquired over territories and states outside the CONUS will require tape recorder development. As shown in Figure 9-17, the proposed recorders will accept a 165 MBPS data stream. If such a

device is not developed by 1984, it would be a simple task to reconfigure the sensor outputs into 16 data streams each operating at a bit rate of approximately 40 MBPS. Of course this would require 12 machines to duplicate the capability shown, but weight would not be a concern. If this configuration was seriously considered, the cost effectiveness of other data processing alternatives might prove to be attractive.

Timely distribution of high data rate and high volume data over a wide geographic area is one of the most challenging aspects of this mission. Several options are obvious:

- 1) Transmit raw data in real time to local users.
- 2) Process on-board and transmit directly to local users.
- 3) Transmit raw (or processed) data to the ground via TDRS; distribute to local users.
- 4) Transmit, process-on-ground, receive/record processed data, retransmit to local user.
- 5) Transmit, process-on-ground, distribute to local users.

Choosing the most cost-effective option depends to a great extent upon the definition of the users. Options 1 and 2 may be selected if the users are few in number (say 3 to 5) and there are no central data stations where all data is required. Option 3 is probably not an acceptable use of TDRS and still leaves the distribution problem to be solved. Option 4 adds a significant data delay in the system and places the recorders in-line for all user data. Option 5, the proposed system configuration, is based on the use of a dedicated satellite which will receive and broadcast data into many small local ground stations. This option was judged to be the only reasonable solution to meeting the demands (perishability, formats, etc.) of a large number of local users disbursed over a wide geographical area.

9.4 Mission 9

9.4.1 Mission Requirements

Mission 9 is designed to provide high resolution data on a frequent basis to aid meteorologists in the detection, monitoring and prediction of dynamic weather systems in tropical latitudes. As such, this is a research and development mission dedicated to meteorology. Multistage

sampling will be accomplished through the use of complementary data supplied by geostationary, low resolution, broad perspective meteorological satellites.

The launch data for Mission 9 is FY 1987. Its sensor complement includes:

- Synthetic aperture radar
- Passive multifrequency microwave radiometer
- Constant resolution meteorological scanner
- Advanced atmospheric sounder
- Data collection and location system.

The mission independent instrument characteristics are depicted in Table 9-17. As in the previous missions, swath width, IFOV, pointing capability and resolution were determined as part of the mission design. (See Section 9.4.2).

The mission must be optimized for routine surveillance of dynamic weather systems in the tropical latitudes at coverage frequencies which satisfy the user observation requirements. Table 9-18 summarizes the data requirements for each data use and indicates the utility of each instrument.

The research and development nature of this mission implies that near raw data should be sent directly to the user for specialized data analyses and interpretation.

9.4.2 Orbit/Satellite - Constellation Design

The basic areal coverage desired for this mission is approximately 14 degrees North and South of the equator. If the satellite flies in an equatorial orbit, the SAR cannot cover this area, but instead will provide one or two strips close to the equator. To approach the desired coverage it is necessary to incline the satellite orbit.

Figure 9-22 shows the coverage pattern of the SAR based on the use of an antenna which provides a swath on both sides of the satellite. To insure complete overlap of the two beams at the equator requires the

Table 9-17. Sensor Complement for Mission 9

INSTRUMENT	DISCIPLINE	APPLICATION	TYPE OF SCAN	SPECTRUM/BANDWIDTH (MICRONS)	ERROR SOURCES	UNIQUE DATA PROCESSING REQUIREMENTS
SYNTHETIC APERTURE RADAR	EARTH RESOURCES	GEOLOGICAL SURVEY, LAND USE MONITORING, WATER, ICE MONITORING	ALONG TRACK - SPACECRAFT MOTION ACROSS TRACK - RANGE DISCRIMINATION	X-BAND/15MHz, DUAL POLARIZATION L-BAND/15MHz DUAL POLARIZATION	GEOMETRIC: • SPACECRAFT ATTITUDE • EARTH ROTATION EFFECTS • SLANT RANGE DISTORTION	AZIMUTH DATA PROCESSING REQUIRED TO ACHIEVE AZIMUTH RESOLUTION. COMPENSATION FOR EARTH ROTATION AND GEOMETRIC EFFECTS
ADVANCED ATMOSPHERIC SOUNDER	METEOROLOGY	TEMPERATURE PROFILES FOR NUMERICAL MODELS AND LOCAL AREA FORECASTS OF POLLUTION TURBULENCE, FOG ETC.	±40°, CROSS TRACK SAMPLES 400KM APART	8 CHANNELS - 15 BAND 4 CHANNELS - 4, 3 1 CHANNEL - 9.6 1 CHANNEL - 11.1 2 CHANNELS - 3.8 3 CHANNELS - 18-30 10 CHANNELS IN MICRO-WAVE NEAR 60 GHz	RADIOMETRIC: • CALIBRATION • DETECTORS, NOISE EQUIVALENT POWER • ATMOSPHERIC ABSORPTION COEFFICIENTS	
PASSIVE MULTICHANNEL AND MICROWAVE RADIOMETER	COASTAL OCEANOGRAPHY AND METEOROLOGY	SEA SURFACE TEMPERATURE AND ROUGHNESS, SEA ICE, WATER VAPOR AND LIQUID WATER IN TROPOSPHERE	CONICAL, APPROXIMATELY 40° FROM NADIR, 1 FREQUENCY (10.7 GHz) CONICAL, APPROXIMATELY 60° FROM NADIR, 2 FREQUENCIES (18 GHz)	4.99 GHz/0.6 GHz 10.7 GHz/0.6 GHz 18.0 GHz/0.6 GHz 21.5 GHz/0.6 GHz 37.0 GHz/0.6 GHz ALL FREQUENCIES DUAL POLARIZATION	GEOMETRIC: • SPACECRAFT VARIATIONS • SCANNING VARIATIONS RADIOMETRIC: • CALIBRATION • ATMOSPHERIC • SIDE LOBES	INVERSION OF DATA TO SEPARATE EFFECTS OF TEMPERATURE, ROUGHNESS, EMISSIVITY, LIQUID WATER AND WATER VAPOR IN ATMOSPHERE AND WATER ICE COVERAGE. CONVERSION OF CONICAL SCAN TO RECTANGULAR GRID FOR DESIRED PROJECTION.
CONSTANT RESOLUTION METEOROLOGICAL SCANNER	EARTH OBSERVATIONS	NEAR REAL-TIME INPUT TO EARTH OBSERVATIONS COMPUTER MODELS, GLOBAL CLOUD COVER IMAGERY	TYPE OF SCAN CONTINUOUS CROSS TRACK 25.5°	0.4 TO 1.1 8 TO 13	GEOMETRIC: • LESS THAN ONE RESOLUTION ELEMENT RADIOMETRIC: • LESS THAN 5 PERCENT ROOT SUM SQUARE	PROVIDE HIGH RESOLUTION DATA IN TERMS OF SCENE RADIANCE WHICH CAN BE USED IN SHORT-TERM (<6 HOURS) FORECASTING COMPUTER PROGRAMS.

Table 9-18. Summary of the Data Requirements and Applicable Instruments for Each Data Use in Mission 9

DATA USE	INSTRUMENTS				DATA REQUIREMENTS SUMMARY										
	SYNTHETIC APERTURE RADAR	PASSIVE MULTICHANNEL MICROWAVE RADIOMETER	CONSTANT RESOLUTION METEOROLOGICAL SCANNER	ADVANCED ATMOSPHERIC SOUNDER	OBSERVATION FREQUENCY (DAYS BETWEEN LOOKS)	PERISHABILITY OF DATA (DAYS)	OVERLAY	SPECIAL MEASUREMENTS	PHOTOMAPS	THEMATIC MAPS	AUTOMATED INVENTORY	GEOMET. REF. SPAT. MEAS.	STATISTICAL SUMMARIES	AUTO. CHANGE DISCRIMINATION	INPUT TO MATH MODELS
SEA SURFACE TEMPERATURE	S	P			1	1-4	•								
SEA SURFACE CURRENTS		S			2	2-5	•								
SEA SURFACE ROUGHNESS		P			1/3-1	1	•								
CLOUD COVER	P	P		P	1/2	1/6	•								
PRECIPITATION	P				1/2-1		•								
OCEANIC RADIATION BUDGETS		P			1		•								
EARTH RADIATION BUDGETS		P			1		•								
CLOUD PHYSICS	S	S		S	1		•								
UPPER ATMOSPHERIC TEMPERATURE				S	2	1	•								
UPPER ATMOSPHERIC COMPOSITION				S	2	1	•								
SEA SURFACE POLLUTION	S				1/4-14	1-14	•								
SEVERE STORM WARNING	P	P		P	1/2-1	1/6	•								

P = PRIMARY APPLICATION, S = SECONDARY APPLICATION
 RANGE COVERING COASTAL TIDAL CYCLE

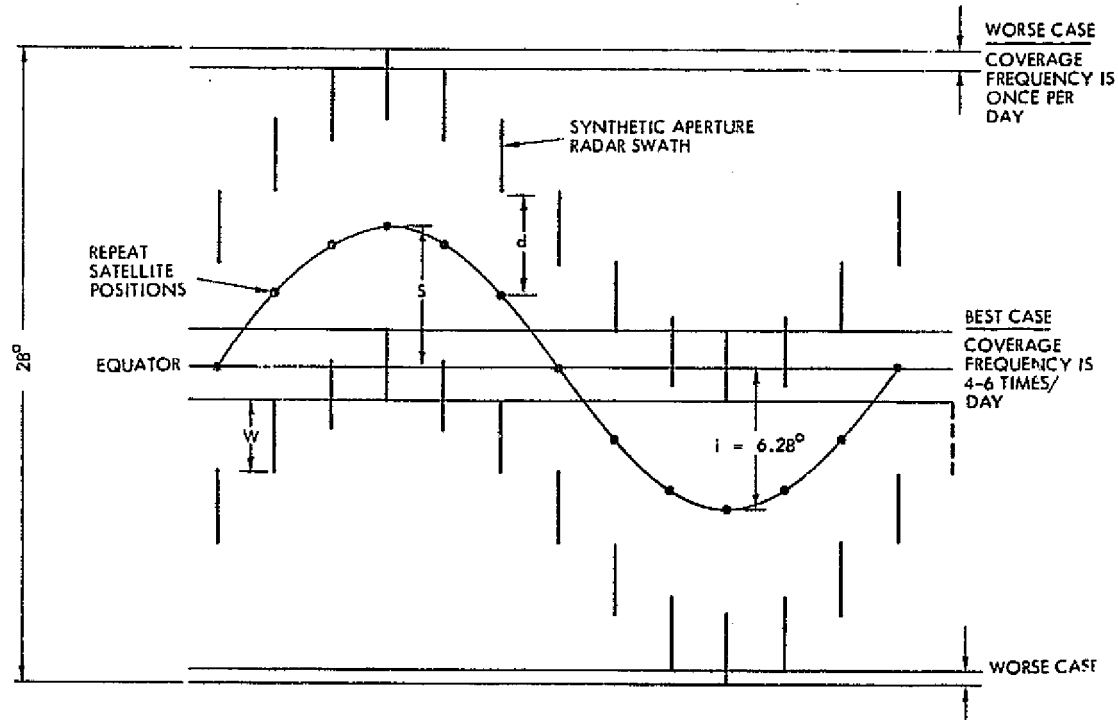


Figure 9-22. Coverage Pattern as a Function of Time for a Given Longitude of the Synthetic Aperture Radar for Mission 9

geometry as shown in Figure 9-23. From this Figure it is possible to derive the following relationships:

$$S = d + \frac{W}{2}$$

$$L = 2S + \frac{W}{2}$$

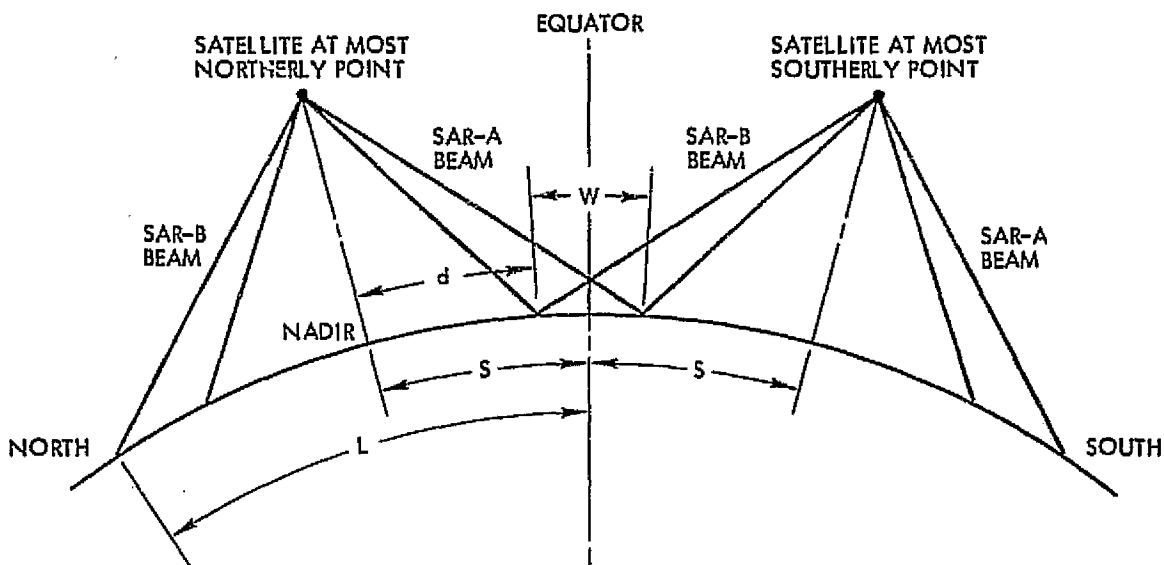


Figure 9-23. View of Orbital Geometry Looking East

To ensure that successive swaths of the same SAR do not leave a gap as the satellite crosses the equator, it is necessary that the orbit-orbit spacing not exceed W or

$$S \sin \frac{2\pi}{N} = W$$

where N is the number of equatorial crossings around the circumference of the earth (assuming that an orbit is selected which repeats the same ground traces on a daily basis). If $N = 11$ is selected, then the orbital altitude can be computed since

$$Q = N + 1 = 11 + 1 = 12$$

$$H = \left(\frac{6.617}{Q^{2/3}} - 1 \right) R_E$$

$$= 1673.8 \text{ KM}$$

To cover +14 degrees of latitude requires that the distance L be equal to 1558.3 KM. Selecting a swath width W of 320 KM yields

$$S = 1/2 \left[L - \frac{W}{2} \right] = 1/2 \left[1558.3 - 160 \right]$$

$$= 699.2$$

$$\text{and } d = S - \frac{W}{2} = 699.2 - 160$$

$$= 539.2 \text{ KM}$$

To provide a 10 KM margin on the overlap, the following values will be used:

$$d^1 = 530 \text{ KM} = (d - 10) \text{ KM}$$

$$W^1 = 340 \text{ KM} = (W + 20) \text{ KM}$$

$$L = 1568 \text{ KM}$$

$$S = 700 \text{ KM}$$

Hence the orbit inclination is: $\left(\frac{S}{RE} \right) \left(\frac{\pi}{180} \right)$ or 6.28 degrees.

The performance of Mission 9, with the orbital characteristics mentioned above, is evaluated in Figure 9-24 in terms of observation requirement. All of these requirements are satisfied by at least one primary instrument.

DATA USE

- SEA SURFACE TEMPERATURE
- SEA SURFACE CURRENTS
- SEA SURFACE ROUGHNESS
- CLOUD COVER
- PRECIPITATION
- OCEANIC RADIATION BUDGET
- EARTH RADIATION BUDGETS
- CLOUD PHYSICS
- UPPER ATM TEMPERATURE
- UPPER ATM COMPOSITION
- SEA SURFACE POLLUTION
- SEVERE STORM WARNING

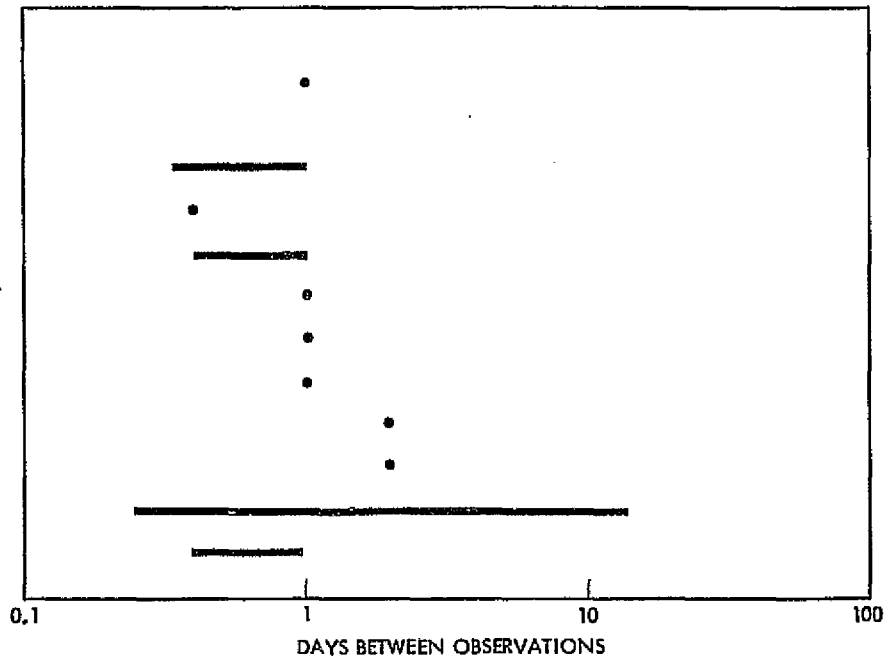


Figure 9-24. A Comparison of the Coverage Frequency of the Mission 9 Sensors in a 1674 km, 6.3 Degree Orbit and the Observation Frequency Requirements

9.4.3 Sensor Design

9.4.3.1 SAR Design

The geometry of Figure 9-25 is appropriate for establishing key parameters in the SAR design. It should be noted that the actual swath of the

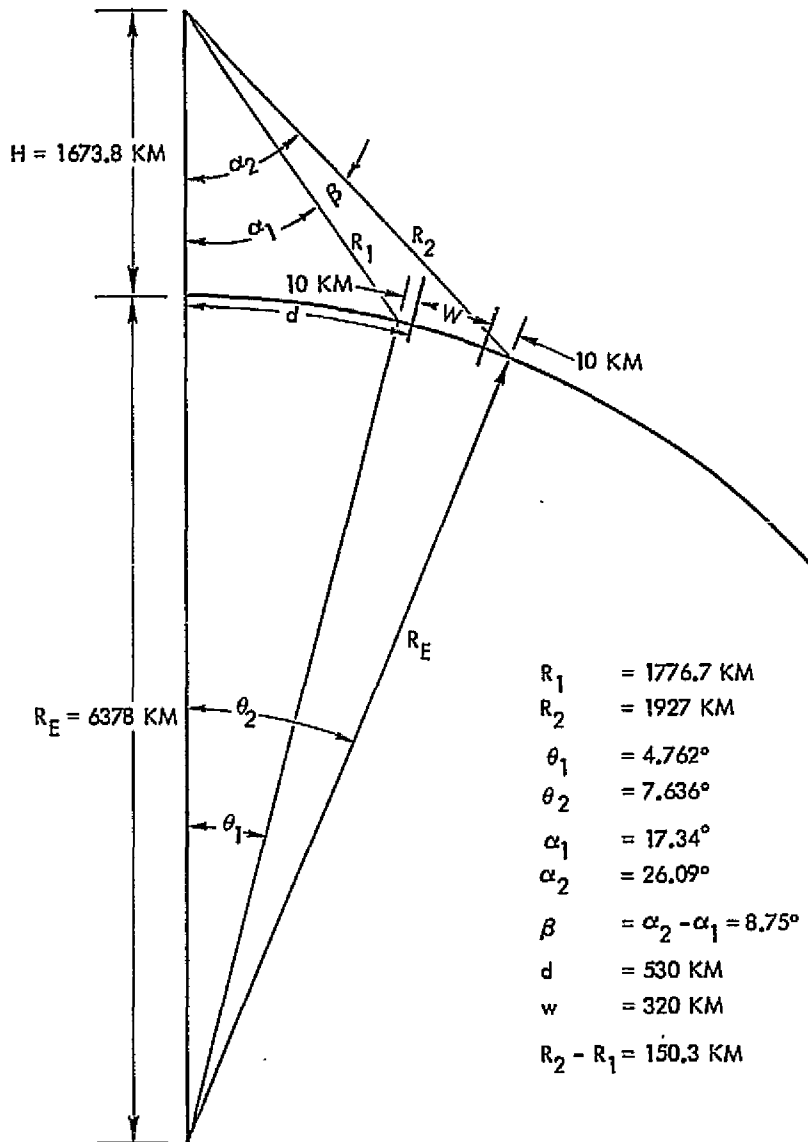


Figure 9-25. SAR Geometry for Mission 9

SAR has been increased over W by 10 km on each side to provide overlap. Using the geometry in this figure one can determine that $R_1 = 1776.7$ km and $R_2 = 1927$ km. The round trip times for these values are 11,844.6 and 12,846 microseconds, respectively. The time difference here is 995.4 μ sec. A pulse repetition interval of 1073.5 μ sec, i.e., 931.5 pulses

per second ensures that the total echo lies between the sixth and seventh pulses transmitted after the one whose echo is being received.

Because there are two SAR's on board, each will have a PRF of half 931.5 or 465.75 pps. In the interval between pulses from each SAR the spacecraft will have advanced 15.085 meters at the orbital velocity of 7.026 km/sec. The SAR antenna should then be twice this long or 30.17 meters.

Antenna size can be determined by evaluating the transverse beam width at the spacecraft. Again using the geometry of Figure 9-25 we determine that the inner beam edge is 17.34 degrees from nadir and the outer beam edge is 26.09 degrees from nadir. By use of the relationship $\beta = K \left(\frac{X}{L} \right)$ (degrees) where $K = 50$ for uniform aperture illumination, it is possible to find the transverse antenna length. Thus, the transverse beam width is seen to be 8.75 degrees at X-band, this corresponds to an antenna width perpendicular to the beam of about 17.1 cm, and at L-band of about 132 cm. Upon orienting the antenna horizontally as was done for Mission 6 the antenna widths become: 18.5 cm at X-band and 142 cm at L-band. Data rate for one SAR is found by calculating the number of range cells and multiplying by the PRF, $\frac{340 \times 10^3}{15} = 22,666$ range cells, $22666 \times 465.75 = 10.6$ mega samples/sec. For 6-bit encoding, two radars, and 4 modes (dual frequency and dual polarization) the data rate equals approximately 506.8 megabits/second. Average power for each X-band SAR is found to be about 263 watts while power for each L-band SAR is about 34 watts. Uncompressed pulse duty cycle is about 21,000 so that pulse compression is called for.

9.4.3.2 Passive Microwave Radiometer

The passive microwave radiometer which gives a measure of ocean surface temperature and roughness may use one of two conical scans (see Figure 9-26. One intersects the surface at 40 degrees and the other at 60 degrees from vertical. Both beams scan over ± 40 degrees from the orbital velocity vector. Scanning is accomplished electronically by a phased array 15 meters by 30 meters lying horizontally under the spacecraft. Five frequencies are scanned at each angle. One scan of ± 40 degrees is accomplished in 1000 steps. The dwell at each step is 0.5 ms. This yields samples collected on approximately a 2.5 km spacing grid. The

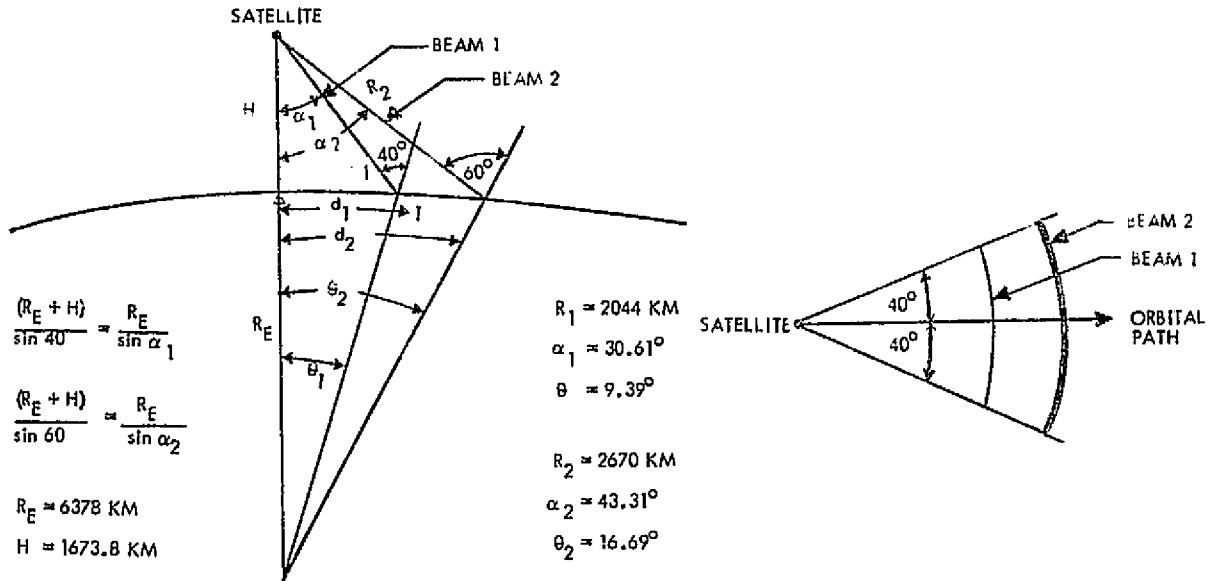


Figure 9-26. Passive Microwave Radiometer Geometry and Scan Pattern

data rate for each channel is 2000 samples per second. Nine bit encoding yields a bit rate of 18,000 bits/sec/channel. The five frequencies each have two polarizations and two beams and hence the system data rate is 360 kb/sec.

9.4.4 Communication System Design

Previous discussions have shown that the SAR is the prime generator of data, operating at 253.4 Mb/sec, all sensors together can be handled with a communication system capable of 510 Mb/sec. The perishability of the data indicates the need for a real time link. The orbit altitude and inclination make TDRSS the logical candidate for accomplishing this real time data gathering. At the 1673.8 km altitudes there will be no blind spots in the TDRSS coverage. The single access Ku-band channel will adequately handle the data rate.

A 30 watt Ku-band amplifier and an 8 foot antenna accomplish transmission with the required margin. Two antennas could be employed for redundancy and to handle the hand-over between relay satellites without data dropouts. The antenna outer gimbals will be along the pitch axis and will require ± 130 degrees of motion from the equatorial plane. No gimbal lock condition occurs. In the 1987 time frame, solid state amplifiers at Ku-band can be expected to develop the required power.

9. 4. 5 Ground Data Handling System

Mission 9 is similar to Mission 2 in that it is a research mission gathering meteorological data using a single data collection platform. However, Mission 9 obtains frequent observations of highly dynamic tropical phenomena through the use of a near-equatorial orbit whereas Mission 2 obtains, at best, two observations per day over CONUS and territories. Because of the perishability of the Mission 9 data, TDRS is used to relay the data to a CDPF at White Sands in real time. The processed data is then distributed to the users via a data dissemination satellite (see Figure 9-27).

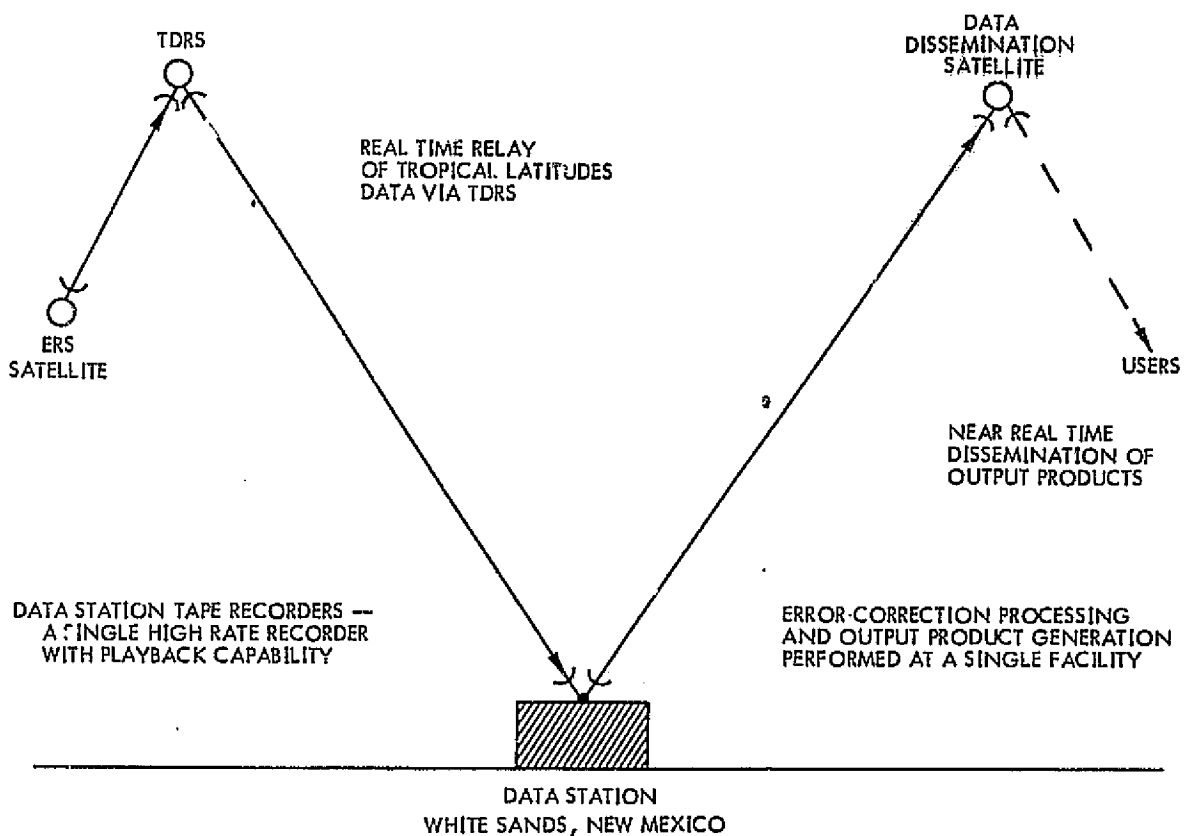


Figure 9-27. Data Routing Scheme for Mission 9

The characteristics of interest for the ground data handling system design driving sensors are shown in Table 9-19. The SARs acquire intermittent data, day or night (approximately 10 percent of total time). The PMMR and CRMS operate approximately 33 percent of the total time (for basic areal coverage--day and night--every six hours).

Table 9-19. Sensor Characteristics Considered in the Ground Data Handling System Parameter Model

PARAMETER	SENSORS		
	SAR	PMMR	CRMS
DATA RATE (Mbps)	125	0.36	1.00
NUMBER OF DETECTORS	N/A	20	3676
ENCODING LEVEL (BITS/PIXEL)	6	9	6
SWATH WIDTH (KM)	320	1450/2557*	3060
RESOLUTION (m)	30	2500	830

* 1450 KM FOR THE 40 DEGREE CONE
2557 KM FOR THE 60 DEGREE CONE

As in the previous applications of the parametric model, Step 1 determined the data volume, processing throughput, detector calibration memory, data frame volume and processing data volume. The resulting throughput rates were:

- SAR: 0.18 μ sec/pixel
- PMMR: 50.0 μ sec/pixel
- CRMS: 12.0 μ sec/pixel

The data handling volume requirements are listed in Table 9-20; they are based on the data in Table 9-19 and the throughput rates. The SARs and PMMR cone angles were each processed sequentially. With respect to the PMMR, the larger cone angle was used as a design driver. The image storage requirement was assumed to be the same as in the other missions, 0.5 percent

In Step 2, a single tape recorder with a playback rate of 40 Mbits/sec was assumed to be adequate. However, a second recorder was included for redundancy. Each recorder would cost 200K.

Table 9-20. Data Handling Volume Requirements
for Mission 9 Design Driving Sensors

PARAMETER	SENSORS		
	SAR	PMMR	CRMS
DATA VOLUME (MBITS/DAY)	2.16×10^6 *	1.03×10^4	2.85×10^4
CALIBRATION DATA VOLUME (MBITS/DAY)	N/A	0.09	1.50
DATA FRAME VOLUME (MPIXELS/FRAME/DAY) (MBITS/FRAME/DAY)	4.55×10^2 (2.73×10^3)	4.68 ** (42.12)	27.0 (162)
PROCESSING DATA VOLUME (MBITS/DAY)	3.41	0.05	0.51

* INCLUDES BOTH RADARS

** BASED ON THE LARGER CONE ANGLE

Two main processing structures were considered adequate in Step 3 to handle the processing throughput rates computed in Step 1, one for the SARs and another for the PMMR and CRMS. The input/output memory costs would be:

- SARs 500K
- PMMR + CRMS 100K

Step 4 determined that three pieces of special purpose hardware were required. As in Mission 6, the SARs required one for fast Fourier transforms and another for convolutions or filtering. Because of the low processing rates of the other two instruments, a single piece of hardware could be used for along-track and cross-track interpolation. (The processing rates for the PMMR and CRMS would be approximately 10^4 nsec/word and approximately 10^3 nsec/word, respectively.) The costs would be:

- SAR pieces 60K each
- PMMR + CRMS piece 50K.

The processing and calibration memory costs derived in Step 5 were:

	<u>Processing Memory</u>	<u>Calibration Memory</u>
• SAR	10K	-
• PMMR	1K	1K
• CRMS	1K	5K

The filmwriter and archiving requirements determined in Step 6 resulted in a cost of 1525K. The general purpose computer would cost 500K.

The cost for the CDPF is summarized in Table 9-21. The most significant cost driver is data archiving.

Table 9-21. Cost Summary for the Ground Data Handling System (\$ Thousands)

ITEM	UNIT COST	QUANTITY	TOTAL COST
TAPE RECORDERS	200	2	400
INPUT/OUTPUT MEMORY	600	-	600
SPECIAL PURPOSE HARDWARE	VARIES	3	170
PROCESSING DATA MEMORY	12	-	12
CALIBRATION DATA MEMORY	6	-	6
MINI-COMPUTER SYSTEMS	100	2	200
FILMWRIER	225	1	225
ARCHIVING	1300	-	1300
GENERAL PURPOSE COMPUTER	500	1	500
TOTAL			3413

9.4.6 Data Dissemination System Design

The Mission 9 data distribution system will employ the same basic elements as Mission 6. Raw data from the spacecraft will be routed (via TDRS) to a ground processing facility. Following the correcting and formatting of raw data, they will be transmitted to a Data Dissemination Satellite for distribution to the users. This system should put near raw data into the hands of the user in near real time.

A worthwhile addition to the basic data distribution system described above would permit small users (ships, for example) access to a limited amount of processed data. Sea surface temperature and salinity are of special interest to fishermen. The location and nature of storm activity are of benefit to all mariners as well as to the general public. Thus an expansion of the data dissemination satellite capabilities to meet the needs of the small data user is highly recommended, and should be a required feature of the operational version of this mission.

9.4.7 System Summary

Figure 9-28 shows a simplified block diagram of the Mission 9 end-to-end data system. System implementation is straightforward although there are several advanced technology items in this configuration. The 506.8 MBPS analog-to-digital converter should be space-qualified in the near future. Data processing capability in 1984 might permit partial or complete synthesis of the SAR antenna beam in which case the data rate could be substantially reduced. This would also alleviate the demultiplex and record hardware required at the White Sands TDRS ground facility. Note that a contiguous data processing and retransmission facility has been proposed for Mission 9. This facility would format data and distribute it to a variety of users via the data dissemination satellite proposed for Mission 6.1.

9.5 SRT and ART Requirements

Throughout this study we have identified areas where technological improvements would lead to better mission fulfillment potential. Only a limited number of these have found application in the three synthesized missions. Here, however, we summarize our findings in all areas.

A statement is in order at this point about the present SRT and ART program. We find, in general, that they are quite effective. Among the items discussed below will be found many, such as solid state power amplifier and tape recorder development, which are currently being pursued. Their inclusion here should help to reinforce the need for continued progress in these areas.

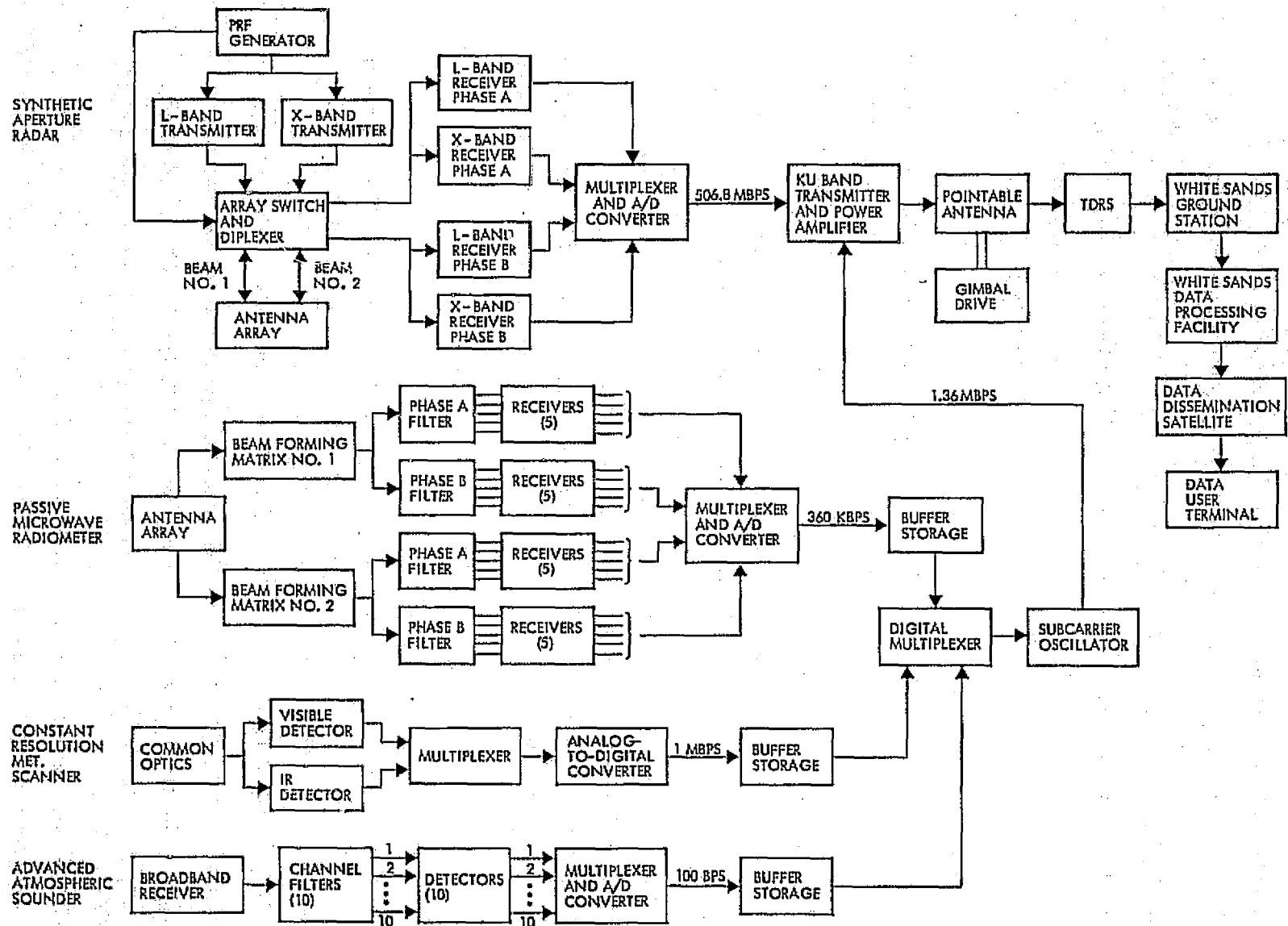


Figure 9-28. Mission 9 Data System Block Diagram

In selecting items for inclusion two qualifications have been imposed.

- a) The desired result would lead to substantially improved performance, increased reliability or reduced cost.
- b) There is a reasonable chance that devoted effort would result in progress.

Items have been grouped into specific technology areas in the discussion which follows.

Instrument Design

Shortcomings in present point-detector design involve a combination of sensitivity, stability, uniformity and reliability. There are detectors which have reasonably good characteristics in each area but none which does well in all areas. Progress here would go a long way toward simplifying some sensor designs.

Mechanical scanning devices in present sensors fall short of desired linearity of scan and scan efficiency. A variety of image and object plane scanning techniques have been proposed but only as part of an overall sensor design. One or more properly directed ART efforts here could develop the technology needed for future instruments before it becomes necessary to rush the effort to meet launch date deadlines.

Over sampling has been used for a long time to offset the effect of resolution degradation resulting from aperture smear. Unfortunately, there is a consequent increase in data rate proportional to the over sampling. A theoretical understanding of the interrelationships between aperture shape and size, spatial sampling interval, pre sample filtering and image reconstruction techniques as they effect signal-to-noise, aliasing, MTF, has been growing but there are still areas not well understood. Furthermore, when aperture shading and/or shaping are called for, techniques for synthesizing them rarely exist. Effort could profitably be spent in increasing our theoretical understanding here and in reducing to practice techniques for synthesizing apertures to control aliasing and minimize smear without loss of MTF or signal-to-noise.

Today's pushbroom scanners suffer from the need to independently calibrate each detector. Through better understanding and more laboratory work it should be possible to control the properties of individual

detectors in an array so as to ensure uniformity. Progress here could yield substantial dividends in the ease of image reconstruction and the elimination of correction equipment.

SAR beam synthesis involves multidimensional processing comparable to taking a Fourier transform. Pursuing algorithms and techniques for doing all or partial beam synthesis on-board would permit a reduction of transmission rates and possibly remove the need for complex ground processing equipment. Similarly, when multi-frequency, multipolarization radars are employed simple range-bin by range-bin redundancy-elimination techniques might substantially reduce data rates with or without on-board beam synthesis. Such improvements will depend both on a better understanding of the problem and on the availability of the proper LSI implementation.

Today's multi-frequency passive microwave radiometers require a multiplicity of large antennas. Technology studies directed toward making use of a common radiating system for all bands would be beneficial. Both mechanical (a common scanning reflector) and electronically scanned arrays should be included.

On-Board Data Processing

Large buffers (from one to several million bits) for use in line stretching, data formatting, sensor calibration, and sample interpolation will be required to optimize future data handling systems. Much of the buffering can be serial but there will also be a need for random access. LSI techniques must be advanced but bubble memories and CCD techniques are worthy of appreciable emphasis.

Large-capacity, serial data storage devices will also be needed. Today tape recorders still hold the greatest promise for accommodating the volume of data needed but increases in reliability and wear-out life time are needed. One of the biggest problems relates to headwear and accumulation of debris. Continued effort should be directed toward minimizing these as problems in future designs. Also continued emphasis must be placed on increasing input and output data rates and total storage capacity.

There is need for developing a large-capacity storage medium for accepting varying input rates. This is easily possible using a combination of existing tape recorder and electronic buffering. Flight-qualified continuously-variable-speed tape recorders currently exist. Their speed is slaved to the frequency of an incoming signal. The inertia of these tape recorders precludes their instantaneous response to data rate changes, so an electronic buffer which can accept data at any rate and feed it to the tape recorder at a different rate must be added. Tape recorder speed would be regulated by the fraction of the buffer that is filled and the data would be transferred from the buffer to tape recorder in synchronism with the locking signal (so as to ensure constant recording density on the tape). The availability of such a system would be invaluable for use with data compression systems of various types.

Likely contenders to replace tape recorders are CCD's and bubble memories. Progress in these areas must be monitored and if the technology advances to where competition with tape recorders is possible, effort should be devoted toward applying it to the creation of flight verification models.

On-board computation today is used for relatively few functions. Computation speeds, instruction sets, and memory sizes are severely limited even in comparison with today's mini-computers for ground usage. In the future, demands for on-board computational capacity will grow. In the future quantities of data processing currently done on the ground may be done in a data processing satellite. To prepare for this, new concepts in "self-healing" architecture will be required, random access memory capacities must be expanded, computational speeds must be increased and new medium-capacity temporary storage devices (whose function on the ground is accomplished in disks) must be developed.

Communications Equipment

The greatest need in communications equipment (which is already being pushed) is for improved efficiency in solid state transmitters at higher power and higher frequencies. A goal of 20 watts at Ku-band at better than 50 percent efficiency is appropriate. Closely related is a need for efficient multipower-level transmitters which can be used at a

variety of data rates. Steerable phased-array antenna development could be beneficial if weight and power requirements were reduced to be competitive with mechanically pointed antennas.

Ground Data Processing

New developments in ground data processing should be directed toward increased throughput, more accurate interpolation algorithms, techniques for linearizing conically scanned data and special equipment for synthesizing SAR beams.

Specialized System

TDRSS capacity should be substantially increased in the single access mode. Larger TDRSS antennas should be used to ease the ERP problem of the using spacecraft. A three satellite constellation should be developed with laser communications between satellites.

In Mission 6 we have identified the need for a dedicated data dissemination satellite. The study of such a system could profitably begin. To achieve best results a two way communication system should be available to permit interactive operations with a central processing and archiving facility. Thus, a user would be able to get not only routine data periodically after each pass but could also request past data.

The key factor in the development of the data dissemination satellite would be establishing an interface with users that can be met with low cost and easily operated and maintained equipment. Items to be considered in establishing this interface include; formats, frequencies, data rates, power flux densities, freedom from dynamic pointing, etc. In the satellite, multiple antennas would be used to permit simultaneous communication to more than one user.